Power System Control for Large-Disturbance Stability: Security, Robustness and Transient Energy

by

Jeffrey Wayne Chapman

B.S., University of California at Santa Barbara, 1990
S.M., Massachusetts Institute of Technology, 1992

Submitted to the Department of Electrical Engineering and Computer Science
in partial fulfillment of the requirements for the degree of

Doctor of Philosophy

at the

MASSACHUSETTS INSTITUTE OF TECHNOLOGY

May 1996

© Massachusetts Institute of Technology 1996. All rights reserved.

Author .....
Department of Electrical Engineering and Computer Science
March 19, 1990

Certified by .....
Marija D. Ilić
Senior Research Scientist
Thesis Supervisor

Accepted by .....
Frederic R. Morgenthaler
Chairman, Departmental Committee on Graduate Students

MASSACHUSETTS INSTITUTE
OF TECHNOLOGY

JUL 16 1996

Eng

LIBRARIES

Power System Control for Large-Disturbance Stability: Security, Robustness and Transient Energy

by

Jeffrey Wayne Chapman

Submitted to the Department of Electrical Engineering and Computer Science
on March 19, 1990, in partial fulfillment of the
requirements for the degree of
Doctor of Philosophy

Abstract

The problem of designing and evaluating controls for the purpose of maximizing transient stability limits of a multimachine power system is considered. Impact of generator excitation control on transient energy functions (TEFs), commonly used in transient stability analysis, is investigated. Modeling issues that simplify analysis of energy functions are developed, and dynamic behavior of several TEFs is derived and related to control design considerations. A time-scale decomposition of control objectives is proposed and formalized as a based on manifold in the state space. Direct Lyapunov-based excitation control is developed and tested, using a common TEF as the basis. Two time scale decoupled excitation control is designed and tested. A two time scale feedback linearizing control (FBLC) for excitation is developed that meets control objectives and provides an advancement both in performance as compared to previous FBLC designs and in terms of decentralization of the control. Concepts are illustrated via simulations on a three-machine test system.

Thesis Supervisor: Marija D. Ilić
Title: Senior Research Scientist

To Vivian.

Acknowledgments

The acknowledgments page is that curious piece of prose that comes first in the document, but is invariably written last. I have always suspected that this custom is observed in case the focus of one's gratitude changes in the course of the effort. In my own case, the list has grown ever longer as things have progressed, even as many of those to be named below have flown to the four winds. I now take this opportunity to express high esteem and deep gratitude to the following people:

First, to the front-line shock troops of survival, my office-mates: charter members L. Haachitaba Mweene and Mary Tolikas, whose wit and compassion kept me smiling through many a tough day, and Joaquin Lacalle, who, sensing depression on my part, would tell bad jokes until cheering up became a matter of self-defense. We were a living, breathing stress-management seminar.

To my academic advisor, Dr. Marija Ilić, a true phenomenon. Many an hour was spent with Dr. Ilić defining and shaping the ideas that went into this thesis. Her enthusiasm was unflagging, and her ideas had a way of worming their way slowly into my consciousness, until the links finally fell into place and I realized she was right on target. Goes to show, if you pour enough water on a rock, some of it will eventually sink in. I am also grateful for her efforts and those of Dr. Richard Tabors in ensuring that my financial support was uninterrupted, and that I had the maximum amount of time for productive research.

To my committee, Professors George Verghese and Munther Dahleh, for their careful reading and comments, without which this thesis would not have been possible. Particular thanks to Professor Verghese for help with structure and syntax that went well beyond the call of duty.

To the graduate students of LEES, always good for advice and conversation on topics technical, practical and metaphysical. They gave the lab its character and made it possible to look forward to being there day after day: Eric Allen, Mary Jane Boyd, Julio Castrillon-Candas, Judy Cardell, Tracy Clark, Brian Eidson, Niels LaWhite, Su-Lin Low, Ahmed Mitwalli, Kwabena Ofori-Tenkorang, Dave Perrault, Ganesh Ramaswamy, Ujjwal Sinha, Kamakshi Sridhar, Alecks Stanković, Assef Zobian, and others too numerous to name. Besides lending life and energy to the place, each has contributed in more concrete ways toward this day.

To Vivian Mizuno for helping every day in every way she could, and to Barbara Connolly and Cathy McCue for office support, commiseration and general camaraderie.

To Wayne Hagman, researcher, philosopher. An excellent fellow to engage in conversation and hoist a beer with.

To Larry Jones, for consulting in matters of PC software and hardware.

To Karen Walrath, grad student, system administrator and UNIX whiz, who ironed out many a problem. I suspect that those now at the mercy of system administrators in the real world will come to a greater appreciation of the functionality that Karen and her husband Jeff Schiller squeezed from a motley assortment of hardware.

To my father, Don L. Chapman, a man I continue to admire, who has been a source of unfailing encouragement and support. Thanks, Dad.

To my in-laws, John and May Sha, who have provided support and love to me and my family.

Finally, to my wife Vivian, whose sacrifices could fill a document twice this size, and to my children, Lee and Katie. Vivian has single-handedly pulled us through ten years of hardship. Lee and Katie have made it all worthwhile. Still the best crowd in this corner of the universe.

Contents

List of Figures

Chapter 1

Introduction

The field of control and stability of large-scale power systems has seen considerable activity in recent years, driven by two major forces. First, existing transmission systems are being operated under loading conditions that challenge the capability of existing control systems [17, 27]. This is a result of changing environmental and economic demands on the power industry coupled with the difficulty and expense of providing new transmission capacity in response to the expansion and geographic redistribution of load. Second, the availability of Flexible AC Transmission System (FACTS) components such as static VAR compensators (SVC's), thyristor controlled series capacitors (TCSC's) and phase shifting transformers is creating opportunities for a redefinition of the transmission grid from an essentially passive system component to an active element that will play a major role in the operation of the power industry [19]. These devices are capable of responding to system transients over a time scale of fractions of a second, making them suitable for use in controlling the short-term system response following system upsets such as equipment outages, short circuits and the like. In addition, the use of microprocessor-based control as an enhancement to established devices such as power system stabilizers (PSS) has created the potential for higher performance control through the application of nonlinear control techniques such as variable structure control, feedback linearization, adaptive control and various paradigms currently lumped under the name of "intelligent" control [8, 34, 35, 5, 52, 18].

The increase in operating demands and proliferation of advanced hardware have cre-

ated a need for more powerful analytical tools for planning and design. In many cases, the function of a particular piece of equipment may be defined in terms of a narrow set of objectives such as the stabilization of a particular bus voltage or modulation of the power flow across a particular transmission interface, without addressing the systemwide effects of the device. This situation follows from the lack of a comprehensive design methodology for power system control. The effect of this is that the selection and application of equipment is done without any systematic method for ensuring that the control objectives are met adequately, efficiently and without unforeseen consequences. Indeed, once the selection of a particular piece of equipment is made, the use of exhaustive time-domain simulations is currently the only method available for ensuring that all of its capabilities are exploited, in the sense of fully realizing systemwide or even local benefits. The development of a coherent set of tools for evaluating the performance of various control devices in terms of immediate control objectives *and* systemwide effects must therefore be viewed as critical to the effective utilization of FACTS technology and advanced control as it becomes available.

1.1 Statement of the Problem

There are several conditions that make the development of such a group of analytical tools a difficult task. First, there is the complexity *and variability* of the power system. The interconnected power system is not a single dynamic system, but rather a set from which the particular system is determined at a given instant by the specifics of load demand, load dynamics, and the generation/transmission configuration. This ranges over a huge number of permutations in response to demand and economic pressures. Therefore, a given control element must remain stable under widely varying conditions, which may change slowly, as in response to the evolution of load demand, or instantaneously, as in the case of a transmission-line outage. Large deviations in the system state may degrade the performance of controls based on linear design techniques. Moreover, any high-performance control that is sensitive to a step change in system parameters may become a liability under faulted conditions. This is a particularly severe challenge to

controls that rely on any sort of parameter identification, since they tend to allow relatively large transients prior to the convergence of the identified parameters, and there is typically an unavoidable trade-off between rapid convergence and tightly-bounded transient behavior.

Several factors may contribute to a system breakdown resulting from a large disturbance. To begin with, any power system has many stable and unstable equilibria, so that a large disturbance may cause the system to settle to a new (and undesirable) equilibrium. The system is also subject to operating constraints such as load voltage limits which must be satisfied in addition to the stability requirement. Under most conditions, an undesirable equilibrium will violate these constraints, causing the protective relaying to remove equipment from service, in which case the net effect may be indistinguishable from actual instability.

Aggravating this condition is the fact that most of the available means of control are severely limited in either magnitude or bandwidth. Control saturation is a commonly-encountered problem and the saturation of a particular control device can be sufficient to cause instability [13]. Given effects such as the foregoing, which result from the variability and nonlinearity of the system, we may ask the following question: How can a workable definition of control quality be developed that will allow the overall performance of the design to be evaluated?

1.2 Control Requirements Unique to Power Systems

Power system operators have traditionally held system reliability as the preemptive design goal, to the extent that in the past transmission capacity and loading were maintained at extremely conservative levels. This conservative design philosophy can no longer be maintained, but system reliability remains a major concern. It is quite possible that as the deregulation of the power industry proceeds, the reliability of the network will decline, as it becomes necessary to justify costs and expenditures that

are related to network reliability in economic terms. This is not necessarily a negative effect, since only the most rudimentary mechanisms now exist to relate the cost of delivered electrical energy to its reliability, forcing many customers to pay for a level of service that may not be optimal for their application. This translates into an inefficient allocation of resources. It should be apparent that if no method currently exists for evaluating the comparative effects of various control designs on reliability, then pricing mechanisms which would lead to an economically optimal level of system reliability cannot be formulated.

Overall reliability is difficult to quantify, and the quantitative assessment of a given design's impact on reliability is still more elusive. Moreover, in many cases, equipment may not be installed for the sole purpose of enhancing system reliability, but its effect on reliability or fault-tolerance as a secondary consequence of its operation is of concern. Therefore it is not immediately apparent how these considerations can be reconciled, to arrive at some working definition of what constitutes "good" control. This question has been addressed extensively in other areas of control (though it is still far from being solved) and some of these approaches have been applied to power systems [24, 36], but the unique characteristics of power system operation make it necessary to revisit the issue in this new context.

In summary, the following conditions are noted:

- The unique characteristics of the bulk power system pose a problem in analyzing control performance that is not adequately addressed by existing methods.
- The need to assess and maximize the survivability of the system through control design may create a need for a new approach to the design process.
- Because of the mutability of the system, robustness to system uncertainty must also be a major concern.
- No existing method for characterizing "good" control appears to directly capture the unique requirements of power system operation.

Since the mechanisms whereby stability is lost on the transient time scale are unique to

nonlinear systems, one approach to analyzing the impact of controls on system reliability would involve an analysis of the effect of a given control scheme on the system energy and the region of attraction of the desired equilibrium point. Lyapunov-based methods have received considerable attention as a method for evaluating the reliability of power systems, but not as an input to the design process. In order to have general application, however, it is important that the process be analytically tractable and general enough to encompass a wide variety of control designs.

1.3 Summary of Existing Theory

1.3.1 Survey of Current Methods of Stability Assessment

The power system is commonly modeled as a nonlinear descriptor system:

$$\begin{aligned} \dot{x} &= f(x, \zeta, u) \\ 0 &= g(x, \zeta) \end{aligned} \tag{1.1}$$

Here, $g(x, \zeta)$ is usually taken to represent the load-flow equations, which, when nonlinear load models are used, do not have a closed-form solution. The vector ζ is an implicit function of x and can be taken to represent load-bus voltages or phase angles, depending on the type of load model used. If constant-admittance loads are assumed, then there is a closed-form solution

$$\zeta = h(x), \tag{1.2}$$

so that (1.1) reduces to the vector O.D.E.

$$\dot{x} = f(x, h(x), u) = f_c(x, u). \tag{1.3}$$

An equilibrium point $(x_o\, \zeta_o\, u_o)$ is a point for which

$$f(x_o, \zeta_o, u_o) = 0, \tag{1.4}$$

and unless (1.4) admits only a single solution (*i.e.* the equilibrium point is unique), the term "stability" must be used only with respect to a given equilibrium point. Moreover, the stability of an equilibrium point may be defined in a number of ways (see, for example, [50]). These definitions are standard material and will be reviewed in somewhat more detail in Chapter 3. We will assume in this thesis that stable, viable equilibrium points are locally asymptotically stable, which essentially means that for disturbances that are sufficiently small, the state deviations may be made arbitrarily small, and the system returns to the stable equilibrium point as the time $t \to \infty$. It may be said that the system returns to a locally asymptotically stable equilibrium point provided that state perturbations remain in the *region of attraction* (ROA), and this may indeed be taken as a working definition of the ROA.

Small-Signal Stability

The purpose of this section is to relate the terms *small-signal* and *transient* stability, common in power-systems jargon, to the more general nonlinear systems terminology. A more complete exposition of this subject is to be found in Chapter 3. As its name indicates, small-signal stability is related to the stability of the linear approximation of the system at a given operating point x_o. This is the familiar "linearized" model, in which a nonlinear system is represented as locally equivalent to a linear state-space form,

$$\begin{aligned} \dot{\tilde{\mathsf{x}}} &= \mathbf{A}\tilde{\mathsf{x}} + \mathbf{B}\tilde{\mathsf{u}}, \\ \mathbf{A} &= \mathbf{J}^{x}_{f_c} \qquad (1.5) \\ \mathbf{B} &= \mathbf{J}^{u}_{f_c} \end{aligned}$$

$$(1.6)$$

where in the context of (1.3), we define $\tilde{\mathsf{x}} = \mathsf{x} - \mathsf{x}_o$, $\mathbf{J}^{x}_{f_c}$ as the Jacobian matrix of f_c taken with respect to x and $\mathbf{J}^{u}_{f_c}$ as the Jacobian with respect to u. If the eigenvalues of the $\mathbf{A}$ matrix are all in the open left half-plane, then the system is stable in some neighborhood of $(\mathsf{x}_o, \zeta_o, \mathsf{u}_o)$ and is said to be small-signal stable.

The fact that the system is small-signal stable at $\mathbf{x}_o$ does not imply anything about other potential operating points, and does not relate to the size of the stability region. Clearly, however, it is of concern to verify that small-signal stability is not lost for any foreseeable operating condition. A well-known example of a system that may lose small-signal stability at certain operating points is a generator which is equipped with a high-gain static exciter and an automatic voltage regulator. Unless some form of rotor angle or frequency feedback is provided, the system Jacobian matrix will exhibit unstable eigenvalues under certain loading conditions (see, *e. g.* [35]).

Transient Stability

A somewhat more difficult concept to grasp is that of transient stability. Some recent work in this area may be found in [39, 9]. Transient stability is related to the fact that, in the more general nonlinear systems terminology, all power system equilibria are only locally stable, if at all. The state space of the system contains large numbers of stable and unstable equilibria and each asymptotically stable equilibrium is associated with its own ROA. If a disturbance is of sufficient severity that the post-disturbance state is outside of the region of attraction of the desired (or, more generally any viable) equilibrium, then the system will not return to a viable operating condition, and some loss of functionality will result. Note that transient stability can only be defined with respect to a given fault. Often it is defined in terms of *critical clearing time* (t_{cr}), that is, the amount of time that a fault may remain uncorrected without causing the system to leave the region of attraction of an acceptable postfault equilibrium.

The event that must be cleared may be a short circuit, in which case t_{cr} is the allowable time before the affected line is removed from service. On the other hand, when a heavily-loaded transmission line is removed from service by its protective devices, generators experience a loss of load that may also result in loss of synchronism, so that the line must be reclosed within a certain time interval in order to preserve the integrity of the system. We must distinguish between the prefault and postfault equilibria, since in general the postfault system is not the same as the prefault system. Faults may result in the removal of transmission lines or generators from service, causing a shift in

the stable equilibria from prefault to postfault periods. Indeed, if extensive structural changes occur as a result of a disturbance, it is conceivable that the prefault equilibrium point could lie outside of the region of attraction of *any* stable postfault equilibrium. Under those circumstances, the system would be transiently unstable with respect to that disturbance, regardless of the clearing time. It is evident that it is the postfault equilibrium that is of primary concern in transient stability analysis. The prefault equilibrium is typically of interest only because it provides the initial conditions for the fault-on stage of the analysis.

In general, a system disturbance causes a change in the power that is supplied by each generator to the grid. Since the mechanical power supplied to the generator by the prime mover cannot be rapidly changed, the mismatch between input and output power results in acceleration of the generator rotor, which "swings," with respect to other generators in the system. When the fault is cleared, the accelerating force is usually reversed, and the speed of the rotor begins to decrease. If the initial swing is eventually reversed and the rotor begins to move back toward its equilibrium angle, the system is said to be *first-swing stable* with respect to that fault. On the other hand, if the generator rotor gains too much kinetic energy during the fault, its speed may not return to the system frequency after the fault is cleared, and it will lose synchronism and be removed from service. The system is then said to be transiently unstable with respect to that fault. Note that a system may be first-swing stable and yet be transiently unstable, as when a generator loses synchronism on the second (or later) swing of an oscillation [31]. In general, although much-used in the past, first-swing stability is not a very useful concept and will not receive much attention here. The more general concept of regions of attraction of the various equilibria must be used to determine the actual security of the system, and the system is said to be transiently stable if it reaches any viable equilibrium following the disturbance. In practice, the exact region of attraction may be difficult or impossible to determine, even in off-line studies. Moreover, the size of the region is a function of the system loading and configuration, and may actually vanish in some cases, driven by the evolution of the loads or other factors. This would correspond to a loss of small-signal stability.

A Lyapunov-based approach has been applied to this problem with some success. In this approach, an attempt is made to capture the total system energy in a scalar, positive-definite function of the system state with a nonincreasing time derivative. Many variations of these functions exist, collectively known as *transient energy functions* (TEF) [45, 37]. Strictly speaking, TEFs are *not* Lyapunov functions, but the analysis is similar. As in Lyapunov analysis, the idea of an "energy" function is that it represents a quantity that is conserved in some sense, so that, absent any net source of "energy," it must be a nonincreasing quantity for a given system configuration. This will be addressed in more detail in Chapter 3, but it may be useful at this point to give a somewhat heuristic outline to illustrate the energy-function method.

Suppose there is a closed, connected, bounded set $\mathcal{B}_o$ containing the postfault equilibrium point, with the following properties: It is contained in the the region of attraction, and for every point on its boundary, the system energy is a constant, E_o. Then if the faulted trajectory remains within $\mathcal{B}_o$ and the system energy at fault clearing is less than E_o, the state trajectory must remain within that region thereafter[1], and the system is considered to be transiently stable. By Lyapunov theory, if the equilibrium is unique and if the boundedness of the energy function implies that the state is also bounded, then one can make some conclusions regarding the global stability of the system. Unfortunately, in power systems, this is never true, since there are many equilibria.

Each stable equilibrium exists in an energy "well," whose boundary is formed by a set of unstable equilibria, together with their stable manifolds [10]. These boundaries separate the regions of attraction of the various stable equilibria, and therefore if the system energy remains below the value of the minimum-energy unstable equilibrium point, the system trajectory will be confined within the region of attraction of the stable equilibrium. The so-called closest unstable equilibrium point (u.e.p.) method attempts to identify the lowest-energy unstable equilibrium point on the boundary of the region of attraction. For a given fault, if the system energy at the time the fault is

[1]since the energy would have to somehow increase in order for the trajectory to penetrate the boundary

cleared is less than the energy of the u.e.p., the system is said to be transiently stable. This method is known as the closest unstable equilibrium or *closest u.e.p* method. In practice it tends to give very conservative results, since the disturbed system trajectory may never approach the minimum energy point on the stability boundary. Refinements to this method have been proposed, but the basic approach of comparing the system energy at the time the fault is cleared to some threshold energy on the stability boundary is unchanged.

Energy-function analysis thus becomes a problem in two parts: First, an appropriate energy function must be found. Second, for each fault of interest, t_{cr} is determined as the point along the faulted system trajectory at which $E(\mathbf{x}(t_{cr})) = E_o$ for some appropriately-determined value of E_o. Many researchers have introduced refinements that increase the accuracy of the TEF method, and many standardized energy functions are available, which yield results of varying but reasonable accuracy.

Several difficulties exist with this method. The first is that it may be numerically difficult to identify the closest u.e.p. The system order is very large, and the large number of unstable equilibria tends to make a brute-force search infeasible for this problem. A second problem is that most methods make the assumption that the system voltages do not affect the power transfer of the grid. While this is justified under many circumstances, in many cases voltage/power coupling does play a significant role in the system dynamics, and it certainly must be considered if the effect of devices such as static VAR compensators and even power system stabilizers is to be analyzed. Unfortunately, the inclusion of voltage/power coupling in the energy-function framework greatly increases the level of complexity, in particular when the dynamics of voltage-control devices are to be included.

A third difficulty with the energy function method arises when system losses are considered. The inclusion of transmission grid losses (*i.e.*, the consideration of transmission line resistance) and machine damping terms creates a path dependency in the system energy function, so that, for instance, the energy of a particular point in the state-space with respect to the post-fault system cannot be calculated without knowing the post-fault trajectory with respect to a given clearing time. Since trajectories differ

for every fault and for each distinct clearing time, this is computationally intensive.

Finally, as with all Lyapunov-based stability methods, there is no systematic method for deriving the least-conservative Lyapunov function for a given system. A given function may satisfy all the conditions of an energy function, but if all mechanisms for energy exchange are not accounted for, the results may be overly conservative. A more serious problem arises when the assumptions upon which the energy function is based are violated. An example in which the voltage/power decoupling assumption is violated is that of a system that is experiencing the so-called inter-area oscillation phenomenon, in which groups of generators participate in oscillations which cause large surges in power transfer to occur across transmission lines. This can cause large deviations in voltage at intermediate points on the transmission grid, which significantly affect its power transfer capability. This is a case in which first-swing analysis might predict a transiently stable condition, but the system may in fact experience a growing oscillation that will ultimately cause a system failure.

In view of the importance of the transient stability problem, one might consider the utilization of some type of control device as a means of increasing the stability margins of a system, in the sense of increasing critical clearing times for a specific fault or group of faults, for example. This is a difficult objective to evaluate directly, however, since current frameworks for considering fast-acting control devices in a transient stability analysis are somewhat cumbersome. Moreover, because existing techniques are complex and computationally unwieldy, the best approach to this problem is not immediately clear.

1.3.2 Specifics of the Power System Control Problem

Several aspects of power systems make their control design problems somewhat unique. To begin with, the system order tends to be very high. A typical interconnected system may involve many hundreds or even thousands of generators, plus other dynamic elements such as SVC's and other FACTS devices. This has an impact on many design methodologies that require numerically intensive calculations, such as $\mathcal{H}_\infty$. Consider the task of accurately solving an algebraic Ricatti equation for a system matrix that

may have a dimension well into the thousands. For this reason, the system model must first be reduced by some method before the control can be designed. This introduces an added level of uncertainty to the problem.

Of course, the system is also nonlinear, but this statement of itself does not mean that linear design techniques are invalid. Almost any system displays some nonlinearity in its behavior at some level of modeling. The question is whether a given system may be adequately modeled for the purpose of control design by a linear model over its expected operating range. If this is not the case, then one must ask whether nonlinear control designs provide sufficient improvement in performance to warrant the abandonment of the powerful and well-tested linear techniques. Without a suitable method for evaluating control performance as it relates to the requirements of the power system, this question cannot be answered.

Many types of nonlinear controllers have been proposed for various FACTS devices, as well as for PSS's [8, 34, 35, 5, 52, 18]. In most cases, the evidence of superiority that is offered consists of a set of simulations of various disturbances. Unfortunately, as previously noted, there is no consensus as to what constitutes "good" control. For example, power system operators tend to desire tight control of system voltages, but are less concerned by a poorly-damped oscillation of a generator rotor, provided that it does eventually disappear. Therefore, a control that provides superior damping of a rotor oscillation is of little interest unless it offers some other benefit, such as increased operating security. This is difficult to show, since current methods for considering advanced control devices in transient stability analysis are not well-developed. This precludes any sort of meaningful comparison, short of exhaustive time-domain simulations, which are computationally expensive and do not provide much useful insight to guide the design process. Therefore, although nonlinear control designs do appear to offer significant improvements in some areas of performance, until some sense of a design's quality can be defined, any potential benefits that might be realized are difficult to quantify.

Another problem in power system control design is that of decentralization. Typically, a given controller will only have access to a very limited set of measurements from a small geographical area. Advanced instrumentation and communications technologies

are changing this factor, but it is safe to assume that in the near future, practical designs will be limited in the information that is available for feedback. This presents a very severe constraint, particularly on high-performance controls, which tend to tolerate less uncertainty. This constraint does not directly bear on the assessment of control quality, but does place limits on the types of controls that may be considered. Clearly, in terms of reliability, it is desirable to limit the amount of instrumentation and information exchange that supports a particular control function. On the other hand, intelligent design choices require that the benefits of an augmented information set be weighed. Unfortunately, this is difficult to quantify in terms of performance.

1.3.3 Review of Linear Control Methodologies

Many types of linear control design methodologies have been applied to power system problems. Classical frequency-domain methods which attempt to maintain specific gain and phase margins continue to find application in the design of power system stabilizers, although more modern methods are also in use. Linear-quadratic (LQ) optimal control designs have also been used [49]. In order to compensate for changes in the small-signal model as the operating point changes, some applications resort to gain-scheduling, in which a series of controls is designed and selected on-line as system conditions change. Robust control paradigms such as $\mathcal{H}_\infty$ are also beginning to find their way into application [36, 24] as are Lyapunov-based controls [16]. Each of these methods has strengths and weaknesses, but none directly addresses the specific requirement for reliability.

A common liability of all linear control designs is that, although the system may operate almost continuously at a given operating point for which the control can be optimized, the most crucial requirement for reliability is that the control operates to stabilize the system during or immediately after a fault, when state deviations are large, and the system characteristics may be significantly different from the usual operating conditions. A fault may involve a change in system topology that will dictate an entirely new equilibrium point, together with state deviations that do violate the small-signal assumptions in the sense that the system behavior is not well-modeled by *any* n^{th}-order

linear system. Inter-area oscillations also present problems, since they appear to involve significant nonlinear coupling between closely-spaced oscillatory modes that appear in the linearized system model [51]. Thus, assuming that a given control is optimal in some sense for the linearized system at a particular operating point, it may not be true that the control is optimal in any sense at all when the disturbance is large. Therefore if existing linear control techniques are to be utilized, it appears at least that some effort will be required to characterize the system performance relevantly and in a form to which the existing theory can be applied.

An interesting note on this point: It has been claimed [43] that by formulating the optimal control as the one which returns the system to equilibrium in the shortest possible time, one also has the optimal control in the sense of maximizing the region of attraction. Unfortunately, formulation of the time-optimal control problem typically involves the calculus of variations and Pontryagin's Principle of the Maximum, and its solution is typically at least as involved as solving the system equations themselves, and therefore is not practical in any but the simplest cases. Some recent work has appeared on the subject with respect to TCSCs, however. The fact that the time-optimal control maximizes the ROA is not intrinsic to the time-optimal problem, however, but results from the fact that it typically includes realistic constraints on control saturation. Therefore, the optimization is done over a set of possible control inputs that are all achievable. Since other common optimization methods provide no direct mechanism for considering control saturation, input signals that are not realizable enter into the search.

The following key points from the foregoing material are of interest here:

- Current methods for evaluating system security (the so-called transient energy methods) involve an approach that is similar to the direct method of Lyapunov.
- Because of the importance of the security margin, it may be desirable to characterize control performance at least partially in terms of a transient energy function.
- No method currently exists for characterizing controls in terms of their impact on transient energy functions or the stability region.

1.4 Thesis Outline

The remainder of this thesis is organized as follows: Chapter 2 sets out the notational conventions to be used in the remainder of the thesis, and develops several of the standard mathematical system models to be utilized in the remainder of the document. The so-called two axis generator model is defined, and used as a baseline to which the single-axis and flux-decay models are compared. In addition, the constant voltage behind the transient reactance model, widely used in early transient stability work, is presented. Generator models are then combined with consideration of the constraints imposed by the transmission network, and are developed in a convenient block-vector notation that clarifies many aspects of the system interactions.

Underlying all of these models is the Park/Blondel transform, which is described briefly. The concept of frames of reference, crucial to the Park/Blondel transform and power system modeling in general, is described and the effects of modeling the system in the so-called network frame of reference are presented. Models of the multimachine power system based on the network frame of reference are derived from models based on the more-common machine frame of reference, and block-form expressions of system quantities of interest, such as the electrical power and reactive power are derived.

Chapter 3 presents background material for transient stability analysis, covering some of the currently-used TEFs and their methods of application. Basic methods for deriving TEFs are described, and the decomposition of these functions into kinetic energy and potential energy terms is explained. TEFs are reformulated in block-vector notation, which clarifies the relationship of the various energy terms to quantities such as the total power produced and the total system reactive power. Some recent refinements of the closest u.e.p. method are presented and are placed into the context that will be used for analyzing the effects of controls that act primarily through variation of the system voltages. This class of controls will be referred to as *voltage-dominant* controls.

Chapter 4 investigates the effects of excitation control on the potential energy associated with a TEF. This is particularly striking when feedback-linearizing control of

the generator excitation is used. It is found that the interaction of voltage-dominant controls with the system energy occurs through variation in the gradient of the potential energy surface. The relationship between the region of attraction and the potential energy surface is described, and the effect of various linear and nonlinear excitation controls on the topology of the potential energy surface is investigated. Simulations are provided to illustrate the concepts involved.

Chapter 5 concludes with a summary of the findings presented in earlier chapters and presents directions for further research.

Appendix C, while somewhat peripheral in its relationship the the body of the thesis, shows how the network-referenced system model can be used to characterize the system nonlinearity as a norm-bounded perturbation to a linear system, and develops a robust control formulation that explicitly characterizes the system nonlinearity as a matrix perturbation to the network-referenced system model. This formulation leads naturally to an $\mathcal{H}^\infty$ framework for control design.

Chapter 2

System Modeling and Notation

2.1 Introduction

The primary purpose of this chapter is to introduce standard mathematical models for the power system on the transient time scale, and to introduce some of the notational conventions that are used to simplify the presentation in later chapters.

An actual power generation and transmission system consists of a large number of dynamic elements, primarily 3-phase synchronous electric generators, coupled across large geographic distances by high-voltage AC transmission lines, and augmented by various automatically-controlled dynamic devices such as FACTS devices for the control of voltage, power, reactive power and other system quantities. The generators supply electrical power to the transmission grid, to be consumed by loads connected at various points in the network. This huge and complex system is modeled in varying degrees of complexity and with various simplifying assumptions. For the topics considered here, the object is to capture the electromagnetic and mechanical interactions of the generators in a system that is in a disturbed condition due to a loss of load, short circuit or other occurrence, over a typical time interval of five to twenty seconds, which is essentially the so-called *transient* time scale. Although the transient time scale is often considered to encompass only the first swing of the generator rotors following a system upset, more recently many researchers have expanded this definition to include the entire interval during which there is risk of loss of synchronism of one or more

generators following an upset. This period may include several swings, particularly if the system is subject to inter-area oscillatory modes, which involve widely-separated groups of generators connected by long transmission lines.

2.2 The Park/Blondel Transform

The use of the Park/Blondel transform considerably simplifies the task of modeling a three-phase power system, particularly when it is assumed that the currents and voltages are balanced. Henceforth, however, we will shorten the name (with apologies to M. Blondel) and refer to it simply as the Park transform. Although the following discussion will use voltages to illustrate the transform, the procedure for transforming a three-phase current is identical.

The three-phase voltages, denoted v_a, v_b and v_c, appear as follows for balanced operation:

$$\begin{aligned} v_a(t) &= V\cos(\omega_o t + \phi) &&= V\cos(\theta(t) + \phi) \\ v_b(t) &= V\cos(\omega_o t - 2\pi/3 + \phi) &&= V\cos(\theta(t) - 2\pi/3 + \phi) \\ v_c(t) &= V\cos(\omega_o t + 2\pi/3 + \phi) &&= V\cos(\theta(t) + 2\pi/3 + \phi) \end{aligned} \tag{2.1}$$

V is the peak magnitude of the wave and $\theta(t)$ is an electrical angle that integrates the base electrical frequency,

$$\theta(t) = \int_{t_o}^{t} \omega_o \, dt \; = \omega_o t - \theta_o. \tag{2.2}$$

Given that there is no natural choice for t_o in a system that operates continuously, θ_o must be chosen arbitrarily. Note that, for a given time waveform as in (2.1), the choice of θ_o induces the value of ϕ.

The Park-transformed analogs of v_a, v_c and v_c appear as V_{D}, V_{Q} and V_0. The transform is as follows:

$$\begin{bmatrix} V_{\mathrm{D}} \\ V_{\mathrm{Q}} \\ V_0 \end{bmatrix} = \sqrt{\frac{2}{3}} \begin{bmatrix} \cos(\theta(t)) & \cos(\theta(t) - 2\pi/3) & \cos(\theta(t) + 2\pi/3) \\ -\sin(\theta(t)) & -\sin(\theta(t) - 2\pi/3) & -\sin(\theta(t) + 2\pi/3) \\ 1/\sqrt{2} & 1/\sqrt{2} & 1/\sqrt{2} \end{bmatrix} \begin{bmatrix} v_a \\ v_b \\ v_c \end{bmatrix}. \tag{2.3}$$

When neither the magnitude V nor the phase ϕ in (2.1) is changing, V_D and V_Q are constant. Moreover, V_0, the so-called zero-sequence component, is identically zero during balanced operation, which allows the considerable simplification of resolving voltages and currents into direct (real) and quadrature (imaginary) components, or equivalently into complex phasor quantities. Referring to (2.1), we have

$$V_D = \sqrt{\frac{3}{2}} V \cos(\phi), \quad V_Q = \sqrt{\frac{3}{2}} \sin(\phi), \quad V_0 = 0. \tag{2.4}$$

Notice that the angle θ has dropped out of the calculation, but as noted earlier, the value of ϕ depends on the choice of θ_o, and indeed we say that ϕ is measured *with respect* to θ_o. The ability to assign an arbitrary value to θ_o rests on the fact that all quantities of interest depend only on *relative* angles, that is, upon the difference between the angles as measured with respect to θ_o. This will presently be illustrated.

A more significant benefit is that when modeled in terms of the DQ voltages and currents, the three-phase generator inductances, which are time-varying functions of the rotor angle when modeled in a static frame of reference, become constant in the Park-transformed model. The mechanism by which this occurs is beyond the scope of this thesis, but can be found in [30]. In order to achieve this simplification for a synchronous machine, however, the reference must be chosen such that the d axis is aligned with the primary axis of the field flux.

Referring to Figure 2.1, observe that the axes marked with the upper-case letters D and Q are the axes induced by the choice of θ_o. The physical position of the rotor with respect to θ is fixed by the offset angle δ. By convention, δ is measured from the direct (D) axis of the arbitrary frame of reference (referred to hereafter as the *network* frame of reference) to the quadrature (q) axis of the machine rotor. The actual value of δ for any given machine depends on θ_o, *i.e.* it is measured relative to the network frame of reference.

A certain difficulty arises in applying the Park transform to a system of interconnected synchronous generators. The offset angle δ in (2.3) must be chosen such that the direct axis is aligned with the primary axis of the machine field flux in order for the

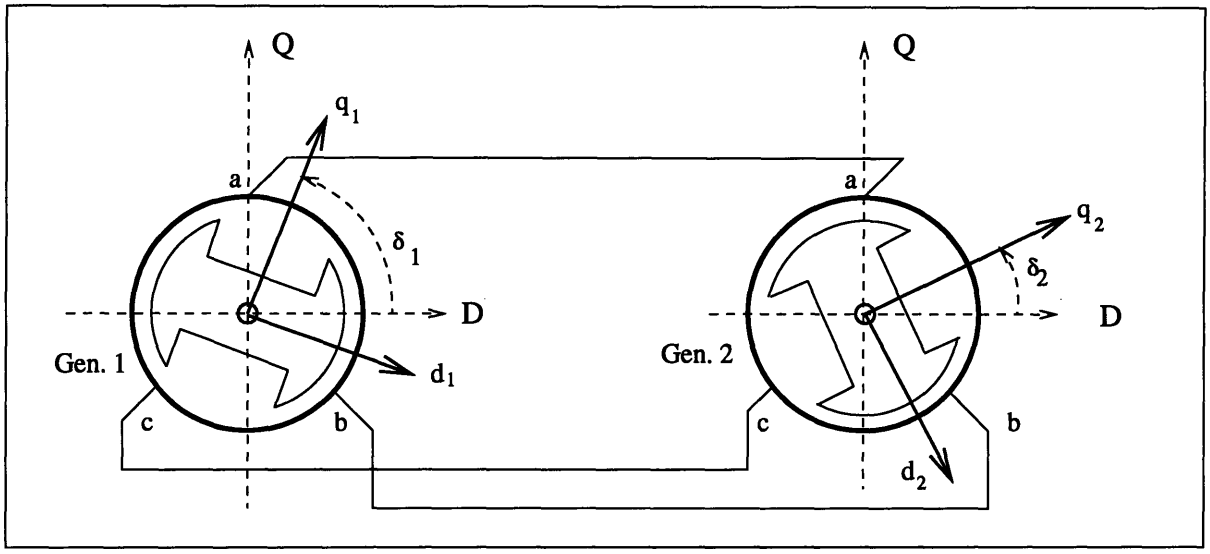

Figure 2.1: Local and Network Coordinates of the Park Transform.

machine inductances to appear as constants. Unfortunately, the particular offset of the field axis with respect to $\theta(t)$ varies from machine to machine, so that a different set of local coordinates is applied to the mathematical model for each machine. This situation is illustrated in Figure 2.1. The dotted axes marked with capital D and Q represent the network frame of reference, induced by the choice of θ_o. Note the alignment of the local axes with the magnetic axis of the rotor. For a synchronous machine, the average (electrical) angular velocity of the shaft matches the base frequency, but the instantaneous velocity may vary, so that for each machine δ_i is a time-varying angle. It is implicit in all that follows that the variation of machine angles, phase angles and magnitudes of the voltages and currents is slow enough to be considered quasi-static with respect to ω_o, and it is this assumption that allows the dynamics of the system to be written in terms of variations in the Park-transformed variables.

All of the axes illustrated rotate at the synchronous frequency. Although the angles $\delta_1(t)$ and $\delta_2(t)$ will change if the reference axes are changed, their difference, $\delta_{ij}(t)$ is invariant to a change in the reference. Hence $\delta_{ij}(t)$ represents the difference between the orientation of the direct field axis in machines i and j, and this angle is independent of the particular reference angle that is chosen. Moreover, as previously observed, given an arbitrary voltage or current measurement (as in Equation (2.1)), the phase angle

ϕ also depends on the choice of the base coordinates[1], so that all relative angles are preserved if the base coordinate system is changed. Since all system quantities depend only on the *relative* angles, the choice of the base coordinates is truly arbitrary.

Once a particular base angle is chosen, the direct and quadrature axes so defined are known as the network frame of reference. On the other hand, the local frame of reference defined at each generator coincides with the axis of the field flux and is known as the machine frame of reference. The particular orientation of the machine frame of reference with respect to the network frame of reference varies with time and from one unit to another. The solid vectors projecting from each machine in Figure 2.1 represent machine frames of reference. The network and machine frames of reference are related via a time-varying coordinate rotation, as should be apparent from the diagram. Adopting the convention of expressing network-referenced values with capital subscripts and machine-referenced variables with lower-case subscripts, we have:

$$\begin{bmatrix} V_{\mathrm{D}_i}(t) \\ V_{\mathrm{Q}_i}(t) \end{bmatrix} = \begin{bmatrix} \sin(\delta_i(t)) & \cos(\delta_i(t)) \\ -\cos(\delta_i(t)) & \sin(\delta_i(t)) \end{bmatrix} \begin{bmatrix} V_{d_i}(t) \\ V_{q_i}(t) \end{bmatrix}, \tag{2.5}$$

and the inverse transform:

$$\begin{bmatrix} V_{d_i}(t) \\ V_{q_i}(t) \end{bmatrix} = \begin{bmatrix} \sin(\delta_i(t)) & -\cos(\delta_i(t)) \\ \cos(\delta_i(t)) & \sin(\delta_i(t)) \end{bmatrix} \begin{bmatrix} V_{\mathrm{D}_i}(t) \\ V_{\mathrm{Q}_i}(t) \end{bmatrix}, \tag{2.6}$$

where δ_i is associated with the i^{th} generator of a multimachine system. Again, the transform is general for any Park-transformed quantity; a voltage is used here only as a specific example. Inspection of Figure 2.1 reveals an important fact regarding the machine frame of reference. It is clear that all of the machine angles (δ_i, for the i_{th} generator) are still measured with respect to the network coordinates. In other words, the rotor angles are defined as offsets from the arbitrary reference angle. Hence, the choice of a reference angle is an indispensable step in defining any Park-transformed model. This has some important consequences, which will motivate the choice of a

[1]or equivalently, on the choice of reference angle.

time-varying reference angle known as the center of inertia, to be dealt with in the sequel.

Because of the fact that the generator voltages and currents are expressed in local coordinates, it is necessary to convert all machine-referenced voltages to a common set of coordinates in order to solve for the currents in the transmission network. Similarly, it is necessary to convert the network-referenced currents back into machine-referenced form in order to solve for the derivatives of the machine states.

At this point it will be useful to defer treating the specifics of the frame-of-reference problem as they relate to system modeling until the dynamic model of the generators and the transmission system has been developed in more detail.

2.3 Single-Machine Models

A generator can be thought of as a combination of two subsystems, which roughly represent the mechanical and the electromagnetic aspects of the machine. The mechanical behavior is dominated by the effects of the rotating turbine/rotor mass, and unless the torsional behavior of the shaft is to be modeled[2], it is represented as a second-order subsystem. The electromagnetic subsystem is coupled to the mechanical subsystem by the energy transfer across the magnetic field in the machine air gap. In contrast to the mechanical model, there is wide variation in the way that the electromagnetic subsystem is modeled, depending primarily upon the time scale at which the phenomena of interest occur.

The dynamic model of interest here is one that will provide good agreement for the behavior of the synchronous generators over a time scale of perhaps twenty seconds following a disturbance. Electromagnetic transients that occur over fractions of a cycle to several cycles are assumed to have stabilized, while longer-term dynamics are assumed to be substantially constant on this time horizon. In particular, most large generating units are not equipped to effect large changes in the input power which the prime mover supplies to the generator itself. Therefore, for short-term simulations, the input torque

[2]We mention this in passing, since we shall not consider shaft dynamics in this document.

is usually considered to be constant, and this convention will be followed in the sequel.

Given these assumptions, several levels of complexity may still be required for the electromagnetic model, which commonly involves anywhere from one to six states, depending on the particular type of dynamics that are to be captured. If it is necessary to capture the fast dynamics that are dominated by the time constants of the generator stator, a sixth-order model (at least) is used. For the purposes of this thesis, however, the stator time constants are assumed to be negligibly small. At the other extreme, the electromagnetic subsystem may be replaced entirely by a voltage phasor of constant magnitude, whose phase angle coincides with the angle deviation of the rotor with respect to a reference angle that rotates at the system frequency. This model is often used for the determination of *first-swing stability*, in which only the first excursion of the rotor angles following a fault is considered.

A final detail to be considered is the almost-universal practice of scaling system variables by base quantities of current, voltage, mass, frequency and power to yield unitless "per-unit" quantities (see, *e.g.* [3]). This is convenient numerically, but can create some confusion. Because of the scaling and the fact that all variables are unitless and deviations from the base frequency are small, the quantities of inductance and reactance are equivalent (*i.e.* x'_d is equivalent to L'_d) and the internal flux of the generators may also be expressed as a voltage. Shaft torque and power are also equivalent in this framework.

A detailed exposition of the meaning and derivation of the various quantities that appear in the machine model is beyond the scope of this document, but each variable will be briefly identified. For a more detailed treatment, see [47], among many expositions on the subject. It will be convenient in the sequel to represent the interconnected system model in vector/matrix format, which will require some care in defining notational conventions. Every effort will be made to preserve standard notation in representing machine and network variables, but a given set of analogous variables may appear variously as a vector quantity, a diagonal matrix or as a more general matrix form. Therefore the following conventions will be adopted:

Diagonal matrices will be denoted by a capital letter in an outline-style font, while

non-diagonal matrices will appear as boldfaced capital letters, and vectors will appear in a boldfaced sans-serif font. For example, x and X are scalars, x and X are vectors, $\mathbf{X}$ is a matrix, and $\mathbb{X}$ is a diagonal matrix. An attempt will be made to denote diagonal matrices in a manner that is suggestive of what is on the diagonal, *e.g.* $\mathbb{E}_{\mathsf{Q}}$ would be a diagonal matrix containing the variable E_{Q} from each machine on the diagonal. A diagonal matrix of direct-axis currents would be $\mathbb{I}_{\mathsf{D}}$, which forces us the make an exception for the identity matrix, which will be shown as $\mathbf{I}$. Occasionally, we will resort to dimensionally-incorrect expressions of the form $\mathsf{x} - x_o$, in which the scalar quantity x_o is subtracted from each element of the vector x. Finally, it is common practice in the power systems literature to utilize a circumflex to denote a complex quantity, and this convention will be followed here as well.

Given this brief motivation, the generator model may now be presented. The multi-machine system model will presently be expressed in vector form, but we begin with the so-called two-axis model for a single unit, which is the most complex single-machine formulation that will appear in these pages. For the i^{th} generator, the machine equations are:

$$\dot{E}'_d = \frac{1}{T'_{qo_i}}\left[-E'_{d_i} + (x_{q_i} - x'_{q_i})i_{q_i}\right] \tag{2.7}$$

$$\dot{E}'_{q_i} = \frac{1}{T'_{do_i}}\left[-E'_{q_i} - (x_{d_i} - x'_{d_i})i_{d_i} + E_{fd_i}\right] \tag{2.8}$$

$$\dot{\delta}_i = \omega_i - \omega_o \tag{2.9}$$

$$\dot{\omega}_i = \frac{1}{m_i}\left[T_{m_i} - P_{e_i} - \frac{D_i}{\omega_o}(\omega_i - \omega_o)\right] \tag{2.10}$$

$$= \frac{1}{m_i}\left[T_{m_i} - E'_{q_i}i_{q_i} - E'_{d_i}i_{d_i} - (x'_{qi} - x'_{d_i})i_{d_i}i_{q_i} - \frac{D_i}{\omega_o}(\omega_i - \omega_o)\right], \tag{2.11}$$

The mechanical variables are ω and δ, representing the frequency and the relative rotor angle of the generator, respectively. The turbine/rotor moment of inertia is m, the input torque is T_m and P_e is the electrical power supplied to the transmission system. D is a catch-all damping term that reflects several different damping effects such as windage, turbine damping and damper winding torques. D tends to be small and is often ignored entirely. The moment of inertia is frequently expressed in terms of the

inertia constant H, where $m = 2H/\omega_o$.

The quantity $E'_d + jE'_q$ is a phasor representation of the Park-transformed three-phase machine voltage. The direct and quadrature transient impedances are denoted by x'_d and x'_q, respectively, while i_d and i_q are the direct and quadrature projections of the machine armature current, in the machine frame of reference . Differences in the values of x'_d and x'_q reflect the condition called transient saliency, which results from asymmetry in the distribution of the rotor iron. Low-speed multi-pole generators (and hydraulic machines in particular) tend to be constructed with the windings supported on isolated iron pole-pieces, so that the effective impedance of the machine varies depending on the relative position of the rotor with respect to the stator windings. This effect is much less pronounced in machines in which the field windings are supported on solid iron rotors, and in this case it is common to take $x'_d = x'_q$. Note that if transient saliency is ignored, the expression for the electrical power reduces to

$$P_e = E'_q i_q + E'_d i_d \tag{2.12}$$

The actual values of i_d and i_q depend on the system load, the grid admittance and the states of the generators connected to it. We make the simplifying assumption that the time constants associated with the transmission line reactances are short enough to allow that part of the system to be taken at sinusoidal steady state, allowing the transmission grid to be represented algebraically as a matrix of complex impedances.

Given a particular set of generator voltages, it is then possible to solve algebraically for the resulting currents. It is common to model the generator voltages as dynamic states, so that the currents become an algebraic function of the voltages. The various elements in the system interact through variations in the network currents. It should be recognized, however, that there is nothing intrinsic in this framework. In a given situation it may be more convenient to consider the currents to be the dynamic states, or indeed to identify some mixed subset of voltages and currents as states, provided that the remaining quantities are uniquely determined thereby. A second assumption is that the three-phase voltages and currents in the transmission network are balanced. Volt-

ages and currents are then projected onto a synchronously-rotating frame of reference via the well-known Park transform (see, *e.g.* [3]).

2.4 The Network Solution

We begin this section with some basic definitions of complex power, real power and reactive and power. The complex-valued power injection at a bus is defined as

$$\hat{S}_i = \hat{V}_i \hat{I}_i^*. \tag{2.13}$$

Recall that the "hat" denotes a complex value and the asterisk denotes the complex conjugate. Current *leaving* the bus is taken to be positive, which causes generated power to be positive and load power to be negative. The real and reactive power are defined as

$$P = \mathcal{R}e(\hat{S}), \;\; Q = \mathcal{I}m(\hat{S}). \tag{2.14}$$

Expanding the real and imaginary parts of the phasor quantities yields:

$$P = V_{\mathrm{D}} I_{\mathrm{D}} + V_{\mathrm{Q}} I_{\mathrm{Q}}, \tag{2.15}$$

$$Q = -V_{\mathrm{D}} I_{\mathrm{Q}} + V_{\mathrm{Q}} I_{\mathrm{D}}. \tag{2.16}$$

Figure 2.2 is a one-line diagram of a very simple power transmission network. Assuming that the generators shown are free of transient saliency, it is possible to represent the internal impedance of the machine as a constant, x'_d. The line admittances are shown symbolically as $G_{ij} + jB_{ij}$, but these may also be denoted by the complex value $\hat{Y}_{ij}$. Two types of load are shown, the one at Bus 2 being a constant-admittance type, with a constant-PQ load shown at bus 4. Impedance-type loads are designated with the bus identifier as $\hat{Y}_{Li} = G_{Li} + jB_{Li}$. A constant-PQ load is one in which the active and reactive power are constant. We now define the complex admittance matrix $\hat{\mathbf{Y}} = [\hat{y}_{ij}]$, in which the ij^{th} element is just the negative admittance of the transmission

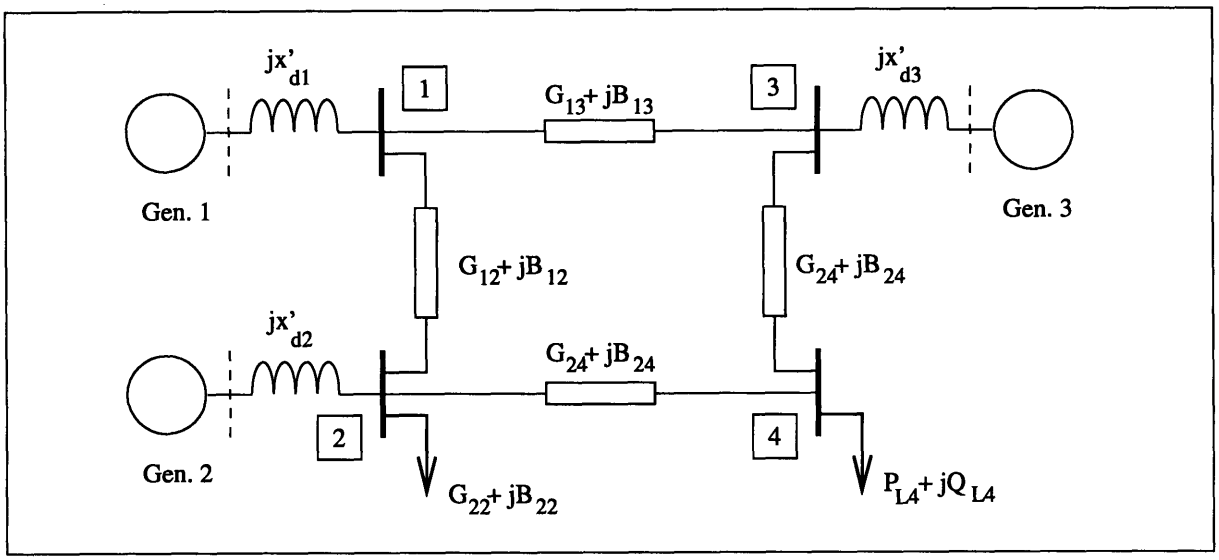

Figure 2.2: A simple transmission network.

line linking busses i and j,

$$\hat{y}_{ij} = -G_{ij} - jB_{ij}, \tag{2.17}$$

while the diagonal elements are defined as

$$\hat{y}_{ii} = G_{Li} + jB_{Li} + \sum_{j=1}^{N}(G_{ij} + jB_{ij}). \tag{2.18}$$

Line shunts, where present, are taken as part of the load admittance. In much of the power systems literature, the signs of B_{ij} and G_{ij} are taken to be the same as their corresponding entries in the admittance matrix, however there does not appear to be a uniform convention in this regard. In this document, the signs will be taken as in (2.17) and (2.18). It is evident that the constant-admittance load can be included naturally in the admittance matrix, but there is no straightforward method for including other types of loads. Kirchoff's current law holds regardless of the load type, however, so that given a vector of complex (Park-transformed) bus voltages in the network frame of reference,

$$\hat{\mathbf{V}} = \begin{bmatrix} \hat{V}_1 & \cdots & \hat{V}_4 \end{bmatrix}^t, \tag{2.19}$$

together with the assumption that the network is in sinusoidal steady state, we may invoke KCL to solve for the complex-valued node currents. The structure of the complex

admittance matrix is such that this yields the following relationship:

$$\hat{\mathbf{I}} = \hat{\mathbf{Y}}\hat{\mathbf{V}}. \tag{2.20}$$

The difficulty with this relationship is that the voltage at constant-PQ busses (e.g. $\hat{V}_4$ in Figure 2.2) is typically unknown. The load voltage at constant-PQ busses depends on the supply voltages via the load-flow equations, which are nonlinear and must be solved iteratively. This presents a problem in the modeling of multimachine systems, since for the purpose of simulations, the load-flow equations must be solved at each step. For short-term stability work it is common to assume that the loads can be represented as constant admittances, and any PQ load that is specified is converted to the equivalent admittance for the nominal bus voltage at equilibrium.

Now, with the load admittance incorporated into the admittance matrix, KCL requires that the node current be zero at any bus that is not connected to a voltage source (as in a load-only bus), hence we have the relationship

$$\begin{bmatrix} \hat{\mathbf{I}}_G \\ 0 \end{bmatrix} = \begin{bmatrix} \hat{\mathbf{Y}}_{GG} & \hat{\mathbf{Y}}_{GL} \\ \hat{\mathbf{Y}}_{LG} & \hat{\mathbf{Y}}_{LL} \end{bmatrix} \begin{bmatrix} \hat{\mathbf{V}}_G \\ \hat{\mathbf{V}}_L \end{bmatrix}, \tag{2.21}$$

where the generator and load nodes have been grouped together as the notation suggests. A simple algebraic manipulation then leads to an algebraic solution for the generator currents, known as the Kron's reduction:

$$\hat{\mathbf{I}}_G = \left(\hat{\mathbf{Y}}_{GG} - \hat{\mathbf{Y}}_{GL}\hat{\mathbf{Y}}_{LL}^{-1}\hat{\mathbf{Y}}_{LG}\right)\hat{\mathbf{V}}_G. \tag{2.22}$$

The matrix within the parentheses is identified as the complex reduced admittance matrix, so that the voltage-current relationship of the interconnected generators may be expressed as follows:

$$\hat{\mathbf{I}}_G = \hat{\mathbf{Y}}_r\hat{\mathbf{V}}_G. \tag{2.23}$$

2.4.1 Network Quantities in the Network Frame of Reference

It is most common to decompose (2.23) into an equivalent real-valued matrix multiplication. Notationally, it is much more convenient to group the real and imaginary parts of the voltages into separate blocks, so that the voltage vector would take the form:

$$\mathsf{V}_{\mathrm{DQ}} = \left[\begin{array}{cccccc} V_{\mathrm{D}_1} & \cdots & V_{\mathrm{D}_p} & V_{\mathrm{Q}_1} & \cdots & V_{\mathrm{Q}_p} \end{array} \right]^t. \tag{2.24}$$

This ordering will be referred to as the *block form*, while the more common order in which variables from each bus are grouped together (*e.g.* $\mathsf{V} = [V_{\mathrm{D}_1}\ V_{\mathrm{Q}_1}\ V_{\mathrm{D}_2}, V_{\mathrm{Q}_2} \ldots]^t$) will be called the *interleaved form.*

Equation (2.23) is then expressed in terms of real numbers by forming the real-valued block-form reduced admittance matrix $\mathbf{Y}_r$ as follows:

$$\mathbf{Y}_r = \left[\begin{array}{cc} \mathcal{R}e\{\hat{\mathbf{Y}}_r\} & -\mathcal{I}m\{\hat{\mathbf{Y}}_r\} \\ \mathcal{I}m\{\hat{\mathbf{Y}}_r\} & \mathcal{R}e\{\hat{\mathbf{Y}}_r\} \end{array} \right] = \left[\begin{array}{cc} \mathbf{G}_r & -\mathbf{B}_r \\ \mathbf{B}_r & \mathbf{G}_r \end{array} \right], \tag{2.25}$$

so that

$$\left[\begin{array}{c} \mathsf{I}_{\mathrm{D}} \\ \mathsf{I}_{\mathrm{Q}} \end{array} \right] = \left[\begin{array}{cc} \mathbf{G}_r & -\mathbf{B}_r \\ \mathbf{B}_r & \mathbf{G}_r \end{array} \right] \left[\begin{array}{c} \mathsf{V}_{\mathrm{D}} \\ \mathsf{V}_{\mathrm{Q}} \end{array} \right], \tag{2.26}$$

or

$$\mathsf{I}_{\mathrm{DQ}} = \mathbf{Y}_r \mathsf{V}_{\mathrm{DQ}}. \tag{2.27}$$

Note that, in (2.22) $\hat{\mathbf{Y}}_{\mathrm{GL}} = \hat{\mathbf{Y}}_{\mathrm{LG}}^t$, so that $\hat{\mathbf{Y}}_r$ is symmetric, hence $\mathbf{G}_r$ and $\mathbf{B}_r$ are also symmetric. The fact that (2.26) is invariant to the choice of reference angle is a simple consequence of the assumption that the voltage phasors represent the steady-state response to a sinusoidal excitation at the frequency ω_o. It was mentioned earlier that the choice of reference angle is equivalent to fixing a time origin, but the steady-state response assumes that $t_o \to -\infty$ and is therefore by definition invariant to a finite shift in the time origin. Thus all voltage-current relationships hold regardless of the choice of reference angle. Moreover, although the actual values of V_{D_i}, V_{Q_i}, I_{D_i} and I_{Q_i} do depend on the reference angle, P_i and Q_i do not, since a shift in the reference

corresponds to a unitary transform on the associated voltage and current vectors. One may resort to the polar form of the power equation $P = |\hat{V}|\,|\hat{I}|\cos(\theta_{\mathrm{V}} - \theta_{\mathrm{I}})$ for algebraic verification of this fact.

It is now a simple matter to write vector equations for the real and reactive power injections at the machine busses:

$$\mathsf{P}_e = \begin{bmatrix} \mathbb{V}_{\mathrm{D}} & \mathbb{V}_{\mathrm{Q}} \end{bmatrix} \begin{bmatrix} \mathbf{G}_r & -\mathbf{B}_r \\ \mathbf{B}_r & \mathbf{G}_r \end{bmatrix} \begin{bmatrix} \mathsf{V}_{\mathrm{D}} \\ \mathsf{V}_{\mathrm{Q}} \end{bmatrix} \tag{2.28}$$

and

$$\mathsf{Q} = \begin{bmatrix} \mathbb{V}_{\mathrm{Q}} & -\mathbb{V}_{\mathrm{D}} \end{bmatrix} \begin{bmatrix} \mathbf{G}_r & -\mathbf{B}_r \\ \mathbf{B}_r & \mathbf{G}_r \end{bmatrix} \begin{bmatrix} \mathsf{V}_{\mathrm{D}} \\ \mathsf{V}_{\mathrm{Q}} \end{bmatrix} \tag{2.29}$$

A block permutation and a sign change of the expression for Q yields:

$$\begin{aligned} \mathsf{Q} &= \begin{bmatrix} \mathbb{V}_{\mathrm{D}} & \mathbb{V}_{\mathrm{Q}} \end{bmatrix} \begin{bmatrix} \mathbf{0} & -\mathbf{I} \\ \mathbf{I} & \mathbf{0} \end{bmatrix} \begin{bmatrix} \mathbf{G}_r & -\mathbf{B}_r \\ \mathbf{B}_r & \mathbf{G}_r \end{bmatrix} \begin{bmatrix} \mathsf{V}_{\mathrm{D}} \\ \mathsf{V}_{\mathrm{Q}} \end{bmatrix} \\ &= \begin{bmatrix} \mathbb{V}_{\mathrm{D}} & \mathbb{V}_{\mathrm{Q}} \end{bmatrix} \begin{bmatrix} -\mathbf{B}_r & -\mathbf{G}_r \\ \mathbf{G}_r & -\mathbf{B}_r \end{bmatrix} \begin{bmatrix} \mathsf{V}_{\mathrm{D}} \\ \mathsf{V}_{\mathrm{Q}} \end{bmatrix} \end{aligned} \tag{2.30}$$

Observe that the sum of the elements of P_e can be expressed as $\mathbf{1}^t\mathsf{P}_e$, where $\mathbf{1}$ is an p-vector whose entries are all ones. Substitution into (2.28) yields:

$$P_{\mathrm{tot}} = \mathbf{1}^t\mathsf{P}_e = \begin{bmatrix} \mathsf{V}_{\mathrm{D}}^t & \mathsf{V}_{\mathrm{Q}}^t \end{bmatrix} \begin{bmatrix} \mathbf{G}_r & -\mathbf{B}_r \\ \mathbf{B}_r & \mathbf{G}_r \end{bmatrix} \begin{bmatrix} \mathsf{V}_{\mathrm{D}} \\ \mathsf{V}_{\mathrm{Q}} \end{bmatrix}. \tag{2.31}$$

This is just a quadratic form, which means that the antisymmetric part of the admittance matrix drops out to leave:

$$P_{\mathrm{tot}} = \begin{bmatrix} \mathsf{V}_{\mathrm{D}}^t & \mathsf{V}_{\mathrm{Q}}^t \end{bmatrix} \begin{bmatrix} \mathbf{G}_r & \mathbf{0} \\ \mathbf{0} & \mathbf{G}_r \end{bmatrix} \begin{bmatrix} \mathsf{V}_{\mathrm{D}} \\ \mathsf{V}_{\mathrm{Q}} \end{bmatrix}. \tag{2.32}$$

Clearly, a similar operation on (2.30) gives:

$$Q_{\text{tot}} = \begin{bmatrix} \mathsf{V}_{\mathrm{D}}^t & \mathsf{V}_{\mathrm{Q}}^t \end{bmatrix} \begin{bmatrix} -\mathbf{B}_r & \mathbf{0} \\ \mathbf{0} & -\mathbf{B}_r \end{bmatrix} \begin{bmatrix} \mathsf{V}_{\mathrm{D}} \\ \mathsf{V}_{\mathrm{Q}} \end{bmatrix}. \tag{2.33}$$

2.4.2 Network Quantities and Modeling in the Machine Frame of Reference

In the previous discussion, the generators were considered as complex voltage sources with with output impedance x'_d, but all equations were written in terms of the terminal voltages rather than the machine voltages, which comprise state variables in the generator models. The major motivation for using a constant admittance load model is that it allows for the solution of the machine currents in terms of the state variables, so that the entire multimachine model may be written as a standard vector O.D.E. Referring to to Figure 2.2, it should be clear that it is possible, in the absence of transient saliency, to incorporate the transient reactances into the admittance matrix, (equivalent to adding the imaginary busses represented by the dotted lines in the figure) and then eliminate the terminal busses by Kron's reduction, so that the machine currents in equations (2.7 – 2.11) become the solution of a matrix multiplication of the machine voltages with a certain admittance matrix. The model so derived is called the *internal node* model.

In fact, for the constant-admittance load model, it is always possible to get a closed-form solution for the network currents in terms of the machine voltages and rotor angles. This will now be derived, starting with the general solution, and then particularizing to the case in which transient saliency is ignored.

In order to express the solution compactly, the coordinate transforms (2.5) and (2.6) must be generalized to the vector case, for a system of p generators. Recall that the lower-case subscripts refer to the machine frame of reference, while the upper-case refers to the network frame. The block-form vector equivalents of (2.5) and (2.6) are

then:

$$\begin{bmatrix} \mathsf{V}_D \\ \mathsf{V}_Q \end{bmatrix} = \mathbf{R}(\boldsymbol{\delta}) \begin{bmatrix} \mathsf{V}_d \\ \mathsf{V}_q \end{bmatrix}, \tag{2.34}$$

where

$$\mathbf{R}(\boldsymbol{\delta}) = \begin{bmatrix} \mathbb{S}(\boldsymbol{\delta}) & \mathbb{C}(\boldsymbol{\delta}) \\ -\mathbb{C}(\boldsymbol{\delta}) & \mathbb{S}(\boldsymbol{\delta}) \end{bmatrix}, \tag{2.35}$$

$$\mathbf{R}^{-1}(\boldsymbol{\delta}) = \begin{bmatrix} \mathbb{S}(\boldsymbol{\delta}) & -\mathbb{C}(\boldsymbol{\delta}) \\ \mathbb{C}(\boldsymbol{\delta}) & \mathbb{S}(\boldsymbol{\delta}) \end{bmatrix} \tag{2.36}$$

and

$$\mathbb{S}(\boldsymbol{\delta}) = \mathrm{diag}(\sin(\delta_1) \ldots \sin(\delta_p))$$

$$\mathbb{C}(\boldsymbol{\delta}) = \mathrm{diag}(\cos(\delta_1) \ldots \cos(\delta_p)).$$

Here δ_i is the rotor angle of the i^{th} generator. $\mathbf{R}(\boldsymbol{\delta})$ is just a pairwise coordinate rotation, which rotates each pair $[\ V_{d_i}\ \ V_{q_i}\ ]$ through an angle of $\delta - \pi/2$. Note the similarity in the form of $\mathbf{R}(\boldsymbol{\delta})$ to (2.5). Indeed, when the voltage vector is expressed in the interleaved form, $\mathbf{R}(\boldsymbol{\delta})$ takes on a block-diagonal form with 2×2 matrices of the form of (2.5) on the diagonal, and it can be directly verified that it is unitary, *i.e.* $\mathbf{R}^t\mathbf{R} = \mathbf{I}$.

The currents i_d and i_q are now expressed in terms of the generator terminal voltages V_d and V_q, taken in the machine frames of reference, and matrix $\mathbf{Y}_r$ as follows:

$$\begin{bmatrix} \mathsf{i}_d \\ \mathsf{i}_q \end{bmatrix} = \mathbf{R}(\boldsymbol{\delta})^{-1}\, \mathbf{Y}_r\, \mathbf{R}(\boldsymbol{\delta}) \begin{bmatrix} \mathsf{V}_d \\ \mathsf{V}_q \end{bmatrix}. \tag{2.37}$$

The following scalar equations relate the terminal voltage to the machine states (the so-called "internal" voltages):

$$V_d = E'_d + x'_q i_q + r_s i_d \tag{2.38}$$

$$V_q = E'_q - x'_d i_d + r_s i_q \tag{2.39}$$

These can be written for an p-machine system as the vector equation

$$\begin{bmatrix} \mathsf{V}_d \\ \mathsf{V}_q \end{bmatrix} = \begin{bmatrix} \mathsf{E}'_d \\ \mathsf{E}'_q \end{bmatrix} + \mathbf{Z} \begin{bmatrix} \mathsf{i}_d \\ \mathsf{i}_q \end{bmatrix}, \tag{2.40}$$

where

$$\begin{aligned} \mathbf{Z} &= \begin{bmatrix} \mathbb{R}_s & \mathbb{X}'_q \\ -\mathbb{X}'_d & \mathbb{R}_s \end{bmatrix} \\ \mathbb{X}'_d &= \mathrm{diag}(\mathsf{x}'_d) \\ \mathbb{X}'_q &= \mathrm{diag}(\mathsf{x}'_q). \end{aligned} \tag{2.41}$$

Substituting (2.40) into (2.37):

$$\begin{bmatrix} \mathsf{i}_d \\ \mathsf{i}_q \end{bmatrix} = \mathbf{R}^{-1}\mathbf{Y}_r\mathbf{R} \left\{ \begin{bmatrix} \mathsf{E}'_d \\ \mathsf{E}'_q \end{bmatrix} + \mathbf{Z} \begin{bmatrix} \mathsf{i}_d \\ \mathsf{i}_q \end{bmatrix} \right\} \tag{2.42}$$

or

$$\begin{aligned} \left[\mathbf{I} - \mathbf{R}^{-1}\mathbf{Y}_r\mathbf{R}\mathbf{Z}\right] \begin{bmatrix} \mathsf{i}_d \\ \mathsf{i}_q \end{bmatrix} &= \mathbf{R}^{-1}\mathbf{Y}_r\mathbf{R}[\mathbf{R}^{-1}\mathbf{Y}_r^{-1}\mathbf{R} - \mathbf{Z}] \begin{bmatrix} \mathsf{i}_d \\ \mathsf{i}_q \end{bmatrix} \\ &= \mathbf{R}^{-1}\mathbf{Y}_r\mathbf{R} \begin{bmatrix} \mathsf{E}'_d \\ \mathsf{E}'_q \end{bmatrix}, \end{aligned} \tag{2.43}$$

where the dependence of the transform upon δ has been suppressed for notational convenience. Finally, premultiplying by $[\mathbf{R}^{-1}\mathbf{Y}_r^{-1}\mathbf{R} - \mathbf{Z}]^{-1}\mathbf{R}^{-1}\mathbf{Y}_r^{-1}\mathbf{R}$ and factoring, we have

$$\begin{bmatrix} \mathsf{i}_d \\ \mathsf{i}_q \end{bmatrix} = \mathbf{R}^{-1}\left[\mathbf{Y}_r^{-1} - \mathbf{R}\mathbf{Z}\mathbf{R}^{-1}\right]^{-1}\mathbf{R} \begin{bmatrix} \mathsf{E}'_d \\ \mathsf{E}'_q \end{bmatrix} = \bar{\mathbf{Y}}_{rs}(\boldsymbol{\delta}) \begin{bmatrix} \mathsf{E}'_d \\ \mathsf{E}'_q \end{bmatrix}. \tag{2.44}$$

This expression may be simplified if $\mathbb{X}'_q = \mathbb{X}'_d$, *i.e.*, when saliency is ignored. Specifically, when $\mathbb{X}'_q = \mathbb{X}'_d$, the matrices $\mathbf{R}$ and $\mathbf{Z}$ commute, so that $\mathbf{R}\mathbf{Z}\mathbf{R}^{-1} = \mathbf{Z}\mathbf{R}\mathbf{R}^{-1} = \mathbf{Z}$,

and

$$\begin{bmatrix} \mathsf{i}_d \\ \mathsf{i}_q \end{bmatrix} = \mathbf{R}^{-1}(\mathbf{Y}_r^{-1} - \mathbf{Z})^{-1}\mathbf{R} \begin{bmatrix} \mathsf{E}'_d \\ \mathsf{E}'_q \end{bmatrix}. \tag{2.45}$$

Denoting this matrix by $\bar{\mathbf{Y}}_r$, we have

$$\begin{bmatrix} \mathsf{i}_d \\ \mathsf{i}_q \end{bmatrix} = \mathbf{R}^{-1}\bar{\mathbf{Y}}_r\mathbf{R} \begin{bmatrix} \mathsf{E}'_d \\ \mathsf{E}'_q \end{bmatrix}. \tag{2.46}$$

It can be shown via simple algebraic manipulations that $(\mathbf{Y}_r^{-1} - \mathbf{Z})^{-1}$ from (2.45) is precisely the reduced admittance matrix that is calculated for the internal node model. In Equation (2.46), the overbar on the symbol $\bar{\mathbf{Y}}_r$ is used to distinguish the reduced matrix for the internal-node model from the matrix that preserves the terminal busses of the generators. Since the internal-node model is used almost exclusively in the sequel, the overbar will be dropped and $\mathbf{Y}_r$ will be understood to refer to the reduced admittance matrix for the internal-node configuration.

Equation (2.46) is defined in terms of the fixed admittance matrix $\mathbf{Y}_r$, under the assumption that transient saliency is negligible, but if the $\boldsymbol{\delta}$-dependent matrix $Y_{rs}(\boldsymbol{\delta})$ from (2.44) is substituted, then it is valid for the more general case. It must be emphasized here that even if saliency is ignored, (2.46) *cannot* in general be reduced to an equivalent expression using machine voltage phasors of magnitude E and phase $\boldsymbol{\delta}$. This is valid only with respect to the single-axis and flux-decay models[3]. The two-axis model does not allow this type of simplification. This is clear from Figure 2.3, which depicts the phase and magnitude relationships of the stator currents and machine voltages in a synchronous generator. This diagram is standard material and can be found *e.g.* in [39]. In general, the machine voltage phasor $\hat{E}$ has magnitude $|E'_d + jE'_q|$ at an angle of $\delta' = \delta - \phi$, where $\phi = \arg(E'_d + jE'_q)$. It is clear that the angle of the machine voltage phasor depends on the machine currents as well as the rotor angle, hence it is not a function of the rotor angle alone.

[3]Some modifications of the machine impedance and voltage magnitude are necessary with the flux-decay model

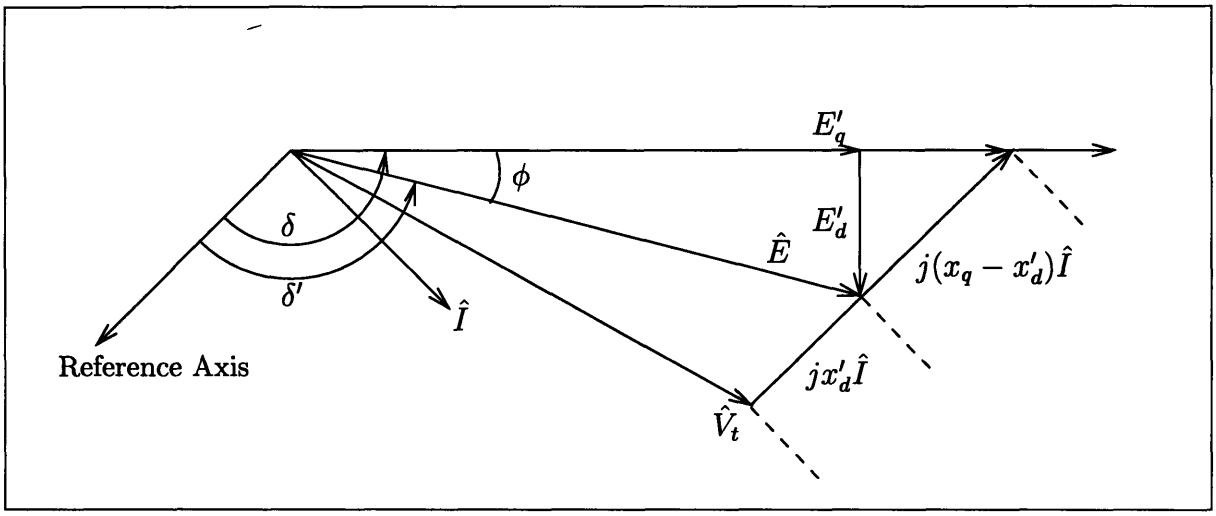

Figure 2.3: Machine Phasor Diagram.

2.5 Multimachine System Models

We are now in a position to develop the model of a multimachine power system having p synchronous generators connected via a transmission grid. We will formulate the model in block form, using the notational conventions described in Section 2.3, so that the state vector has the form:

$$\begin{bmatrix} \mathsf{E}'_d \\ \mathsf{E}'_q \\ \boldsymbol{\delta} \\ \boldsymbol{\omega} \end{bmatrix} = \begin{bmatrix} E_{d_1} & \cdots & E_{d_p} & E_{q_1} & \cdots & E_{q_p} & \delta_1 & \cdots & \delta_p & \omega_1 & \cdots & \omega_p \end{bmatrix}^t. \qquad (2.47)$$

In the process some block-form expressions will be developed for the basic system quantities of power and reactive power analogous to those in Section 2.4.1. These will be useful in the chapters to follow.

It is straightforward to generalize the model of equations (2.7) – (2.11) to a basic vector form. It will be most convenient to group the electromagnetic subsystems into a matrix expression. Defining $\tilde{x}_{d_i} = x_{d_i} - x'_{d_i}$ and $\tilde{x}_{q_i} = x_{q_i} - x'_{q_i}$, along with the associated

diagonal matrices $\tilde{\mathbf{X}}_d$ and $\tilde{\mathbf{X}}_q$, we have

$$\begin{bmatrix} \mathbb{T}'_{qo} & \mathbf{0} \\ \mathbf{0} & \mathbb{T}'_{do} \end{bmatrix} \begin{bmatrix} \dot{\mathsf{E}}'_d \\ \dot{\mathsf{E}}'_q \end{bmatrix} = -\begin{bmatrix} \mathsf{E}'_d \\ \mathsf{E}'_q \end{bmatrix} - \begin{bmatrix} \mathbf{0} & -\tilde{\mathbb{X}}_q \\ \tilde{\mathbb{X}}_d & \mathbf{0} \end{bmatrix} \begin{bmatrix} \mathsf{i}_d \\ \mathsf{i}_q \end{bmatrix} + \begin{bmatrix} \mathbf{0} \\ \mathsf{E}_{fd} \end{bmatrix} \tag{2.48}$$

$$\dot{\boldsymbol{\delta}} = \boldsymbol{\omega} - \boldsymbol{\omega}_o \tag{2.49}$$

$$\mathbb{M}\dot{\boldsymbol{\omega}} = \mathsf{T}_m - \mathsf{P}_e - \frac{1}{\omega_o}\mathbb{D}(\boldsymbol{\omega} - \boldsymbol{\omega}_o) \tag{2.50}$$

$$= \mathsf{T}_m - \begin{bmatrix} \mathbb{E}'_d & \mathbb{E}'_q \end{bmatrix} \begin{bmatrix} \mathsf{i}_d \\ \mathsf{i}_q \end{bmatrix} - \frac{1}{\omega_o}\mathbb{D}(\boldsymbol{\omega} - \boldsymbol{\omega}_o). \tag{2.51}$$

The matrix $[\mathbb{E}'_d \;\; \mathbb{E}'_q]$ is a rectangular composite of the two $p \times p$ diagonal matrices. One may now substitute (2.46) into these equations to express the currents as functions of the state:

$$\begin{bmatrix} \mathbb{T}'_{qo} & \mathbf{0} \\ \mathbf{0} & \mathbb{T}'_{do} \end{bmatrix} \begin{bmatrix} \dot{\mathsf{E}}'_d \\ \dot{\mathsf{E}}'_q \end{bmatrix} = \left(I + \tilde{\mathbf{X}}_{dq}\mathbf{R}^t(\boldsymbol{\delta})\mathbf{Y}_r\mathbf{R}(\boldsymbol{\delta})\right) \begin{bmatrix} \mathsf{E}'_d \\ \mathsf{E}'_q \end{bmatrix} + \begin{bmatrix} \mathbf{0} \\ \mathbf{I} \end{bmatrix} \mathsf{E}_{fd} \tag{2.52}$$

$$\dot{\boldsymbol{\delta}} = \boldsymbol{\omega} - \boldsymbol{\omega}_o \tag{2.53}$$

$$\mathbb{M}\dot{\boldsymbol{\omega}} = \left(\mathsf{T}_m - \begin{bmatrix} \mathbb{E}'_d & \mathbb{E}'_q \end{bmatrix} \mathbf{R}^t(\boldsymbol{\delta})\mathbf{Y}_r\mathbf{R}(\boldsymbol{\delta}) \begin{bmatrix} \mathsf{E}'_d \\ \mathsf{E}'_q \end{bmatrix} - \frac{1}{\omega_o}\mathbb{D}(\boldsymbol{\omega} - \boldsymbol{\omega}_o)\right). \tag{2.54}$$

Note particularly the vector expression for P_e in (2.54),

$$\mathsf{P}_e = \begin{bmatrix} \mathbb{E}'_d & \mathbb{E}'_q \end{bmatrix} \mathbf{R}^t(\boldsymbol{\delta})\mathbf{Y}_r\mathbf{R}(\boldsymbol{\delta}) \begin{bmatrix} \mathsf{E}'_d \\ \mathsf{E}'_q \end{bmatrix}. \tag{2.55}$$

The presence of the matrix $\mathbf{R}(\boldsymbol{\delta})$ and its inverse in the expression is a reflection of the fact that the machine voltages must be expressed in a common frame of reference in order to solve the network equations. The expression (2.55) is not seen in the literature, so it may be instructive to compare it to the more commonly-used equation. Using a phasor representation $E_i \angle \phi_i$ for the machine voltage, taken in a common frame

of reference, the expression for the power output of a single machine connected in a multimachine system is typically written as

$$P_{e_i} = E_i^2 G_{ii} - E_i \sum_{\substack{j=1 \\ j \neq i}}^{p} E_j (G_{ij} \cos(\phi_i - \phi_j) + B_{ij} \sin(\phi_i - \phi_j)). \tag{2.56}$$

As long as saliency is ignored, (2.26) may be applied to internal voltages as well as to terminal quantities, using the internal-node reduced admittance matrix:

$$\begin{bmatrix} \mathsf{I}_{\mathrm{D}} \\ \mathsf{I}_{\mathrm{Q}} \end{bmatrix} = \begin{bmatrix} \mathbf{G}_r & -\mathbf{B}_r \\ \mathbf{B}_r & \mathbf{G}_r \end{bmatrix} \begin{bmatrix} \mathsf{E}_{\mathrm{D}} \\ \mathsf{E}_{\mathrm{Q}} \end{bmatrix}, \tag{2.57}$$

hence one may identify the components of the machine voltage in the network frame of reference, and express the equivalents of (2.28) and (2.30), taken at the internal nodes. By expanding the transform matrix $\mathbf{R}^t(\boldsymbol{\delta})$ it is easy to see that

$$\begin{bmatrix} \mathbb{E}'_d & \mathbb{E}'_q \end{bmatrix} \mathbf{R}^t(\boldsymbol{\delta}) = \begin{bmatrix} \mathbb{E}'_d & \mathbb{E}'_q \end{bmatrix} \begin{bmatrix} \mathbb{S}(\boldsymbol{\delta}) & -\mathbb{C}(\boldsymbol{\delta}) \\ \mathbb{C}(\boldsymbol{\delta}) & \mathbb{S}(\boldsymbol{\delta}) \end{bmatrix} = \begin{bmatrix} \mathbb{E}_{\mathrm{D}} & \mathbb{E}_{\mathrm{Q}} \end{bmatrix}, \tag{2.58}$$

For the network-referenced machine voltages, we have dropped the prime notation which is used by convention to denote the transient machine voltages. It will henceforth be understood that E_{D} and E_{Q} are derived from one of the transient voltage models. We now have a direct analogy of the internal-node model to (2.28) and (2.31) via the following expressions:

$$\mathsf{P}_e = \begin{bmatrix} \mathbb{E}_{\mathrm{D}} & \mathbb{E}_{\mathrm{Q}} \end{bmatrix} \mathbf{Y}_r \begin{bmatrix} \mathsf{E}_{\mathrm{D}} \\ \mathsf{E}_{\mathrm{Q}} \end{bmatrix} \tag{2.59}$$

$$P_{\mathrm{tot}} = \begin{bmatrix} \mathsf{E}_{\mathrm{D}}^t & \mathsf{E}_{\mathrm{Q}}^t \end{bmatrix} \underline{\underline{\mathbf{G}}} \begin{bmatrix} \mathsf{E}_{\mathrm{D}} \\ \mathsf{E}_{\mathrm{Q}} \end{bmatrix}, \tag{2.60}$$

where we have defined

$$\underline{\underline{\mathbf{G}}} = \begin{bmatrix} \mathbf{G} & \mathbf{0} \\ \mathbf{0} & \mathbf{G} \end{bmatrix} \tag{2.61}$$

Similarly, with respect to (2.30) and (2.33), we have

$$\mathbf{Q} = \begin{bmatrix} \mathbb{E}_{\mathrm{D}} & \mathbb{E}_{\mathrm{Q}} \end{bmatrix} \begin{bmatrix} -\mathbf{B} & -\mathbf{G} \\ \mathbf{G} & -\mathbf{B} \end{bmatrix} \begin{bmatrix} \mathsf{E}_{\mathrm{D}}^{t} \\ \mathsf{E}_{\mathrm{Q}}^{t} \end{bmatrix} \tag{2.62}$$

$$Q_{\mathrm{tot}} = \begin{bmatrix} \mathsf{E}_{\mathrm{D}} & \mathsf{E}_{\mathrm{Q}} \end{bmatrix} \underline{\underline{\mathbf{B}}} \begin{bmatrix} \mathsf{E}_{\mathrm{D}} \\ \mathsf{E}_{\mathrm{Q}} \end{bmatrix}, \tag{2.63}$$

using the analogous definition for $\underline{\underline{\mathbf{B}}}$.

Clearly, by reflecting the machine voltages into the network frame of reference, a significant simplification is achieved in the expressions of real and reactive power. However, as noted in Section 2.2, the machine models are more complex if the alignment of the Park-transform coordinates is not maintained at each machine. Nonetheless, since it is the interaction of the various generators that is of interest in many cases, it may be advantageous to sacrifice the simplicity of the individual machine models in order to attain a simplification of the network quantities of real and reactive power.

2.6 System Models in the Network Frame of Reference

The derivation of the machine equations in the network frame of reference will be accomplished by direct differentiation of the transformed variables for a single machine, from which the generalization to the vector case will be immediate. For the scalar case, the following equations relate the two frames of reference, as applied to the machine voltages:

$$E_{\mathrm{D}} = E'_d \sin\delta + E'_q \cos(\delta), \tag{2.64}$$

$$E_{\mathrm{Q}} = E'_d \cos(\delta) - E'_q \sin(\delta). \tag{2.65}$$

Differentiating, we have

$$\dot{E}_{\mathrm{D}} = (\omega-\omega_o)(E'_d\cos(\delta)-E'_q\sin(\delta))+\dot{E}'_d\sin(\delta)+\dot{E}'_q\cos(\delta) \tag{2.66}$$

$$\dot{E}_{\mathrm{Q}} = (\omega-\omega_o)(-E'_d\sin(\delta)-E'_q\cos(\delta))+\dot{E}'_d\cos(\delta)-\dot{E}'_q\sin(\delta) \tag{2.67}$$

$$\tag{2.68}$$

Proceeding now with the equation for $\dot{E}_{\mathrm{D}}$, it is possible to identify E_{Q} in the first term and expand the derivatives on the RHS:

$$\begin{aligned}\dot{E}_{\mathrm{D}} &= -(\omega-\omega_o)E_{\mathrm{Q}}-\frac{1}{T'_{q0}}\left[E'_d-(x_q-x'_q)i_q\right]\sin(\delta)\\ &\quad -\frac{1}{T'_{d0}}\left[E'_q+(x_d-x'_d)i_d\right]\cos(\delta)+\frac{1}{T'_{d0}}\cos(\delta)E_{fd}.\end{aligned} \tag{2.69}$$

Observe that

$$\begin{aligned}\frac{1}{T'_{q0}}E'_d\sin(\delta)+\frac{1}{T'_{d0}}E'_q\cos(\delta) &= \frac{1}{2}\left(\frac{1}{T'_{d0}}+\frac{1}{T'_{q0}}\right)\underbrace{\left(E'_d\sin(\delta)+E'_q\cos(\delta)\right)}_{E_{\mathrm{D}}}\\ &\quad +\frac{1}{2}\left(\frac{1}{T'_{d0}}-\frac{1}{T'_{q0}}\right)\left(-E'_d\sin(\delta)+E'_q\cos(\delta)\right).\end{aligned} \tag{2.70}$$

Now, making the definitions

$$T_1=\frac{1}{2}\left(\frac{1}{T'_{d0}}+\frac{1}{T'_{q0}}\right),\qquad T_2=\frac{1}{2}\left(\frac{1}{T'_{d0}}-\frac{1}{T'_{q0}}\right), \tag{2.71}$$

identifying E_{D} in the first expression on the RHS of (2.70) and using trigonometric identities to find that

$$-E'_d\sin(\delta)+E'_q\cos(\delta)=E_{\mathrm{D}}\cos(2\delta)+E_{\mathrm{Q}}\sin(2\delta), \tag{2.72}$$

(2.70) becomes

$$\frac{1}{T'_{q0}}E'_d\sin(\delta)+\frac{1}{T'_{d0}}E'_q\cos(\delta)=T_1E_{\mathrm{D}}+T_2\left(E_{\mathrm{D}}\cos(2\delta)+E_{\mathrm{Q}}\sin(2\delta)\right). \tag{2.73}$$

Similarly, the definitions

$$\begin{aligned} \bar{x}_d &= \frac{(x_d - x'_d)}{T'_{d0}} \qquad \bar{x}_q = \frac{(x_q - x'_q)}{T'_{q0}} \\ x_1 &= \frac{\bar{x}_d + \bar{x}_q}{2} \qquad x_2 = \frac{\bar{x}_d - \bar{x}_q}{2}, \end{aligned} \tag{2.74}$$

lead to the following form:

$$\bar{x}_d i_d \cos(\delta) - \bar{x}_q i_q \sin(\delta) = x_1 \underbrace{\Big(i_d \cos(\delta) - i_q \sin(\delta)\Big)}_{i_{\mathrm{Q}}} + x_2 \Big(i_d \cos(\delta) + i_q \sin(\delta)\Big), \tag{2.75}$$

which in turn leads to

$$\bar{x}_d i_d \cos(\delta) - \bar{x}_q i_q \sin(\delta) = -x_1 i_{\mathrm{Q}} + x_2 \Big(i_{\mathrm{D}} \sin(2\delta) - i_{\mathrm{Q}} \cos(2\delta)\Big). \tag{2.76}$$

At this point it is only necessary to collect terms from (2.73) and (2.76) and substitute into (2.66):

$$\begin{aligned} \dot{E}_{\mathrm{D}} &= -T_1 E_{\mathrm{D}} - T_2 \Big(E_{\mathrm{D}} \cos(2\delta) + E_{\mathrm{Q}} \sin(2\delta)\Big) + x_1 i_{\mathrm{Q}} - x_2 \Big(i_{\mathrm{D}} \sin(2\delta) - i_{\mathrm{Q}} \cos(2\delta)\Big) \\ &\quad + (\omega - \omega_o) E_{\mathrm{Q}} + T_{do}^{-1} \cos(\delta) E_{fd} \end{aligned} \tag{2.77}$$

By a similar procedure the state equation for E_{Q} may be derived, with the following result:

$$\begin{aligned} \dot{E}_{\mathrm{Q}} &= -T_1 E_{\mathrm{Q}} - T_2 \Big(E_{\mathrm{D}} \sin(2\delta) - E_{\mathrm{Q}} \cos(2\delta)\Big) - x_1 i_{\mathrm{D}} + x_2 \Big(i_{\mathrm{D}} \cos(2\delta) + i_{\mathrm{Q}} \sin(2\delta)\Big) \\ &\quad - (\omega - \omega_o) E_{\mathrm{D}} + T_{do}^{-1} \sin(\delta) E_{fd}. \end{aligned} \tag{2.78}$$

At this point it is not difficult to collect variables, make the substitution for the currents indicated by (2.57) and express the electromagnetics of a multimachine system in the

network frame of reference in block-vector form:

$$\begin{aligned}
\begin{bmatrix} \dot{\mathsf{E}}_{\mathrm{D}} \\ \dot{\mathsf{E}}_{\mathrm{Q}} \end{bmatrix} &= -\left\{ \begin{bmatrix} \mathbb{T}_1 & \mathbf{0} \\ \mathbf{0} & \mathbb{T}_1 \end{bmatrix} + \begin{bmatrix} \mathbf{0} & -\mathbb{X}_1 \\ \mathbb{X}_1 & \mathbf{0} \end{bmatrix} \begin{bmatrix} \mathbf{G}_r & -\mathbf{B}_r \\ \mathbf{B}_r & \mathbf{G}_r \end{bmatrix} \right\} \begin{bmatrix} \mathsf{E}_D \\ \mathsf{E}_Q \end{bmatrix} \\
&\quad -\left\{ \begin{bmatrix} \mathbb{T}_2 & \mathbf{0} \\ \mathbf{0} & \mathbb{T}_2 \end{bmatrix} \begin{bmatrix} \mathbb{C}(2\boldsymbol{\delta}) & \mathbb{S}(2\boldsymbol{\delta}) \\ \mathbb{S}(2\boldsymbol{\delta}) & -\mathbb{C}(2\boldsymbol{\delta}) \end{bmatrix} \right. \\
&\quad \left. + \begin{bmatrix} \mathbf{0} & \mathbb{X}_2 \\ -\mathbb{X}_2 & \mathbf{0} \end{bmatrix} \begin{bmatrix} \mathbb{C}(2\boldsymbol{\delta}) & \mathbb{S}(2\boldsymbol{\delta}) \\ \mathbb{S}(2\boldsymbol{\delta}) & -\mathbb{C}(2\boldsymbol{\delta}) \end{bmatrix} \begin{bmatrix} \mathbf{G}_r & -\mathbf{B}_r \\ \mathbf{B}_r & \mathbf{G}_r \end{bmatrix} \right\} \begin{bmatrix} \mathsf{E}_D \\ \mathsf{E}_Q \end{bmatrix} \\
&\quad - \begin{bmatrix} \mathbf{0} & -\mathbb{W} \\ \mathbb{W} & \mathbf{0} \end{bmatrix} \begin{bmatrix} \mathsf{E}_D \\ \mathsf{E}_Q \end{bmatrix} + \begin{bmatrix} \mathbb{C}(\boldsymbol{\delta}) \\ \mathbb{S}(\boldsymbol{\delta}) \end{bmatrix} \mathbb{T}_{do}^{-1} \mathsf{E}_{fd},
\end{aligned} \tag{2.79}$$

where $\mathbb{W} = \mathrm{diag}(\boldsymbol{\omega} - \omega_o)$. This can be rearranged into a somewhat more convenient form. Observe that

$$\begin{bmatrix} \mathbb{T}_2 & \mathbf{0} \\ \mathbf{0} & \mathbb{T}_2 \end{bmatrix} \begin{bmatrix} \mathbb{C}(2\boldsymbol{\delta}) & \mathbb{S}(2\boldsymbol{\delta}) \\ \mathbb{S}(2\boldsymbol{\delta}) & -\mathbb{C}(2\boldsymbol{\delta}) \end{bmatrix} = \begin{bmatrix} \mathbb{C}(2\boldsymbol{\delta}) & \mathbb{S}(2\boldsymbol{\delta}) \\ \mathbb{S}(2\boldsymbol{\delta}) & -\mathbb{C}(2\boldsymbol{\delta}) \end{bmatrix} \begin{bmatrix} \mathbb{T}_2 & \mathbf{0} \\ \mathbf{0} & \mathbb{T}_2 \end{bmatrix} \tag{2.80}$$

and that

$$\begin{bmatrix} \mathbf{0} & \mathbb{X}_2 \\ -\mathbb{X}_2 & \mathbf{0} \end{bmatrix} \begin{bmatrix} \mathbb{C}(2\boldsymbol{\delta}) & \mathbb{S}(2\boldsymbol{\delta}) \\ \mathbb{S}(2\boldsymbol{\delta}) & -\mathbb{C}(2\boldsymbol{\delta}) \end{bmatrix} = \begin{bmatrix} \mathbb{C}(2\boldsymbol{\delta}) & \mathbb{S}(2\boldsymbol{\delta}) \\ \mathbb{S}(2\boldsymbol{\delta}) & -\mathbb{C}(2\boldsymbol{\delta}) \end{bmatrix} \begin{bmatrix} \mathbf{0} & -\mathbb{X}_2 \\ \mathbb{X}_2 & \mathbf{0} \end{bmatrix}. \tag{2.81}$$

Thus, the rotation matrix may be factored to the left to yield

$$\begin{aligned}
\begin{bmatrix} \dot{\mathsf{E}}_{\mathrm{D}} \\ \dot{\mathsf{E}}_{\mathrm{Q}} \end{bmatrix} &= -\left\{ \begin{bmatrix} \mathbb{T}_1 & \mathbf{0} \\ \mathbf{0} & \mathbb{T}_1 \end{bmatrix} + \begin{bmatrix} \mathbf{0} & \mathbb{X}_1 \\ -\mathbb{X}_1 & \mathbf{0} \end{bmatrix} \begin{bmatrix} \mathbf{G}_r & -\mathbf{B}_r \\ \mathbf{B}_r & \mathbf{G}_r \end{bmatrix} \right\} \begin{bmatrix} \mathsf{E}_D \\ \mathsf{E}_Q \end{bmatrix} \\
&\quad - \begin{bmatrix} \mathbb{C}(2\boldsymbol{\delta}) & \mathbb{S}(2\boldsymbol{\delta}) \\ \mathbb{S}(2\boldsymbol{\delta}) & -\mathbb{C}(2\boldsymbol{\delta}) \end{bmatrix} \left\{ \begin{bmatrix} \mathbb{T}_2 & \mathbf{0} \\ \mathbf{0} & \mathbb{T}_2 \end{bmatrix} + \begin{bmatrix} \mathbf{0} & -\mathbb{X}_2 \\ \mathbb{X}_2 & \mathbf{0} \end{bmatrix} \begin{bmatrix} \mathbf{G}_r & -\mathbf{B}_r \\ \mathbf{B}_r & \mathbf{G}_r \end{bmatrix} \right\} \begin{bmatrix} \mathsf{E}_D \\ \mathsf{E}_Q \end{bmatrix} \\
&\quad - \begin{bmatrix} \mathbf{0} & -\mathbb{W} \\ \mathbb{W} & \mathbf{0} \end{bmatrix} \begin{bmatrix} \mathsf{E}_D \\ \mathsf{E}_Q \end{bmatrix} + \begin{bmatrix} \mathbb{C}(\boldsymbol{\delta}) \\ \mathbb{S}(\boldsymbol{\delta}) \end{bmatrix} \mathbb{T}_{do}^{-1} \mathsf{E}_{fd}
\end{aligned} \tag{2.82}$$

These equations take the form:

$$\dot{\mathsf{E}}_{\mathrm{DQ}} = \left\{ \mathbf{A}_1 + \mathbf{R}_{\mathrm{N}}(2\boldsymbol{\delta})\, \mathbf{A}_2 + \mathbf{W}(\boldsymbol{\omega}) \right\} \mathsf{E}_{\mathrm{DQ}} + \mathbf{U}(\boldsymbol{\delta}) \mathsf{E}_{fd}, \tag{2.83}$$

where

$$\mathsf{E}_{\mathrm{DQ}} = [\, \mathsf{E}_{\mathrm{D}} \;\; \mathsf{E}_{\mathrm{Q}} \,]^t \tag{2.84}$$

$$\mathbf{A}_1 = \begin{bmatrix} \mathbb{T}_1 & \mathbf{0} \\ \mathbf{0} & \mathbb{T}_1 \end{bmatrix} + \begin{bmatrix} \mathbf{0} & \mathbb{X}_1 \\ -\mathbb{X}_1 & \mathbf{0} \end{bmatrix} \begin{bmatrix} \mathbf{G}_r & -\mathbf{B}_r \\ \mathbf{B}_r & \mathbf{G}_r \end{bmatrix} \tag{2.85}$$

$$\mathbf{A}_2 = \begin{bmatrix} \mathbb{T}_2 & \mathbf{0} \\ \mathbf{0} & \mathbb{T}_2 \end{bmatrix} + \begin{bmatrix} \mathbf{0} & -\mathbb{X}_2 \\ \mathbb{X}_2 & \mathbf{0} \end{bmatrix} \begin{bmatrix} \mathbf{G}_r & -\mathbf{B}_r \\ \mathbf{B}_r & \mathbf{G}_r \end{bmatrix} \tag{2.86}$$

$$\mathbf{R}_{\mathrm{N}}(2\boldsymbol{\delta}) = \begin{bmatrix} \mathbb{C}(2\boldsymbol{\delta}) & \mathbb{S}(2\boldsymbol{\delta}) \\ \mathbb{S}(2\boldsymbol{\delta}) & -\mathbb{C}(2\boldsymbol{\delta}) \end{bmatrix} \tag{2.87}$$

$$\mathbf{W} = \begin{bmatrix} \mathbf{0} & -\mathbb{W} \\ \mathbb{W} & \mathbf{0} \end{bmatrix} \tag{2.88}$$

$$\mathbf{U}(\boldsymbol{\delta}) = \begin{bmatrix} \mathbb{C}(\boldsymbol{\delta}) \\ \mathbb{S}(\boldsymbol{\delta}) \end{bmatrix} \mathbb{T}_{do}^{-1}. \tag{2.89}$$

Equation (2.83) expresses the machine dynamics of a multimachine power system in a common frame of reference. To complete the model, we restate (2.83) and add the mechanical states, expressed in the network frame of reference:

$$\begin{aligned} \dot{\mathsf{E}}_{\mathrm{DQ}} &= \left\{ \mathbf{A}_1 + \mathbf{R}_{\mathrm{N}}(2\boldsymbol{\delta})\, \mathbf{A}_2 + \mathbf{W}(\boldsymbol{\omega}) \right\} \mathsf{E}_{\mathrm{DQ}} + \mathbf{U}(\boldsymbol{\delta}) \mathsf{E}_{fd}, \\ \dot{\boldsymbol{\delta}} &= \boldsymbol{\omega} - \omega_o \\ \mathbb{M}\dot{\boldsymbol{\omega}} &= \mathsf{T}_m - \begin{bmatrix} \mathbb{E}_{\mathrm{D}} & \mathbb{E}_{\mathrm{Q}} \end{bmatrix} \mathbf{Y}_r \begin{bmatrix} \mathsf{E}_{\mathrm{D}} \\ \mathsf{E}_{\mathrm{Q}} \end{bmatrix} - \mathbb{D} \frac{(\boldsymbol{\omega} - \omega_o)}{\omega_o} \end{aligned} \tag{2.90}$$

It is important to recognize that the basic form of (2.90) is similar for a number of underlying electromagnetic models. In particular, it is preserved with minor modifications for the single-axis model, and for the flux decay model. This observation will be useful

as the various types of transient energy functions are explored. First, however these simplified models must be introduced and their connection to the network-referenced model made clear.

2.7 Simplified Electromagnetic Models

The first level of simplification that may be applied to the two-axis model involves a time-scale separation. Note that the time constant T'_{do} that governs the quadrature axis equations is normally several times larger than T'_{qo}, which is associated with the direct axis equations. This reflects the fact that the inductance of the field winding, which is typically quite large, is associated solely with the quadrature axis. The direct-axis time constant reflects only the dynamics of the damper winding, which physically is a series of shorted turns of conductor embedded in the circumference of the rotor. Because of the large difference in the time constants, the direct-axis equations (2.7) are often taken to be algebraic constraints by setting the time derivative to 0, *i.e.*

$$E'_d = (x_q - x'_q) i_q \tag{2.91}$$

This may be justified rigorously via singular perturbation analysis, as in [32]. This model is known as the *flux-decay model*, and it may be represented as a voltage source of magnitude $E'_q + (x_q - x'_d) i_d$ and phase δ, in series with the synchronous reactance x_q.

At the cost of some loss of accuracy, it is often assumed that $x_q = x'_d$, in which case the direct-axis voltage vanishes, and we are left with the *single-axis model*, in which the entirety of the electromagnetic dynamics is represented in the quadrature axis by equation (2.9). This model is also known as the *voltage behind the transient reactance* model. The internal voltage of the machine is then simply given as a phasor with magnitude E'_q and phase δ. In this case it can be seen that the map from the machine frame of reference to the network frame of reference becomes:

$$\begin{bmatrix} \mathsf{E}_{\mathsf{D}} \\ \mathsf{E}_{\mathsf{Q}} \end{bmatrix} = \begin{bmatrix} \mathbb{C}(\delta) \\ \mathbb{S}(\delta) \end{bmatrix} \mathsf{E}'_q. \tag{2.92}$$

Note that the Jacobian of the transform from the network frame of reference to the machine frame of reference for the two-axis model is

$$\begin{bmatrix} \mathbb{C}(\delta) & -\mathbb{S}(\delta) & \mathbf{0} \\ \mathbb{S}(\delta) & \mathbb{C}(\delta) & \mathbf{0} \\ \mathbf{0} & \mathbf{0} & \mathbf{I} \end{bmatrix}, \tag{2.93}$$

which is always nonsingular, *i.e.* the transform is globally valid. For the reduced-order models, the 3-into-3 transform $[\ \mathsf{E}'_q \quad \boldsymbol{\delta} \quad \boldsymbol{\omega}\ ]^t \rightarrow [\ \mathsf{E}_{\mathrm{D}} \quad \mathsf{E}_{\mathrm{Q}} \quad \boldsymbol{\omega}\ ]^t$ is also globally nonsingular, making the preservation of δ in the reduced network-referenced model unnecessary, although it is often convenient to preserve δ in the electromagnetic equations, since it is somewhat cumbersome to express δ in terms of E_{D} and E_{Q}.

2.8 The Relative-Angle and Center-of-Inertia Models

Two facts that were mentioned in Section 2.2 motivate the present one. First, the rotor angle δ is always expressed with respect to a predefined reference angle. Second, recall that all network quantities which affect the electromechanical subsystems are invariant to a change in the reference angle. Moreover, since the machine frame of reference is physically meaningful in the sense that it represents the axis of the machine rotor, one would intuitively expect that the machine voltages E'_d and E'_q would be invariant to a shift in the absolute reference, and this is indeed the case. On the other hand, the network-referenced machine voltages do depend on the reference angle, but their interaction with the electromechanical subsystems is invariant to a shift in the reference.

Suppose that the vector $[\ \mathsf{E}'_{d_o} \quad \mathsf{E}'_{q_o} \quad \boldsymbol{\delta}_o \quad \boldsymbol{\omega}_o\ ]$ represents a system equilibrium for the machine-referenced model. Then for any angle ϕ, $[\ \mathsf{E}'_{d_o} \quad \mathsf{E}'_{q_o} \quad (\boldsymbol{\delta}_o + \phi) \quad \boldsymbol{\omega}_o\ ]$ is also an equilibrium. Stated in another way, one may observe that the equilibria of the model of (2.90) are degenerate in the sense that if $\boldsymbol{\delta}$ is a system equilibrium, then $\boldsymbol{\delta} + \phi$ is also an equilibrium for any ϕ. In linear systems, this would correspond to the presence of a zero

eigenvalue, and any linearization of this model does indeed exhibit a zero eigenvalue. Moreover, when the input torque is taken to be constant, this zero eigenvalue is also uncontrollable, which means that the system representation is not minimal.

Two common methods exist for dealing with this problem, both of which involve defining a reference angle that evolves with time. In both cases, the transformation is such that the variation in the reference angle renders any two angle vectors $\boldsymbol{\delta}_i$, $\boldsymbol{\delta}_j$ equivalent if $\boldsymbol{\delta}_i - \boldsymbol{\delta}_j = k\mathbf{1}$, where $\mathbf{1} = [\ 1,\ \cdots, 1\ ]^t$. Under certain assumptions, the frequency of the reference machine may also be eliminated from the model, thus reducing the dimension of the model by 2.

2.8.1 The Relative-Angle Model

The first method is known as the *relative-angle model*, in which one of the machines is arbitrarily declared to be the reference. Enumerating the machines such that, for a p-machine system, the p^{th} machine is taken as the reference, we define the rotor angles in the relative model as

$$\delta_i^r = \delta_i - \delta_p. \tag{2.94}$$

Clearly, $\delta_p^r \equiv 0$ in the relative-angle model. Since δ_p is fixed at 0, it no longer has any dynamic properties and can be eliminated, reducing the dimension by 1. There are two cases in which the frequency of the reference machine may also be eliminated from the relative-angle model. In the first case, if the moment of inertia of the reference machine, m_p, is large, then it may be possible without undue loss of accuracy to assume that $m_p \to \infty$, so that $\dot{\omega}_p \to 0$, in which case both the frequency and angle are fixed and may be eliminated as state variables. In the second case, as will presently be shown, ω_p may be eliminated if *uniform damping* is assumed, *i.e.* the damping constants are assumed to satisfy the relationship

$$\frac{D_i}{\omega_o} = m_i D \tag{2.95}$$

for some constant D.

In order to eliminate ω_p, the following state transformation is made:

$$\begin{aligned} \omega_i^r &= \dot{\delta}_i^r = \omega_i - \omega_p \quad ; \quad i = 1, \cdots, p-1 \\ &\equiv 0 \qquad\qquad\quad ; \quad i = p \end{aligned} \quad , \tag{2.96}$$

so that ω_p also is eliminated as a distinct state variable if the dynamics of the remaining states can be expressed independently of ω_p. Referring to (2.10) we write $\dot{\omega}_i - \dot{\omega}_p$ as

$$\dot{\omega}_i^r = \frac{1}{m_i}\left[T_{m_i} - P_{e_i} - \frac{D_i}{\omega_o}(\omega_i - \omega_o)\right] - \frac{1}{m_p}\left[T_{m_p} - P_{e_p} - \frac{D_p}{\omega_o}(\omega_p - \omega_o)\right]. \tag{2.97}$$

The electrical power output of the reference machine is independent of its frequency, but the damping term involving ω_p cannot in general be eliminated. The uniform damping assumption yields $\frac{D_p}{m_p\omega_o} = D$, however, so that

$$\begin{aligned} \dot{\omega}_i^r &= \frac{1}{m_i}\left[T_{m_i} - P_{e_i} - \frac{m_i}{m_p}(T_{m_p} - P_{e_p}) - m_i D\omega_i^r\right]. \\ &= \frac{1}{m_i}(T_m^r - P_e^r) - D\omega^r, \end{aligned} \tag{2.98}$$

where the obvious definitions have been made. The electromechanical subsystems for the first $p-1$ machines may now be expressed without reference to the frequency of the base machine, allowing both δ_p and ω_p to be eliminated from the relative angle model. Thus the frequency of the reference machine becomes the base frequency for the system. Two items are of note here: First, uniform damping includes zero damping

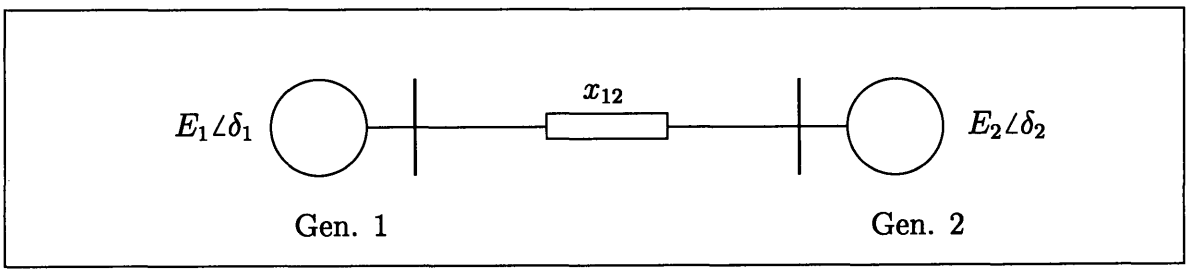

Figure 2.4: Two-Machine Example.

as a special case, and indeed, setting all damping terms to zero creates a second zero eigenvalue when angles are expressed as relative quantities. Second, when damping is

uniform but nonzero, it is still possible to define a subsystem of order $n-2$ which depends only on the relative angles and frequencies, but a nonzero eigenvalue exists which is not accounted for by the relative-angle subsystem. Hence, there must exist a variable x_{n-1} whose dynamics do not affect the relative subsystem. There is a certain amount of freedom in defining this last state, but there is a natural choice, which will be motivated by an example.

Example 2.1

Consider a two-machine swing-model system coupled by a lossless transmission line, taken at the internal nodes, as in Figure 2.4. Assuming that $E_1 = E_2 = 1$, the equations for this system are

$$\dot{\delta}_1 = (\omega_1 - \omega_o) \tag{2.99}$$

$$\dot{\delta}_2 = (\omega_2 - \omega_o) \tag{2.100}$$

$$\dot{\omega}_1 = \frac{1}{m_1}\left\{T_{m_1} - \frac{1}{x_{12}}\sin(\delta_1 - \delta_2) - \frac{D_1}{\omega_o}(\omega_1 - \omega_o)\right\} \tag{2.101}$$

$$\dot{\omega}_2 = \frac{1}{m_2}\left\{T_{m_2} + \frac{1}{x_{12}}\sin(\delta_1 - \delta_2) - \frac{D_2}{\omega_o}(\omega_2 - \omega_o)\right\}. \tag{2.102}$$

The linearized system matrix is

$$\mathbf{A}_s = \begin{bmatrix} 0 & 0 & 1 & 0 \\ 0 & 0 & 0 & 1 \\ -\frac{1}{x_{12}m_1}\cos(\delta_1 - \delta_2) & \frac{1}{x_{12}m_1}\cos(\delta_1 - \delta_2) & -\frac{D_1}{m_1\omega_o} & 0 \\ \frac{1}{x_{12}m_2}\cos(\delta_1 - \delta_2) & -\frac{1}{x_{12}m_2}\cos(\delta_1 - \delta_2) & 0 & -\frac{D_2}{m_2\omega_o} \end{bmatrix} \tag{2.103}$$

As expected, this has a zero eigenvector, namely $[\ 1 \quad 1 \quad 0 \quad 0\ ]^t$, which illustrates the fact that the equilibrium value of $\boldsymbol{\delta}$ is nonunique. Now, if δ_2 is taken as the reference angle, the model becomes

$$\dot{\delta}_{12} = (\omega_1 - \omega_2) \tag{2.104}$$

$$\dot{\omega}_1 = \frac{1}{m_1}\left\{T_{m_1} - \frac{1}{x_{12}}\sin(\delta_{12}) - \frac{D_1}{\omega_o}(\omega_1 - \omega_o)\right\} \tag{2.105}$$

$$\dot{\omega}_2 = \frac{1}{m_2}\left\{T_{m_2} + \frac{1}{x_{12}}\sin(\delta_{12}) - \frac{D_2}{\omega_o}(\omega_2 - \omega_o)\right\}, \tag{2.106}$$

for which the (now full-rank) reduced system matrix is

$$\mathbf{A}_s^r = \begin{bmatrix} 0 & 1 & -1 \\ \frac{1}{x_{12}m_1}\cos(\delta_{12}) & -\frac{D_1}{m_1\omega_o} & 0 \\ -\frac{1}{x_{12}m_2}\cos(\delta_{12}) & 0 & -\frac{D_2}{m_2\omega_o} \end{bmatrix} = \underbrace{\begin{bmatrix} 0 & 1 & -1 \\ \frac{1}{x_{12}m_1}\cos(\delta_{12}) & -D & 0 \\ -\frac{1}{x_{12}m_2}\cos(\delta_{12}) & 0 & -D \end{bmatrix}}_{\text{uniform damping}} \tag{2.107}$$

For uniform damping with a lossless transmission grid, the vector $[\ 0 \quad 1 \quad 1\ ]$ is both a left and right eigenvector. This suggests the following definition for the remaining state:

$$x_{n-1} = \sum_{i=1}^{p}(\omega_i - \omega_o), \tag{2.108}$$

which satisfies the differential equation

$$\dot{x}_{n-1} = \sum_{i=1}^{p}\left[\frac{1}{m_i}(T_{m_i} - P_{e_i}) - D(\omega_i - \omega_o)\right], \tag{2.109}$$

$$= -Dx_{n-1} + \sum_{i=1}^{p}\frac{1}{m_i}(T_{m_i} - P_{e_i}) \tag{2.110}$$

This has the form of a bounded-input bounded-output (BIBO)-stable first-order scalar system whose input is a scaled sum of the power mismatch at each machine. Since the system is stable, it is clear that the input is bounded, so that as long as $D > 0$, x_{n-1} is also stable. Now, given the singular state transform $[\ \delta_1 \quad \delta_2 \quad \omega_1 \quad \omega_2\ ] \rightarrow [\ \delta_r \quad \omega_r \quad x_{n-1}\ ]$, the resulting linearized system matrix is

$$\mathbf{A}_s^{r'} = \begin{bmatrix} 0 & 1 & 0 \\ \frac{m_1-m_2}{m_1m_2x_{12}}\cos(\delta_{12}) & -D & 0 \\ -\frac{m_1+m_2}{m_1m_2x_{12}}\cos(\delta_{12}) & 0 & -D \end{bmatrix}. \tag{2.111}$$

The decoupling of the upper 2×2 block is apparent here. ∎

Up to this point, the electromagnetic subsystem has not been addressed; however,

as outlined in Section 2.7, several levels of simplification are available. Unlike the electromechanical subsystem, no naturally occurring zero mode exists. Therefore the full set of machine voltages may be preserved in a minimal state realization, or reductions may be made as the application demands. If the direct-axis electromagnetic dynamics are eliminated (by setting $x_{q_p} = x'_{d_p}$), then $E'_{d_p} \equiv 0$, which effectively fixes the phase of the voltage at the (internal-node) reference bus. Since the reference bus angle is taken to be 0, we have $E'_{q_p} = E_{\mathrm{D}_p} = E_p$. Finally, if the electromagnetic time constants of the reference machine are allowed to approach infinity, then the reference node becomes an infinite bus, equivalent to a voltage source with fixed magnitude and phase $\theta_p = \delta_p = 0$.

In order to determine the effect of the relative-angle transformation on the dynamic equations of the network-referenced voltages, recall that the machine-referenced voltages are invariant to a change in reference, time-varying or otherwise. In order to determine the effect in the network-referenced model, we proceed from the definitions (2.64) and (2.65). In order to relate these to a time-varying frame of reference, it is only necessary to express δ_i relative to that reference. In the present case, one substitutes δ_i^r for δ_i. From that point forward, the derivation of the network-referenced system equations is identical, with the obvious exception that differentiation of δ_i^r produces ω_i^r rather than ω_i. Based on the foregoing treatment, we may express the relative-angle state vector (given uniform damping) as $[\ (\mathsf{E}^r_{\mathrm{DQ}})^t \quad (\boldsymbol{\delta}^r)^t \quad (\boldsymbol{\omega}^r)^t\ ]^t$, where $\mathsf{E}^r_{\mathrm{DQ}}$ is the machine voltage vector, projected onto the relative reference, $\boldsymbol{\delta}^r = [\ \delta_1^r, \ \cdots, \ \delta_{p-1}^r\ ]$ and $\boldsymbol{\omega}^r = [\ \omega_1^r, \ \cdots, \ \omega_{p-1}^r\ ]$. The generator torque is redefined as $T^r_{p_i} = T_{m_i} - m_i/m_p T_{m_p}$. The rotation matrix becomes

$$R^r_{\mathrm{N}}(2\boldsymbol{\delta}^r) = \left[\begin{array}{cc|cc} \mathbb{C}(2\boldsymbol{\delta}^r) & 0 & \mathbb{S}(2\boldsymbol{\delta}^r) & 0 \\ 0 & 1 & 0 & 0 \\ \hline \mathbb{S}(2\boldsymbol{\delta}^r) & 0 & \mathbb{C}(2\boldsymbol{\delta}^r) & 0 \\ 0 & 0 & 0 & 1 \end{array}\right], \tag{2.112}$$

while the matrix $\mathbf{W}(\boldsymbol{\omega})$ takes the form

$$\mathbf{W} = \begin{bmatrix} \mathbf{0} & -\mathbb{W}^r \\ \mathbb{W}^r & \mathbf{0} \end{bmatrix} \tag{2.113}$$

with $\mathbb{W}^r = \text{diag}(\omega_1^r, \cdots, \omega_{p-1}^r, 0)$. Therefore, with minor modifications, the form of the equations that govern the behavior of the electromagnetic variables in the network frame of reference is unchanged.

2.8.2 The Center-of-Inertia Model

An alternative method for dealing with the degenerate equilibrium is to define a time-varying reference angle called the *center of inertia*, δ_{COI} as follows:

$$\delta_{\text{COI}} = \frac{1}{m_{\text{T}}} \sum_{i=1}^{p} m_i \delta_i \qquad ; \qquad m_{\text{T}} = \sum_{i=1}^{p} m_i. \tag{2.114}$$

All rotor angles are then defined with respect to δ_{COI} as

$$\delta_i^c = \delta_i - \delta_{\text{COI}}. \tag{2.115}$$

This method does not actually reduce the state order, but introduces a constraint on the δ vector such that

$$\sum_{i=1}^{p} m_i \delta_i^c = 0. \tag{2.116}$$

This corresponds to a linear transform,

$$\boldsymbol{\omega}^c = \left(\mathbf{I} - 1 \begin{bmatrix} \frac{m_1}{m_{\text{T}}} & \cdots & \frac{m_p}{m_{\text{T}}} \end{bmatrix} \boldsymbol{\omega}, \right) \tag{2.117}$$

This is actually a singular transform. The eigenvector corresponding to the zero eigenvalue of the transform is $\mathbf{1}$, which coincides with the zero mode of the original system. It therefore annihilates any projection along the zero mode of the original system, and this is sufficient to uniquely determine the state at any operating point. Since the transformation is singular but does not reduce the dimension of the state, the state-

space model that will be derived in the sequel is not strictly valid, since it contains an implicit algebraic relationship that is not captured in the model. In particular, in order for the model to be well-defined, an additional constraint must be placed on the transform. Observe that if (2.116) is to be satisfied along system trajectories, it must also be satisfied at initial conditions, *i.e.* the initial conditions of the COI model are not arbitrary, but must lie on the manifold defined by (2.116).

In order to complete the model we define:

$$\omega_i^c = \dot{\delta}_i^c = \omega_i - \omega_o - \omega_{\text{COI}}, \tag{2.118}$$

where we differentiate δ_{COI} to find

$$\omega_{\text{COI}} = \frac{1}{m_{\text{T}}} \sum_{i=1}^{p} m_i(\omega_i - \omega_o). \tag{2.119}$$

Differentiating a second time yields:

$$\dot{\omega}_{\text{COI}} = \frac{1}{m_{\text{T}}} \sum_{j=1}^{p} \left(T_{m_j} - P_{e_j} - \frac{1}{\omega_o} D_j(\omega_j - \omega_0) \right) = \frac{1}{m_{\text{T}}} P_{\text{COI}} + \frac{1}{m_{\text{T}}} \sum_{j=1}^{p} \frac{D_j}{\omega_o}(\omega_j - \omega_0) \tag{2.120}$$

By substitution, we can now express the dynamics of ω_i^c:

$$m_i \dot{\omega}_i^c = T_{m_i} - P_{e_i} - \frac{D_i}{\omega_o}(\omega_i - \omega_o) - \frac{m_i}{m_{\text{T}}} P_{\text{COI}} - \frac{1}{m_{\text{T}}} \sum_{j=1}^{p} \frac{D_j}{\omega_o}(\omega_j - \omega_0) \tag{2.121}$$

The presence of ω_o in (2.121) presents some difficulty, first because it makes it impossible to express the equation exclusively in terms of the COI-referenced states, and second since $\dot{\boldsymbol{\omega}}^c$ may not equal zero when $\boldsymbol{\omega} = \omega_{\text{COI}}$, so that $\boldsymbol{\omega} = \omega_{\text{COI}}$ will not be an equilibrium. The difficulty arises because of the damping term, and it can be seen that for the lossless case, the system model is well-defined in terms of the COI states. For nonzero damping, it is again common to make the uniform damping assumption (2.95). Making the substitution, we find that

$$\frac{1}{m_{\text{T}}} \sum_{j=1}^{p} \frac{D_j}{\omega_o}(\omega_j - \omega_o) = \frac{D}{m_{\text{T}}} \sum_{j=1}^{p} m_j(\omega_j - \omega_0) = D(\omega_{\text{COI}} - \omega_o), \tag{2.122}$$

so that (2.121) becomes

$$m_i\dot{\omega}_i^c = T_{m_i} - P_{e_i} - m_i D(\omega_i - \omega_o) - \frac{m_i}{m_{\mathrm{T}}} P_{\mathrm{COI}} - m_i D(\omega_{\mathrm{COI}} - \omega_o). \tag{2.123}$$

Thus the COI model becomes

$$\begin{aligned} \dot{\delta}_i^c &= \omega_i^c \\ \dot{\omega}_i^c &= \frac{1}{m_i}(T_{m_i} - P_{e_i}) - D\omega_i^c - \frac{1}{m_{\mathrm{T}}} P_{\mathrm{COI}}. \end{aligned} \tag{2.124}$$

Expressed in the vector form of (2.90), this is

$$\begin{aligned} \dot{\boldsymbol{\delta}}^c &= \boldsymbol{\omega}^c \\ \dot{\boldsymbol{\omega}}^c &= \mathbb{M}^{-1}\left(T_m - \left[\begin{array}{c|c} \mathbb{E}_{\mathrm{D}} & \mathbb{E}_{\mathrm{Q}} \end{array}\right] \mathbf{Y}_r \begin{bmatrix} \mathsf{E}_{\mathrm{D}} \\ \mathsf{E}_{\mathrm{Q}} \end{bmatrix}\right) - \frac{1}{m_{\mathrm{T}}} P_{\mathrm{COI}} - \mathbb{D}\boldsymbol{\omega}. \end{aligned} \tag{2.125}$$

Since the COI model does not reduce the state dimension and the movement of the angle reference is captured in $\boldsymbol{\omega}^c$, the voltage equations in the COI model are unchanged from (2.83). Note that the transformation matrix that maps $\boldsymbol{\omega} \to \boldsymbol{\omega}^c$ is identical to the matrix that maps $\boldsymbol{\delta} \to \boldsymbol{\delta}^c$. There is actually another assumption implicit in (2.124). Note that in order for (2.116) to be satisfied along trajectories, we must have

$$\frac{d}{dt}\left(\sum_{i=1}^{p} m_i \delta_i^c\right) = \sum_{i=1}^{p} m_i \omega_i^c = \omega_{\mathrm{COI}} = 0, \tag{2.126}$$

and so initial conditions must also satisfy (2.126). We will refer to the surface defined by (2.116) and (2.126) as the *COI manifold*:

Definition 2.1 *The* COI manifold *is the set of states* $\{[\boldsymbol{\delta}^t, \boldsymbol{\omega}^t]^t\}$ *that satisfy the constraint equation (2.116) and (2.126). Moreover, the COI manifold is an invariant manifold for the model of (2.124)*

The invariance of the COI manifold follows from the fact that (*cf* (2.124)):

$$\frac{d}{dt}\left(\sum_{i=1}^{p} m_i \omega_i^c\right) = -D\omega_{\mathrm{COI}}. \tag{2.127}$$

Since $\omega_{\text{COI}} = 0$ on the COI manifold, the invariance of the manifold follows.

It may be useful at this point to relate this discussion to Example 2.1, via the following,

Example 2.2

For the system of Figure 2.4, we have $P_{\text{COI}} = T_{m_1} + T_{m_2}$. In this case the transmission grid is lossless, so the electrical power drops out of P_{COI}, but in general this will not be the case. The COI model takes the form

$$\begin{aligned}
\dot{\delta}_1^c &= \omega_1^c \\
\dot{\delta}_2^c &= \omega_2^c \\
\dot{\omega}_1^c &= \frac{1}{m_1}\left\{T_{m_1} - \frac{1}{x_{12}}\sin(\delta_1^c - \delta_2^c)\right\} - D\omega_1^c - \frac{1}{m_{\text{T}}}(T_{m_1} + T_{m_2}) \\
\dot{\omega}_2^c &= \frac{1}{m_2}\left\{T_{m_2} + \frac{1}{x_{12}}\sin(\delta_1^c - \delta_2^c)\right\} - D\omega_2^c - \frac{1}{m_{\text{T}}}(T_{m_1} + T_{m_2}).
\end{aligned}$$

The linearized system matrix in this case is identical to (2.103), and displays a single zero eigenvalue. This may be somewhat surprising, since the transforms for both the angle and the frequency are singular. Note, however, that (2.103) has an eigenvector $[0\,0\,1\,1]^t$ that corresponds to the eigenvalue D. This eigenvector is orthogonal to the COI manifold, and therefore it cannot be excited by the initial conditions of the COI model. This example illustrates two facts: first, that the COI model does not eliminate the zero eigenvalue of the linearized system model, and second, that the assumptions upon which the COI model is based cannot be captured in a linearized model. ∎

It should be clear that, for any initial conditions, the COI manifold constraints may be satisfied by selecting the proper value for the arbitrary reference angle δ_o in (2.116) and by allowing for the selection of the proper value of ω_o in (2.119). Thus, although we have defined a moving frame of reference that may simplify some aspects of system analysis, we have not solved the problem of the arbitrariness of the initial reference point. It might therefore be of value to consider a model in which the time-varying reference is allowed to be arbitrary, but which asymptotically approaches the point for

which the COI manifold conditions are satisfied. Then, using the theory of singular perturbations, the time constant associated with the motion of the reference point is allowed to approach zero, thereby recovering the COI model. It is a fairly simple matter to do this.

First, however, a very brief review of singular perturbation theory will be presented. In the interest of brevity, we will not attempt to rigorously present the assumptions under which the arguments hold; more thorough expositions of the theory may be found in [23, 28] and elsewhere.

Suppose that the equations for a given autonomous dynamic system take the following form:

$$\dot{\mathsf{x}} = \mathsf{f}(\mathsf{x}, \mathsf{z}, \varepsilon),\ \mathsf{x}(t_o) = \mathsf{x}_o(\varepsilon) \tag{2.128}$$

$$\varepsilon\dot{\mathsf{z}} = \mathsf{g}(\mathsf{x}, \mathsf{z}, \varepsilon),\ \mathsf{z}(t_o) = \mathsf{z}_o(\varepsilon) \tag{2.129}$$

where ε is a small positive parameter, and we allow the initial conditions of the system to have some dependence on it. It is assumed that solutions of (2.128), (2.129) exist and are unique over some time interval $[t_o,\ t_1]$, in some neighborhood of the equilibrium, $\mathcal{B}_\rho(\mathsf{x}_o, \mathsf{z}_o)$, and for some range of ε, $\varepsilon \in [0,\ \varepsilon_o]$. Moreover, we assume that f and g are locally continuously differentiable in x, z and ε. Note that the presence of the small parameter ε in (2.129) means that the dynamics associated with z are in some sense "fast" with respect to the evolution of x, since $\dot{\mathsf{z}} = \mathsf{g}/\varepsilon$ implies that small perturbations in the state give rise to large values of $\dot{\mathsf{z}}$, and we will consequently refer to (2.129) as the fast subsystem and to (2.128) as the slow subsystem.

If ε is allowed to approach 0, then the model (2.129) degenerates to an algebraic equation (hence, it is a "singular" perturbation):

$$0 = \mathsf{g}(\mathsf{x}, \mathsf{z}) \tag{2.130}$$

Given that at least one root of (2.130) exists and that the root(s) are distinct, then the assumptions on $\mathsf{g}(\mathsf{x}, \mathsf{z})$ imply that z may be approximated locally around an appropriate

root of $\mathbf{g}(\mathbf{x}, \mathbf{z})$ as

$$\bar{\mathbf{z}} = \mathbf{h}(\mathbf{x}). \tag{2.131}$$

This is known as the *quasi-steady-state* approximation of $\mathbf{z}$. Clearly, since (2.131) represents a steady-state approximation of $\mathbf{z}$, it may be subject to large errors when initial conditions are far from the equilibrium, hence it may not be a good approximation of $\mathbf{z}$ over the entire interval $[t_o, t_1]$. If the fast dynamics are stable, however, the approximation will improve after a short interval, such that

$$\mathbf{z}(t, \varepsilon) - \bar{\mathbf{z}}(t) = O(\varepsilon) \tag{2.132}$$

on some sub-interval of $[t_o, t_1]$. We may then define the *slow model*,

$$\dot{\bar{\mathbf{x}}} = \mathbf{f}(\mathbf{x}, \mathbf{h}(\mathbf{x}, 0), 0). \tag{2.133}$$

We denote the solution of this model as $\bar{\mathbf{x}}(t)$. Since we are free to specify the initial conditions for this reduced-order model, it is reasonable to expect that

$$\mathbf{x}_o(\varepsilon) - \mathbf{x}_o(o) = O(\varepsilon) \tag{2.134}$$

and hence that

$$\mathbf{x}(t) - \bar{\mathbf{x}}(t) = O(\varepsilon) \tag{2.135}$$

on the entire interval $[t_o, t_1]$.

Returning to the power system model, suppose the following two dynamic variables are defined:

$$\varepsilon\dot{\delta}_r = -\left(\delta_r - \frac{1}{m_{\mathrm{T}}}\sum_{i=1}^{p} m_i\delta_i\right) \tag{2.136}$$

$$\varepsilon\dot{\omega}_r = -\left(\omega_r - \frac{1}{m_{\mathrm{T}}}\sum_{i=1}^{p} m_i(\omega_i - \omega_o)\right). \tag{2.137}$$

We may then define the state transformation $\delta_i^c = \delta_i - \delta_r$, $i = 1, \cdots, m$, $z = \delta_r$, which

corresponds to the matrix equation

$$\begin{bmatrix} \boldsymbol{\delta}^c \\ z_1 \end{bmatrix} = \left[\begin{array}{ccc|c} 1 & & & -1 \\ & \ddots & & \vdots \\ & & 1 & -1 \\ \hline & 0 & & 1 \end{array}\right] \begin{bmatrix} \boldsymbol{\delta} \\ \delta_r \end{bmatrix}. \tag{2.138}$$

The matrix is upper-triangular with nonzero diagonal entries, hence it is nonsingular. We may define a similar transformation on $\boldsymbol{\omega}$, which is also nonsingular. Given arbitrary initial conditions, the auxiliary variables act to translate the system to the COI manifold by shifting the angle and frequency references. The dynamic equations for δ_r may be expressed in terms of the transformed states by substituting $\delta_i = \delta_i^c + \delta_r$ into (2.137) to yield

$$\varepsilon\dot{\delta}_r = \sum_{i=1}^{p} \delta_i^c, \tag{2.139}$$

and similarly for ω_r:

$$\varepsilon\dot{\omega}_r = \sum_{i=1}^{p} \omega_i^c, \tag{2.140}$$

Now, since $\dot{\delta}_r = \omega_r$, $\dot{\boldsymbol{\delta}}^c = \boldsymbol{\omega} - \omega_r = \boldsymbol{\omega}^c$, so that the transformed states are independent of δ_r ω_r. At this point it is tempting to simply ignore the auxiliary states, but it remains to deal with initial conditions. By allowing $\varepsilon \to 0$ in (2.139) and (2.140) the manifold conditions of (2.116) and (2.126) are reproduced. Now, in order to maintain an $O(\varepsilon)$ approximation as $\varepsilon \to 0$, the initial conditions must satisfy the COI-manifold conditions to within $O(\varepsilon)$. Given an arbitrary initial condition $[\,\mathsf{x}_o(\varepsilon_o),\ \mathsf{z}_o(\varepsilon_o)\,]$, we must define $\mathsf{x}_o(\varepsilon)$ to be a smooth interpolation between the initial condition and its projection onto the COI manifold, *e.g.*

$$\mathsf{x}_o(\varepsilon) = \mathsf{x}(t_o) - (1 - \frac{\varepsilon}{\varepsilon_o})(\mathsf{x}_{\text{COI}} - \mathsf{x}(t_o)). \tag{2.141}$$

Equation (2.141) actually recreates the constraints on initial conditions that were indicated in the original derivation of the COI model as $\varepsilon \to 0$, hence either approach yields an identical result, however the singular perturbations method provides a rigorous

framework for achieving it.

As noted in the foregoing discussion, no states are actually eliminated from the COI model. Indeed, although the equilibrium is unique in the COI model, the COI transform depends on initial conditions, projecting them onto the COI manifold. The COI model does not lend itself to control design, since the linearized system will not be stabilizable due to the zero eigenvalue, however it is quite useful in transient stability work, since it leads to simpler expressions of the transient energy functions, as compared to the relative-angle model. For this reason the COI model is used exclusively in Chapters 3 and 4.

Chapter 3

Transient Stability

It was observed in Chapter 1 that one of the main considerations in power system operation is to enhance the ability of the system, at any given operating point, to remain in operation within acceptable limits on voltage, real and reactive power transfer and so forth in the event of an equipment failure or other system disturbance. Several modes of failure may be of concern, however the most immediate concern following a system disturbance is the preservation of transient stability. For the purposes of this thesis, transient stability will be defined as the ability of the power system to return to a viable operating condition that satisfies operating constraints following a system disturbance. Typically, this will encompass a time frame up to about twenty seconds following the disturbance. This definition excludes some types of system failure that occur over a somewhat longer period of time, most notably the phenomenon of voltage collapse, which tends to occur over a span of several minutes. On the other hand, it encompasses a broader range of phenomena than "first-swing" stability, which is only concerned with the ability of affected generators to maintain synchronism on the first swing of the rotor angles following a disturbance.

It will be assumed in all that follows that a viable equilibrium point[1] exists for the postfault system. In general, there will be a continuum of possible equilibria available to the postfault system. One of the available equilibria will be assumed to be optimal

[1] A viable equilibrium point is one at which all quantities such as voltages and reactive power outputs are within sustainable limits.

in some sense, and will be designated as the *nominal* equilibrium. The existence of the nominal equilibrium is all that will concern us here; the method by which it is selected is outside the scope of this thesis, but typically the nominal equilibrium for the postfault system will preserve some prefault parameters such as the machine voltage or the field voltage magnitudes. We will assume that some best or most reasonable equilibrium exists among the available equilibria, and will not require that any prefault parameters be preserved at the postfault equilibrium. This distinction is important in formulating advanced excitation controls, since it is common practice to include "washout" stages in excitation controllers (power system stabilizers, or PSS) which force the terminal voltage to return to the prefault setpoint irrespective of whether there is a postfault equilibrium available at that voltage. The assumption that a viable equilibrium exists is implicit in most transient stability work involving transient energy functions, since one must assume the existence of a stable postfault equilibrium in order to formulate the transient energy functions that are used for the analysis.

In this chapter, some of the common methodologies for analyzing system security in terms of transient stability will be reviewed with respect to some common transient energy functions. We will begin by outlining some of the nonlinear system theory that will be necessary for understanding the transient energy method, followed by a presentation of a commonly-used energy function for the constant-voltage classical machine model. This energy function will then be generalized, and its dynamic characteristics derived for the single-axis model. Our intent is to utilize these energy functions as a means of gaining insight into the problem of designing controls for maximum system security; such a control would maximize the ability of the system to return to a viable equilibrium point following severe system upsets.

3.1 Notions of Stability

In contrast to linear systems, which have a single equilibrium point that may be marginally stable, asymptotically stable or unstable, nonlinear systems may have many equilibria, each of which may be characterized in terms of various definitions of stability.

We will apply these definitions of stability to systems of the form

$$\dot{\mathsf{x}} = \mathsf{f}(\mathsf{x}) \tag{3.1}$$

This system is said to be *autonomous*, *i.e.*, it is time-invariant. Note that it does not depend on an external input, but does include feedback systems in which the input is some (non-time-varying) function of x.

Definition 3.1 *The point x_o is an equilibrium point of the system (3.1) if $\mathsf{f}(\mathsf{x}_o) = 0$.*

Now, for some $r > 0$, we define the set $\mathcal{B}_r(\mathsf{x}_o) \subset \mathbb{R}^n$ as $\mathcal{B}_r(\mathsf{x}_o) = \{\mathsf{x} \in \mathbb{R}^n \mid \|\mathsf{x} - \mathsf{x}_o\| < r\}$.

Definition 3.2 *An equilibrium point associated with the system of (3.1) is said to be* locally stable in the sense of Lyapunov (i.s.L) *about an equilibrium point x_o if, given any $\varepsilon > 0$, there is a $\delta > 0$ such that for any initial condition $\mathsf{x}(t_o) \in \mathcal{B}_\delta(\mathsf{x}_0)$, $\mathsf{x}(t) \in \mathcal{B}_\varepsilon(\mathsf{x}_o)$, for all $t \geq t_o$. It is said to be* globally stable i.s.L. *if it is locally stable i.s.L. and if, for every $\delta > 0$ there is an $\varepsilon < \infty$ such that for all $\mathsf{x}(t_o) \in \mathcal{B}_\delta(\mathsf{x}_o)$, $\mathsf{x}(t) \in \mathcal{B}_\varepsilon(\mathsf{x}_o)$, for all $t > t_o$.*

Note that this definition does not require the state vector to approach the equilibrium in any sense, it only says that we may confine system trajectories arbitrarily closely to x_o by choosing the state $\mathsf{x}(t_o)$ to be close enough to the equilibrium. For example, a linear system that exhibits a nontrivial periodic solution but whose other eigenvalues are strictly in the left half-plane is globally stable i.s.L.

A type of stability that does require trajectories to approach the equilibrium is asymptotic stability.

Definition 3.3 *An equilibrium point associated with the system (3.1) is said to be* locally asymptotically stable (l.a.s.) *if it is stable i.s.L., and if, furthermore, there exists some $\delta > 0$ such that for any initial condition $\mathsf{x}(t_o) \in \mathcal{B}_\delta(\mathsf{x}_o)$, $\mathsf{x}(t) \to \mathsf{x}_o$ as $t \to \infty$. It is said to be* globally asymptotically stable (g.a.s.) *if it is globally stable i.s.L and l.a.s. for all $\delta \in [0, \infty)$*

Asymptotic stability is stricter than stability i.s.L.; however it says nothing about the *rate* at which trajectories approach the equilibrium. Two definitions that put require-

ments on the convergence rate are *exponential stability* and *quadratic stability.* Exponential stability will not be used in the sequel, so we will not dwell on it further. Quadratic stability will be defined and explored in Chapter C

It should be apparent that for any system with more than a single equilibrium point, no global asymptotic stability results are possible. It is actually true that global stability i.s.L. is also impossible except in systems with a single equilibrium, but we will not prove it here. Since power systems always have multiple equilibria, we will only be concerned with local stability in this thesis. For every equilibrium point x_o that is l.a.s., there is a region in the state space, referred to as the *region of attraction* of x_o, that is defined as follows:

Definition 3.4 *Suppose that, for the system of (3.1),* x_o *is l.a.s. Then there is an open, connected set* $\mathcal{A}(\mathsf{x}_o)$*, known as the* region of attraction *(or* ROA*) of* x_o*, defined as follows:* $\mathcal{A}(\mathsf{x}_o) = \{\mathsf{z} \in \mathbb{R}^n \mid \mathsf{x}(t) \to \mathsf{x}_o \text{ as } t \to \infty, \text{ if } \mathsf{x}(t_o) = \mathsf{z}\}$*. Furthermore, if* $\mathcal{A}(\mathsf{x}_o) \neq \mathbb{R}^n$*, the* closure *of* $\mathcal{A}(\mathsf{x}_o)$ *will be denoted as* $\bar{\mathcal{A}}(\mathsf{x}_o)$*. The* boundary *of* $\mathcal{A}(\mathsf{x}_o)$ *will be denoted* $\partial\mathcal{A}(\mathsf{x}_o) = \bar{\mathcal{A}}(\mathsf{x}_o)\backslash\mathcal{A}(\mathsf{x}_o)$[2]*, and will be referred to as the* stability boundary *of the system with respect to* x_o*.*

The primary concern of transient stability analysis is to determine, for a given fault scenario and given postfault equilibrium point x_s, whether the system state at the instant of fault clearing, $\mathsf{x}(t_{cl})$, remains within $\mathcal{A}(\mathsf{x}_s)$. If this is the case, then the system will settle to the desired equilibrium. If, on the other hand, $\mathsf{x}(t_{cl}) \notin \mathcal{A}(x_s)$, then the system may settle to an undesirable equilibrium point or become unbounded. There is little practical difference between the two, however, since an undesirable equilibrium point will almost invariably be one at which system operating constraints are violated, in which case protective relaying will act to remove equipment from service.

The general idea of local asymptotic stability and regions of attraction is illustrated in Figure 3.1[3]. The bead is free to slide on the wire under the force of gravity. Several stable and unstable equilibria exist along the wire, corresponding to "peaks" (unstable)

[2]The notation $\mathcal{A}\backslash\mathcal{B}$ means "All points in $\mathcal{A}$ that are not in $\mathcal{B}$"

[3]This example shamelessly lifted from Professor J.L. Wyatt's class on nonlinear systems, M.I.T. course 6.243.

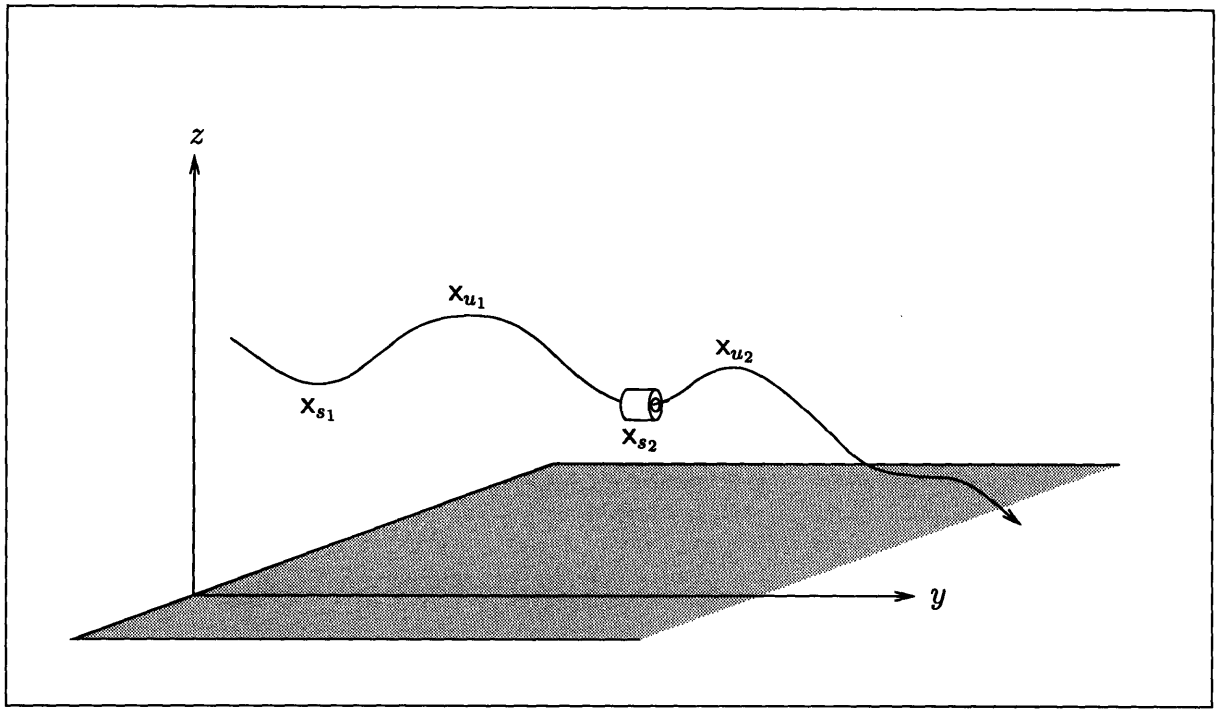

Figure 3.1: Example of System With Multiple Equilibria.

and "valleys" (stable). Equilibria are labeled x_{s_i} (stable) and x_{u_i} (unstable). The axes represent a set of space coordinates, y and z, and gravity is assumed to act along the z axis. If the bead is pushed slightly away from a stable equilibrium, it will experience a restoring force that will bring it back to rest at the same equilibrium. However, if the bead is given sufficient velocity (or, more to the point, sufficient kinetic energy) and/or sufficient potential energy, it will overshoot the original equilibrium point, pass one of the unstable equilibria, and proceed to either settle at a different stable equilibrium, or continue *ad infinitum* along the wire, its position becoming unbounded.

Note that if the system has friction, then all locally stable equilibria are l.a.s. Intuitively speaking, this is clear since as long as the bead is moving it must be losing energy to friction. If the bead is in the ROA of a stable equilibrium point, its energy must eventually approach a minimum, and the minimum must occur at the stable equilibrium point. If the model is assumed to be frictionless, then the energy of the bead will remain constant, since there is no mechanism for its dissipation. A small perturbation away from a stable equilibrium point will lead to a bounded periodic os-

cillation, in which the potential energy (height) of the bead is converted into kinetic energy which in turn is converted back to potential energy. In this case the stable equilibria are locally stable i.s.L., since vanishingly small perturbations lead to vanishingly small oscillations. If the bead has mass m, then we may define the potential energy at any point as $PE(y,z) = mgz$, and the kinetic energy as $KE(y,z) = \frac{1}{2}m(\dot{y}^2 + \dot{z}^2)$. Each stable and unstable equilibrium point has an energy associated with it, which is just the potential energy, PE_i. For the frictionless case, it is clear by the conservation of energy that, with respect to a given stable equilibrium point, if the total energy of the bead is greater than the potential energy associated with the lower of the two adjacent unstable equilibria, then the bead will pass over the "peak" and will not return to the original equilibrium point.

The preceding argument is a heuristic example of Lyapunov's direct method for assessing the stability of nonlinear systems. In this example, conservation of energy led to conclusions about stability and regions of attraction. In a more general sense, if a function of the state can be defined that represents a scalar quantity that is conserved, in the sense that it is nonincreasing as the system evolves, then stability information may be derived from it via Lyapunov's direct method.

3.2 Lyapunov Functions and Energy Functions

Once again, we will not present rigorous derivations of the following theorems, but will rely on the energy-based intuition of the previous section to motivate them. It will be convenient to assume that the equilibrium point of interest is 0, which can always be achieved by an appropriate translation of the state variables.

Theorem 3.1 (Lyapunov's direct method) *For the system of (3.1), suppose there exists a continuously-differentiable scalar function V(x), defined in some neighborhood*

of 0. *Consider the following properties:*

$$\left.\begin{array}{rcl} \mathcal{V}(\mathsf{x}) & \geq & 0, \\ \mathcal{V}(\mathsf{x}) & = & 0 \text{ only for } \mathsf{x} = 0 \\ \frac{d\mathcal{V}(\mathsf{x})}{dt} & \leq & 0 \end{array}\right\} \tag{3.2}$$

and

$$\frac{d\mathcal{V}(\mathsf{x})}{dt} = 0 \Longleftrightarrow \mathsf{x} = 0 \tag{3.3}$$

If (3.2) holds, then the system is locally stable i.s.L. If, in addition, (3.3) holds, then the system is l.a.s. If the conditions of (3.2) and (3.3) hold globally and additionally, if $\mathcal{V}(\mathsf{x})$ *is* radially unbounded, *i.e. if* $\mathcal{V}(\mathsf{x}) \to \infty$ *as* $\|\mathsf{x}\| \to \infty$, *then the stability (i.s.L and asymptotic, respectively,) is global.*

A function $\mathcal{V}(\mathsf{x})$ with the above properties is known as a *Lyapunov function* or an *energy function.* The proof of Theorem 3.1 is standard material, and may be found in several references, *e.g.* [50]. Many refinements of this theorem are available, most notably the LaSalle-Krasovski theorem, but these are peripheral to the material in this chapter and will not be stated in detail here. It should be emphasized that if the direct method fails to predict stability for a given candidate Lyapunov function, then nothing can be concluded. In this sense, all stability results related to Lyapunov's direct method are only *sufficient* conditions. It has been shown that under mild assumptions, a Lyapunov function exists for any system with a stable equilibrium, but unfortunately no systematic method exists for finding valid Lyapunov functions for general nonlinear systems.

Theorem 3.1 motivates the primary method for assessing transient stability. During a fault, a power system typically gains "energy" due to changes in loads seen by the generators. Given some function that expresses this energy in a meaningful way, the energy of the state may be calculated at the time of fault clearing, t_{cl}. If the system energy at the time of fault clearing is greater than some critical value $\mathcal{V}_{cr}$, then it may be deduced that the system has exited the ROA of the postfault equilibrium point and will not approach it as the system evolves. The system is therefore pronounced transiently

unstable for that fault. The value of t for which $\mathcal{V}(\mathbf{x}(t)) = \mathcal{V}_{cr}$ is known as the *critical clearing time* and is denoted t_{cr}. The determination of an appropriate energy function and the critical energy is not as straightforward as the example of Figure 3.1 might lead one to expect, however. For the power system model, the ROA boundary $\partial\mathcal{A}(x_s)$ is very difficult to compute exactly, and dissipative terms are difficult to account for in the energy function. This leads to conservative determinations of t_{cr}. Moreover, the energy of points in $\partial\mathcal{A}(\mathbf{x}_o)$ is not constant, hence the value of $\mathcal{V}_{cr}$ depends on the fault trajectory, taking different values for different faults.

Several methods exist for approximating the exact value of $\mathcal{V}_{cr}$. The *controlling unstable equilibrium point* (u.e.p.) method attempts to locate the lowest-energy unstable equilibrium point on $\partial\mathcal{A}(\mathbf{x}_s)$, as characterized by the transient energy function (TEF). Several difficulties exist with this method. First, it may be difficult in a high-dimension system to locate all of the relevant unstable equilibria. Second, a given trajectory may never approach the controlling equilibrium point, hence t_{cr} as calculated by the u.e.p. method may be very conservative.

Another method for determining $\mathcal{V}_{cr}$ is the so-called *potential energy boundary surface (PEBS) method.* The potential energy is defined as the value of the TEF when all frequencies are at the nominal value (0 in COI). This can be thought of as a manifold (defined by the constraint implicit in the TEF) that exists in a reduced-order space consisting only of the machine rotor angles, and will be of great importance in the following chapter. The PEBS may then be defined as the stability boundary of a reduced-order *gradient system.* The PEBS approach attempts to locate the maximum of the potential energy along the faulted trajectory. Wherever this maximum may occur, it is taken as an approximation of the actual stability boundary. It is well-known, however, that the potential energy boundary does not coincide with the actual stability boundary of the system, hence results based on this method may have unpredictable results.

A refinement of this method advanced by Chiang et. al. [12] is the *boundary controlling unstable equilibrium* (BCU) method, in which the PEBS method is used to locate the crossing of the potential energy boundary. This point is then used as the starting point of an algorithm that locates the unstable equilibrium point nearest the

crossing, whose energy is then taken as $\mathcal{V}_{cr}$.

Transient stability determination differs from a typical Lyapunov stability analysis because the equilibrium point of interest is l.a.s. *by assumption*: It is pointless to attempt to determine the ROA of an equilibrium point that is not l.a.s., and the determination of local stability is typically done by examining the eigenvalues of the linearized system matrix. If this matrix is not strictly stable about a given equilibrium point, it is not considered to be viable and hence is not a candidate for transient stability analysis. Because of the *a priori* assumption of asymptotic stability and difficulty in accounting for losses in the transmission grid and in the real part of constant-admittance loads, the strict definition of the Lyapunov function is typically relaxed to include functions which satisfy all the requirements for a Lyapunov function, but which may not be bounded below. This approach leads to an adequate determination of t_{cr}.

The preceding introduction is by no means comprehensive. It is included in order to give the reader a flavor of the issues involved in transient stability analysis, but since the objective of this thesis is not to determine t_{cr}, this quick introduction will be sufficient for understanding the material to follow. In particular, the importance of the PEBS and BCU methods is evidence of the close association between the region of attraction and the PE surface. This concept will be developed in more detail in Chapter 4 with respect to the effect of various types of compensators on the dynamics of the PE surface.

An important distinction must now be made between the objectives of transient stability and those of Lyapunov-based control. Although we do not present any Lyapunov-based controls in this chapter, the energy functions presented in following sections are described to some extent from the perspective of control, so that certain aspects that would be important to transient stability analysis are minimized or omitted. Since transient stability is concerned with the ability of an existing system to ride through a disturbance, many TEFs go to great lengths to include energy terms that are associated with particular types of control and auxiliary equipment. Moreover, it is important that the energy functions used are nonincreasing, given the existing system dynamics. For control purposes, the main interest is that the energy function captures some meaning-

ful quantity in such a way as to allow for control design. Typically, this means that the function must at least be positive semidefinite, but there is no *a priori* requirement on its behavior in the time domain. The control will be designed to ensure that the selected energy function is decreasing in closed loop. If the function is not strictly positive definite, then there is no guarantee that the control will return the system to the desired equilibrium, and in this case some additional analysis is required.

3.3 Transient Energy Functions

We begin with a statement of a TEF for the classical machine model, in which the voltage behind the transient reactance is held constant. Thus we may write (3.1) in the COI frame of reference as

$$\dot{x} = \begin{bmatrix} \dot{\delta}^c \\ \dot{\omega}^c \end{bmatrix} = f(\delta^c, \omega^c). \tag{3.4}$$

From this point forward, all derivations will be based on the COI model, unless otherwise indicated, and we will drop the "c" superscript in the interest of notational simplicity

For a single-machine infinite-bus model, this function can be derived directly as the first integral for the lossless system. In the multimachine case, a similar formulation is derived with some effort by writing the model as a Luré system and resorting to the Moore-Anderson theorem, which is a multivariable generalization of the Popov criterion (see *e.g.* [38]). Although a simple energy function will be derived in this chapter as an illustration of some of the concerns involved in the use of these functions, the full derivation of the more complex multimachine TEFs will not be presented here, as it tends to be rather involved algebraically, and is available in the literature, *e.g.* [39, 22, 21].

For this simple energy function, the loads are modeled as constant admittances. The generators are modeled as voltage sources of constant magnitude and phase δ, connected in series with the transient reactance, x'_d. The internal-node representation of the system is used, and load-only busses are eliminated by Kron's reduction (see Chapter 2). In order to derive a closed-form expression for the system energy, it is then

necessary to ignore the transconductances, *i.e.* the real part of the off-diagonal elements of the reduced admittance matrix. On the other hand, the power dissipated by the real parts of the diagonal elements G_{ii} of the reduced admittance matrix is constant in the internal-node classical model, since they are connected to voltage sources of constant magnitude. This power may be subtracted from the input torque of the associated machines,

$$T'_{m_i} = T_{m_i} - E_i^2 G_{ii} \tag{3.5}$$

This renders the reduced admittance matrix completely lossless, so that that $P_{\text{tot}} = 0$, for P_{tot} as defined in (2.60), since the matrix $\mathbf{G}$ is zero. For models in which the machine voltage varies, the elimination of G_{ii} is equivalent to the conversion of G_{ii} to a constant-power load. Initially, we will consider the lossy model in order to illustrate the difficulties presented by the lossy terms. In all that follows, machine angles and frequencies will be expressed in the COI frame of reference, and the superscript c that was used to denote the COI-referenced state variables in Chapter 2 will be dropped in the interest of notational simplicity. The operative dynamic equations will be (2.125) and, if voltage dynamics are to be considered, they will be governed by (2.90), with the single-axis model as the underlying basis. We will begin by deriving the function with respect to the machine-referenced coordinates, following a treatment by [38]. We will then convert to network-referenced quantities, and finally extend the network-referenced energy function to account for time-varying machine voltages.

3.3.1 A Classical TEF in Machine Coordinates

The most straightforward method for deriving a TEF is to look for a function that is constant along the system trajectories, *i.e.*, to calculate the first integral of motion. This is quite simple, at least for the single-machine infinite-bus model, but somewhat lacking in intuition, so we will preface this exercise with some comments about the energy interpretation of the classical TEF. The classical TEF accounts for three types of energy storage: the kinetic energy manifested as a change in the angular velocity of the turbine/generator mass, the potential energy accumulated as the integral of the input

torque through the angular displacement of the machine rotor, and the average energy stored in the electromagnetic fields of reactive elements such as generator windings and transmission lines. In a lossless system the sum of these energies must remain constant, so it should not be surprising that in calculating the first integral, which is always constant along system trajectories, we arrive at an expression that reflects each of these terms. To calculate the first integral we define

$$\nabla \mathcal{V} = \left[\; -m_1\dot{\omega}_1, \;\; \ldots, \;\; -m_p\dot{\omega}_p, \;\; m_1\dot{\delta}_1, \;\; \ldots, \;\; m_p\dot{\delta}_p \; \right], \Rightarrow \dot{\mathcal{V}}_i = \nabla\mathcal{V}\dot{\mathsf{x}} \equiv 0, \qquad (3.6)$$

which is now formally integrated in pairs, so that each machine is associated with an *individual machine* TEF. These will be summed to generate a system TEF. The calculation of the individual TEF starts with the formal integration:

$$\mathcal{V}_i(\delta_i, \omega_i) = \int_{\delta_o,0}^{\delta,\omega} \left(m_i\dot{\delta}_i \, d\omega_i - m_i\dot{\omega}_i \, d\delta_i \right), \qquad (3.7)$$

into which the machine equations are substituted, utilizing the power equation from (2.56):

$$\begin{aligned} \mathcal{V}_i(\mathsf{x}) \;\; &= \;\; \int_0^{\omega_i} m_i\omega_i \, d\omega_i \\ &- \;\; \int_{\delta_{oi}}^{\delta_i} \Big\{ \underbrace{T_{m_i} - E_i^2 G_{ii}}_{T'_{mi}} + E_i \sum_{\substack{j=1 \\ j\neq i}}^{p} E_j \left[G_{ij}\cos(\delta_i - \delta_j) + B_{ij}\sin(\delta_i - \delta_j) \right] \Big\} \, d\delta_i \\ &- \;\; \int_{\delta_{oi}}^{\delta_i} \left(m_i D\omega_i + \frac{m_i}{m_{\mathrm{T}}} P_{\mathrm{COI}} \right) d\delta_i \end{aligned} \qquad (3.8)$$

For the classical model, this may be reduced to

$$\begin{aligned} \mathcal{V}_i(\mathsf{x}) \;\; &= \;\; m_i{\omega_i}^2 - T'_{m_i}(\delta_i - \delta_{o_i}) \\ - \int_{\delta_{oi}}^{\delta_i} \Big\{ E_i \sum_{\substack{j=1 \\ j\neq i}}^{p} E_j \left[G_{ij}\cos(\delta_i - \delta_j) + B_{ij}\sin(\delta_i - \delta_j) \right] &+ m_i D\omega_i + \frac{m_i}{m_{\mathrm{T}}} P_{\mathrm{COI}} \Big\} \, d\delta_i \end{aligned} \qquad (3.9)$$

We now sum the individual machine TEFs over i and collect similar terms in the summation of the power-related terms to arrive at the system TEF. In view of (3.9),

this yields

$$\begin{aligned}\mathcal{V}(\mathsf{x}) &= \frac{1}{2}\boldsymbol{\omega}^t\mathbb{M}\boldsymbol{\omega} - \mathsf{T}_m^t(\boldsymbol{\delta}-\boldsymbol{\delta}_o) \\ &- \int_{\boldsymbol{\delta}_o}^{\boldsymbol{\delta}} \sum_{i=1}^{p-1}\sum_{j=i+1}^{p} E_iE_jB_{ij}\sin(\delta_i-\delta_j)\,d(\delta_i-\delta_j) \\ &- \underbrace{\int_{\boldsymbol{\delta}_o}^{\boldsymbol{\delta}} \sum_{i-1}^{p-1}\sum_{j=i+1}^{p} E_iE_jG_{ij}\cos(\delta_i-\delta_j)\,d(\delta_i+\delta_j) - \int_{\boldsymbol{\delta}_o}^{\boldsymbol{\delta}}\sum_{i=1}^{p} m_iD\omega_i\,d\delta_i}_{\text{path-dependent}} \qquad (3.10)\end{aligned}$$

The terms involving P_{COI} have vanished, since in the COI model, $\sum_{i=1}^{p} m_i d\delta_i = 0$. Here it is clear that the integrals involving the lossy terms are path-dependent, making it impossible to express the TEF as a closed-form function of the state variables. We now make the typical assumption that the transconductances and the damping constant are equal to 0, and we have the classical multimachine TEF:

$$\begin{aligned}\mathcal{V}(\mathsf{x}) &= \frac{1}{2}\boldsymbol{\omega}^t\mathbb{M}\boldsymbol{\omega} - \mathsf{T}_m^t(\boldsymbol{\delta}-\boldsymbol{\delta}_o) \\ &- \sum_{i=1}^{p-1}\sum_{j=i+1}^{p} E_iE_jB_{ij}\cos(\delta_i-\delta_j) + \sum_{i=1}^{p-1}\sum_{j=i+1}^{p} E_iE_jB_{ij}\cos(\delta_{o_i}-\delta_{o_j}) \qquad (3.11)\end{aligned}$$

The kinetic energy and the potential energy associated with integrating a torque through an angular displacement are evident in the first two terms of (3.11), but the interpretation of the final two terms is not as clear as could be desired. This shortcoming will be remedied in the section to follow.

This derivation is not quite as straightforward as the foregoing procedure makes it seem, since it has not been shown that (3.11) is positive-definite. As noted earlier, this requires an appeal to the Moore-Anderson theorem, which can be used to show that (3.11) is actually a Lyapunov function for the idealized system. The details of this are somewhat involved and will not be presented.

It is also true that for the lossless system, none of the stable equilibria is asymptotically stable, which is not surprising, since $\dot{\mathcal{V}} \equiv 0$. Equation (3.11) may nonetheless be used to show asymptotic stability for systems in which the grid is lossless, but $D > 0$. In this case, $\nabla\mathcal{V}_i(\mathsf{x}) = [-m_i(\dot{\omega}_i - D\omega_i),\ \dot{\delta}_i]$ and hence, $\dot{\mathcal{V}}_i(\mathsf{x}) = \nabla\mathcal{V}_i(\mathsf{x})\dot{x} = -m_iD{\omega_i}^2$,

so that $\dot{\mathcal{V}}(\mathsf{x}) = -D\sum_{i=1}^{p} m_i\omega_i{}^2$. This is strictly negative except when $\boldsymbol{\omega} = 0$, but may be zero when $\boldsymbol{\delta} \neq \boldsymbol{\delta}_o$. One must resort to the LaSalle-Krasovski theorem to complete the proof of asymptotic stability, using the fact that the largest invariant set contained within the set $\{\mathsf{x} \mid \dot{\mathcal{V}}(\mathsf{x}) = 0\}$ is the equilibrium point x_o.

3.3.2 The Classical TEF in Network Coordinates

It is possible to obtain a simpler form for the classical TEF by expressing it in terms of the network-referenced state variables. Recall that the classical model assumes that the machine voltages are constant. Therefore the "voltage dynamics" in this case are nonexistent, but the form that is derived in this section will provide a convenient working framework for more complex energy functions. Recall from Section 2.7 that the relationship between the two frames of reference in the single-axis machine model is just

$$\mathsf{E}_{\mathsf{D}} = \mathbb{C}(\boldsymbol{\delta})\mathsf{E}'_q; \qquad \mathsf{E}_{\mathsf{Q}} = \mathbb{S}(\boldsymbol{\delta})\mathsf{E}'_q, \tag{3.12}$$

which also holds for the classical model. To begin the derivation of $\mathcal{V}(\mathsf{x})$ in the network frame of reference, (3.11) is rewritten as

$$\begin{aligned} \mathcal{V} &= \frac{1}{2}\boldsymbol{\omega}^t\mathbb{M}\boldsymbol{\omega} - \mathsf{T}_m^t(\boldsymbol{\delta} - \boldsymbol{\delta}_o) \\ &- \underbrace{\frac{1}{2}\sum_{j=1}^{p}\sum_{i=1}^{p} E_iE_jB_{ij}\cos(\delta_i - \delta_j)}_{(**)} + \frac{1}{2}\sum_{j=1}^{p}\sum_{i=1}^{p} E_iE_jB_{ij}\cos(\delta_i^o - \delta_j^o). \end{aligned} \tag{3.13}$$

Note that each of the summations in (3.13) contains an extra term, $\frac{1}{2}\sum_{i=1}^{p} E_i^2B_{ii}$, which cancels out. The inclusion of these terms leads to a notationally simpler form and motivates some of the work presented in Chapter 4.

Application of the trigonometric identity $\cos(\delta_i - \delta_j) = \cos(\delta_i)\cos(\delta_j) + \sin(\delta_i)\sin(\delta_j)$ allows the final term to be written as

$$(**) = -\frac{1}{2}\mathsf{E}^t\left(\mathbb{C}(\boldsymbol{\delta})\,\mathbf{B}\,\mathbb{C}(\boldsymbol{\delta}) + \mathbb{S}(\boldsymbol{\delta})\mathbf{B}\mathbb{S}(\boldsymbol{\delta})\right)\mathsf{E}, \tag{3.14}$$

which in turn yields

$$(**) = \frac{1}{2}\mathsf{E}^t \begin{bmatrix} \mathbb{C}(\boldsymbol{\delta}) & \mathbb{S}(\boldsymbol{\delta}) \end{bmatrix} \begin{bmatrix} -\mathbf{B} & 0 \\ 0 & -\mathbf{B} \end{bmatrix} \begin{bmatrix} \mathbb{C}(\boldsymbol{\delta}) \\ \mathbb{S}(\boldsymbol{\delta}) \end{bmatrix} \mathsf{E}, \tag{3.15}$$

and finally,

$$(**) = \frac{1}{2} \begin{bmatrix} E_{\mathrm{D}}^t & E_{\mathrm{Q}}^t \end{bmatrix} \underline{\underline{\mathbf{B}}} \begin{bmatrix} E_{\mathrm{D}} \\ E_{\mathrm{Q}} \end{bmatrix} = -\frac{1}{2} Q_{\mathrm{tot}}. \tag{3.16}$$

The final equality in (3.16) just restates (2.33). Since the second summation in (3.13) is identical to the first, except that the angles are fixed, we may express (3.13) as

$$\begin{aligned} \mathcal{V} &= \frac{1}{2}\boldsymbol{\omega}^t \mathbb{M}\boldsymbol{\omega} - \mathsf{T}_m^t(\boldsymbol{\delta} - \boldsymbol{\delta}_o) \\ &+ \frac{1}{2} \begin{bmatrix} \mathsf{E}_{\mathrm{D}}^t & \mathsf{E}_{\mathrm{Q}}^t \end{bmatrix} \underline{\underline{\mathbf{B}}} \begin{bmatrix} \mathsf{E}_{\mathrm{D}} \\ \mathsf{E}_{\mathrm{Q}} \end{bmatrix} - \frac{1}{2} \begin{bmatrix} \mathsf{E}_{\mathrm{D}_o}^t & \mathsf{E}_{\mathrm{Q}_o}^t \end{bmatrix} \underline{\underline{\mathbf{B}}} \begin{bmatrix} \mathsf{E}_{\mathrm{D}_o} \\ \mathsf{E}_{\mathrm{Q}_o} \end{bmatrix} \\ &= \frac{1}{2}\boldsymbol{\omega}^t \mathbb{M}\boldsymbol{\omega} - \mathsf{T}_m^t(\boldsymbol{\delta} - \boldsymbol{\delta}_o) + \frac{1}{2}(Q_{\mathrm{tot}} - Q_{\mathrm{tot}}^o) \end{aligned} \tag{3.17}$$

This form of the classical TEF is appears to be new, though it is quite similar in spirit to the expressions derived in [21]. The final term of (3.17) is unaffected if a lossy system is considered; to account for the losses, path-dependent integral terms from (3.10) are simply added to (3.17).

This function is locally positive-definite and nonincreasing only if E'_q remains constant. Thus, if one wishes to evaluate the stability of a system in which variation of the machine voltage is a significant factor, more complex energy functions are required. At the next level of complexity, there is the so-called flux-decay model, in which the field voltage is considered constant, but the effects of flux decay due to armature currents are modeled (See Section 2.7).

3.3.3 A TEF for the Flux-Decay Model

Several energy functions have been developed for the flux-decay model, most notably in [46, 21]. The magnitude of the machine voltage phasor for the flux-decay model will

be denoted as $E = |E'_{q_i} + j(x_{d_i} - x'_{d_i})i_{d_i}|$. For this model, (3.1) takes the form

$$\dot{\mathsf{x}} = \mathsf{f}(\mathsf{x}) = \mathsf{f}(\mathsf{E}, \boldsymbol{\delta}, \boldsymbol{\omega}) \tag{3.18}$$

The classical TEF is invalid for this model, since $\mathcal{V}(\mathsf{E}_o, \boldsymbol{\delta}_o, \boldsymbol{\omega}_o)$ is not a local minimum if E is allowed to vary. One method for dealing with this problem has been advanced by Sasaki [46]. In this method as it was originally proposed, (3.11) is used, but E is not considered to be a dynamic variable, rather it is taken as a vector of variable parameters. The unstable equilibria are then found under the assumption that the magnitude of the generator voltage at the unstable equilibrium is the same as the magnitude at the stable equilibrium. This method is somewhat cumbersome for transient stability work, since not only the energy margin, but also the location of the stable and unstable equilibria depend directly on the value of the "parameters," *i.e.*, the magnitude of the generator voltage. This means that the location of both the stable and unstable equilibria must be recalculated at each step.

For the purposes of this thesis, it will be necessary to derive the dynamic behavior of Sasaki's function, and that is the goal of this section. In order to achieve this, it is necessary to cast the point-by-point recalculation of the stable equilibrium as a type of dynamic process, associated with an extra set of dynamic variables called the *tracking variables.* The function of the tracking system is to perform a dynamic recalculation of the stable equilibrium in response to variation in the machine voltage magnitude, and the time-domain behavior of the tracking states may be derived in terms of the machine dynamics. The tracking variables will be denoted by an asterisk, *e.g.* $\boldsymbol{\delta}^*$ is the tracking vector associated with the virtual equilibrium of the rotor angles. It will be shown that when expressed in this fashion, Sasaki's TEF is a positive semidefinite function of $\boldsymbol{\delta}$, $\boldsymbol{\omega}$ and E over a certain range of variation in the machine voltages, so that the parametric interpretation is unnecessary. Hereafter, the Sasaki TEF will be referred to as the STEF.

Several technical assumptions are made in order to justify the energy interpretation of the STEF, the primary one being that the ratio between the q component E'_q and

the d component $(x_q - x'_q)i_q$ remains fixed. This assumption means that the angle ϕ in Figure 2.3 is fixed, so that the change in angle of the machine voltage phasor is strictly a function of the change in the rotor angle δ. Under these circumstances, the flux-decay model can be reduced to a single-axis model, with the appropriate choice of initial conditions and machine impedance (x_q rather than x'_d).

Several other issues arise regarding the use of the STEF for transient stability work, but these are not of concern here, since our interest in the STEF is as a type of control Lyapunov function. The areas of primary interest for control are the types of system energy expressed by the STEF, the mechanisms for conversion of one type of energy to another, and the dissipation of energy via the action of the control.

Given the foregoing discussion, Equation (3.11) is sufficient for transient stability analysis using Sasaki's method. In the sequel, however, we will be interested in the dynamic behavior of (3.11) as the system evolves, with and without field voltage control. Therefore, beginning with the expression of the classical TEF in network coordinates, (3.13), we utilize the tracking variables to reformulate Sasaki's TEF in the network frame of reference as:

$$\begin{aligned} \mathcal{V}^* &= \frac{1}{2}\boldsymbol{\omega}^t\mathbb{M}\boldsymbol{\omega} - \mathsf{T}_m^t(\boldsymbol{\delta} - \boldsymbol{\delta}^*) \\ &+ \frac{1}{2}\begin{bmatrix} \mathsf{E}_{\mathrm{D}}^t & \mathsf{E}_{\mathrm{Q}}^t \end{bmatrix}\underline{\underline{\mathbf{B}}}\begin{bmatrix} \mathsf{E}_{\mathrm{D}} \\ \mathsf{E}_{\mathrm{Q}} \end{bmatrix} - \frac{1}{2}\begin{bmatrix} \mathsf{E}_{\mathrm{D}}^{*t} & \mathsf{E}_{\mathrm{Q}}^{*t} \end{bmatrix}\underline{\underline{\mathbf{B}}}\begin{bmatrix} \mathsf{E}_{\mathrm{D}}^* \\ \mathsf{E}_{\mathrm{Q}}^* \end{bmatrix} \\ &= \frac{1}{2}\boldsymbol{\omega}^t\mathbb{M}\boldsymbol{\omega} - \mathsf{T}_m^t(\boldsymbol{\delta} - \boldsymbol{\delta}^*) + \frac{1}{2}(Q_{\mathrm{tot}} - Q_{\mathrm{tot}}^*) \end{aligned} \tag{3.19}$$

As mentioned earlier, the tracking variables $\mathsf{E}_{\mathrm{D}}^*$, $\mathsf{E}_{\mathrm{Q}}^*$ and $\boldsymbol{\delta}^*$ are introduced here as a means of following the equilibrium as the magnitude of the generator voltages changes. This may be motivated as follows. Given any vector of machine voltage magnitudes, say E, there will be some vector of rotor angles, $\boldsymbol{\delta}^*$, such that the state vector $[\ \boldsymbol{\delta}^t\ \boldsymbol{\omega}^t\ ]^t = [\ \boldsymbol{\delta}^{*t}\ 0\ ]^t$ would be an equilibrium if the voltage magnitudes were fixed at that value[4].

[4]Actually, we must confine E to some neighborhood of a nominal equilibrium point in order for this to be strictly true, since there are values of E for which no equilibria exist.

This is the stable equilibrium for a particular voltage condition, and we will refer to it as the *virtual equilibrium.* It can be seen that for any fixed vector of voltage magnitudes, say E_o, the tracking variables assure that the STEF is completely analogous to the classical TEF *at that value of* E_o. Therefore the STEF is positive definite for E_o, and positive semidefinite for some range of variation about E_o.

The kinetic energy term in the STEF is identical the the KE term in the classical TEF, and indeed identical to the KE expressed by most if not all TEFs.

$$\mathcal{V}^*_{\text{KE}} = \mathcal{V}_{\text{KE}} = \frac{1}{2}\boldsymbol{\omega}^t \mathbb{M} \boldsymbol{\omega}, \tag{3.20}$$

The remaining terms are collectively taken to represent some type of potential energy; what distinguishes one energy function from another is typically the treatment of the PE terms. In the classical TEF, interpretation of the PE terms is fairly direct. In contrast, no straightforward interpretation exists for the STEF. In this case, $\mathcal{V}^*_{\text{PE}}$ is given by

$$\mathcal{V}^*_{\text{PE}} = \mathsf{T}^t_m(\boldsymbol{\delta} - \boldsymbol{\delta}^*) + \frac{1}{2}(Q_{\text{tot}} - Q^*_{\text{tot}}). \tag{3.21}$$

Since no accounting is provided for the energy exchange inherent in the dynamic effects of flux decay, the interpretation of $\mathcal{V}^*_{\text{PE}}$ is not as direct as for the constant-voltage classical TEF. One interpretation is to consider $\mathcal{V}^*_{\text{PE}}$ to be a measure of the energy available for conversion to KE, if the voltage magnitudes are fixed at a given instantaneous value. If the voltages change in such a manner as to reduce the PE, the total possible gain in KE is also reduced.

The defining relationship for the tracking voltages is simply that they must represent a stable point at which the input and output power is balanced at each generator:

$$\mathsf{P}^* \;=\; \mathsf{T}_m = \left[\; \mathbb{E}^*_{\text{D}} \;\middle|\; \mathbb{E}^*_{\text{Q}} \;\right] \mathbf{Y}_r \begin{bmatrix} \mathsf{E}^*_{\text{D}} \\ \mathsf{E}^*_{\text{Q}} \end{bmatrix}. \tag{3.22}$$

The use of the tracking variables will allow us to derive and work with the dynamic characteristics of the STEF. The tracking voltages are essentially the solution of a load-flow problem, and are therefore related algebraically to the system voltages and

rotor angles. Therefore the STEF is actually a positive-semidefinite function of the full system state vector, and no parametric interpretation is necessary. Unfortunately, there is no closed-form solution to the load-flow problem, so it is impossible to express the tracking variables directly in terms of the system variables, but it is feasible to construct a fictitious dynamic system whose inputs are the actual system states and whose outputs are the tracking variables. In this way it is possible to derive the overall dynamics of the STEF. The task of constructing and initializing such a system is addressed in Appendix A. In the following it is assumed that the tracking variables follow the stable equilibrium, but if the tracking system is initialized at an unstable equilibrium, then the tracking variables will follow it as the voltages vary, and $\mathcal{V}^*$ would represent the energy difference between the system and the unstable equilibrium. This is just the transient energy margin of the system with respect to that equilibrium.

Before we proceed, the variables $\boldsymbol{\lambda}_{\|}$ and $\boldsymbol{\lambda}_{\perp}$ will be introduced. These are used to express the rates of change of both the system voltages and the tracking voltages in an alternative form that will simplify many of the expressions that are to come, allowing them to be written in terms of familiar system quantities such as the reactive power Q. Expressions written in these forms are independent of the underlying machine model, and in that sense are more general than they would be if written in more conventional notation. The voltage at each machine is expressed in rectangular coordinates as $E_{\mathsf{D}} + jE_{\mathsf{Q}}$, and its rates of change along the direct and quadrature axes are expressed as $\dot{E}_{\mathsf{D}}$ and $\dot{E}_{\mathsf{Q}}$, respectively. $\boldsymbol{\lambda}_{\|}$ and $\boldsymbol{\lambda}_{\perp}$ are a type of polar representation of the machine voltage phasor, except that $\boldsymbol{\lambda}_{\|}$, is actually the time derivative of the log magnitude of the machine voltage. $\boldsymbol{\lambda}_{\perp}$ is the rate of change of the phase of the machine voltage vector, which in the single-axis model is the same as the frequency $\boldsymbol{\omega}$. In more complex models, the relationship between the phase angle and rotor angle is not direct, but it is the change in the voltage phasor that affects the power output of the machine. The main utility of the new variables derives from the way in which they are related to

the original quantities $\dot{E}_D$ and $\dot{E}_Q$:

$$\begin{bmatrix} \dot{\mathsf{E}}_D \\ \dot{\mathsf{E}}_Q \end{bmatrix} = \begin{bmatrix} \mathbb{E}_D \\ \mathbb{E}_Q \end{bmatrix} \boldsymbol{\lambda}_{\|} + \begin{bmatrix} -\mathbb{E}_Q \\ \mathbb{E}_D \end{bmatrix} \boldsymbol{\lambda}_{\perp}. \tag{3.23}$$

An identical relationship may be used to define the analogous quantities $\boldsymbol{\lambda}^*_{\|}$ and $\boldsymbol{\lambda}^*_{\perp}$, but it is not necessary to distinguish between $\boldsymbol{\lambda}_{\|}$ and $\boldsymbol{\lambda}_{\perp}$, since they are equal by definition. Again, this is treated in more detail in Appendix A.

We may now express the dynamics of the STEF through the following claim:

Claim 3.1 *The time-domain behavior of the STEF for the lossless single-axis power system model is expressed through the following equation:*

$$\dot{\mathcal{V}}^*(\mathsf{x}) = (\mathsf{Q}^t - \mathsf{Q}^{*t})\boldsymbol{\lambda}_{\|}, \tag{3.24}$$

where Q^* *is a vector of virtual reactive power outputs, defined analogously to (2.62) as*

$$\mathsf{Q}^* = \begin{bmatrix} \mathsf{E}^*_D & \mathsf{E}^*_Q \end{bmatrix} \underline{\underline{\mathbf{B}}} \begin{bmatrix} \mathbb{E}^*_D \\ \mathbb{E}^*_Q \end{bmatrix} \tag{3.25}$$

Proof:

Direct differentiation of (3.19) yields:

$$\begin{aligned} \dot{\mathcal{V}}^* &= \boldsymbol{\omega}^t \mathbb{M} \dot{\boldsymbol{\omega}} - \mathsf{T}^t_m(\boldsymbol{\omega} - \boldsymbol{\omega}^*) \\ &+ \begin{bmatrix} \mathsf{E}^t_D & \mathsf{E}^t_Q \end{bmatrix} \underline{\underline{\mathbf{B}}} \begin{bmatrix} \dot{\mathsf{E}}_D \\ \dot{\mathsf{E}}_Q \end{bmatrix} - \begin{bmatrix} \mathsf{E}^{*t}_D & \mathsf{E}^{*t}_Q \end{bmatrix} \underline{\underline{\mathbf{B}}} \begin{bmatrix} \dot{\mathsf{E}}^*_D \\ \dot{\mathsf{E}}^*_Q \end{bmatrix} \end{aligned} \tag{3.26}$$

As was done with the tracking voltages, the derivatives of the machine voltages are projected onto a parallel and a perp component. In this case, however, we will use projection matrices. Recall that for a rank-deficient $m \times n$ matrix $\mathbf{A}$, where $m > n$,

the projection matrix is $\Pi_{\mathbf{A}} = \mathbf{A}^t(\mathbf{A}\mathbf{A}^t)^{-1}\mathbf{A}$. Define

$$\Pi_{\parallel} \quad = \quad |\mathbb{E}|^{-2}\begin{bmatrix} \mathbb{E}_{\mathrm{D}} \\ \mathbb{E}_{\mathrm{Q}} \end{bmatrix}\begin{bmatrix} \mathbb{E}_{\mathrm{D}} & \mathbb{E}_{\mathrm{Q}} \end{bmatrix} \tag{3.27}$$

$$\Pi_{\perp} \quad = \quad |\mathbb{E}|^{-2}\begin{bmatrix} -\mathbb{E}_{\mathrm{Q}} \\ \mathbb{E}_{\mathrm{D}} \end{bmatrix}\begin{bmatrix} -\mathbb{E}_{\mathrm{Q}} & \mathbb{E}_{\mathrm{D}} \end{bmatrix}, \tag{3.28}$$

where the commutativity of diagonal matrices has been exploited in (3.27) and (3.28) to allow factoring of the matrix $|\mathbb{E}|^{-2}$ to the left. Now, $\Pi_{\parallel} + \Pi_{\perp} = \mathbf{I}$, so that (3.26) may now be reformulated as

$$\dot{\mathcal{V}}^* \quad = \quad \boldsymbol{\omega}^t\mathbf{M}\dot{\boldsymbol{\omega}} - \mathsf{T}_m^t\boldsymbol{\omega} + \begin{bmatrix} \mathsf{E}_{\mathrm{D}}^t & \mathsf{E}_{\mathrm{Q}}^t \end{bmatrix}\underline{\underline{\mathbf{B}}}\,\Pi_{\perp}\begin{bmatrix} \dot{\mathsf{E}}_{\mathrm{D}} \\ \dot{\mathsf{E}}_{\mathrm{Q}} \end{bmatrix} \tag{3.29}$$

....

$$+ \quad \mathsf{T}_m^t\boldsymbol{\omega}^* + \begin{bmatrix} \mathsf{E}_{\mathrm{D}}^t & \mathsf{E}_{\mathrm{Q}}^t \end{bmatrix}\underline{\underline{\mathbf{B}}}\,\Pi_{\parallel}\begin{bmatrix} \dot{\mathsf{E}}_{\mathrm{D}} \\ \dot{\mathsf{E}}_{\mathrm{Q}} \end{bmatrix}$$

$$- \quad \begin{bmatrix} \mathsf{E}_{\mathrm{D}}^{*t} & \mathsf{E}_{\mathrm{Q}}^{*t} \end{bmatrix}\underline{\underline{\mathbf{B}}}\left(\begin{bmatrix} \mathbb{E}_{\mathrm{D}}^* \\ \mathbb{E}_{\mathrm{Q}}^* \end{bmatrix}\boldsymbol{\lambda}_{\parallel} + \begin{bmatrix} -\mathbb{E}_{\mathrm{Q}}^* \\ \mathbb{E}_{\mathrm{D}}^* \end{bmatrix}\boldsymbol{\lambda}_{\perp}^*\right) \tag{3.30}$$

Let us compare the part of (3.30) above the dotted line to the derivative of the classical transient energy function presented in (3.11). Again by direct differentiation:

$$0 = \dot{\mathcal{V}} = \boldsymbol{\omega}^t\mathbf{M}\dot{\boldsymbol{\omega}} - \mathsf{T}_m^t\boldsymbol{\omega} + \begin{bmatrix} \mathsf{E}_{\mathrm{D}}^t & \mathsf{E}_{\mathrm{Q}}^t \end{bmatrix}\underline{\underline{\mathbf{B}}}\begin{bmatrix} \dot{\mathsf{E}}_{\mathrm{D}} \\ \dot{\mathsf{E}}_{\mathrm{Q}} \end{bmatrix}. \tag{3.31}$$

Since the perp projection matrix annihilates any parallel component of the voltage derivatives, it is clear that the part of (3.30) above the dotted line is invariant to any component of change in magnitude of the generator voltages.

Now suppose that the magnitudes of the generator voltages are fixed. Then any change must occur along the perp component, which means that the projection matrix $\Pi_{\perp}$ acts as an identity. Thus, the expression above the dotted line is equivalent to (3.31) when the magnitude of the voltages is not changing. Since (3.31) vanishes for a lossless

system, both expressions are identically zero. But the expression above the dotted line is invariant to any component of change along the parallel direction, hence it vanishes identically for any value of $[\,\dot{\mathsf{E}}_{\mathrm{D}}\ \dot{\mathsf{E}}_{\mathrm{Q}}\,]^t$. Consequently, the time-domain behavior of $\mathcal{V}^*$ is governed by the portion of (3.30) below the dotted line. Expanding $\Pi_{\|}$, we have

$$\begin{aligned}\dot{\mathcal{V}}^* &= \mathsf{T}_m^t\boldsymbol{\omega}^* + \left[\begin{array}{cc}\mathsf{E}_{\mathrm{D}} & \mathsf{E}_{\mathrm{Q}}\end{array}\right]\underline{\underline{\mathbf{B}}}\,|\mathbb{E}|^{-2}\left[\begin{array}{c}\mathbb{E}_{\mathrm{D}}\\ \mathbb{E}_{\mathrm{Q}}\end{array}\right]\left[\begin{array}{cc}\mathbb{E}_{\mathrm{D}} & \mathbb{E}_{\mathrm{Q}}\end{array}\right]\left[\begin{array}{c}\dot{\mathsf{E}}_{\mathrm{D}}\\ \dot{\mathsf{E}}_{\mathrm{Q}}\end{array}\right]\\ &\quad - \left[\begin{array}{cc}\mathsf{E}_{\mathrm{D}}^{*t} & \mathsf{E}_{\mathrm{Q}}^{*t}\end{array}\right]\underline{\underline{\mathbf{B}}}\left(\left[\begin{array}{c}\mathbb{E}_{\mathrm{D}}^{*}\\ \mathbb{E}_{\mathrm{Q}}^{*}\end{array}\right]\boldsymbol{\lambda}_{\|}^{*} + \left[\begin{array}{c}-\mathbb{E}_{\mathrm{Q}}^{*}\\ \mathbb{E}_{\mathrm{D}}^{*}\end{array}\right]\boldsymbol{\lambda}_{\perp}^{*}\right)\end{aligned} \tag{3.32}$$

Several substitutions must now be made. Observe that

$$\begin{aligned}\left[\begin{array}{cc}\mathsf{E}_{\mathrm{D}}^{*t} & \mathsf{E}_{\mathrm{Q}}^{*t}\end{array}\right]\underline{\underline{\mathbf{B}}}\left[\begin{array}{c}\mathbb{E}_{\mathrm{D}}^{*}\\ \mathbb{E}_{\mathrm{Q}}^{*}\end{array}\right] &= \left[\begin{array}{cc}\mathsf{E}_{\mathrm{D}}^{*t} & \mathsf{E}_{\mathrm{Q}}^{*t}\end{array}\right]\left[\begin{array}{cc}-\mathbf{B} & 0\\ 0 & -\mathbf{B}\end{array}\right]\left[\begin{array}{c}\mathbb{E}_{\mathrm{D}}^{*}\\ \mathbb{E}_{\mathrm{Q}}^{*}\end{array}\right]\\ &= \left[\begin{array}{cc}\mathsf{E}_{\mathrm{D}}^{*t} & \mathsf{E}_{\mathrm{Q}}^{*t}\end{array}\right]\left[\begin{array}{cc}0 & -\mathbf{I}\\ \mathbf{I} & 0\end{array}\right]Y_r^t\left[\begin{array}{c}\mathbb{E}_{\mathrm{D}}^{*}\\ \mathbb{E}_{\mathrm{Q}}^{*}\end{array}\right] = \mathsf{Q}^{*t}.\end{aligned} \tag{3.33}$$

Similarly,

$$\begin{aligned}\left[\begin{array}{cc}\mathsf{E}_{\mathrm{D}}^{*t} & \mathsf{E}_{\mathrm{Q}}^{*t}\end{array}\right]\underline{\underline{\mathbf{B}}}\left[\begin{array}{c}-\mathbb{E}_{\mathrm{Q}}^{*}\\ \mathbb{E}_{\mathrm{D}}^{*}\end{array}\right] &= \left[\begin{array}{cc}\mathsf{E}_{\mathrm{D}}^{*t} & \mathsf{E}_{\mathrm{Q}}^{*t}\end{array}\right]\left[\begin{array}{cc}-\mathbf{B} & 0\\ 0 & -\mathbf{B}\end{array}\right]\left[\begin{array}{c}-\mathbb{E}_{\mathrm{Q}}^{*}\\ \mathbb{E}_{\mathrm{D}}^{*}\end{array}\right]\\ &= \left[\begin{array}{cc}\mathsf{E}_{\mathrm{D}}^{*t} & \mathsf{E}_{\mathrm{Q}}^{*t}\end{array}\right]Y_r^t\left[\begin{array}{c}\mathbb{E}_{\mathrm{D}}^{*}\\ \mathbb{E}_{\mathrm{Q}}^{*}\end{array}\right] = \mathsf{P}^{*t} = \mathsf{T}_m^t.\end{aligned} \tag{3.34}$$

Substituting into (3.32) yields

$$\begin{aligned}\dot{\mathcal{V}}^* &= \mathsf{T}_m^t\boldsymbol{\omega}^* + \mathsf{Q}^t|\mathbb{E}|^{-2}\left[\begin{array}{cc}\mathbb{E}_{\mathrm{D}} & \mathbb{E}_{\mathrm{Q}}\end{array}\right]\left[\begin{array}{c}\dot{\mathsf{E}}_{\mathrm{D}}\\ \dot{\mathsf{E}}_{\mathrm{Q}}\end{array}\right]\\ &\quad - \mathsf{Q}^{*t}\boldsymbol{\lambda}_{\|}^{*} - \mathsf{T}_m\boldsymbol{\lambda}_{\perp}^{*}\end{aligned} \tag{3.35}$$

Now, under the assumption that $|\mathbb{E}|^* = |\mathbb{E}|$,

$$|\mathbb{E}|^{-2} \begin{bmatrix} \mathbb{E}_D & \mathbb{E}_Q \end{bmatrix} \begin{bmatrix} \dot{E}_D \\ \dot{E}_Q \end{bmatrix} = |\mathbb{E}|^{*-1}|\mathbb{E}|^{-1} \begin{bmatrix} \mathbb{E}_D & \mathbb{E}_Q \end{bmatrix} \begin{bmatrix} \dot{E}_D \\ \dot{E}_Q \end{bmatrix} = \boldsymbol{\lambda}_{\|}^*. \tag{3.36}$$

The term involving $\boldsymbol{\omega}^*$ may be expressed in terms of the tracking voltage components. In order to minimize the complexity, this will be derived for the scalar case, from which the generalization to the vector case is trivial, since all matrices involved are diagonal. Note:

$$\delta^* = \tan^{-1}(\frac{E_D^*}{E_Q^*}). \tag{3.37}$$

Differentiating,

$$\omega^* = \dot{\delta}^* = \frac{-E_Q^*}{E_D^{*2} + E_Q^{*2}} \dot{E}_D^* + \frac{E_D^*}{E^{*2}_D + E^{*2}_Q} \dot{E}_Q^*. \tag{3.38}$$

Going to vector notation and exploiting the commutativity of the diagonal matrices,

$$\begin{aligned} \boldsymbol{\omega}^* &= |\mathbb{E}^*|^{-2} \begin{bmatrix} -\mathbb{E}_Q^* & \mathbb{E}_D^* \end{bmatrix} \begin{bmatrix} \dot{E}_D^* \\ \dot{E}_Q^* \end{bmatrix} \\ &= |\mathbb{E}^*|^{-2} \begin{bmatrix} -\mathbb{E}_Q^* & \mathbb{E}_D^* \end{bmatrix} \left(\begin{bmatrix} \mathbb{E}_D^* \\ \mathbb{E}_Q^* \end{bmatrix} \boldsymbol{\lambda}_{\|}^* + \begin{bmatrix} -\mathbb{E}_Q^* \\ \mathbb{E}_D^* \end{bmatrix} \boldsymbol{\lambda}_{\perp}^* \right) \\ &= \boldsymbol{\lambda}_{\perp}^* \end{aligned} \tag{3.39}$$

By substitution, then,

$$\begin{aligned} \dot{\mathcal{V}}^* &= \mathsf{T}_m^t \boldsymbol{\lambda}_{\perp}^* + \mathsf{Q}^t \boldsymbol{\lambda}_{\|}^* - \mathsf{Q}^* \boldsymbol{\lambda}_{\|}^* - \mathsf{T}_m^t \boldsymbol{\lambda}_{\perp}^* \\ &= (\mathsf{Q}^t - \mathsf{Q}^{*t}) \boldsymbol{\lambda}_{\|}^*. \end{aligned} \tag{3.40}$$

■

This equation relates the change in value of the STEF to the change in the magnitudes of the generator voltages; the increment in "energy" is directly related to the change in magnitude at each generator, and the sign of the increment in energy is de-

termined by the difference between the reactive power at each generator bus and the virtual reactive power that would be supplied if the system were operating at an equilibrium point associated with the instantaneous voltage E. The implications of this will be explored in Chapter 4.

Chapter 4

Kinetic Energy, Potential Energy and Energy-Based Control

4.1 Introduction

Chapter 3 introduced some basic TEFs and began an investigation of the dynamic behavior of Sasaki's TEF when variations in the magnitude of the generator voltages are present. This topic will be explored in more depth in this chapter, and generator excitation control strategies that are based on the dynamic behavior of these functions will be developed. Some work has recently appeared in the literature that addresses Lyapunov-based control of a range of control devices [16]. Excitation control is notably absent from this work, however. Moreover, Lyapunov-based controls typically provide sufficient conditions for stability of a given control, but do not directly address enhancement of the system's ability to survive a more severe disturbance as a result of the control action. Our approach in this chapter will be to use the intuition gained by studying the behavior of some simple energy functions, together with the concept of a time-scale decoupling of control objectives, to guide the control design process.

Two general approaches will be developed in parallel, and will be illustrated and motivated through a series of simulations of a three-machine test system. First, the time-scale separation of control objectives will be made more concrete by defining a set of target states for the short-term control objective. This set will be referred to

as the objective manifold. The short-term control task may then be defined as an effort to minimize some measure of distance from the objective manifold. Second, the control objectives and the system behavior will be related to the interchange between kinetic and potential energy via the gradient of the PE surface. This gives an intuitive understanding of the effect of excitation control on the interchange of PE and KE, providing an understanding of the limitations imposed by input saturation and the implications of saturation on control design. In particular, the mechanisms by which kinetic energy is converted into potential energy and dissipated via control action will be of interest. This interchange is governed by some fundamental structural properties of the power system that are independent of the particulars of the control design, and for this reason, we do not make use of the more complex energy functions that account for the effects of voltage regulators and other devices.

It will be seen that the STEF may be interpreted as a measure of the distance of the state variables from the objective manifold. Therefore if a control is designed to effect the most rapid decrease in the value of the STEF, it can be seen as an effort to drive the system toward the objective manifold as quickly as possible. This leads to a type of control in which the field voltage is forced to its most positive or negative value, depending on some measured signal. This approach is quite similar to the time-optimal control problem, except that maximizing the rate of decline of an energy function in a pointwise manner does not guarantee the most rapid return to zero. The time-optimal control problem has been extensively addressed in the literature [43, 29, 44], via the calculus of variations and the Hamilton-Jacobi-Bellman equations, but except in special cases it has not been solved. In the present case there is the extra dimension that we desire the most rapid return to a *set*, rather than a single point. Therefore we will typically be forced to adopt the pointwise minimization approach. As the simulations will show, however, control based on the STEF has serious shortcomings. An evaluation of simulation results and an assessment of the knowledge gained through this effort will lead to a more effective measure of the short-term control task and a more effective control.

In most cases, the system is closed-loop stable with the controls to be investigated

in this chapter, but the controls vary widely in their influence on the survivability of the system during large system upsets. Lyapunov-based methods for assessing local stability are therefore not emphasized in this chapter; rather, information gleaned from the dynamic behavior of energy functions and their associated regions of stability along system trajectories will be the main focus. In the interest of arriving at some general insights linking the behavior of excitation controls with the time-domain behavior of the TEFs, it will be assumed that a fast (*e.g.* static) exciter is available on each generator, such that the field voltage E_{fd} may be taken directly as a system input. In some sections, a further assumption will be made that $\boldsymbol{\lambda}_{\|}$ is the control signal, since it has a direct algebraic relationship to E_{fd}. This provides a considerable notational and conceptual simplification.

4.2 Time-Scale Separation of Control Objectives via the Objective Manifold

Up to this point, some general observations have been made regarding the time frames over which the objectives of excitation control operate. It has been noted that in the immediate postfault period, the overriding goal is to prevent a system failure by preventing loss of synchronism of the constituent generators. It may be somewhat difficult to confine this objective to a very short time frame, since in many cases generators may be at risk over the course of several seconds and several oscillations of the frequency and rotor angles. Nonetheless, a deviation from desired operating parameters is preferable to an outright failure[1], so that preventing loss of synchronism must be the primary goal as long as the system is at risk. Once the level of risk has been reduced (in a manner yet to be defined), the restoration of a *desirable* operating point becomes the primary goal. Thus, there is a natural prioritization of control objectives that, at least conceptually, could lead to some type of sequential tasking of the controller, *i.e.*,

[1]This is true at least in the sense that other variables such as voltage remain within safe (as opposed to desirable) limits. In many cases such deviations exhibit an inverse-time characteristic, being sustainable in inverse proportion to their severity, so that relatively large deviations may be tolerable provided they are of short duration.

a time-scale separation of objectives. In order to make this more precise, it is necessary to define the conditions under which the transition is made from the primary to the secondary control objective. We consider this transition to occur on a manifold in the state space, and we will refer to it as the *objective manifold.*

Informally, we may observe that the objective manifold should reflect a definitive transition to a condition of less risk. When a disturbance occurs, transient energy is invariably injected into the system. In the COI model, this causes some machines to accelerate and some to decelerate, which in turn increases the difference in rotor angles between accelerating and decelerating machines. If these angle deviations can be kept small, the system will experience little risk. If rotor angle deviations continue to increase, some machines or groups of machines will lose synchronism from others. Consider a point at which the rotor angles are fixed; this implies that $\omega_i = 0$ at each machine, and at this point in time, although the system may not be at equilibrium, the risk is neither increasing nor decreasing. It may also be said that, momentarily at least, the kinetic energy is zero, *i.e.* $\mathcal{V}_{\text{KE}} = 0$. If in addition, $\dot{\omega}_i = 0$ at each machine, then the system is at least marginally secure, since kinetic energy is not being gained by the system and consequently the relative positions of the machine rotors are fixed. Although there may be serious deviations in other variables such as the system voltages, in the absence of a second event there is no immediate risk of losing synchronism. Under these circumstances we say that the system is on the objective manifold. We make this working definition somewhat more precise as follows:

Definition 4.1 *Consider a p-machine power system model of the form*

$$\dot{\mathsf{E}} = \mathsf{f}_e(\mathsf{E}, \boldsymbol{\delta}, \boldsymbol{\omega}, \mathsf{E}_{fd}) \tag{4.1}$$

$$\begin{bmatrix} \dot{\boldsymbol{\delta}} \\ \dot{\boldsymbol{\omega}} \end{bmatrix} = \mathsf{f}_p(\mathsf{E}, \boldsymbol{\delta}, \boldsymbol{\omega}) \tag{4.2}$$

where the vector $\mathsf{E} \in \mathbb{R}^q$ *reflects the electromagnetic subsystem of the chosen machine model, whose dimension may differ depending on the model selected. The* objective

manifold $\mathcal{O}$ *is defined as follows:*

$$\mathcal{O} = \left\{ (\bar{\mathsf{E}},\, \bar{\boldsymbol{\delta}},\, \bar{\boldsymbol{\omega}}) \in \mathbb{R}^q \times \mathbb{R}^p \times \mathbb{R}^p \;\middle|\; \mathsf{f}_p(\bar{\mathsf{E}},\, \bar{\boldsymbol{\delta}},\, \bar{\boldsymbol{\omega}}) = 0 \right\}. \tag{4.3}$$

We also refer to points on the objective manifold as potential equilibria because each point on $\mathcal{O}$ must be associated with a specific value of E_{fd} in order to become an actual equilibrium.

We may now restate our previous observation that the most immediate goal of the excitation control is to restore *some* equilibrium following a fault, in the context of the following time-scale separation of control objectives: We define the *fast objective* as the effort to bring the system state to the objective manifold in the shortest possible time. The *slow objective* is defined as the movement of the system state along the objective manifold to the nominal or desired equilibrium point. In order to achieve both goals via excitation control, we will define a composite control input of the form

$$\mathsf{E}_{fd} = \mathsf{u}_f(\mathsf{x}) + \varepsilon \mathsf{u}_s(\mathsf{x}) \tag{4.4}$$

where the small positive parameter ε reflects the time-scale separation.

4.3 Sasaki's TEF and the Objective Manifold

There is nothing intrinsic in the STEF that distinguishes the desired equilibrium from any of a continuum of equilibria that may arise as continuous perturbations of the nominal equilibrium point when the magnitudes of the machine voltages are allowed to vary. In other words, although the STEF is positive definite (by analogy to the classical TEF) for any fixed set of machine voltage magnitudes, it is also zero for any of the equilibria that may be achieved by continuous perturbation of the magnitudes, provided that the augmented Jacobian matrix $\mathbf{J}_\perp^a$ from (A.25) remains nonsingular[2]. Let $\mathcal{X}_s$ denote the set of equilibria achievable via continuous perturbations of the generator

[2] $\mathbf{J}_\perp^a$ is related to the load flow Jacobian taken with respect to δ, but is modified to alleviate the generic singularity of that matrix.

voltages around the nominal equilibrium x_o over a region in which $\mathbf{J}_\perp^a$ is nonsingular. The inverse function theorem implies that the stable equilibrium point x_s is a smooth, single-valued function of the voltages on $\mathcal{X}_s$, so that x_s may be followed by the tracking variables, and the STEF is well-defined. Clearly, though, the system state coincides with the tracking variables when $\mathsf{x} = \mathsf{x}_s$, so that $\mathcal{V}^*(\mathsf{x}_s) = 0$ for any $\mathsf{x}_s \in \mathcal{X}_s$. The difficulty that may arise when $\mathbf{J}_\perp^a$ is singular is that the tracking variables are not well-defined at those points.

We may use the STEF to define a manifold $\mathcal{O}'$ locally about x_o as follows:

$$\mathcal{O}' = \{\mathsf{x} \in \mathbb{R}_n | \mathcal{V}^*(\mathsf{x}) = 0\}. \tag{4.5}$$

It is not hard to see that $\mathcal{O}'$ is a submanifold of $\mathcal{O}$. Moreover, there exists a neighborhood of x_o such that for all $\mathsf{x} \notin \mathcal{O}'$, $\mathcal{V}^*(\mathsf{x}) > 0$. Therefore we may take $\mathcal{V}^*(\mathsf{x})$ as a local measure of the distance of the system from the objective manifold. In view of this, a Lyapunov-based control that attempts the most rapid reduction of the STEF may be seen as a direct effort to realize the fast control objective. In this light, the failure of the STEF to distinguish between various achievable equilibria in $\mathcal{X}_s$ may be seen as a desirable characteristic that allows an explicit decoupling of the slow and fast objectives.

The form of (3.40) suggests an attractive possibility. As will presently be shown, the value of $\boldsymbol{\lambda}_\parallel$ is directly related to the generator field voltage, E_{fd}. From (3.40), it is clear from Claim 3.1 that if the elements of $\boldsymbol{\lambda}_\parallel$ are subject to magnitude bounds, then we may maximize the rate of decline of the STEF by setting

$$\lambda_{\parallel i} = \begin{cases} \lambda_{\max} \;\; ; \;\; (Q_i - Q_i^*) \;\; < \;\; 0 \\ \lambda_{min} \;\; ; \;\; (Q_i - Q_i^*) \;\; > \;\; 0\,. \end{cases} \tag{4.6}$$

This minimization of $\dot{\mathcal{V}}^*(\mathsf{x})$ is not equivalent to a time-optimal control, since it is done pointwise, but it is conceptually simple and Q_i at least is a locally-measurable quantity, *i.e.* it can be measured at each generating site, without relying on information from geographically distant parts of the system.

In order to implement this control, it is also necessary to calculate the value of Q^*. This may be done using the dynamic model of (A.27), which essentially computes the load-flow solution of the system, given the input torques to the machines and the current magnitudes of the machine voltages. This of course requires measurements or estimates of the relevant voltages, as well as complete knowledge of the grid and load admittances, which is not practical with the current level of technology. The type of bang-bang control suggested by (4.6) must therefore be viewed as an academic exercise, in the sense that it is approached in this thesis as a vehicle for obtaining knowledge about the interaction of excitation control with the system energy as expressed by the STEF. If it were desired to use the value of Q^* as a measured output for the purpose of control, however, it might be possible to estimate its value locally (again in the geographic sense) using a process similar to the observation decoupled state-space method of [8], but this is beyond the scope of this document.

Note that, from the definition of $\boldsymbol{\lambda}_{\|}$ in (3.23) and in view of (2.7) and (2.9), one may deduce that

$$\begin{aligned} \lambda_{\|i} &= \frac{E'_{q_i}}{T'_{do}}(-E'_{q_i} - (x_{i_i} - x'_{d_i})i_{d_i} + E_{fd_i}) \\ &= f_{e_i}(\mathsf{x}) + \frac{E'_{q_i}}{T'_{do_i}}E_{fd_i}. \end{aligned} \tag{4.7}$$

Since $f_{e_i}(\mathsf{x})$ does not depend on the state derivatives (*i.e.* it is independent of the value of E_{fd}) and E'_{q_i} is invariably positive, it is clear that $\lambda_{\|_i}$ is maximized by maximizing E_{fd_i}, so (4.6) is realized by setting

$$E_{fd_i} = \begin{cases} E_{fd\_\max} & ; \quad (Q_i - Q_i^*) < 0 \\ E_{fd\_\min} & ; \quad (Q_i - Q_i^*) > 0 \end{cases} \tag{4.8}$$

This control law guarantees that $\dot{\mathcal{V}}^*(\mathsf{x})$ is always negative, provided that the magnitude of the field voltage saturation limits are broad enough to allow E_{fd} to dominate $f_e(\mathsf{x})$ along any system trajectory. Even when this is not true, however, this control always minimizes the time derivative of $\mathcal{V}^*$.

Therefore, since the value of the STEF is bounded below and $\mathcal{V}^*(\mathsf{x}) = 0$ only if $\mathsf{x} \in \mathcal{O}'$ one would expect that this control would always return the system to the objective manifold. Driving the STEF to zero thus explicitly achieves the fast objective. Since the STEF does not differentiate between points on $\mathcal{O}'$, however, it will clearly be necessary to augment the control in some manner in order to achieve the slow objective. This might be done by adding some type of supplemental voltage control, or by modifying the STEF to account for the slow objective in some way. It is instructive nonetheless to investigate the behavior of an STEF-based control, so at this point a three-machine test model will be introduced for the purpose of simulating this control and others to follow.

4.4 A Test Model for Energy-Based Control

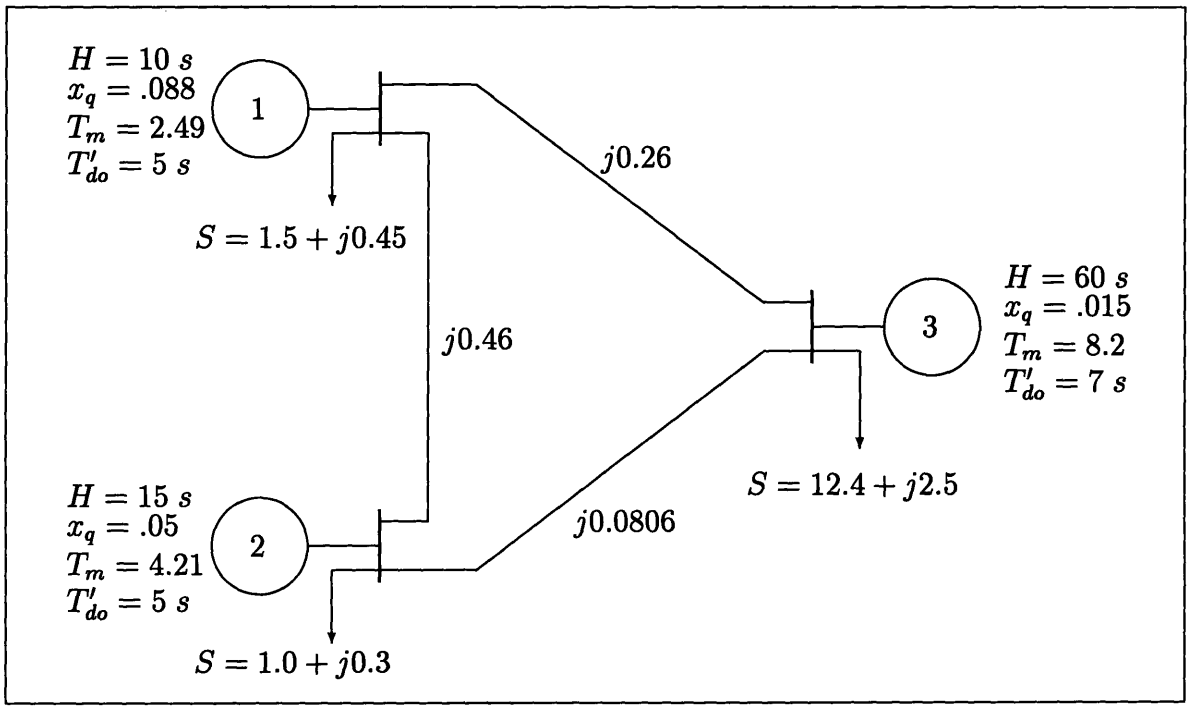

Figure 4.1: 3-Machine Test System.

Figure 4.1 is a schematic of a three-machine model that will be used throughout the chapter to illustrate the concepts that are developed. This model was introduced in [4], and subsequently has appeared elsewhere in the literature. The bus loads are of the

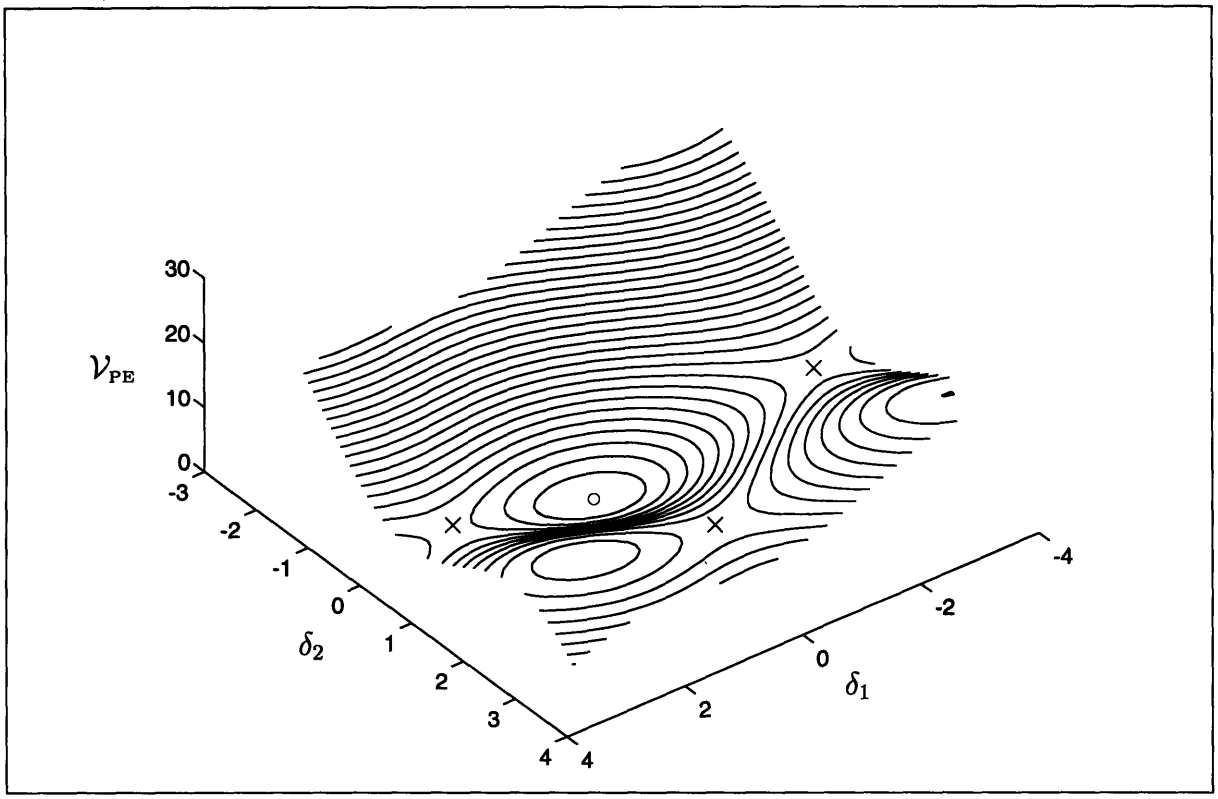

Figure 4.2: Classical-Model Potential Energy Surface.

constant-impedance type. For this chapter, the model has been modified to convert it to a lossless model. This was done by reducing the admittance matrix, setting the real part of the admittance matrix to zero, and subtracting the nominal power dissipated by the conductances on the matrix diagonal from the input torque of the associated generator. For the simulations, when a ground fault is applied to the terminal bus of a particular generator, the input torque is adjusted to account for the fact that the constant-power load at that bus would be lost for the period of the fault. Note that, since the terminal bus is not preserved in the admittance matrix, it is necessary to create a full admittance matrix for the faulted and postfault system, and then reduce them separately.

Since $\mathcal{V}_{\rm PE}$ is independent of the frequency, it is possible to plot the potential energy in a three-dimensional mesh plot, as a function of two of the three rotor angles. Recall that in the COI frame of reference, $\sum_{i=1}^{p} \frac{m_i}{m_{\rm T}} \delta_i = 0$, so the rotor angles are subject to an algebraic constraint and only two of the three rotor angles are required to completely

characterize $\mathcal{V}_{\text{PE}}$. The potential energy surface represents the system energy in the special case in which the frequency of all machines is at 0. Note also that the extrema of the potential energy surface represent points at which the load-flow equations are satisfied, that is, points at which $\mathsf{P}_e = \mathsf{T}_m$. Since any system equilibrium point requires that $\boldsymbol{\omega} = 0$ and $\mathsf{P}_e = \mathsf{T}_m$, the extrema of the potential energy surface represent system equilibria, at least for the classical model. For the STEF, where the machine voltages may vary, the extrema represent equilibria only if the machine voltage magnitudes are also at equilibrium.

The potential energy surface for the test system with the classical model is shown in the contour plot of Figure 4.2. Note that the stable equilibrium (marked with an "o") exists at a minimum of this function, and there are also three other "saddle" equilibria (marked with "×") evident in the plot. It is tempting to consider the energies associated with the saddle equilibria as critical energies with respect to the transient stability of the system, but the connection is far from direct, since the actual stability boundary does not always pass through the "boundary" equilibria on the potential energy surface [31, 39, 11]. In this document, our main concern will be with the *slope* of the potential energy surface and its influence on the acceleration of the machine rotors and the conversion of KE to PE.

For most of the work in this chapter, the fault that is simulated (referred to hereafter as case 1) is a three-phase ground fault at bus 1, with fault impedance $j10^{-6}$, followed by the tripping of line 1-2. The fault is applied at $t_1 = 0.04$ sec., and cleared at a time t_2 whose value varies depending on the simulation. Because the fault is not applied at $t = 0$, the fault clearing time is calculated as $t_{c\ell} = t_2 - t_1$. The critical clearing time, t_{cr}, is defined as the maximum value of $t_{c\ell}$ for which the system returns to an acceptable equilibrium.

For the purpose of comparison, we first present a baseline simulation of case 1, using the classical model, with $t_{cr} \approx t_{c\ell} = 0.191$ sec. The rotor-angle response is plotted in Figure 4.3, and the transient energy as expressed by the STEF is plotted in Figure 4.4 (solid line), along with the kinetic and potential components, $\mathcal{V}_{\text{KE}}$ and $\mathcal{V}_{\text{PE}}$ (dashed and dash-dot plots, respectively). The transient energy is constant for the entire postfault

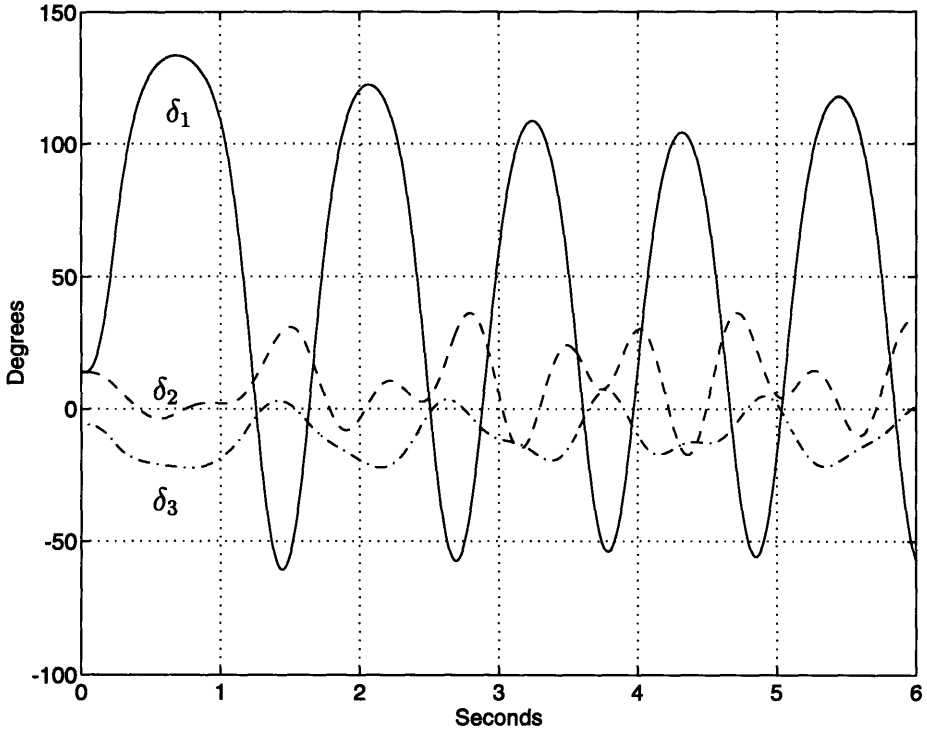

Figure 4.3: Case 1: Classical model rotor angle response.

period, as would be expected for the lossless, constant-voltage model, while the kinetic and potential energy display the Hamiltonian relationship $\dot{\mathcal{V}}_{\text{KE}} = -\dot{\mathcal{V}}_{\text{PE}}$.

As a comparison, Figures 4.5 through 4.7 are plots of the same system, this time using a single-axis model with constant field excitation. Because of flux decay, the critical clearing time is significantly shorter, approximately 0.176 sec.

4.5 Mechanisms for Energy Conversion

For the classical TEF in a lossless system, $\dot{\mathcal{V}}(\mathsf{x}) \equiv 0$. Hence the system is conservative with respect to the classical TEF, which is not surprising since the classical TEF was derived as the first integral of the lossless classical model. It must therefore be true that $\dot{\mathcal{V}}_{\text{KE}}(\mathsf{x}) = -\dot{\mathcal{V}}_{\text{PE}}(\mathsf{x})$, and indeed, consideration of (3.8) reveals that

$$\dot{\mathcal{V}}_{\text{KE}} = \boldsymbol{\omega}^t \mathbb{M} \boldsymbol{\omega} = (\mathsf{T}_m - \mathsf{P}_e)^t \boldsymbol{\omega}. \tag{4.9}$$

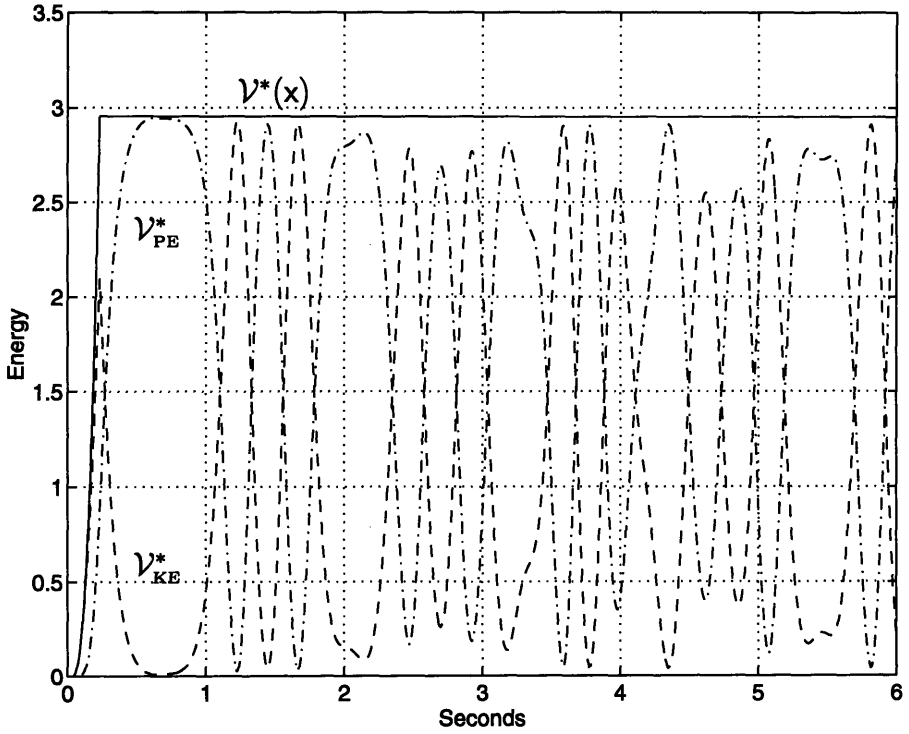

Figure 4.4: Case 1: Transient, Kinetic and Potential Energy.

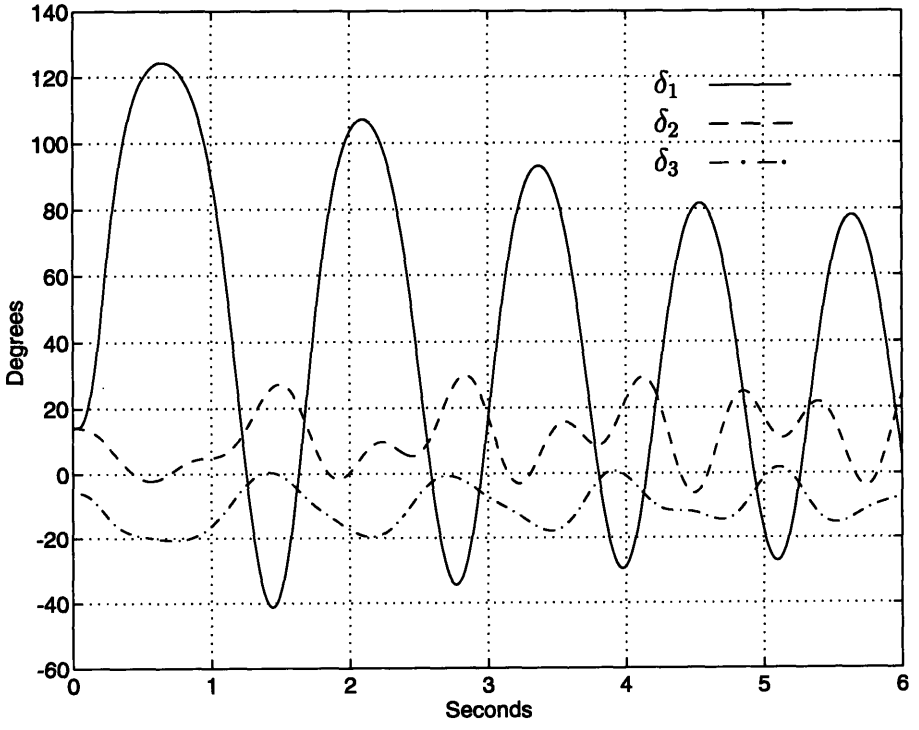

Figure 4.5: Case 1 Rotor Angle: Single-Axis, Constant Excitation.

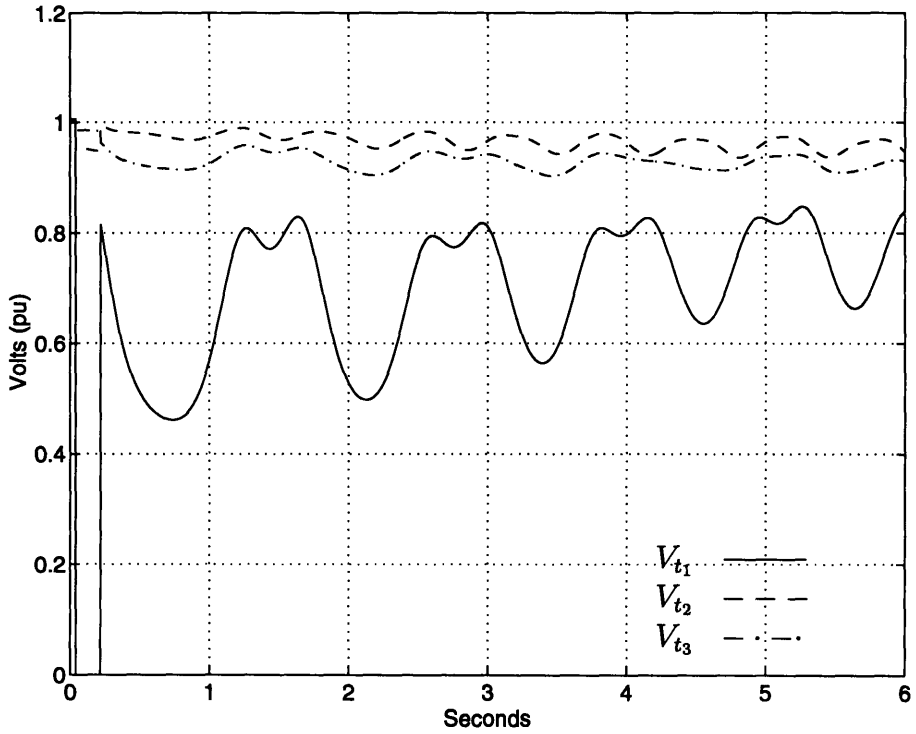

Figure 4.6: Case 1 Terminal Voltage: Single-Axis, Constant Excitation.

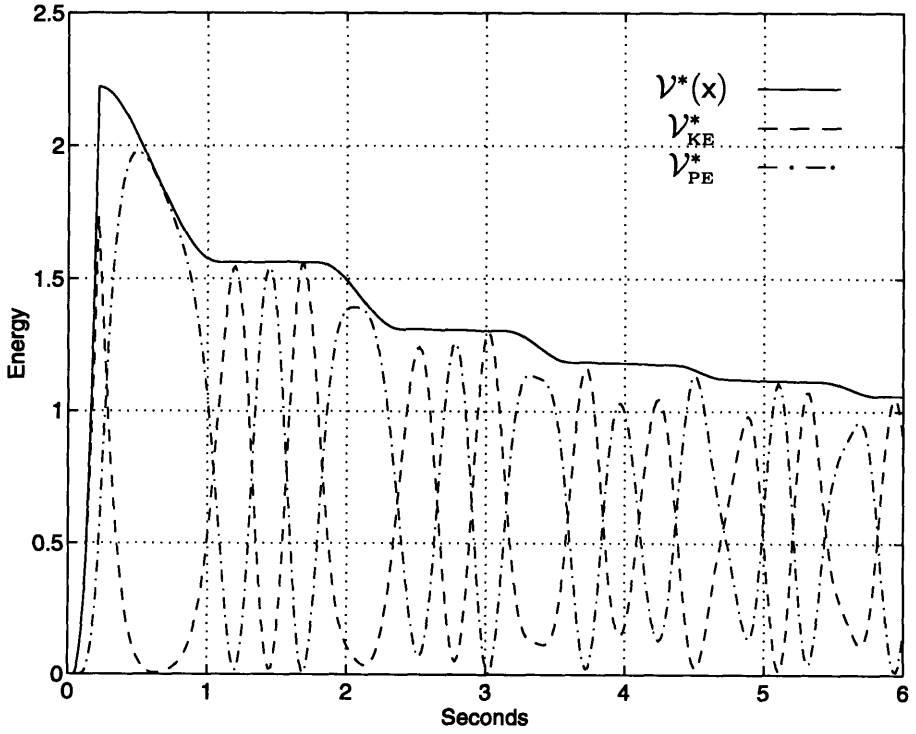

Figure 4.7: Case 1 TEF: Single-Axis, Constant Excitation.

With a little more effort it may be shown algebraically that $\dot{\mathcal{V}}_{\text{KE}} = -\dot{\mathcal{V}}_{\text{PE}}$, as Figure 4.4 suggests. When the damping coefficients are greater than zero we have

$$\dot{\mathcal{V}}_{\text{KE}} = (\mathsf{T}_m - \mathsf{P}_e - \mathbb{D}\boldsymbol{\omega})^t\boldsymbol{\omega}. \tag{4.10}$$

The form of (4.10) suggests that

$$\frac{\partial \mathcal{V}_{\text{KE}}}{\partial \boldsymbol{\delta}} = (\mathsf{T}_m - \mathsf{P}_e - \mathbb{D}\boldsymbol{\omega})^t, \tag{4.11}$$

which may be verified for the more general Luré form where

$$\begin{aligned} \dot{\mathsf{x}}_1 &= \mathsf{x}_2 \\ \dot{\mathsf{x}}_2 &= \mathsf{f}(\mathsf{x}_1, \mathsf{x}_2). \end{aligned} \tag{4.12}$$

For any symmetric matrix $\mathbf{N}$,

$$\begin{bmatrix} \dot{\mathsf{x}}_2^t\mathbf{N} & -\dot{\mathsf{x}}_1^t\mathbf{N} \end{bmatrix} \begin{bmatrix} \dot{\mathsf{x}}_1 \\ \dot{\mathsf{x}}_2 \end{bmatrix} = 0, \tag{4.13}$$

which implies the equality of the path integrals,

$$\int_{\mathsf{x}_1(0)}^{\mathsf{x}_1(t)} \mathsf{f}(\mathsf{x}_1, \mathsf{x}_2)^t\mathbf{N}\, d\mathsf{x}_1 = \int_{x_2(0)}^{\mathsf{x}_2(t)} \mathsf{x}_2^t\mathbf{N}\, d\mathsf{x}_2 = \frac{1}{2}\mathsf{x}_2^t\mathbf{N}\mathsf{x}_2, \tag{4.14}$$

hence, along system trajectories,

$$\frac{\partial}{\partial \mathsf{x}_1}\mathsf{x}_2^t\mathbf{N}\mathsf{x}_2 = \mathsf{f}(\mathsf{x}_1, \mathsf{x}_2)^t\mathbf{N}. \tag{4.15}$$

For Sasaki's TEF the energy exchange situation is somewhat different. We must again insert the disclaimer that the "potential" energy terms with respect to the STEF are not cleanly related to a physical energy. We will, however, continue to refer to any terms other than kinetic energy as potential energies. Thus, we define

$$\mathcal{V}_{\text{PE}}^* = -\mathsf{T}_m'(\boldsymbol{\delta} - \boldsymbol{\delta}^*) + \frac{1}{2}(Q_{\text{tot}} - Q_{\text{tot}}^*), \tag{4.16}$$

which facilitates the statement of the following claim:

Claim 4.1 *With respect to the STEF, field voltage control directly affects* only *the time rate of change of* $\mathcal{V}^*_{\text{PE}}$. $\dot{\mathcal{V}}_{\text{KE}}$ *is invariant to changes in the field voltage.*

Proof:

The second part is direct from (4.10), since P_e does not depend on E_{fd}. For the first part, using the form of (2.63) for Q_{tot} and Q^*_{tot},

$$\dot{\mathcal{V}}^*_{\text{PE}} = \mathsf{T}'_m(\boldsymbol{\omega} - \boldsymbol{\omega}^*) + \begin{bmatrix} \mathsf{E}^t_{\text{D}} & \mathsf{E}^t_{\text{Q}} \end{bmatrix} \underline{\underline{\mathbf{B}}} \begin{bmatrix} \dot{\mathsf{E}}_{\text{D}} \\ \dot{\mathsf{E}}_{\text{Q}} \end{bmatrix} - \begin{bmatrix} \mathsf{E}^{*t}_{\text{D}} & \mathsf{E}^{*t}_{\text{Q}} \end{bmatrix} \underline{\underline{\mathbf{B}}} \begin{bmatrix} \dot{\mathsf{E}}^*_{\text{D}} \\ \dot{\mathsf{E}}^*_{\text{Q}} \end{bmatrix}. \tag{4.17}$$

Separating the parallel and perp components of this expression, we have

$$\begin{aligned} \dot{\mathcal{V}}^*_{\text{PE}} \;=\; & -\mathsf{T}_m(\boldsymbol{\omega} - \boldsymbol{\omega}^*) + \underbrace{\begin{bmatrix} \mathsf{E}^t_{\text{D}} & \mathsf{E}^t_{\text{Q}} \end{bmatrix} \underline{\underline{\mathbf{B}}} \begin{bmatrix} \mathbb{E}_{\text{D}} \\ \mathbb{E}_{\text{Q}} \end{bmatrix}}_{\mathsf{Q}^t} \boldsymbol{\lambda}_{\parallel} + \underbrace{\begin{bmatrix} \mathsf{E}^t_{\text{D}} & \mathsf{E}^t_{\text{Q}} \end{bmatrix} \underline{\underline{\mathbf{B}}} \begin{bmatrix} -\mathbb{E}_{\text{Q}} \\ \mathbb{E}_{\text{D}} \end{bmatrix}}_{\mathsf{P}^t_e} \boldsymbol{\lambda}_{\perp} \\ & - \underbrace{\begin{bmatrix} \mathsf{E}^{*t}_{\text{D}} & \mathsf{E}^{*t}_{\text{Q}} \end{bmatrix} \underline{\underline{\mathbf{B}}} \begin{bmatrix} \mathbb{E}^*_{\text{D}} \\ \mathbb{E}^*_{\text{Q}} \end{bmatrix}}_{\mathsf{Q}^{*t}} \boldsymbol{\lambda}_{\parallel} + \underbrace{\begin{bmatrix} \mathsf{E}^{*t}_{\text{D}} & \mathsf{E}^{*t}_{\text{Q}} \end{bmatrix} \underline{\underline{\mathbf{B}}} \begin{bmatrix} -\mathbb{E}^*_{\text{Q}} \\ \mathbb{E}^*_{\text{D}} \end{bmatrix}}_{\mathsf{P}^{*t}_e = \mathsf{T}_m} \boldsymbol{\lambda}^*_{\perp}. \end{aligned} \tag{4.18}$$

Grouping terms, transposing some quantities and recognizing that for the lossless single-axis model, $\boldsymbol{\lambda}_{\perp} = \boldsymbol{\omega}$, $\boldsymbol{\lambda}^*_{\perp} = \boldsymbol{\omega}^*$ yields

$$\dot{\mathcal{V}}^*_{\text{PE}} = -(\mathsf{T}_m - \mathsf{P}_e)^t \boldsymbol{\omega} + (\mathsf{Q} - \mathsf{Q}^*)^t \boldsymbol{\lambda}_{\parallel} \tag{4.19}$$

Since the value of $\boldsymbol{\lambda}_{\parallel}$ is directly related to the field voltage response of the generators, (4.19) makes it clear that field voltage control has a direct influence *only* on $\dot{\mathcal{V}}^*_{\text{PE}}$. ∎

Claim 4.1 makes it clear that in order for the control to have an effect on $\mathcal{V}_{\text{KE}}$, the kinetic energy must first be converted to potential energy. To the extent that the action of the control prevents conversion of accumulated PE back into KE, this energy may be considered to have been dissipated. In fact, in the lossless system, this "dissipation"

is actually the result of a redirection of differences in the relative frequencies of the various generators into a uniform increment in the frequency at each machine, which vanishes in the COI model. This increment is not seen in the plots presented in this thesis, since they are all plotted in COI. If the machine angles were plotted with respect to an arbitrary fixed reference, the "steady-state" in each case would show a steady, uniform increase in the rotor angle at each machine.

Although field voltage control does not directly affect the rate of change of the KE, it does have a crucial effect on the manner and rate at which the conversion to PE takes place, since it affects the gradient of the potential energy surface with respect to $\boldsymbol{\delta}$, which in conjunction with the machine frequencies determines the rate of conversion of KE to PE. Examination of (4.19) reveals that for the lossless STEF, as for the classical TEF,

$$\frac{\partial \mathcal{V}_{\mathrm{KE}}}{\partial \boldsymbol{\delta}} = -\frac{\partial \mathcal{V}_{\mathrm{PE}}}{\partial \boldsymbol{\delta}} = (\mathsf{T}_m - \mathsf{P}_e)^t, \tag{4.20}$$

which is just the slope of the PE surface for a fixed set of generator voltages. Henceforth the gradient taken with respect to $\boldsymbol{\delta}$ will be referred to simply as the gradient, ignoring the fact the the PE surface also depends on the machine voltages, since we will typically be concerned with the topology of the PE surface for a given fixed set of voltages, and we will use the notation $\nabla_{\delta}\mathcal{V}^*_{\mathrm{PE}}$ to express it.

4.5.1 Simulations of the Steepest-Descent Control

The performance of the steepest-descent control will be examined here via two simulations: case 1a is a very minor instance of case 1, cleared in only 0.02 sec. case 1b is the same fault, with a slightly longer clearing time of 0.06 seconds. An approximate implementation of the bang-bang control is used, where $(Q - Q^*)$ appears as an input, multiplied by a gain of -200, followed by a saturation block that limits the magnitude of E_{fd} to 4.5 pu. A small dead zone of $\pm 5 \times 10^{-4}$ is also used on $(Q - Q^*)$. The signal $\tilde{E}_{fd} = E'_q + (x_d - x'_d)i_d$ is an offset signal which ensures that $\lambda_{\|_i} = 0$ when $Q_i - Q_i^* = 0$. This subsystem, as implemented in the Simulink package by The Mathworks, is illustrated in Figure 4.8.

Figure 4.9 shows the rotor angle response (solid lines), compared with the trajectory of the virtual equilibrium (dashed lines) that would exist if the instantaneous magnitude of the machine voltages were fixed. Note that the virtual equilibrium moves rapidly toward the system trajectory, so that it nearly coincides with the actual machine angles shortly after the fault clears. It appears that the steepest descent control acts most directly to move the virtual equilibrium point, rather than bringing the machine angles back to the original equilibrium point. The magnitude of the angle deviation from the original equilibrium point is out of proportion to the magnitude of the fault, and this condition is maintained in more severe faults, with the result that the critical clearing time of the system is seriously reduced. Moreover, consistent with the shift in the system equilibrium, the terminal voltages are depressed well beyond acceptable operating limits and do not recover following the fault, as shown in Figure 4.10. Thus, the most rapid reduction of the system energy does not lead to more secure operation, but indeed achieves the reverse. Figure 4.11 illustrates the transient, kinetic and potential energies (solid, dashed and dash-dot curves, respectively).

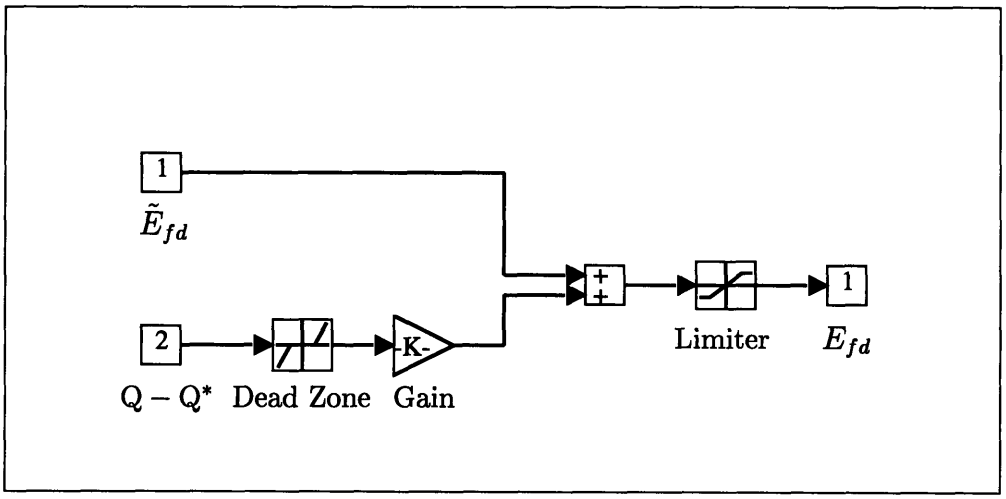

Figure 4.8: Steepest-Descent Excitation Implementation.

The transient energy curve bears out the fact that the energy declines rather rapidly, approaching zero in about two seconds. The kinetic component accounts for almost all of the transient energy at fault clearing. The potential energy initially rises slightly, as KE is converted to PE, but the fact that the total PE never approaches the peak value

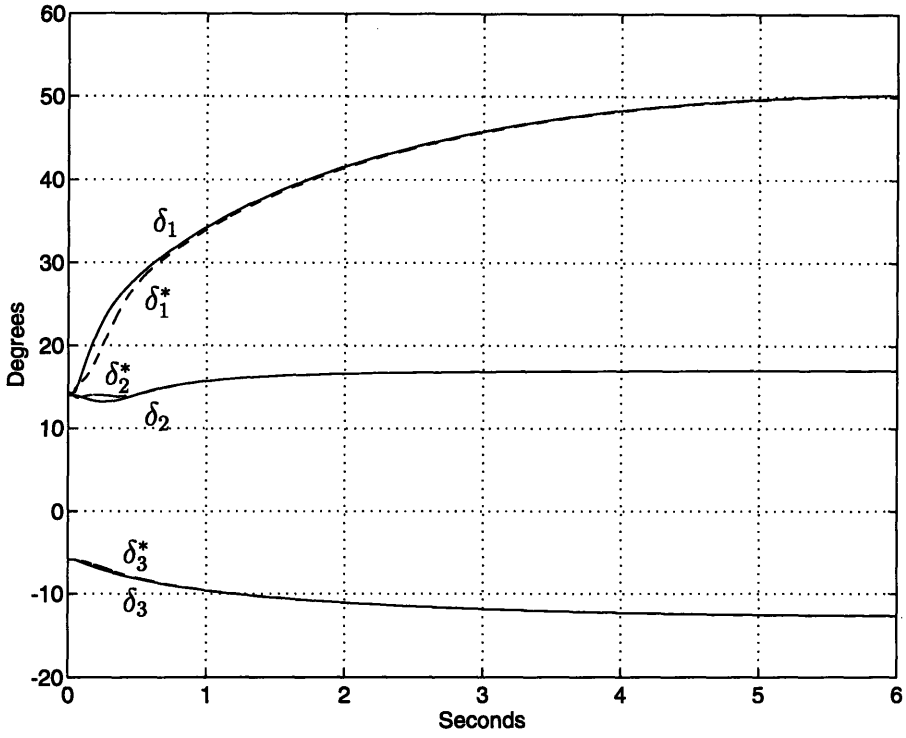

Figure 4.9: Case 1a: Rotor Angles for Steepest-Descent Control.

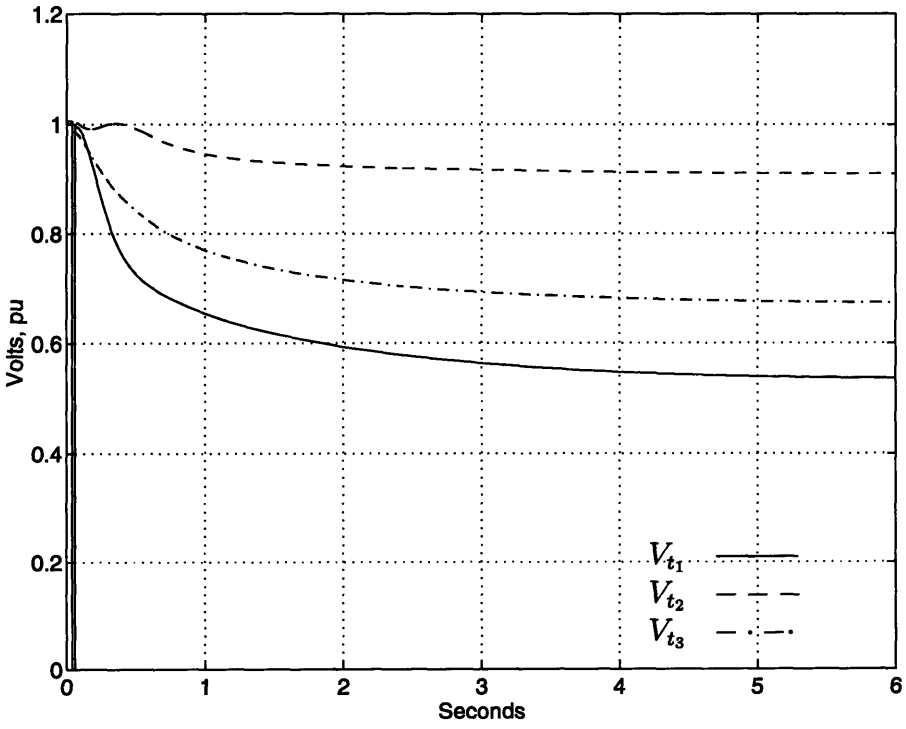

Figure 4.10: Case 1a: Terminal Voltages for Steepest-Descent Control.

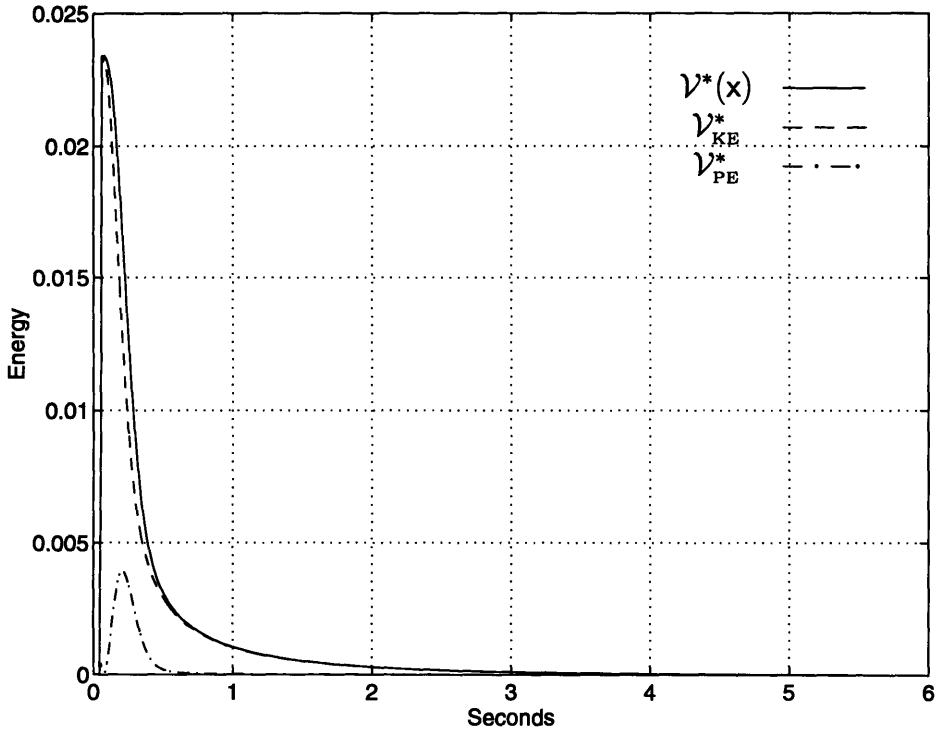

Figure 4.11: Case 1a: Transient, Kinetic, Potential Energy for Steepest-Descent Control.

of the KE indicates that PE is being continuously dissipated.

The potential energy surface is plotted in Figures 4.12 and 4.13, the latter of which is an enlargement of the former, showing the angle trajectory. Note the flattening of the region of attraction, as compared to Figure 4.2. The rotor angle trajectories are also shown, with the initial point denoted by an "o" and the final point denoted by an "×". Because of the variation in machine voltages (and attendant warping of the potential energy surface), only the endpoint of the trajectory actually lies on the PE surface. The initial rise and sharp decline in the PE are evident in the system path.

A more telling example of the steepest-descent control is presented in Figures 4.14 through 4.16. In these simulations, the fault clearing time is somewhat longer than the previous example, but is still comparatively short at 0.06 sec. The abrupt change in system behavior that is seen in Figure 4.14 is the result of the fact that the "tracking" voltages actually jump to a different load-flow solution at that point. Once again, the virtual equilibrium angles as followed by the tracking voltages are plotted as dashed

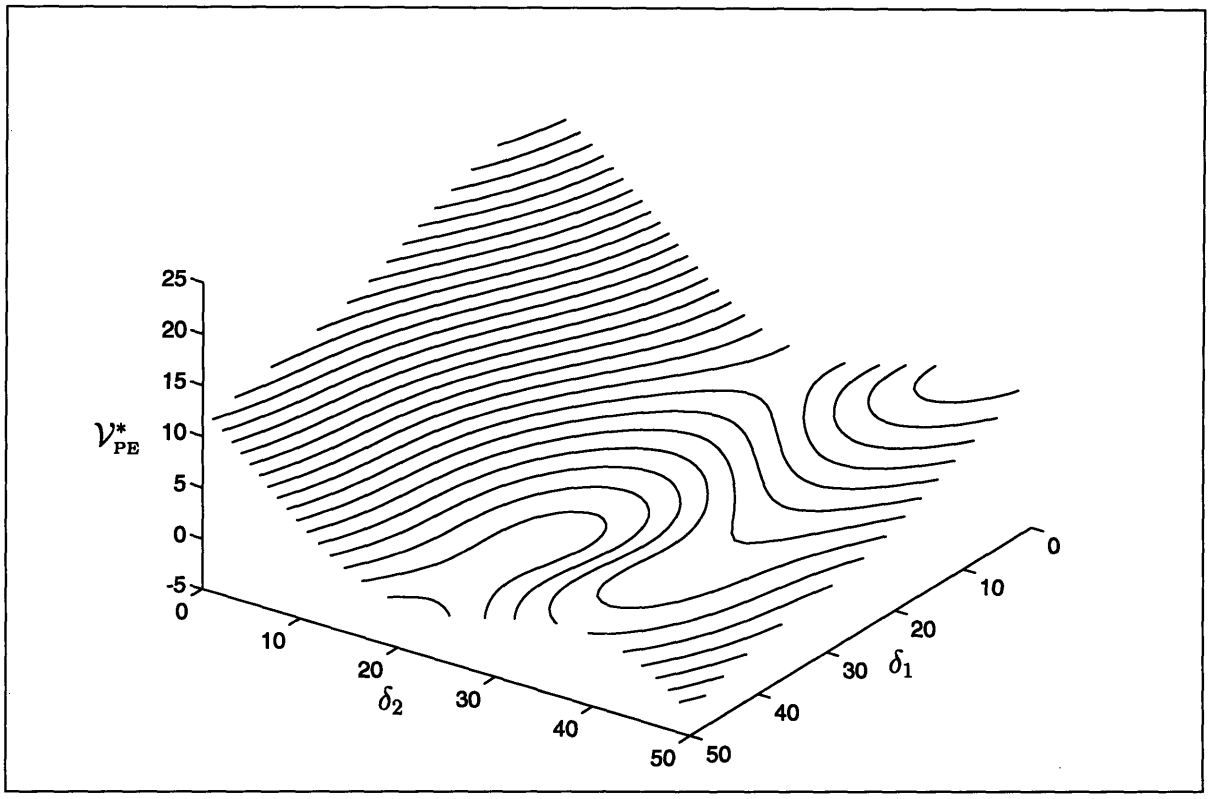

Figure 4.12: Case 1a PE Surface, Steepest-Descent Control at t = 6 sec.

lines. The point at which the solution changes is quite evident. What is actually happening is that, because of the depression in the system voltages, the stable equilibrium point draws near to an unstable equilibrium in an incipient saddle-node bifurcation.

In a saddle-node bifurcation, a stable and unstable equilibrium approach each other as a system parameter is varied, (in this case the variation is in the generator voltages). The bifurcation point is the point at which the equilibria actually meet. If the variation of the parameters proceeds past this point, the equilibrium vanishes altogether. In the present case, as the system approaches the bifurcation point, the numerical error in the calculation causes the "tracking" voltages to jump to the unstable equilibrium. Following the point at which the tracking voltages jump to the unstable equilibrium, the system no longer tracks the STEF *per se*, but acts to minimize an analogous function defined with respect to an unstable equilibrium. Because this new function is not positive-definite, its value becomes increasingly negative. The control continues to effect the most rapid decline in the transient energy, but when defined with respect to

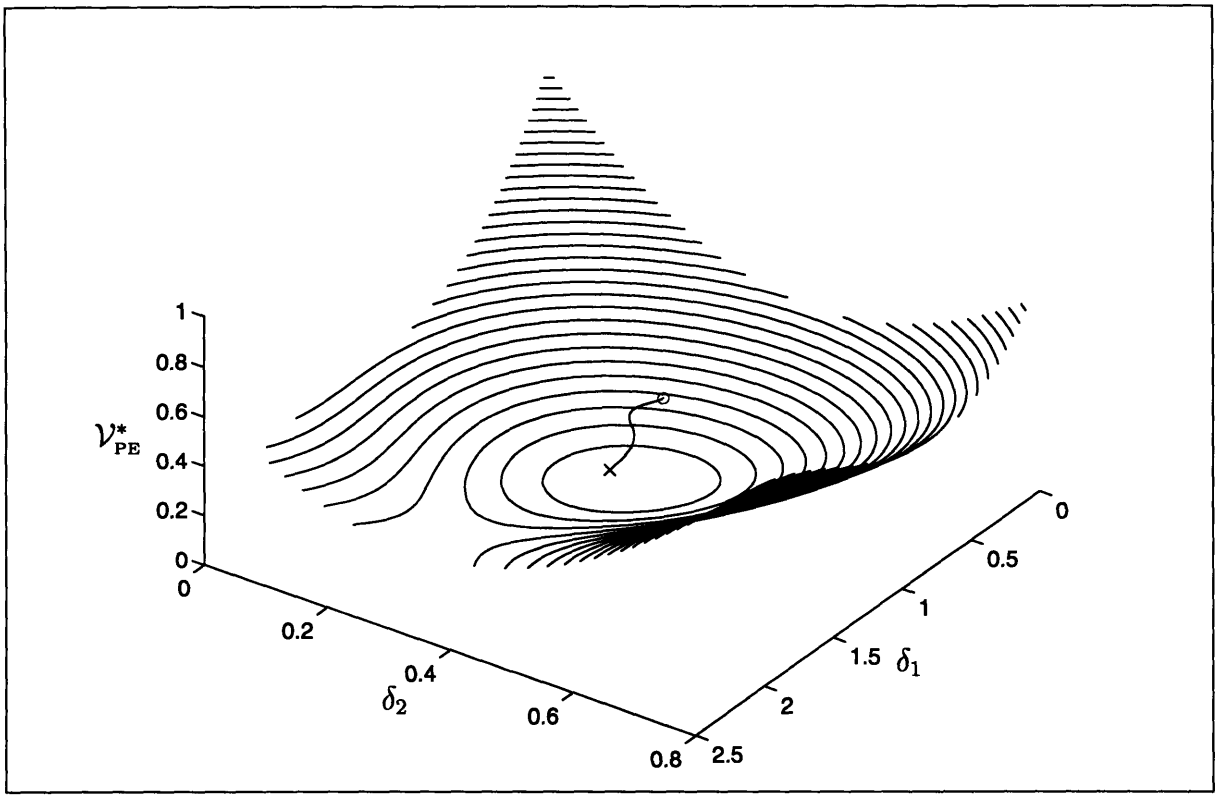

Figure 4.13: Case 1a PE Surface, Steepest-Descent Control at t = 6 sec.

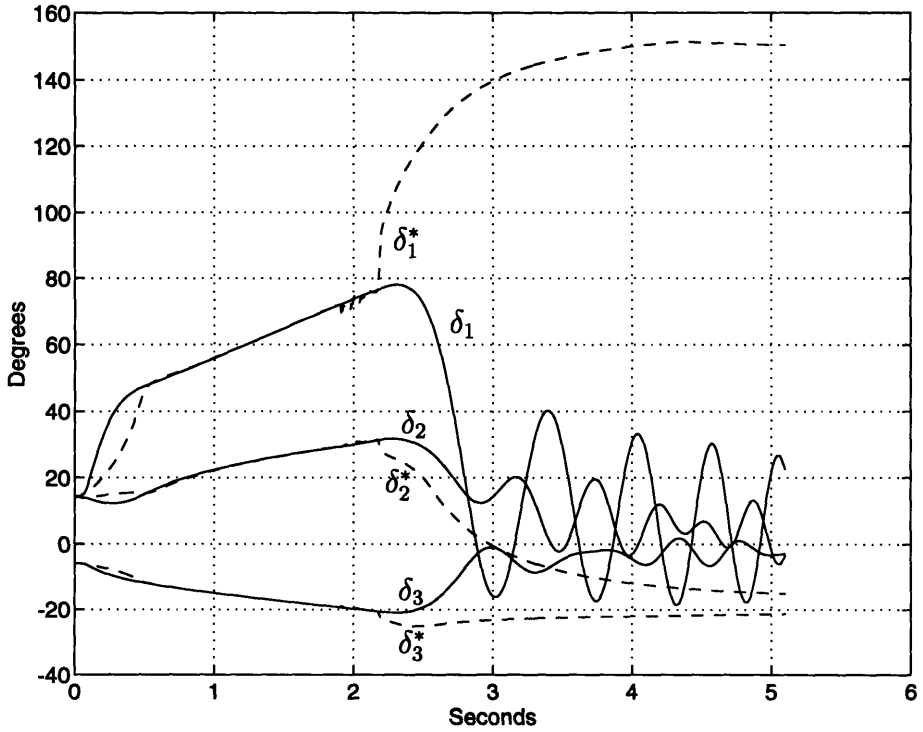

Figure 4.14: Case 1b: Rotor Angles for Steepest-Descent Control.

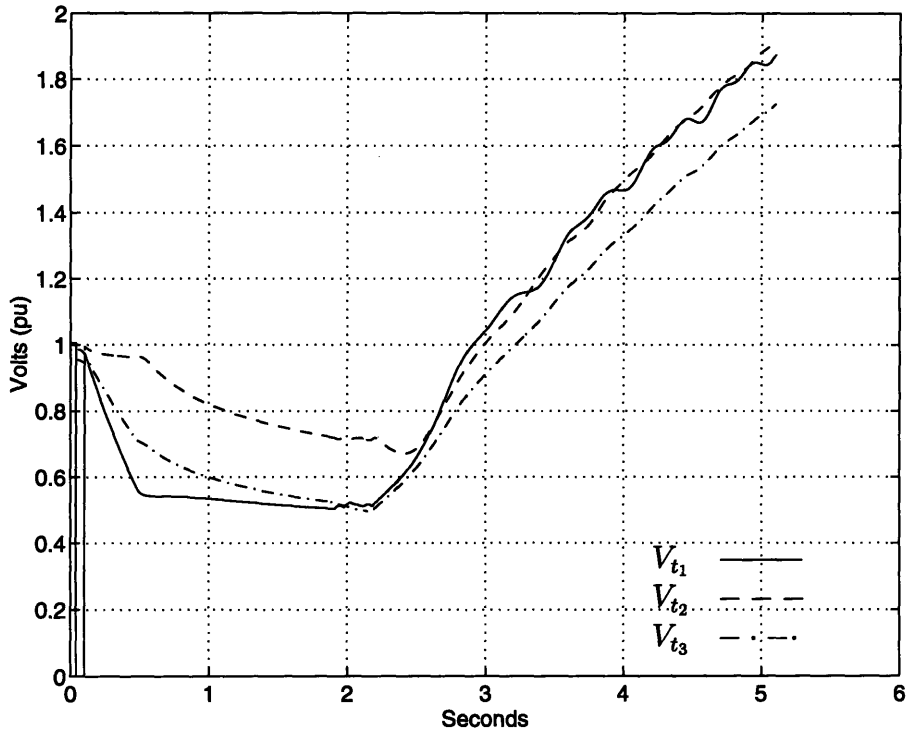

Figure 4.15: Case 1b: Terminal Voltages for Steepest-Descent Control.

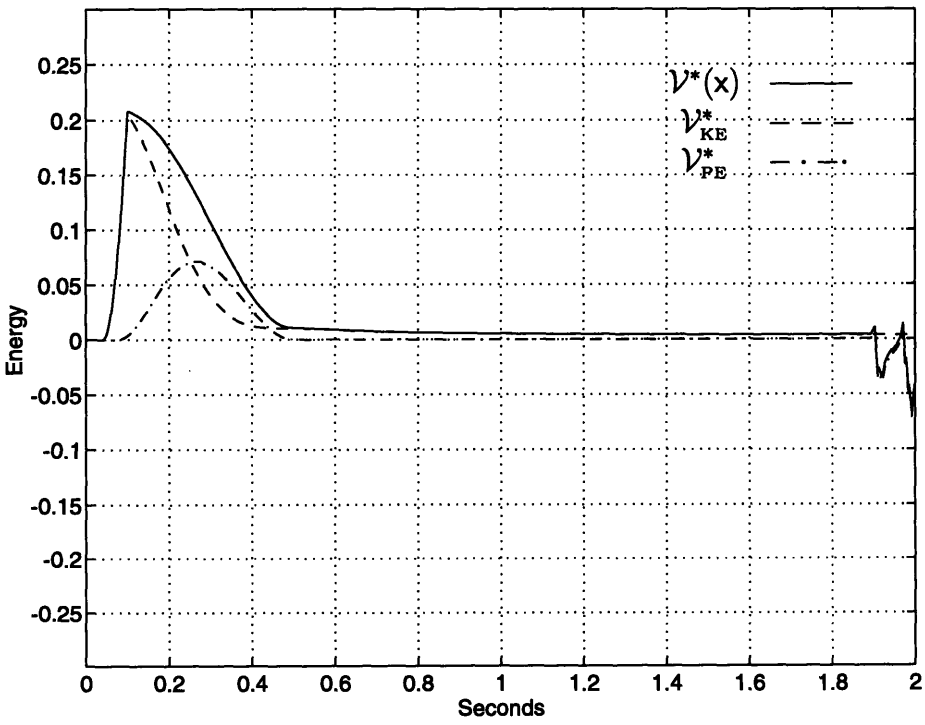

Figure 4.16: Case 1b: Transient, Kinetic, Potential Energy for Steepest-Descent Control.

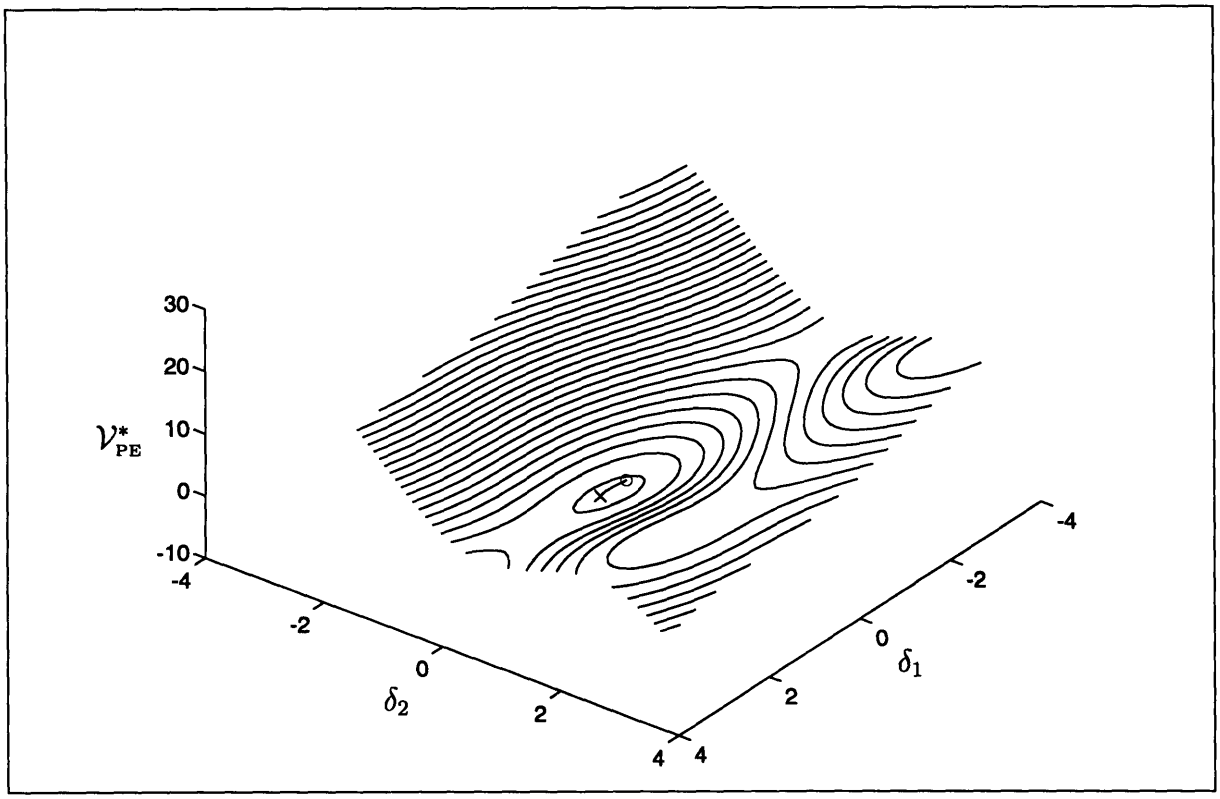

Figure 4.17: Case 1b PE Surface, Steepest-Descent Control at t = 0.4 sec.

an unstable equilibrium, the new energy function is not bounded below. The control acts to push this defective STEF to increasingly negative values, driving the system *away* from the unstable equilibrium. Obviously, this radically changes the character of the control, causing the behavior displayed in the second half of the simulation. Note the instability in the value of $\mathcal{V}^*_{PE}$ which is caused by oscillation in the value of the tracking voltages at $t = 1.9$, a point at which the load-flow Jacobian is very close to singular.

The time axis of the transient energy plot (Figure 4.16) is limited to the first 2 seconds to capture the behavior in the first part of the simulation. Note that the control does indeed reduce the value of the STEF in very short order to a value close to zero. As in case 1b, however, this does not result in an increase in the transient stability margin of the system. Rather, as one might expect in retrospect, it acts most directly to reduce potential energy of the system associated with whatever rotor angle the system happens to assume along its trajectory. In doing this, the gradient of the

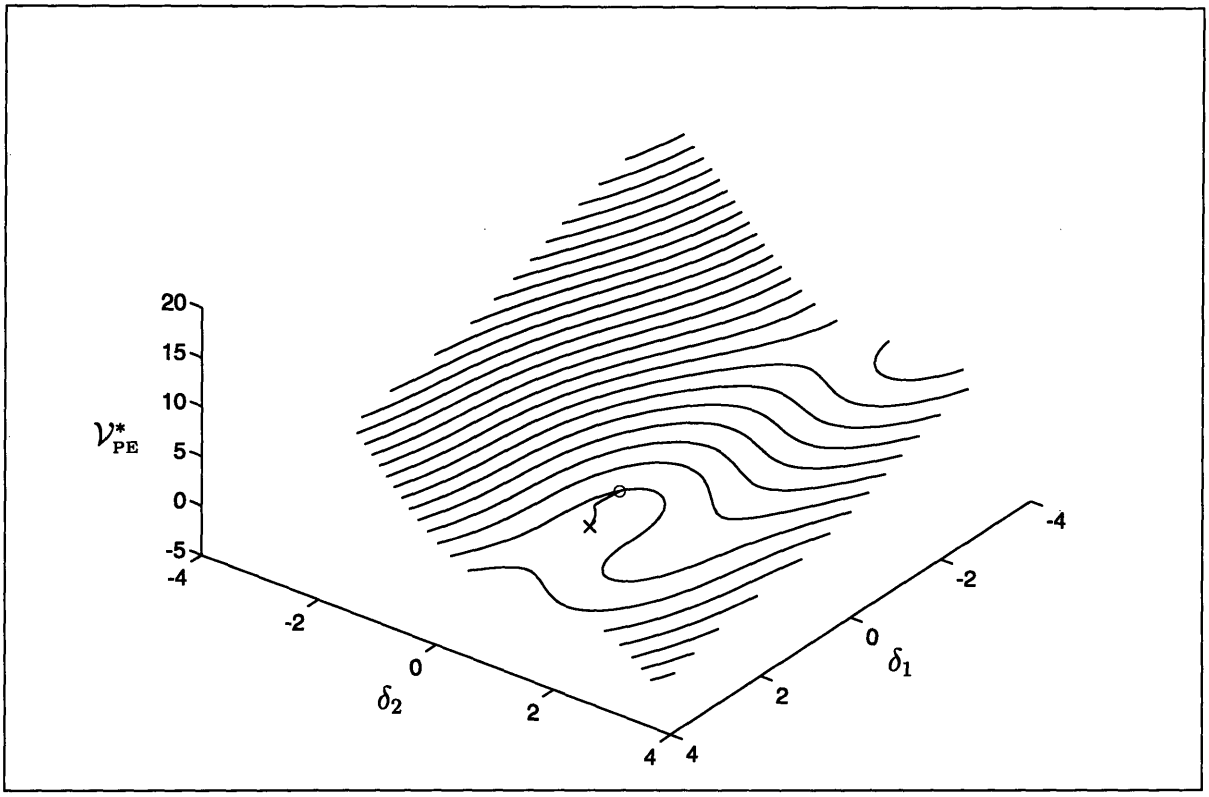

Figure 4.18: Case 1b PE Surface, Steepest-Descent Control at t = 1.9 sec.

PE surface must also be reduced. The inevitable consequence is that the capability of the system for converting the KE associated with the frequency deviation into PE and thereby making it available for dissipation by the control is reduced. The result in both case 1a and 1b is the increase in magnitude of the first postfault rotor swing as compared to the classical model, and consequent reduction in the first-swing stability margin. Indeed, for clearing times much in excess of 0.06, the system is first-swing unstable.

A careful inspection of Figure 4.16 reveals that the potential energy is very close to zero at about 0.5 sec. At this point the residual transient energy is made up almost entirely of KE, and slope of the transient energy curve also approaches zero. The fact that there is a residual amount of energy that is never dissipated means that *the fast objective is never achieved.* When the system voltages and angles coincide with the tracking variables, as is evident in Figure 4.14, then $(\mathbf{Q}-\mathbf{Q}^*) \approx \mathbf{0}$, which means that the input no longer has any effect on $\mathcal{V}^*(\mathbf{x})$. Hence it appears that the pointwise steepest-

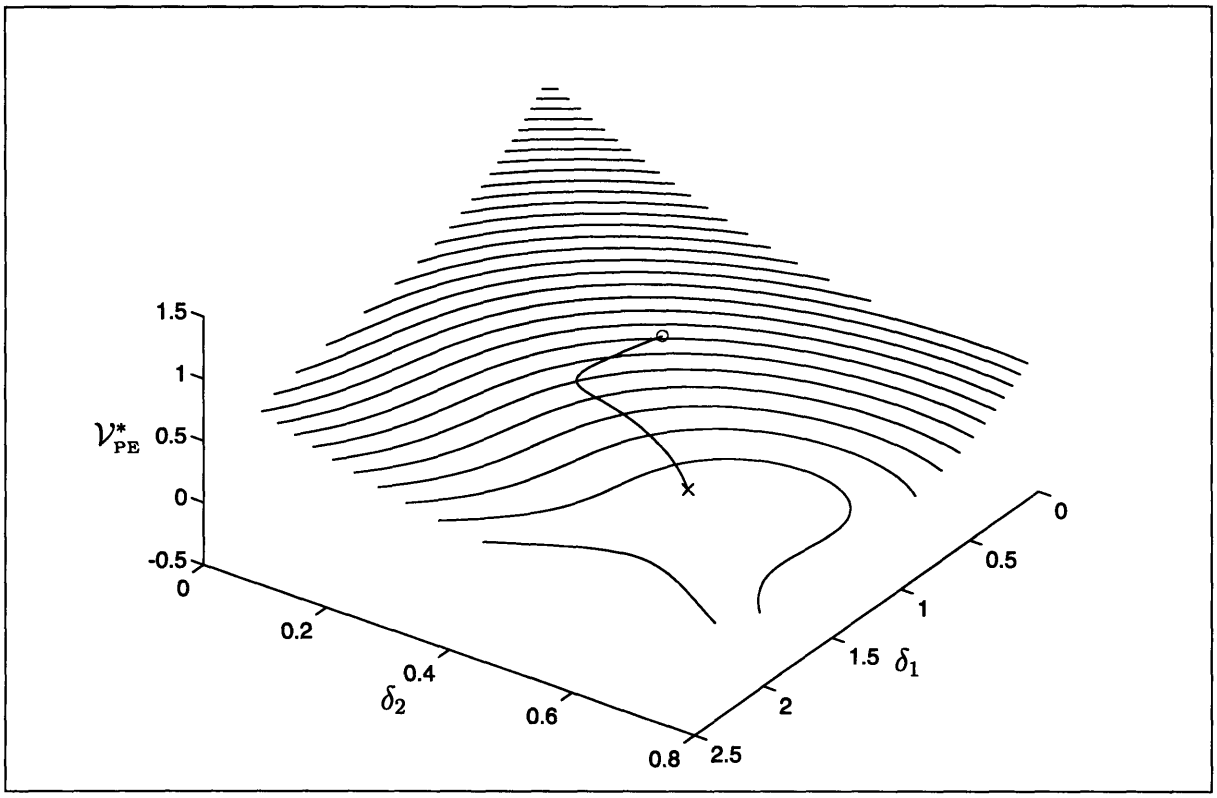

Figure 4.19: Case 1b PE Surface, Steepest-Descent Control at t = 1.9 sec.

descent method, while it does cause an initial rapid decline in the system energy, is not effective in reducing the energy to zero.

Figures 4.17 through 4.19 are contour plots of the potential energy surface at two points along the system trajectory. At $t = 0$, the voltage magnitudes are identical to the classical model, hence the initial potential energy surface is given in Figure 4.2. In Figure 4.17, calculated at $t = 0.41$ in the case 1b simulation, the potential energy "well" is significantly shallower than in the initial surface, which is identical to the one plotted in Figure 4.2. At $t = 1.9$, as depicted in Figures 4.18 and 4.19, the region of attraction of the stable equilibrium point has essentially vanished. Notice that the unstable equilibrium point associated with the saddle point to the left of the stable equilibrium in Figure 4.2 has approached the stable equilibrium, and the system is on the verge of a saddle-node bifurcation in which both equilibria may actually vanish. Very shortly after this, the tracking voltages jump to the unstable load-flow solution and the system voltages rise, prompting the change in behavior that is observed in the

last part of the simulation.

4.5.2 A Modified STEF with a Unique Equilibrium

Although the STEF-based steepest-descent control appeared to be ineffective in increasing stability margins, and in fact did not completely achieve the fast objective of driving the system to the manifold $\mathcal{O}'$, it did rapidly reduce the transient energy to a small value. In order to achieve the slow objective in finite time, the trajectory cannot in any event actually operate *on* $\mathcal{O}$, but must operate within $O(\varepsilon)$ of it. Since the STEF-based control does bring the system close to $\mathcal{O}$ quite rapidly, one might conjecture that by modifying the STEF to account in some way for the slow objective of driving the system to the nominal equilibrium, a viable control might be developed.

In order to account for the slow objective, the STEF may be modified, or we may resort to other energy functions that are available in the literature, *e.g.* Kakimoto's energy function [21]. The underlying idea is to construct an energy function that provides some penalty for departure from the nominal equilibrium. To preserve the slow/fast decoupling of the control objectives, this penalty should be small compared to the energy associated with the distance from $\mathcal{O}$. One method for modifying the STEF to create a unique local minimum at the desired equilibrium point (thereby accounting for the slow objective) will now be outlined.

We begin by *assuming* that there exists a viable equilibrium point $\mathsf{x}_s = [\,\mathsf{E}'^t_{qs} \quad \boldsymbol{\delta}^t_s \quad \boldsymbol{\omega}^t_s\,]^t$ at which the function Q^*_{tot} as defined in (3.19) has a constrained local minimum, Q^*_{min}. The constraint is implicit in (3.19), since Q^* is a function of the tracking voltages, which by definition must satisfy the load-flow constraint $\mathsf{P}_e = \mathsf{T}_m$. If such a point exists, then $Q^*_{\text{tot}}(\mathsf{x}_s) - Q^*_{\text{min}}$ and the function

$$\mathcal{V}^{\mathsf{Q}}(\mathsf{x}) = \frac{1}{2}(Q^*_{\text{tot}}(\mathsf{x}) - Q^*_{\text{min}}) \tag{4.21}$$

is locally positive-definite about x_s, since Q^*_{min} is a local minimum of $Q^*_{\text{tot}}(\mathsf{x})$ by assump-

tion. Hence, for any constant $k_q \in [0,\ 1]$, the function

$$\mathcal{V}^{\circ}(\mathsf{x}) = (1 - k_q)\mathcal{V}^{*}(\mathsf{x}) + k_q\mathcal{V}^{\mathsf{Q}}(\mathsf{x}) \tag{4.22}$$

is also locally positive-definite, since $\mathcal{V}^{\mathsf{Q}}(\mathsf{x})$ is locally positive-definite and $\mathcal{V}^{*}_{\mathrm{PE}}$ is locally positive-semidefinite. Moreover, $\mathcal{V}^{\mathsf{Q}}(\mathsf{x}_s) = 0$. Now, since $\dot{\mathcal{V}}^{*}(\mathsf{x})$ has already been calculated, the time derivative of $\mathcal{V}^{\circ}(\mathsf{x})$ may be found by calculating $\dot{\mathcal{V}}^{\mathsf{Q}}(\mathsf{x})$. Since $Q_{\min}$ is constant, this is just

$$\dot{\mathcal{V}}^{\mathsf{Q}}(\mathsf{x}) = \dot{Q}^{*}_{\mathrm{tot}}(\mathsf{x}) = \left[\begin{array}{cc} \mathsf{E}^{*}_{\mathsf{D}} & \mathsf{E}^{*}_{\mathsf{Q}} \end{array}\right] \underline{\underline{\mathbf{B}}} \left[\begin{array}{c} \dot{\mathsf{E}}^{*}_{\mathsf{D}} \\ \dot{\mathsf{E}}^{*}_{\mathsf{Q}} \end{array}\right]. \tag{4.23}$$

This may be expressed in terms of $\boldsymbol{\lambda}_{\|}$ and $\boldsymbol{\lambda}^{*}_{\perp}$ as

$$\begin{aligned} \dot{\mathcal{V}}^{\mathsf{Q}}(\mathsf{x}) &= \left[\begin{array}{cc} \mathsf{E}^{*}_{\mathsf{D}} & \mathsf{E}^{*}_{\mathsf{Q}} \end{array}\right] \underline{\underline{\mathbf{B}}} \left[\begin{array}{c} \mathbb{E}^{*}_{\mathsf{D}} \\ \mathbb{E}^{*}_{\mathsf{Q}} \end{array}\right] \boldsymbol{\lambda}_{\|} + \left[\begin{array}{cc} \mathsf{E}^{*}_{\mathsf{D}} & \mathsf{E}^{*}_{\mathsf{Q}} \end{array}\right] \underline{\underline{\mathbf{B}}} \left[\begin{array}{c} -\mathbb{E}^{*}_{\mathsf{Q}} \\ \mathbb{E}^{*}_{\mathsf{D}} \end{array}\right] \boldsymbol{\lambda}^{*}_{\perp} && (4.24) \\ &= Q^{*t}\boldsymbol{\lambda}_{\|} + \mathsf{P}^{*t}\boldsymbol{\lambda}^{*}_{\perp} && (4.25) \end{aligned}$$

Now, in view of (A.26) and recognizing that $\mathsf{P}^{*} = \mathsf{T}_m$ we have

$$\dot{\mathcal{V}}^{\mathsf{Q}}(\mathsf{x}) = Q^{*t}\boldsymbol{\lambda}_{\|} - \mathsf{T}^{t}_{m}(\mathbf{J}^{a}_{\perp})^{-1}\mathbf{J}^{*}_{\|}\boldsymbol{\lambda}_{\|}. \tag{4.26}$$

Hence,

$$\dot{\mathcal{V}}^{\circ}(\mathsf{x}) = (1 - k_q)(\mathsf{Q} - \mathsf{Q}^{*})^{t}\boldsymbol{\lambda}_{\|} + k_q(Q^{*t} - \mathsf{T}^{t}_{m}(\mathbf{J}^{a}_{\perp})^{-1}\mathbf{J}^{*}_{\|})\boldsymbol{\lambda}_{\|} \tag{4.27}$$

Setting $k_q = 0.5$ leads to a particularly simple function,

$$\frac{1}{2}\mathcal{V}^{\circ}(\mathsf{x}) = \frac{1}{2}\boldsymbol{\omega}^{t}\mathbb{M}\boldsymbol{\omega} - \mathsf{T}^{t}_{m}(\boldsymbol{\delta} - \boldsymbol{\delta}^{*}) + \frac{1}{2}(Q_{\mathrm{tot}} - Q^{*}_{\min}), \tag{4.28}$$

for which (4.27) reduces to

$$\dot{\mathcal{V}}^{\circ}(\mathsf{x}) = \frac{1}{2}(\mathsf{Q} - \mathsf{T}^{t}_{m}(\mathbf{J}^{a}_{\perp})^{-1}\mathbf{J}^{*}_{\|})\boldsymbol{\lambda}_{\|}. \tag{4.29}$$

Once again, this lends itself to a bang-bang type control. Selecting a small value of k_q preserves the time-scale separation of objectives, but in practice a larger value of k_q gives a somewhat better response. Before considering any type of control, however, we must address the fact that in general Q^* is not minimized at x_s, as we have assumed to this point.

Note that the STEF is not affected by a change in the diagonal elements of the $\mathbf{B}$ matrix. This is because the terms associated with the diagonal elements cancel from the expression $Q_{\text{tot}} - Q^*_{\text{tot}}$. A similar condition[3] was noted in Chapter 3. It is a simple matter to show that this holds for the STEF as well. For convenience, we extract the definition of $Q_{\text{tot}} - Q^*_{\text{tot}}$ from (3.19):

$$\begin{aligned} Q_{\text{tot}} - Q^*_{\text{tot}} &= \begin{bmatrix} \mathsf{E}_{\text{D}}^t & \mathsf{E}_{\text{Q}}^t \end{bmatrix} \underline{\underline{\mathbf{B}}} \begin{bmatrix} \mathsf{E}_{\text{D}} \\ \mathsf{E}_{\text{Q}} \end{bmatrix} - \begin{bmatrix} \mathsf{E}_{\text{D}}^{*t} & \mathsf{E}_{\text{Q}}^{*t} \end{bmatrix} \underline{\underline{\mathbf{B}}} \begin{bmatrix} \mathsf{E}_{\text{D}}^* \\ \mathsf{E}_{\text{Q}}^* \end{bmatrix} \\ &= \begin{bmatrix} \mathsf{E}_{\text{D}}^t & \mathsf{E}_{\text{Q}}^t \end{bmatrix} \begin{bmatrix} -\mathbf{B} & \mathbf{0} \\ \mathbf{0} & -\mathbf{B} \end{bmatrix} \begin{bmatrix} \mathsf{E}_{\text{D}} \\ \mathsf{E}_{\text{Q}} \end{bmatrix} - \begin{bmatrix} \mathsf{E}_{\text{D}}^{*t} & \mathsf{E}_{\text{Q}}^{*t} \end{bmatrix} \begin{bmatrix} -\mathbf{B} & \mathbf{0} \\ \mathbf{0} & -\mathbf{B} \end{bmatrix} \begin{bmatrix} \mathsf{E}_{\text{D}}^* \\ \mathsf{E}_{\text{Q}}^* \end{bmatrix}. \end{aligned} \tag{4.30}$$

Each diagonal element b_{ii} of $\mathbf{B}$ appears twice in $\underline{\underline{\mathbf{B}}}$, and gives rise to the following terms in (4.30):

$$b_{ii}(E_{\text{D}_i}^2 + E_{\text{Q}_i}^2) - b_{ii}(E_{\text{D}_i}^{*2} + E_{\text{Q}_i}^{*2}), \tag{4.31}$$

but these terms all vanish, since $|E_{\text{D}} + jE_{\text{Q}}| = |E_{\text{D}}^* + jE_{\text{Q}}^*|$. Hence, as far as the STEF is concerned, any diagonal weighting matrix may be added to $\mathbf{B}$ without affecting the value of the function. Although this does not bear directly on the attempt to force a minimum of $\mathcal{V}^{\text{Q}}(\mathsf{x})$ to appear at a desired location, it will considerably simplify the task of deriving the dynamic behavior of $\mathcal{V}^{\text{o}}(\mathsf{x})$.

We may proceed by attempting to find a diagonal weighting matrix $\mathbb{B}_\ell = \text{diag}(\mathsf{b}_\ell)$ which, when added to $\mathbf{B}$, causes a constrained minimum to appear in $Q^*_{\text{tot}}(\mathsf{x})$ at the

[3]See discussion following (3.13)

desired equilibrium. We form the Lagrangian

$$L = \begin{bmatrix} \mathsf{E}_{\mathrm{D}}^{*t} & \mathsf{E}_{\mathrm{Q}}^{*t} \end{bmatrix} \begin{bmatrix} -(\mathbf{B}+\mathbb{B}_\ell) & \mathbf{0} \\ \mathbf{0} & -(\mathbf{B}+\mathbb{B}_\ell) \end{bmatrix} \begin{bmatrix} \mathsf{E}_{\mathrm{D}}^{*} \\ \mathsf{E}_{\mathrm{Q}}^{*} \end{bmatrix} + \boldsymbol{\xi}^t(\mathsf{P}_{er} - \mathsf{T}_{mr}), \tag{4.32}$$

where P_{er} and T_{mr} are the power output and input torque, respectively, of the first $p-1$ machines. This is sufficient to completely specify the load-flow constraints in a lossless system, since the sum of the input powers of all machines must equal zero. The necessary conditions for a constrained minimum to occur are

$$\nabla Q_{\mathrm{tot}}^{*} + \boldsymbol{\xi}^t \mathbf{J}_r^p = 0; \qquad \mathsf{P}_{er}^{*} - \mathsf{T}_{mr} = 0 \tag{4.33}$$

where $\nabla Q_{\mathrm{tot}}^{*}$ is the gradient of Q^* and $\mathbf{J}_r^p$ is the first $p-1$ rows of the jacobian of the machine power output, taken with respect to the network-referenced machine voltages. Since our object is to select an appropriate value of b_ℓ such that a constrained minimum appears at x_s, we will fix the machine voltages at the desired equilibrium and allow $\boldsymbol{\xi}$ and b_ℓ to vary. Thus, the load-flow constraints will be automatically satisfied, and we will concentrate on finding a solution to the first condition in (4.33). Expanding (4.33) and substituting in the equilibrium voltages,

$$2\begin{bmatrix} \mathsf{E}_{\mathrm{D}_s}^{*t} & \mathsf{E}_{\mathrm{Q}_s}^{*t} \end{bmatrix} \begin{bmatrix} -(\mathbf{B}+\mathbb{B}_\ell) & \mathbf{0} \\ \mathbf{0} & -(\mathbf{B}+\mathbb{B}_\ell) \end{bmatrix} + \boldsymbol{\xi}^t \mathbf{J}_r^p = 0. \tag{4.34}$$

This is rewritten as

$$\nabla Q_o + 2\begin{bmatrix} \mathsf{E}_{\mathrm{D}_s}^{*t} & \mathsf{E}_{\mathrm{Q}_s}^{*t} \end{bmatrix} \begin{bmatrix} -\mathbb{B}_\ell & \mathbf{0} \\ \mathbf{0} & -\mathbb{B}_\ell \end{bmatrix} + \boldsymbol{\xi}^t \mathbf{J}_r^p = 0, \tag{4.35}$$

where the obvious definition has been made for ∇Q_o. Rearranging,

$$(\nabla Q_o)^t = 2\begin{bmatrix} \mathbb{E}_{\mathrm{D}_s}^{*} \\ \mathbb{E}_{\mathrm{Q}_s}^{*} \end{bmatrix} \mathsf{b}_\ell - (\mathbf{J}_r^p)^t \boldsymbol{\xi} = \left[\begin{array}{c|c} \mathbb{E}_{\mathrm{D}_s}^{*} & \\ \mathbb{E}_{\mathrm{Q}_s}^{*} & (\mathbf{J}_r^p)^t \end{array}\right] \begin{bmatrix} \mathsf{b}_\ell \\ -\boldsymbol{\xi} \end{bmatrix} \tag{4.36}$$

The matrix on the RHS of (4.36) has dimensions $2p \times (2p-1)$, which means that the equation is overdetermined. Dimensionally speaking, the problem is that $\boldsymbol{\xi}$ is only of dimension $p-1$. If we were to somehow specify an additional independent constraint in (4.32), then assuming that the problem is otherwise well-posed, the solution would always exist. The simplest way to do this is to specify the angle of the p^{th} machine. Note that we are free to specify the value of one angle (or some linear combination of angles, as in the COI), without affecting the result of the minimization. Hence, by adding the constraint term

$$\xi_p \left(\tan^{-1} \frac{E_{\mathrm{Q}_p}}{E_{\mathrm{D}_p}} - \theta_p \right) = 0 \tag{4.37}$$

to the Lagrangian of (4.32), equation (4.36) takes the form

$$(\nabla Q_o)^t = \left[\begin{array}{c|c|c} \mathbb{E}^*_{\mathrm{D}_s} & (\mathbf{J}^p_r)^t & \mathsf{e}_p \\ \mathbb{E}^*_{\mathrm{Q}_s} & & \end{array} \right] \left[\begin{array}{c} \mathsf{b}_\ell \\ -\boldsymbol{\xi} \\ \xi_p \end{array} \right] \tag{4.38}$$

where

$$\mathsf{e}_p = \left[\begin{array}{ccccccc} 0 & \cdots & -\frac{E_{\mathrm{Q}_p}}{|E_p|} & 0 & \cdots & \frac{E_{\mathrm{D}_p}}{|E_p|} \end{array} \right]^t. \tag{4.39}$$

In practice, it is not necessary to consider the p^{th} constraint, since the exact solution may be obtained from the overdetermined system of (4.36).

Given the above procedure for placing the constrained minimum of Q^*_{tot} in the desired location, the function of (4.22) becomes a locally positive-definite function, whose derivative may be made nonpositive by the proper choice of control. The continued presence of the virtual equilibrium angle $\boldsymbol{\delta}^*$ in $\mathcal{V}^{\circ}(\mathsf{x})$ means that, in order to implement a Lyapunov-style control, it will still be necessary to follow the virtual equilibrium via the tracking voltages. It would be attractive to attempt to eliminate $\boldsymbol{\delta}^*$ by applying a similar procedure to the classical TEF, but this is not possible, since that function is not semidefinite for time-varying voltage magnitudes, hence its sum with $\mathcal{V}^{\mathrm{Q}}(\mathsf{x})$ is not positive-definite in general.

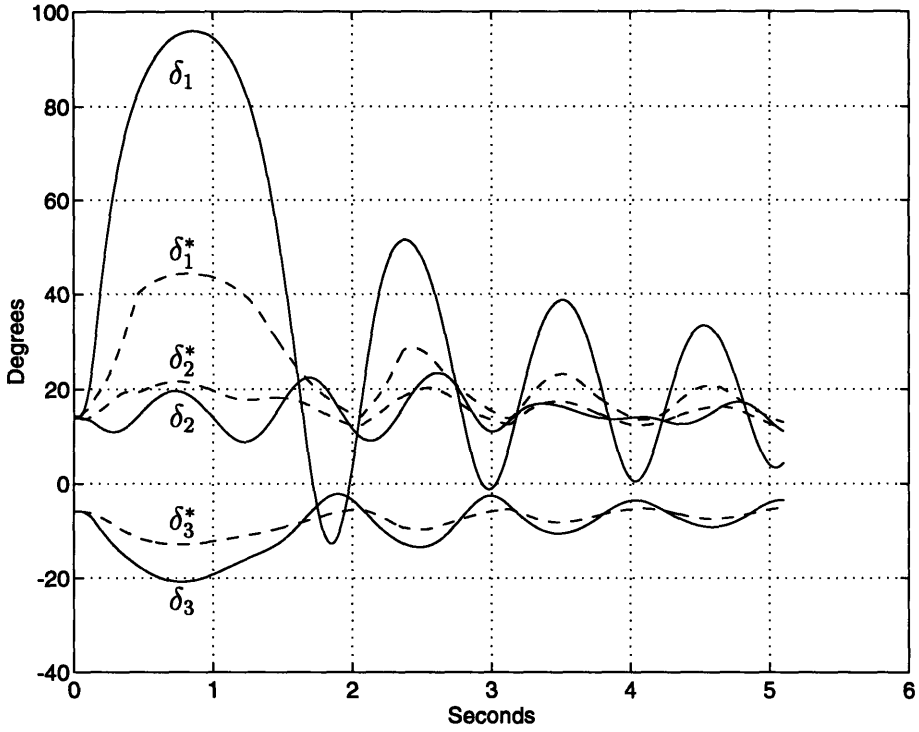

Figure 4.20: Case 1: Rotor Angles for Steepest-Descent Control, Modified TEF.

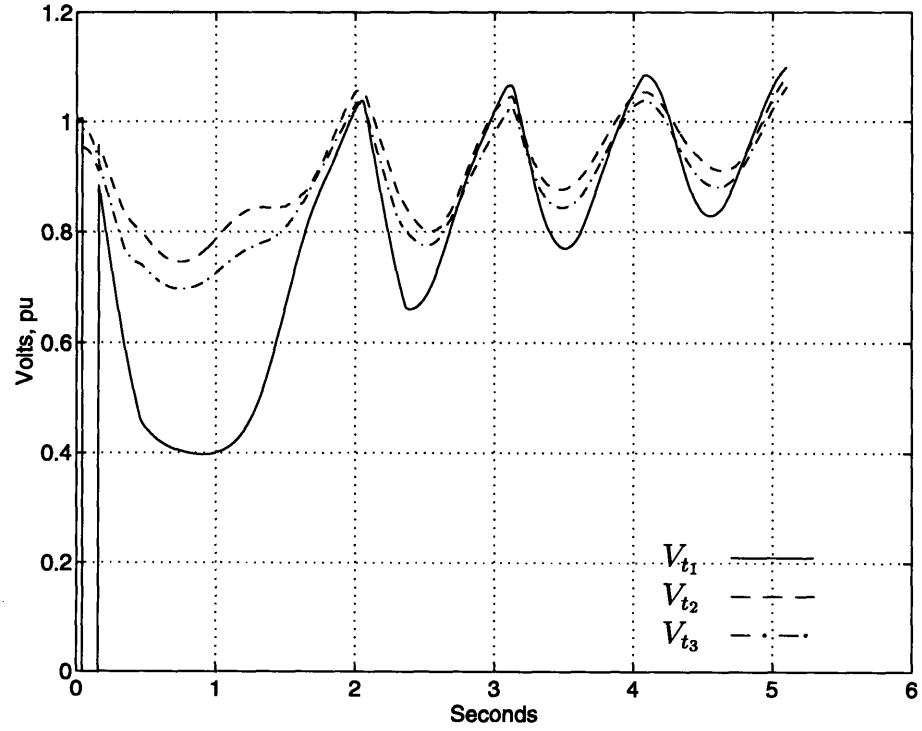

Figure 4.21: Case 1: Terminal Voltages for Steepest-Descent Control, Modified TEF.

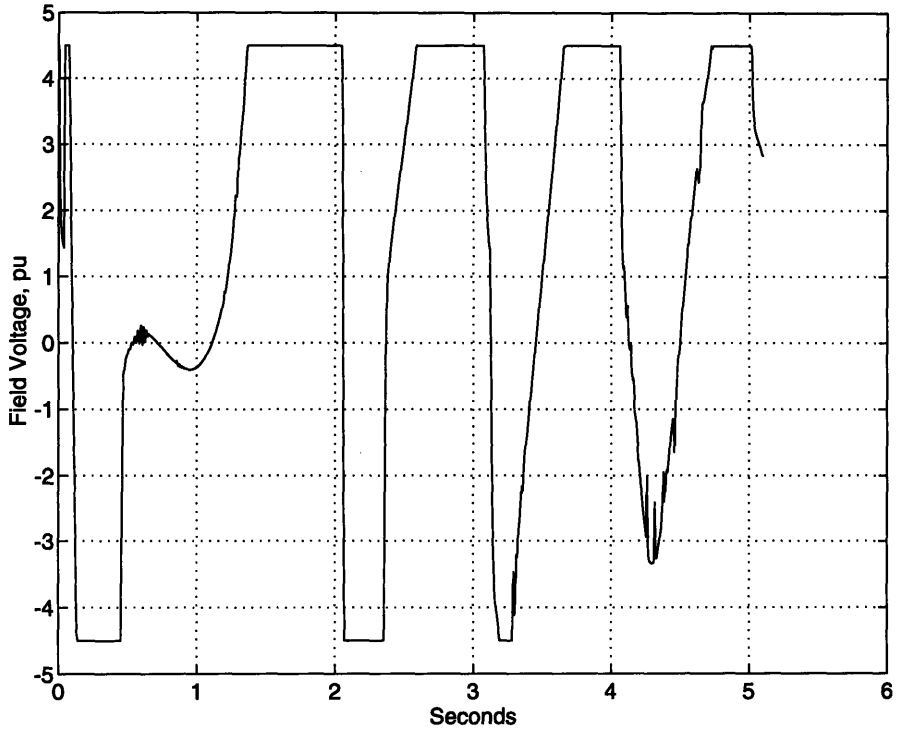

Figure 4.22: Case 1: Machine 1 Field Voltage for Steepest-Descent Control, Modified TEF.

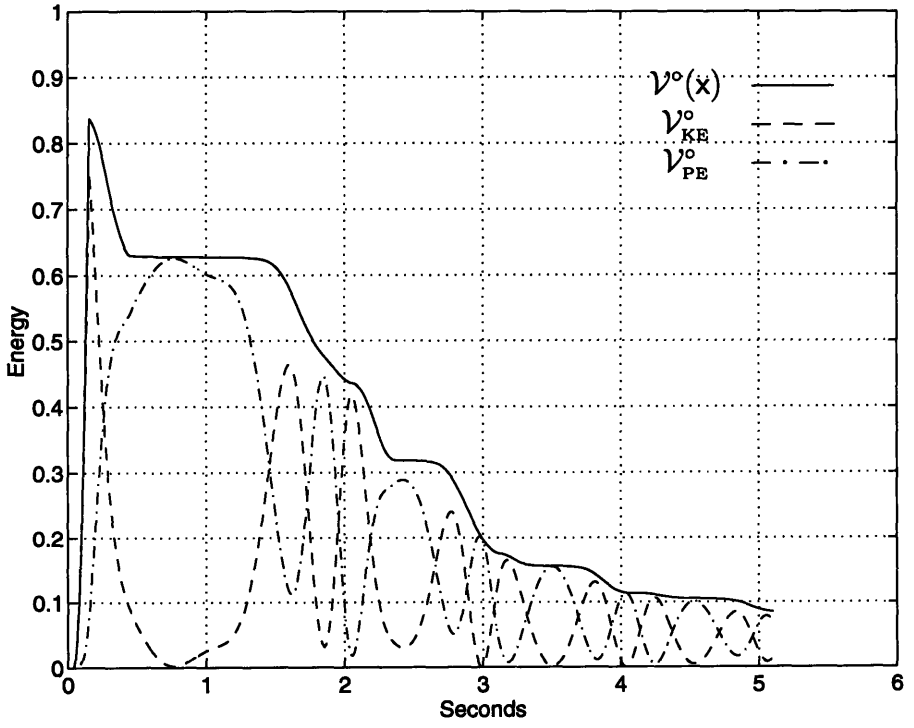

Figure 4.23: Case 1: Transient, Kinetic and Potential Energy for Steepest-Descent Control, Modified TEF.

The following simulation illustrates the system behavior for a steepest-descent control using $k_q = 1/2$, *i.e.* the function (4.29). This simulation represents a critically-cleared instance of case 1, which for this control is $t_{cr} = 0.115$ sec. The field voltage subsystem is the same as for the STEF steepest-descent control, given in Figure 4.8, except that the gain is -100. Although the simulation was not continued until the system had completely settled, the difference between this control and the one based on the STEF is clear in the rotor angle response of Figure 4.20, and the system does settle eventually to the desired equilibrium. Also plotted as dotted lines in Figure 4.20 are the trajectories of the virtual equilibrium angles.

Although the damping of the oscillation has improved significantly, it comes at the expense of a rather large decrease in the critical clearing time. Consequently, there is little incentive for using this type of control. The terminal and field voltage plots (Figures 4.21 and 4.22) show that the field voltage does respond to the rotor angle swings in such a way as to damp the oscillation. During the crucial first swing, however, the field voltage is at its minimum value, which accounts for the higher-magnitude deviation and consequent decrease in critical clearing time, as compared to constant field excitation. The transient energy plot of Figure 4.23 shows that the TEF is nonincreasing, but it does not have the steep slope of the STEF control. This seems to indicate that the attempt to simultaneously minimize the two halves of the modified TEF presents conflicting objectives. Note that $\mathcal{V}^{\mathrm{Q}}$ penalizes any deviation in the voltage magnitude from the equilibrium values, and this is apparently at odds with reducing the energy in the STEF. This is made clearer if the constant k_q is changed. For larger values of k_q (which give proportionally greater weighting to $\mathcal{V}^{\mathrm{Q}}(\mathsf{x})$), the response of the system begins to resemble the constant-voltage (or classical) response. For smaller values of k_q, the response approaches that of the STEF steepest-descent control, which has been seen to be far from ideal in terms of system security.

4.5.3 Tracking Two Equilibria

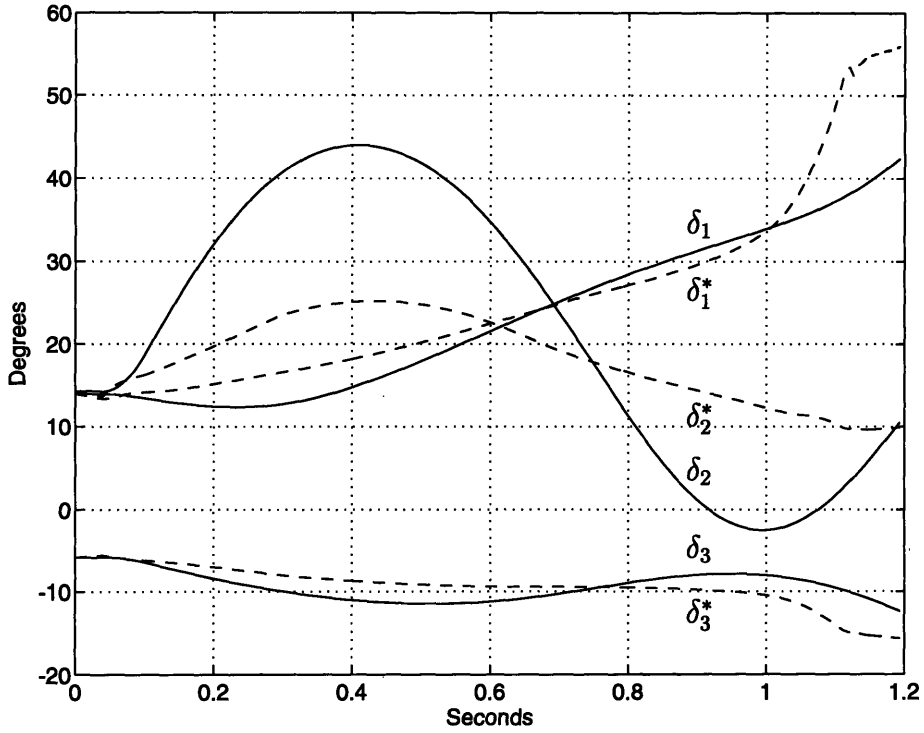

Figure 4.24: Case 1: Rotor Angles, Tracking Two Equilibria.

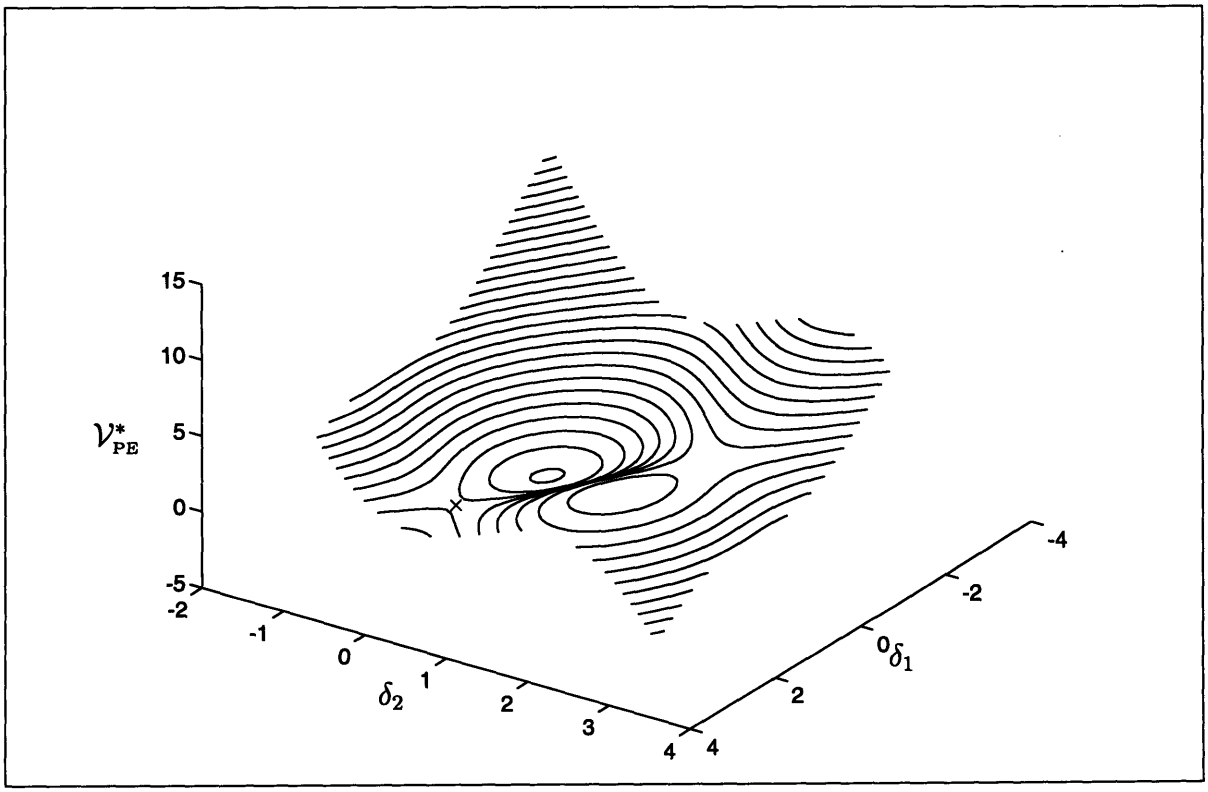

Figure 4.25: Case 1: Potential Energy Surface at t = 0.5, Tracking Two Equilibria.

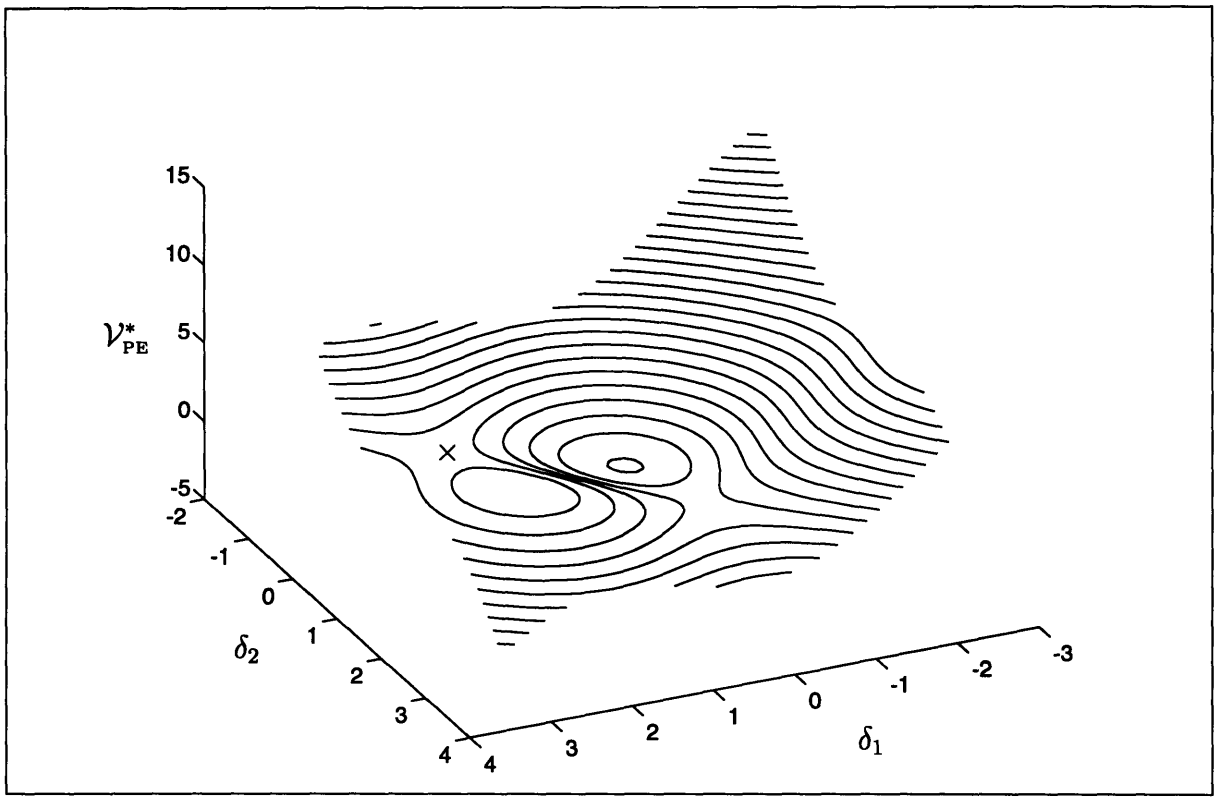

Figure 4.26: Case 1: Potential Energy Surface at t = 1.0, Tracking Two Equilibria.

An interesting (if equally unsuccessful) variant of this approach is developed as follows: Suppose we define the function

$$\mathcal{V}_2^Q = Q_{tot}^{s*} - Q_{\text{tot}}^{u*} \tag{4.40}$$

where Q_{tot}^{s*} is the reactive power associated with the tracking voltages as we have defined them, and Q_{tot}^{u*} is the reactive power associated with a second set of tracking voltages that follows one of the boundary unstable equilibria, as the magnitudes of the machine voltages change. In the same manner as was used to derive the modified TEF, we can calculate diagonal loads for the admittance matrix (one diagonal load for each equilibrium to be tracked) such that $\mathcal{V}_2^Q$ is minimized when the machine voltages are at their desired equilibrium values. This is added to the STEF as in (4.21). This function tracks the difference in energy between the stable equilibrium point and a single boundary unstable equilibrium point, and is designed to maintain the separation be-

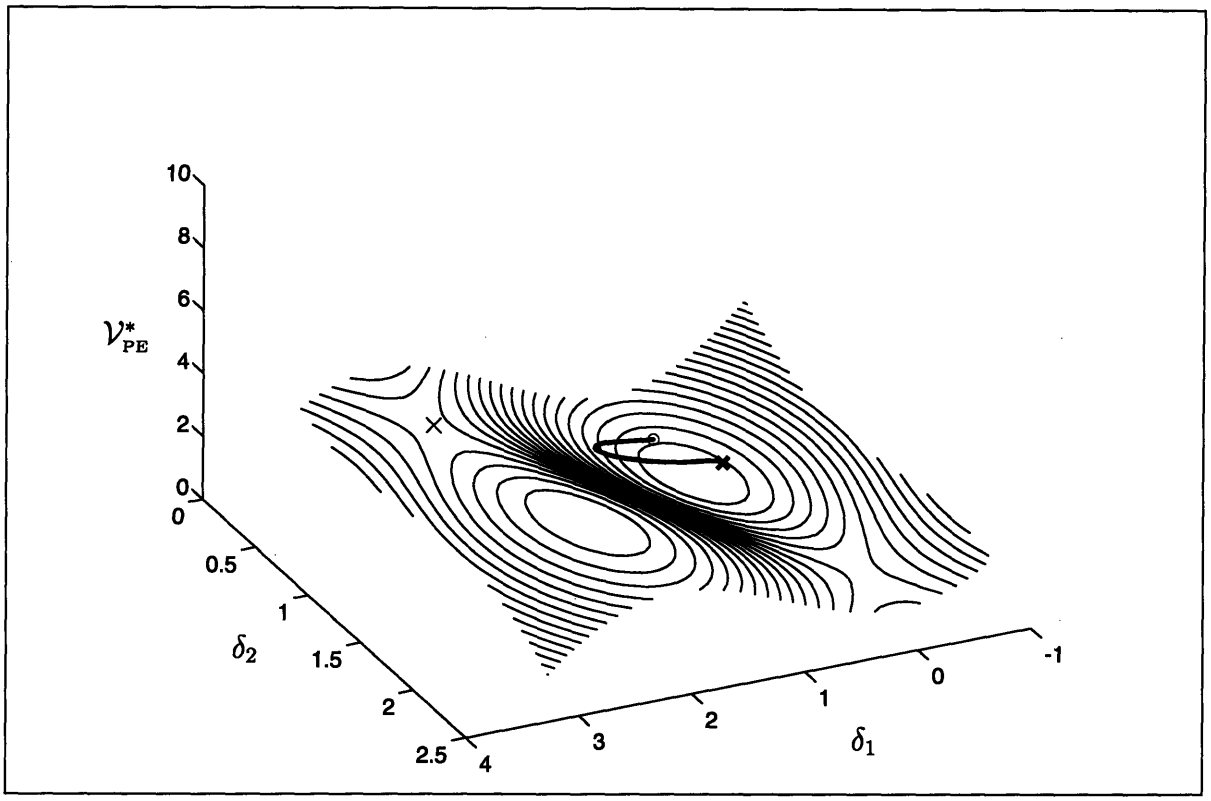

Figure 4.27: Case 1: Potential Energy Surface at t = 1.0, Tracking Two Equilibria.

tween the stable and unstable equilibria, preventing the two equilibria from approaching each other in the type of incipient bifurcation that was observed in the steepest-descent STEF control. The unstable equilibrium point is followed with a set of tracking voltages whose dynamics are identical to those that follow the stable equilibrium point, the only distinction being that the second set of tracking voltages is initialized at the unstable equilibrium point of interest. For the simulations depicted here, we select the unstable equilibrium point closest to the case 1 first-swing exit point. At the prefault machine voltage magnitudes, this equilibrium occurs at $\boldsymbol{\delta}_u = [\,2.4404 \quad -0.0339 \quad -0.3983\,]^t$ in COI coordinates.

This control will not be dealt with in any detail, but we will present a series of plots to illustrate the effect that it has on the potential energy surface. Case 1 was simulated with a clearing time $t_{c\ell} = 0.06$. Figure 4.24 shows the rotor angle response, which survives the first swing only to have Machine 2 lose synchronism on the second. As the contour plots will illustrate, tracking the unstable equilibrium has the desirable effect

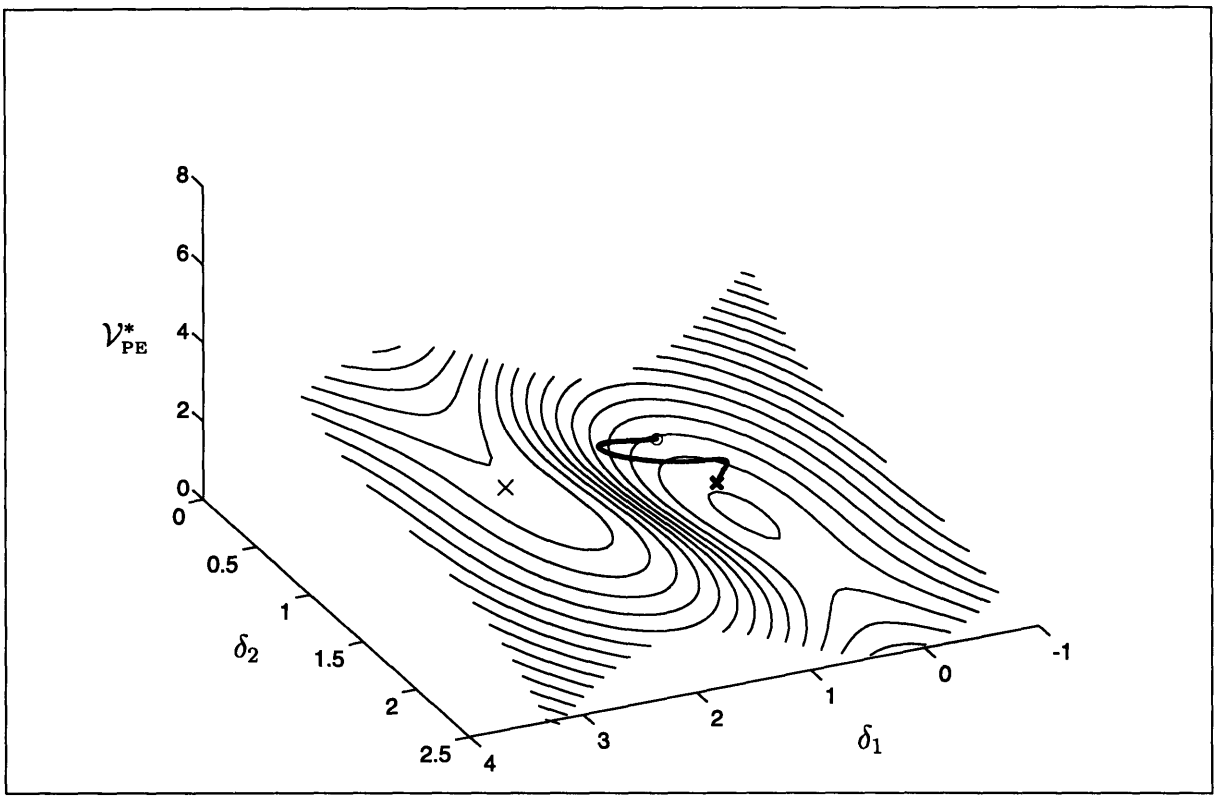

Figure 4.28: Case 1: Potential Energy Surface at t = 1.2, Tracking Two Equilibria.

of maintaining the energy threshold associated with the tracked equilibrium. Unfortunately, it does not prevent a deterioration in the security of other boundary equilibria. Figure 4.25 is the potential energy surface at $t = 0.5$ and is quite similar to the equilibrium PE surface of Figure 4.2. The equilibrium point that is being tracked is marked in this plot with an $\times$. As time evolves, the "height" of the critical equilibrium point is substantially preserved, as Figure 4.26 attests, but the height of a second equilibrium point declines. Enlarged plots with the rotor angle trajectories superimposed are shown in Figures 4.27 and 4.28, taken at $t = 1$ and $t = 1.2$, respectively. The beginning of the trajectories are marked with circles and the ends are marked with '$\times$'. In the last plot, the region of attraction has again all but vanished, but in this case the equilibrium point associated with the bifurcation is different. The control has indeed forced the stable and (originally) critical equilibria to maintain a separation, but without contributing materially to the stability of the system.

Although it might be theoretically possible to track larger numbers of equilibria

and thus support the entire stability boundary, it is not practical to do so. Tracking each equilibrium requires that $2p$ new states be added to the controller (albeit that this is only 2 states per machine), and there are great practical difficulties involved with tracking even one. Moreover, determination of the correct set of unstable equilibria to track would be a difficult task. These simulations do make it clear that at least for the type of TEF dealt with here, the steepest-descent approach does not lead to a viable control. Also apparent is the dependence of the PE surface on the machine voltage magnitudes, and it is possible to observe that the amount of KE that may be absorbed by the system is roughly related to the magnitude of the PE at the stability boundary. In order to maximize the first-swing stability of the system, it appears that an initial *increase* in the system energy, which would be manifested as an increase in the PE component, may be necessary. This does not necessarily correlate with the ability to maintain stability on second and later swings, or with the problem of returning the system voltage profile to an acceptable level, however.

4.6 An Alternative Measure of the Objective Manifold

The observation that good first-swing stability may require an initial rise in the transient energy, at least as measured by the STEF and related functions, means that the STEF is not an effective measure of the distance to $\mathcal{O}$, at least in terms of control design. Therefore it may be advantageous to revisit the definition of $\mathcal{O}$ and attempt to develop a more suitable measure. Recall that one may think of the STEF as a constraint that defines the submanifold $\mathcal{O}'$ and measures the distance from it. It may be that $\mathcal{O}'$ is too restrictive a set, particularly since the attempt to bring the state to $\mathcal{O}'$ seems to result in an unavoidable reduction in the ROA of the stable equilibrium. A more effective control might be developed if a measure could be found that reflected the entire object manifold $\mathcal{O}$.

Let the vector of angular accelerations of the generator rotors be denoted by $\boldsymbol{\alpha}$.

Note that $\boldsymbol{\alpha} = \dot{\boldsymbol{\omega}}$. The condition of Definition 4.1 may be restated as

$$\mathcal{O} = \left\{ (\bar{\mathsf{E}},\, \bar{\boldsymbol{\delta}},\, \bar{\boldsymbol{\omega}}) \in \mathbb{R}^q \times \mathbb{R}p \times \mathbb{R}^p \mid \boldsymbol{\omega} = 0;\ \boldsymbol{\alpha} = 0 \right\}. \tag{4.41}$$

Based on this definition, it is clear that any norm applied to $[\boldsymbol{\omega}^t \ \ \boldsymbol{\alpha}^t]^t$ is a measure of the distance to $\mathcal{O}$, and any norm may be taken as the definition of $\mathcal{O}$ as follows:

$$\mathsf{x} \in \mathcal{O} \Longleftrightarrow \left\| \begin{bmatrix} \boldsymbol{\omega} \\ \boldsymbol{\alpha} \end{bmatrix} \right\| = 0. \tag{4.42}$$

As compared to the STEF, this a a very simple measure. Unfortunately, this is achieved by using the variable $\boldsymbol{\alpha}$, and reverts to Definition 4.1 when expressed in terms of the system states E, $\boldsymbol{\delta}$ and $\boldsymbol{\omega}$. To take advantage of the apparent simplicity of this measure, one might consider the following state transformation, applied to the single-axis model:

$$\mathsf{z} = \begin{bmatrix} (\boldsymbol{\delta} - \boldsymbol{\delta}_o) \\ \boldsymbol{\omega} \\ \boldsymbol{\alpha} \end{bmatrix} = \mathsf{T}(\mathsf{E}'_q,\, \boldsymbol{\delta},\, \boldsymbol{\omega}), \tag{4.43}$$

When considering this state transformation as applied to a multimachine system, the use of the network-referenced coordinates in conjunction with the quantities $\boldsymbol{\lambda}_{\|}$ and $\boldsymbol{\lambda}_{\perp}$ will yield a simpler form. Referring to (2.90), using the COI model and again setting $\mathbb{D} = 0$, we differentiate $\boldsymbol{\alpha} = \dot{\boldsymbol{\omega}}$ with respect to time, which allows the system model to be written in the following form:

$$\dot{\boldsymbol{\delta}} = \boldsymbol{\omega} \tag{4.44}$$

$$\dot{\boldsymbol{\omega}} = \boldsymbol{\alpha} \tag{4.45}$$

$$\dot{\boldsymbol{\alpha}} = -\mathbb{M}^{-1} \left(\mathbf{J}^p_{\perp} \boldsymbol{\lambda}_{\perp} + \mathbf{J}^p_{\|} \boldsymbol{\lambda}_{\|} \right) - \frac{1}{m_{\mathrm{T}}} \frac{dP_{\mathrm{tot}}}{dt}. \tag{4.46}$$

For the lossless system, $P_{\mathrm{tot}} \equiv 0$, so it is dropped from the equation. For lossy systems, it may be necessary to consider the effect of P_{coi}, but it tends to be small. If $\boldsymbol{\lambda}_{\|}$ is considered to be the input, this system in affine in the control (actually it is affine with

respect to E_{fd} as well), and moreover is in the so-called Brunovsky canonical form. It also exhibits a natural state decomposition associated with the fast and slow control objectives. Clearly, if (4.42) is satisfied, the system is on $\mathcal{O}$, regardless of the value of $\boldsymbol{\delta}$. Therefore the fast objective may be formulated as the most rapid minimization of the deviation in $\boldsymbol{\omega}$ and $\boldsymbol{\alpha}$, while the slow objective may involve a slower reduction in the norm $\|\boldsymbol{\delta} - \boldsymbol{\delta}_o\|$.

Another interesting aspect of this state transformation is that it is possible to perform *feedback linearizing control* (FBLC) on a system in Brunovsky form, and this leads to a number of interesting results. Several technical considerations arise when FBLC is implemented on all machines of a lossless system, and these will be dealt with in the course of formulating controls for security in following sections. Another issue that is quite well-documented [6, 8, 26] is the difficulty in achieving acceptable voltage control with FBLC. Some new results are reported on this issue as well. Initially, however, some brief introductory material on FBLC will be presented.

4.7 Interaction of Feedback Linearizing Control with the STEF

Although it did not lead to a viable control, the investigation of the steepest-descent methods did provide some insight into the issues of energy interchange and the effects on the PE surface engendered by excitation control. We now turn our attention toward the impact of FBLC on the interchange of energy and the PE surface. The particular type of FBLC that is of interest here is an excitation control developed, in approximately chronological order, in [33, 32, 6, 8, 26]. Although the use of FBLC raises issues of robustness and practicality in implementation [7], it provides a framework in which several fundamental issues regarding the use of excitation control for enhancement of transient stability are brought to light in a particularly simple form. Moreover, other types of control that are based on linear systems theory are locally equivalent to FBLC, so that the investigation of its affects on the system energy leads to more generally-

applicable insights.

Feedback linearizing control attempts to use the input to cancel any system nonlinearities, substituting a linear response. The theoretical details of this type of control will not be examined in any detail here, but may be found in several references, *e.g.* [48, 20]. For our purposes, a simplified version of the FBLC formulation will suffice; hence, in the interest of simplicity, the more general form will not be used. Moreover, several conditions on the well-behavedness of the vector fields that define the dynamics of the system under consideration will be assumed to be satisfied, at least for the present. In fact, these conditions are violated at certain points in the state-space of the power system model, and indeed are generically false for the lossless model, but it will be shown that even for the lossless case, a type of FBLC can be formulated. The implications of this on the operation of feedback-linearizing excitation control will be noted in the sequel.

4.7.1 The FBLC Framework

A very brief introduction to feedback linearizing excitation control as it relates to a single-machine system will now be presented, followed by a generalization to the multimachine case.

In order to perform feedback linearization of a single-input system described by the equations

$$\dot{\mathsf{x}} = \mathsf{f}(\mathsf{x}, u), \tag{4.47}$$

we search for a nonlinear state transformation

$$T : \mathbb{R}^n \to \mathbb{R}^n, \ \mathsf{x} = T(\mathsf{z}), \tag{4.48}$$

such that in the new coordinates, the system appears in the affine chain-of-integrators (or *Brunovsky Canonical*) form, which for a single-input single-output (SISO) system

is of the form:

$$\begin{bmatrix} \dot{z}_1 \\ \dot{z}_2 \\ \vdots \\ \dot{z}_n \end{bmatrix} = \begin{bmatrix} z_2 \\ z_3 \\ \vdots \\ f(\mathbf{z}) + b(\mathbf{z})u \end{bmatrix} \tag{4.49}$$

The control input is now defined as

$$u = \frac{1}{b(\mathbf{z})}(-\mathbf{f}(\mathbf{z}) + v), \tag{4.50}$$

so that the resulting system has the following closed-loop system equation:

$$\begin{bmatrix} \dot{z}_1 \\ \dot{z}_2 \\ \vdots \\ \dot{z}_n \end{bmatrix} = \begin{bmatrix} 0 & 1 & \cdots & 0 \\ \vdots & & \ddots & \vdots \\ 0 & \cdots & \cdots & 1 \\ 0 & \cdots & \cdots & 0 \end{bmatrix} \begin{bmatrix} z_1 \\ \vdots \\ \vdots \\ z_n \end{bmatrix} + \begin{bmatrix} 0 \\ \vdots \\ 0 \\ 1 \end{bmatrix} v. \tag{4.51}$$

Usually, one sets $v = \begin{bmatrix} a_0 & a_1 & \cdots & a_{n-1} \end{bmatrix} \mathbf{z}$, so that (4.51) becomes

$$\begin{bmatrix} \dot{z}_1 \\ \dot{z}_2 \\ \vdots \\ \dot{z}_n \end{bmatrix} = \begin{bmatrix} 0 & 1 & \cdots & 0 \\ \vdots & & \ddots & \vdots \\ 0 & \cdots & \cdots & 1 \\ a_0 & a_1 & \cdots & a_{n-1} \end{bmatrix} \begin{bmatrix} z_1 \\ \vdots \\ \vdots \\ z_n \end{bmatrix}, \tag{4.52}$$

which is clearly a linear system. More generally, v can be any time signal, including of course any linear or nonlinear function of the state. Briefly, the conditions under which such a control may be implemented are that $T(\mathbf{z})$ exists and is locally a C^1 diffeomorphism (*i.e.* continuously differentiable, and with a continuously differentiable inverse) and that the system vector field satisfies certain rank and regularity conditions. These conditions are locally satisfied for the flux-decay and single-axis machine models around most if not all viable equilibria. The transformation is similar for the single and multimachine cases, and is identical to the transformation suggested by the norm

condition of (4.42).

At this point, we will proceed to derive the feedback linearizing control for the multimachine system, utilizing $\boldsymbol{\lambda}_{\|}$ as the input. This is much more direct and convenient notationally, but is not standard notation. A derivation of a similar control using standard notation for a single machine infinite-bus system is given in Appendix B Referring to (4.46), we now define the feedback linearizing input as

$$\boldsymbol{\lambda}_{\|} = -(\mathbf{J}_{\|}^{p})^{-1}\,(\mathbf{J}_{\perp}\boldsymbol{\lambda}_{\perp}) + (\mathbf{J}_{\|}^{p})^{-1}\mathbb{M}\mathsf{v}. \tag{4.53}$$

where, in order to achieve a linear response, one sets

$$\mathsf{v} = \mathbf{A}_3\mathsf{z} \tag{4.54}$$

With this control, the system takes the form

$$\frac{d}{dt}\begin{bmatrix} \boldsymbol{\delta} \\ \boldsymbol{\omega} \\ \boldsymbol{\alpha} \end{bmatrix} = \left[\begin{array}{ccc} \mathbf{0} & \mathbf{I} & \mathbf{0} \\ \mathbf{0} & \mathbf{0} & \mathbf{I} \\ \hline \multicolumn{3}{c}{\mathbf{A}_3} \end{array}\right] \begin{bmatrix} (\boldsymbol{\delta} - \boldsymbol{\delta}_o) \\ \boldsymbol{\omega} \\ \boldsymbol{\alpha} \end{bmatrix}. \tag{4.55}$$

If the rectangular matrix A_3 is specified as

$$\mathbf{A}_3 = \begin{bmatrix} \mathbb{A}_0 & \mathbb{A}_1 & \mathbb{A}_2 \end{bmatrix} \tag{4.56}$$

where $\mathbb{A}_i = \mathrm{diag}(a_{i1}, a_{i2}, \ldots, a_{ip})$, then the system matrix is equivalent (via a state permutation into the interleaved state ordering) to a block-diagonal form, with each diagonal block being a 3×3 "companion" form similar to (4.52). The control in this case effectively reduces each machine to a decoupled linear system (subject to limits on control magnitude and the invertibility of $\mathbf{J}_{\|}^{p}$). Note that there are two steps to FBLC, the first being the cancellation or inversion of the natural plant dynamics (this is the function of the term $-(\mathbf{J}_{\|}^{p})^{-1}\,(\mathbf{J}_{\perp}\boldsymbol{\lambda}_{\perp})$ in (4.53)), the second being the substitution of some desired dynamics (represented by the term $(\mathbf{J}_{\|}^{p})^{-1}\mathbb{M}\mathsf{v}$ in the same equation).

In general, it is impractical or impossible to calculate $\mathbf{J}_{\|}^{p}$ or $\mathbf{J}_{\perp}^{p}$, or their inverses.

Because of the difficulty of obtaining the actual admittance matrix of a system of the geographical size and complexity of a typical power system, it is typically impractical to operate any control that requires measurements from distant parts of the system, hence any practical control must be formulated in a decentralized framework, using measurements obtained only at the site at which the equipment is installed. This requirement is becoming less strict as technology for obtaining reliable and timely measurements from distant locations evolves, but it remains a major design constraint. In [32, 6, 8], methods were outlined for circumventing this difficulty, but we shall not be concerned with them here.

Our primary interest is to investigate the effects of FBLC on the STEF and PE surface, as well as the limitations inherent in the system, in order to obtain insights that may be generally applicable to any type of control. Consequently, implementation issues will be relegated to a secondary role.

Our first result relates FBLC to the gradient of the PE surface, $\nabla_\delta \mathcal{V}^*_{\text{PE}}(\mathsf{x})$, which is equal to $-\nabla_\delta \mathcal{V}^*_{\text{KE}}(\mathsf{x})$:

Claim 4.2 *For the lossless single-axis multimachine power system model using FBLC as in (4.53), the time rate of change of the KE/PE gradient along system trajectories is given by*

$$\frac{d}{dt}\left(\frac{\partial \mathcal{V}_{\text{KE}}}{\partial \boldsymbol{\delta}}\right) = \mathbb{M}\mathsf{v} = \mathbb{M}\mathbf{A}_3\mathsf{z}. \tag{4.57}$$

Proof:

From (4.11), we have that

$$\frac{d}{dt}\left(\frac{\partial \mathcal{V}_{\text{KE}}}{\partial \boldsymbol{\delta}}\right) = -(\mathbf{J}^p_\perp \lambda_\perp + \mathbf{J}^p_\parallel \lambda_\parallel) = \mathbb{M}\dot{\alpha}, \tag{4.58}$$

where we are again assuming that $\mathbb{D} = 0$. Substitution of the FBLC control law (4.53) into (4.58) yields the result. ∎

Note that, although we have used $\mathsf{v} = \mathbf{A}_3\mathsf{z}$ in the claim, v may actually be defined arbitrarily. In fact, for any input vector $\boldsymbol{\lambda}_\parallel = \mathsf{h}(\mathsf{z}, t)$ it is true that

$$\frac{d}{dt}\left(\frac{\partial \mathcal{V}_{\text{KE}}}{\partial \boldsymbol{\delta}}\right) = \mathbb{M}\mathbf{J}^p_\parallel \mathsf{h}(\mathsf{z}, t) \tag{4.59}$$

Hence, FBLC (in this more general sense) allows for essentially arbitrary control of the rate of change of the slope of the classical potential energy surface. In view of the fact that in the undamped system, the only mechanism available for change in the KE is through conversion to PE, any damping of rotor angle/frequency oscillations will be achieved by manipulation of the potential energy surface such that energy converted to PE is not recovered later as KE. The ability to exercise direct control of the gradient is limited by both control saturation and the fact that the gradient at any point is related to the integral of the control rather than the control signal itself. This geometrically-based intuition will presently be shown to be related in a direct way to the time-scale separation of the control objectives and to the objective manifold.

4.7.2 Some Effects of Transformation Singularity

Some practical issues arise in the implementation of FBLC on the lossless model. To begin with, for the lossless system, $\mathbf{J}_{\|}^{p}$ is always singular. This is a consequence of the fact that the sum over all generator power outputs must equal zero for a lossless system, hence the sum over the elements of any vector of increments in the generator power outputs must also equal zero. We may verify this by noting that the block-form lossless admittance matrix is skew-symmetric,

$$\mathbf{Y}_r^t = \begin{bmatrix} \mathbf{0} & -\mathbf{B} \\ \mathbf{B} & \mathbf{0} \end{bmatrix}^t = \begin{bmatrix} \mathbf{0} & \mathbf{B} \\ -\mathbf{B} & \mathbf{0} \end{bmatrix} = -\mathbf{Y}_r. \tag{4.60}$$

hence

$$\begin{aligned} (1^t \mathbf{J}_{\|}^{p})^t &= \left(1^t \left\{ \begin{bmatrix} \mathbb{E}_D & \mathbb{E}_Q \end{bmatrix} \mathbf{Y}_r \begin{bmatrix} \mathbb{E}_D \\ \mathbb{E}_Q \end{bmatrix} + \mathrm{diag}(\mathsf{P}) \right\} \right)^t \\ &= \left\{ -\begin{bmatrix} \mathbb{E}_D & \mathbb{E}_Q \end{bmatrix} \mathbf{Y}_r \begin{bmatrix} \mathbb{E}_D \\ \mathbb{E}_Q \end{bmatrix} + \mathrm{diag}(\mathsf{P}) \right\} 1 = -\mathsf{P}_e + \mathsf{P}_e = 0. \end{aligned} \tag{4.61}$$

Although we do not explicitly consider the constant-power load model in this thesis, the same argument holds for constant-power loads as well, since they are invariant with

respect to voltage. This relationship does not hold, however, when $\mathbf{G} \neq \mathbf{0}$, and in that case, $\mathbf{J}_{\|}^{p}$ is normally nonsingular about any viable equilibrium point. Throughout this section, it will be assumed that the $p \times p$ matrix $\mathbf{J}_{\|}^{p}$ has rank $p-1$. This appears to be generically true locally about viable equilibria, but as in the lossy case, the matrix may drop rank or become ill-conditioned (with respect to the $p-1$ nonzero singular values) at other points in the state space.

Since it is really the increment in $\dot{\mathsf{P}}_e$ created by variation in the field voltage that controls the angle/frequency dynamics of the machines, it would appear that no more than $p-1$ of the system generators could be fitted with FBLC. There is a method for avoiding this problem, however. The problem that is to be solved takes the form

$$\dot{\mathsf{P}}_e = \mathbf{J}_{\|}^{p}\boldsymbol{\lambda}_{\|} + \mathbf{J}_{\perp}^{p}\boldsymbol{\lambda}_{\perp}. \tag{4.62}$$

Because of the rank deficiency of $\mathbf{J}_{\|}^{p}$, there may be no solution for arbitrary $\dot{\mathsf{P}}_e$. However, under certain circumstances, it may be shown that the desired value of $\dot{\mathsf{P}}_e$ always lies in the range space of $\mathbf{J}_{\|}^{p}$, at least in COI coordinates.

Claim 4.3 *Suppose that in (4.56),* $\mathbf{A}_3$ *takes the form*

$$\mathbf{A}_3 = \begin{bmatrix} a_0\mathbf{I} & a_1\mathbf{I} & a_2\mathbf{I} \end{bmatrix} \tag{4.63}$$

Then the equation

$$\mathbf{J}_{\|}^{p}\boldsymbol{\lambda}_{\|} = \mathbf{J}_{\perp}^{p}\boldsymbol{\lambda}_{\perp} + \mathbb{M}\mathbf{A}_3 \begin{bmatrix} (\boldsymbol{\delta} - \boldsymbol{\delta}_o) \\ \boldsymbol{\omega} \\ \boldsymbol{\alpha} \end{bmatrix}, \tag{4.64}$$

has an exact solution for all $[\boldsymbol{\delta}^t \quad \boldsymbol{\omega}^t \quad \boldsymbol{\alpha}^t]^t$ *in some neighborhood of the equilibrium* x_o.

Proof:

The claim follows from the fact that

$$1^t \left(\mathbf{J}_{\perp}^{p} \boldsymbol{\lambda}_{\perp} + \mathbb{M}\mathbf{A}_3 \begin{bmatrix} (\boldsymbol{\delta} - \boldsymbol{\delta}_o) \\ \boldsymbol{\omega} \\ \boldsymbol{\alpha} \end{bmatrix} \right) = 0. \tag{4.65}$$

This holds since $1^t \mathbf{J}_{\perp}^{p} = 0$ in a lossless system, and the second term on the RHS may be reduced to

$$\begin{aligned} 1^t \mathbb{M}\mathbf{A}_3 \begin{bmatrix} (\boldsymbol{\delta} - \boldsymbol{\delta}_o) \\ \boldsymbol{\omega} \\ \boldsymbol{\alpha} \end{bmatrix} &= 1^t \begin{bmatrix} a_0 m_1(\delta_1 - \delta_o) + a_1 m_1 \omega_1 + a_2 m_1 \alpha_1 \\ a_0 m_2(\delta_2 - \delta_o) + a_1 m_2 \omega_2 + a_3 m_2 \alpha_2 \\ \vdots \\ a_0 m_p(\delta_p - \delta_o) + a_1 m_p \omega_p + a_3 m_p \alpha_p \end{bmatrix} \\ &= a_0 \sum_{i=1}^{p} m_i(\delta_i - \delta_o) + a_1 \sum_{i=1}^{p} m_i \omega_i + a_2 \sum_{i=1}^{p} m_i \alpha_i = 0, \end{aligned} \tag{4.66}$$

with the final equality being true because each of the constituent summations is equal to zero in COI. Hence, it is clear that in actual operation, $\dot{\mathsf{P}}_e$ never has any projection along the vector 1, *i.e.* it has no component in the left nullspace of $\mathbf{J}_{\|}^{p}$, provided that the coefficients of $\mathbf{A}_3$ are chosen so as to select the same triplet of poles for each machine in the system. But this means that $\dot{\mathsf{P}}_e$ must lie in the column space of $\mathbf{J}_{\|}^{p}$, hence (4.64) has an exact solution. ∎

It is possible to generalize the subsystem pole-matching requirement to a certain extent. Suppose that a rotor-angle reference is defined as a convex combination of the rotor angles taken with respect to a fixed arbitrary reference, *i.e.*

$$\delta_r = \sum_{i=1}^{p} k_i \delta_i, \quad k_i > 0, \quad \sum_{i=1}^{p} k_i = 1. \tag{4.67}$$

It may be shown by the same procedure as in Claim 4.3 that for $\mathbb{K} = \mathrm{diag}(k_1, k_2, \ldots, k_p)$, if

$$\mathbf{A}_3 = \mathbb{M}^{-1}\mathbb{K} \begin{bmatrix} a_0\mathbf{I} & a_1\mathbf{I} & a_2\mathbf{I} \end{bmatrix}, \tag{4.68}$$

then $\dot{\mathsf{P}}_e$ is in the range of $\mathbf{J}_{\|}^{p}$, provided that all angle, frequency and acceleration mea-

surements are taken with respect to δ_r as defined in (4.67). In the special case where the COI reference is used, $\mathbb{K} = \mathbb{M}$.

In order for this to be valid, of course, measurements of $\boldsymbol{\delta}$, $\boldsymbol{\omega}$ and $\boldsymbol{\alpha}$ must be taken in COI (or in the generalized COI of (4.67)). Practically speaking, it is impossible to obtain measurements of the machine states in COI. There are similarities between the COI frame of reference and the Observation Decoupled State Space (ODSS) of Zaborszky *et. al.*, however [54, 55]. A modified ODSS was used in formulating a type of decentralized FBLC in [8]. It may also be possible to approximate the COI reference in a similar manner, particularly in view of the emerging phasor-measurement technology, but this is beyond the scope of this thesis.

When (4.68) is satisfied, $\boldsymbol{\lambda}_{\|}$ may be found by using the Moore-Penrose inverse (also known as the pseudoinverse) in (4.53). If, on the other hand, the selected subsystem poles are such that the required control signal is not in the range of $\mathbf{J}^p_{\|}$, the actual system poles are shifted from the design locations, but the response of the system remains linear. This can be shown as follows: Recall that for the lossless system, $\mathbf{1}^t\mathbf{J}^p_{\|} = \mathbf{1}^t\mathbf{J}^p_{\perp} = 0$, that is, the vector $\mathbf{1}$ is orthogonal to the column space of both $\mathbf{J}^p_{\|}$ and $\mathbf{J}^p_{\perp}$. We project the RHS of (4.64) onto the column space of $\mathbf{J}^p_{\|}$ by subtracting the projection along the vector $\mathbf{1}$, yielding the following equation, which has an exact solution provided that $[\,\mathbf{J}^p_{\|} \quad \mathbf{1}\,]$ has full row rank:

$$\mathbf{J}^p_{\|}\boldsymbol{\lambda}_{\|} = \mathbf{J}^p_{\perp}\boldsymbol{\lambda}_{\perp} + \mathbb{M}\mathbf{A}_3\mathbf{z} - \frac{1}{p}\mathbf{1}\mathbf{1}^t\mathbb{M}\mathbf{A}_3\mathbf{z}. \tag{4.69}$$

Setting $\eta = \frac{1}{m}\mathbf{1}^t\mathbf{A}_3\mathbf{z}$ yields

$$\begin{bmatrix} \mathbf{J}^p_{\|} & \mathbf{1} \end{bmatrix} \begin{bmatrix} \boldsymbol{\lambda}_{\|} \\ \eta \end{bmatrix} = \mathbf{J}^p_{\perp}\boldsymbol{\lambda}_{\perp} + \mathbb{M}\mathbf{A}_3\mathbf{z}. \tag{4.70}$$

Since $\mathbf{1}$ is orthogonal to the column space of $\mathbf{J}^p_{\|}$, the value of η is unique, and is as we have defined it. Moreover, we now have a underdetermined set of equations, which

always has a solution. Let

$$\begin{bmatrix} \boldsymbol{\lambda}_{\|} \\ \eta \end{bmatrix} = \begin{bmatrix} \mathbf{J}_{\|}^{p} & 1 \end{bmatrix}^{+} \mathbf{J}_{\perp}^{p} \boldsymbol{\lambda}_{\perp} + \mathbb{M}\mathbf{A}_3\mathbf{z}, \tag{4.71}$$

where the "+" superscript denotes the pseudoinverse. This $\boldsymbol{\lambda}_{\|}$ solves (4.69) and is also the minimum-norm solution. Hence, from (4.69) and (4.46), the system dynamics will be governed by

$$\dot{\boldsymbol{\alpha}} = A_3\mathbf{z} - \frac{1}{p}\mathbb{M}^{-1}11^{t}\mathbb{M}\mathbf{A}_3\mathbf{z}, \tag{4.72}$$

which is linear. Note that if $\mathbf{A}_3$ has the form of (4.63), $1^{t}\mathbb{M}\mathbf{A}_3\mathbf{z} = 0$, which recovers the original special case.

If the grid is not lossless (or if constant-impedance loads are present), then $\mathbf{J}_{\|}^{p}$ will normally be nonsingular. Nonetheless, it may still be of interest to satisfy a condition similar to (4.66) in order to avoid unnecessary control saturation. For instance, it may be desirable to minimize the projection of the RHS of (4.64) along singular vectors of $\mathbf{J}_{\|}^{p}$ which are associated with singular values of small magnitude. This is more difficult to formalize, since the singular values and singular vectors will be state-dependent, but if the real part of the admittance matrix is small, then there will remain a singular vector that is close to 1 associated with a small singular value, and this will not vary significantly along system trajectories.

All of the foregoing discussion has the flavor of a modal reachability condition, but there is no specific unreachable mode involved; instead, the condition of (4.68) must be satisfied. In particular, even if $\mathbf{A}_3$ satisfies (4.68), $1^{t}\mathbf{A}_3 \neq 0$.

4.7.3 Noninteracting Voltage Control

The use of FBLC presents a problem, in that it provides no direct means for regulating the terminal voltages of the generators [8]. The only quantities that are directly regulated are $\boldsymbol{\delta}$, $\boldsymbol{\omega}$ and $\boldsymbol{\alpha}$, so that the voltages achieved at the various generators are a by-product of network loading, configuration and the rotor reference angle that is provided to each control. It is important to distinguish here between the reference

angle that is provided as an equilibrium point for each generator and the systemwide reference angle (such as the COI reference) that was discussed in Chapter 2. Here we are referring to a reference signal that is used as an input to the FBLC, from which the rotor angle error signal is derived. For instance, if δ_{oi} is selected as the reference angle for FBLC at the i^{th} machine, it becomes the equilibrium angle for that machine. If the value of δ_{oi} is improperly selected, the machine will not operate with the desired terminal voltage. A simple example will illustrate this problem.

Consider a single-machine, single-axis, infinite-bus internal-node model. Let x_{eq} be the equivalent line impedance (lumped with the machine impedance) and let the infinite-bus voltage have a phase angle of 0 and magnitude E_∞. At equilibrium, given a reference angle δ_o, the load-flow equation for this system is

$$P_e = T_m = \frac{EE_\infty}{x_{eq}} \sin(\delta_o). \tag{4.73}$$

Assuming that FBLC is used, the control will act to maintain a rotor angle of δ_o as, for instance, the effective impedance or the input torque changes. Consequently, the only free variable at equilibrium is the machine voltage magnitude E. If the machine is to operate within a prescribed voltage range, some method must be found for making the reference angle sensitive to changes in network loading and configuration. In the multimachine case, this means that a set of reference angles must be found that solves the load-flow equations for a given set of desired terminal voltage magnitudes[4], and this procedure must be repeated for every significant change in the operating condition of the system. This has been the subject of some research [6, 8], but the point to be made here is that achieving tight voltage control with FBLC is a difficult problem, and that voltage control objectives tend to be at odds with the task of achieving rapid stabilization of angle/frequency dynamics.

A consequence of the singularity of $\mathbf{J}_{\|}^p$ is that $\boldsymbol{\lambda}_{\|}$ is not uniquely determined. This is easily seen, since if $\boldsymbol{\lambda}_{\|}^o$ solves (4.64), then $\boldsymbol{\lambda}_{\|}^o + \tilde{\boldsymbol{\lambda}}_{\|}$ is also a solution for any $\tilde{\boldsymbol{\lambda}}_{\|}$ such that $\mathbf{J}_{\|}^p \tilde{\boldsymbol{\lambda}}_{\|} = 0$. In the initial seconds following a major system disturbance, it may

[4] *i.e.* some reasonable approximation of a full-scale load-flow calculation must be performed

seem sensible to attempt to minimize $\|\boldsymbol{\lambda}_{\|}\|_2$, in an effort to avoid unnecessary control saturation, and indeed, this is precisely the solution that is achieved through the use of the Moore-Penrose inverse. This is only a pointwise minimization, however, and there is no guarantee that it will lead to an overall minimization of any signal norm with respect to the input. Another possibility that presents itself is the potential for utilizing the extra degree of freedom in $\boldsymbol{\lambda}_{\|}$ to implement a type of non-interacting voltage control, and indeed, when $\mathbf{J}_{\|}^{p}$ is singular, it is actually necessary to implement some sort of voltage control, since even with the proper selection of $\boldsymbol{\delta}_o$, the equilibrium voltage magnitudes are not uniquely determined. This would be the situation if, in the example above, both E and E_∞ were allowed to vary. Given a particular selection of δ_o, the two voltages are only subject to a single constraint, hence they are not uniquely determined.

A conceptually simple method for achieving a type of noninteracting voltage control when $\mathbf{J}_{\|}^{p}$ is singular is to project the voltage error vector onto the nullspace of $\mathbf{J}_{\|}^{p}$, as follows:

$$\tilde{\boldsymbol{\lambda}}_{\|} = k_v(\mathbf{I} - \mathbf{J}_{\|}^{p}(\mathbf{J}_{\|}^{p\,t}\mathbf{J}_{\|}^{p})^{-1}\mathbf{J}_{\|}^{p\,t}) \begin{bmatrix} (V_1 - V_{ref_1}) \\ \vdots \\ (V_p - V_{ref_p}) \end{bmatrix}, \tag{4.74}$$

where k_v is a scalar gain. Using this method, the voltage correction term $\tilde{\boldsymbol{\lambda}}_{\|}$ affects the magnitudes of the machine voltages, but has no effect on the generator output power, hence is not seen in the frequency/angle dynamics of the system. This is true only as long as control saturation is avoided, so that if a truly noninteracting control were desired, it would be necessary to disable the voltage control during the immediate postfault period following a large disturbance. The use of a noninteracting voltage control will presently be demonstrated via a series of simulations.

Although all of the foregoing has been expressed in terms of implementation issues with respect to FBLC, these findings have impact on the design of other types of field voltage control, since they represent fundamental limits on the behavior of the power/angle subsystem with respect to field voltage control. In particular, even if $\mathbf{J}_{\|}^{p}$ is nonsingular, it will be of interest to avoid damping controls that require a signifi-

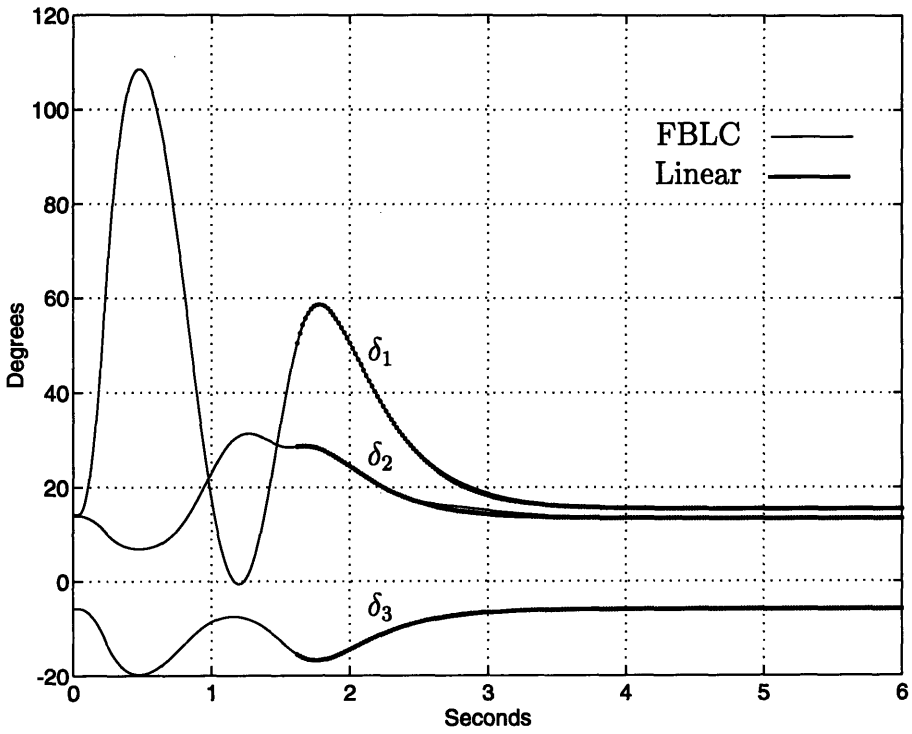

Figure 4.29: Rotor Angle Response Compared to Linear Response.

cant projection along the singular vectors of $\mathbf{J}_{\|}^{p}$ that are associated with small singular values. Similarly, these same singular vectors represent directions along which voltage control may be achieved with the smallest possible interaction with the angle/frequency dynamics of the system. Because of the fact that most power system controls are designed as decentralized units, the type of control interaction involved here may not be properly expressed in the reduced-order models used in control design, and in particular may not show up as modal controllability problems when viewed from a single input, particularly when detailed modeling of existing damping controls is not utilized in the design phase.

4.7.4 Simulations

We will now demonstrate some of the foregoing concepts through simulations of the three-machine test system, again using the case 1 fault. Initially, it is of interest to compare a simulation in which the control input is taken as the least-norm solution of (4.64) and one in which the noninteracting voltage control is utilized. In both these

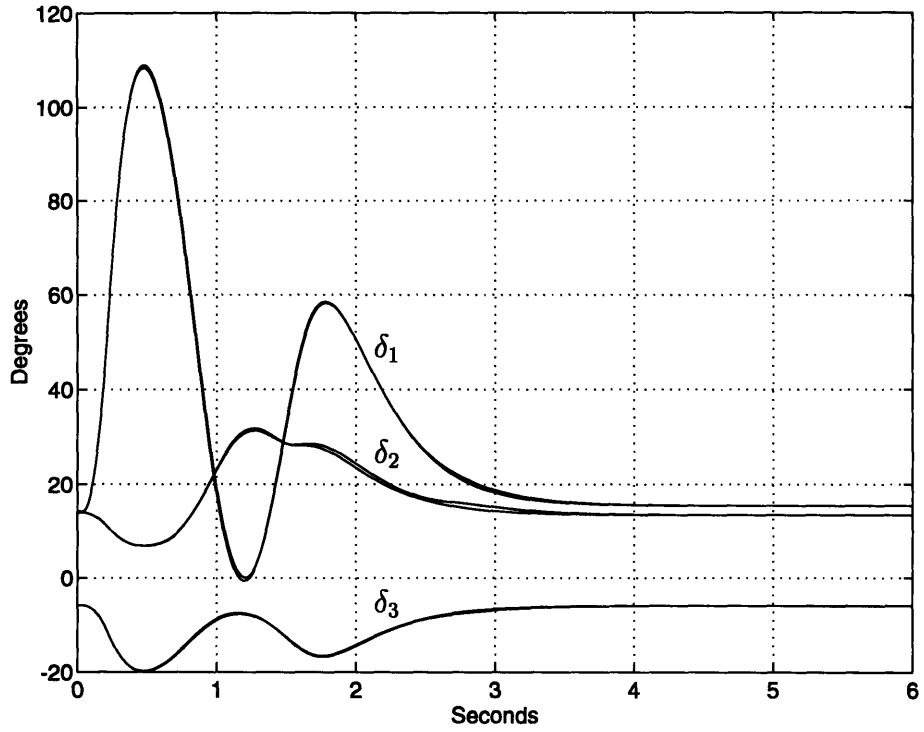

Figure 4.30: Rotor Angle Response With and Without Voltage Control.

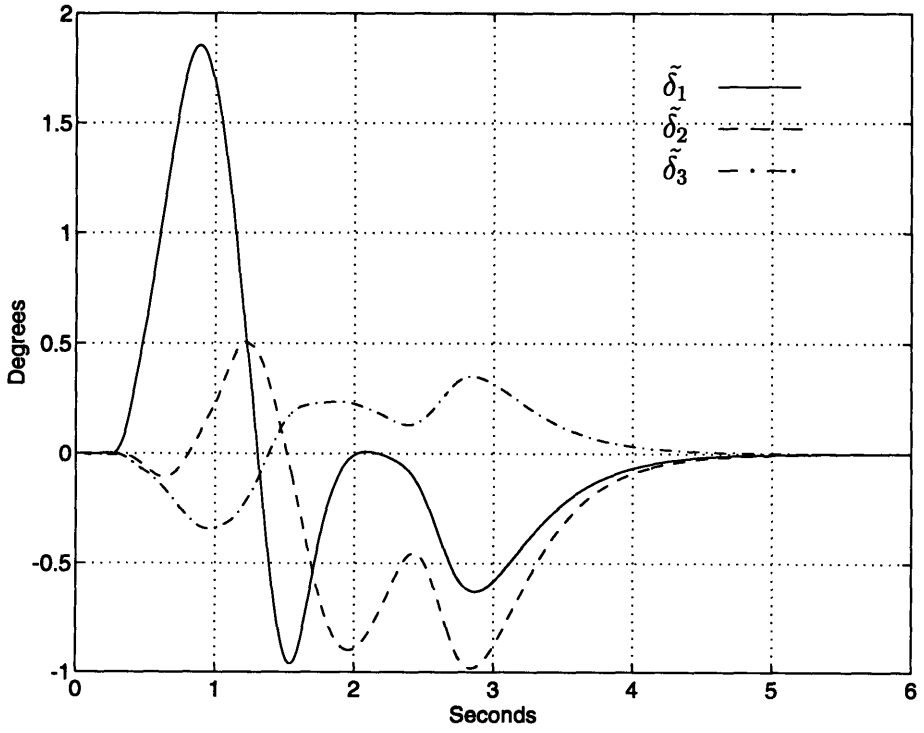

Figure 4.31: Rotor Angle Difference, With and Without Voltage Control.

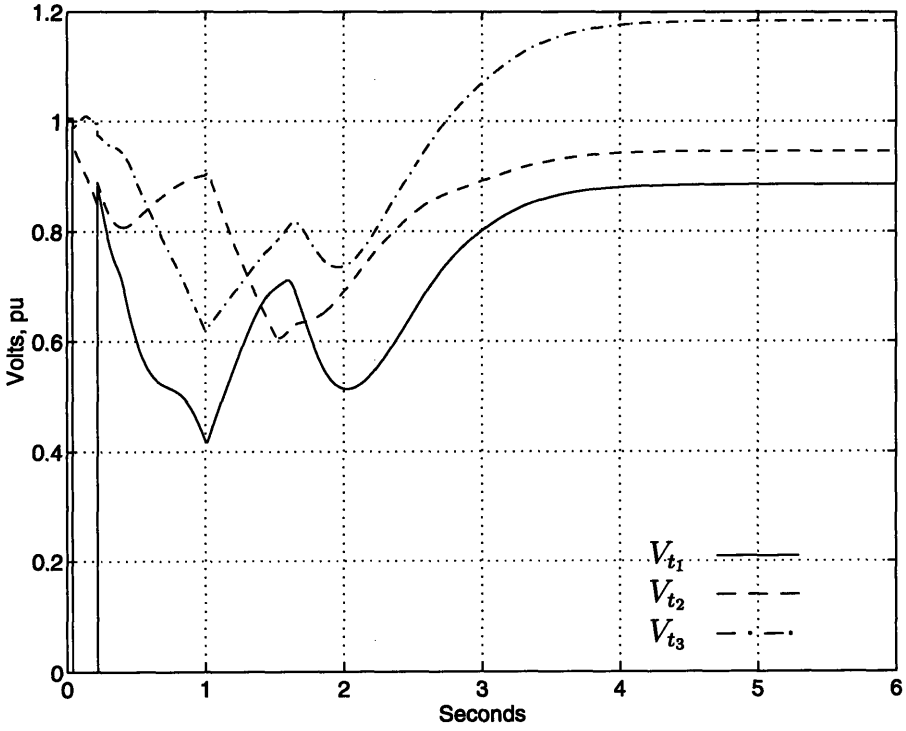

Figure 4.32: Terminal Voltage: No Supplementary Voltage Control.

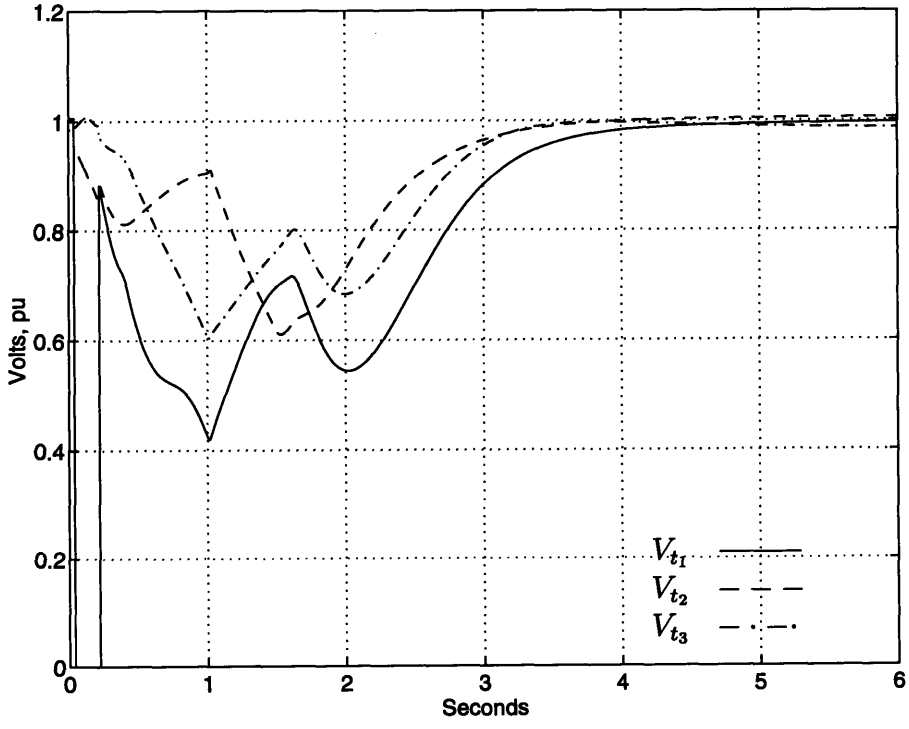

Figure 4.33: Terminal Voltage: Noninteracting Voltage Control.

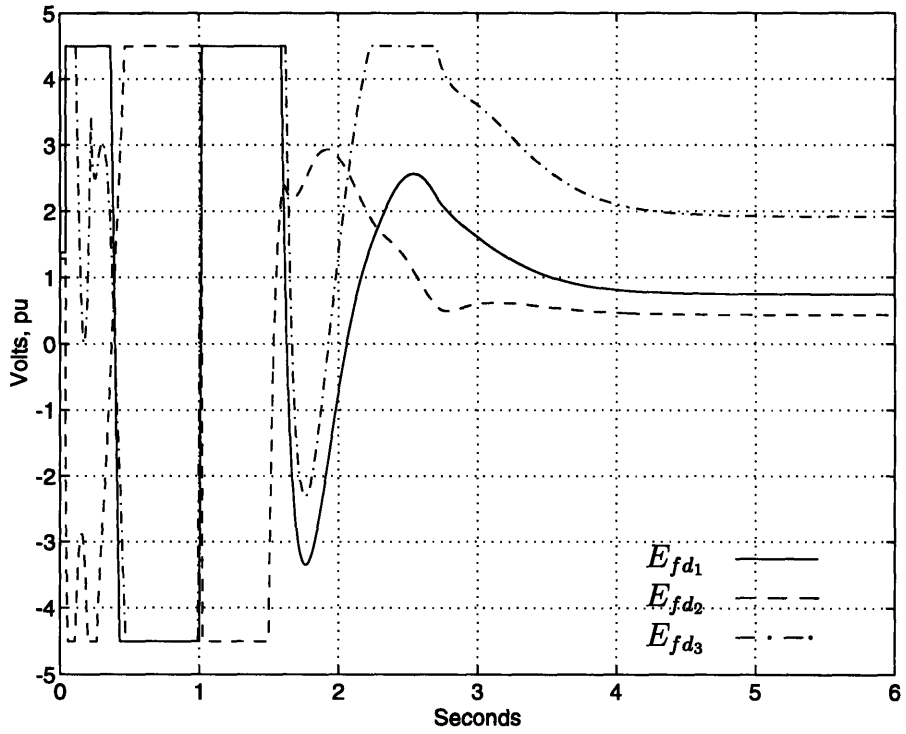

Figure 4.34: Field Voltage: No Supplementary Voltage Control.

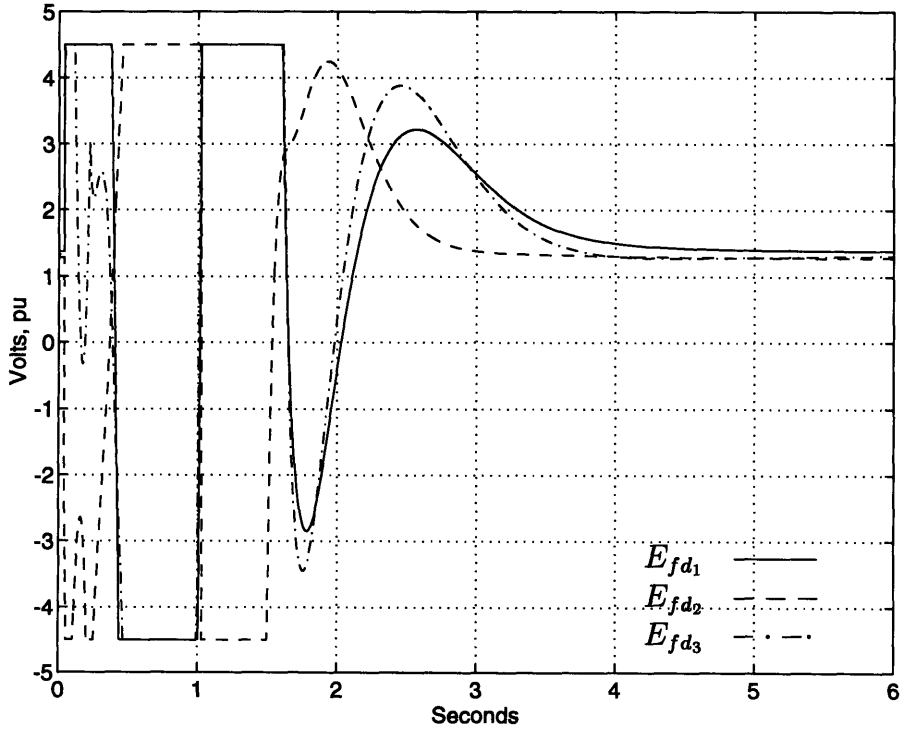

Figure 4.35: Field Voltage: Noninteracting Voltage Control.

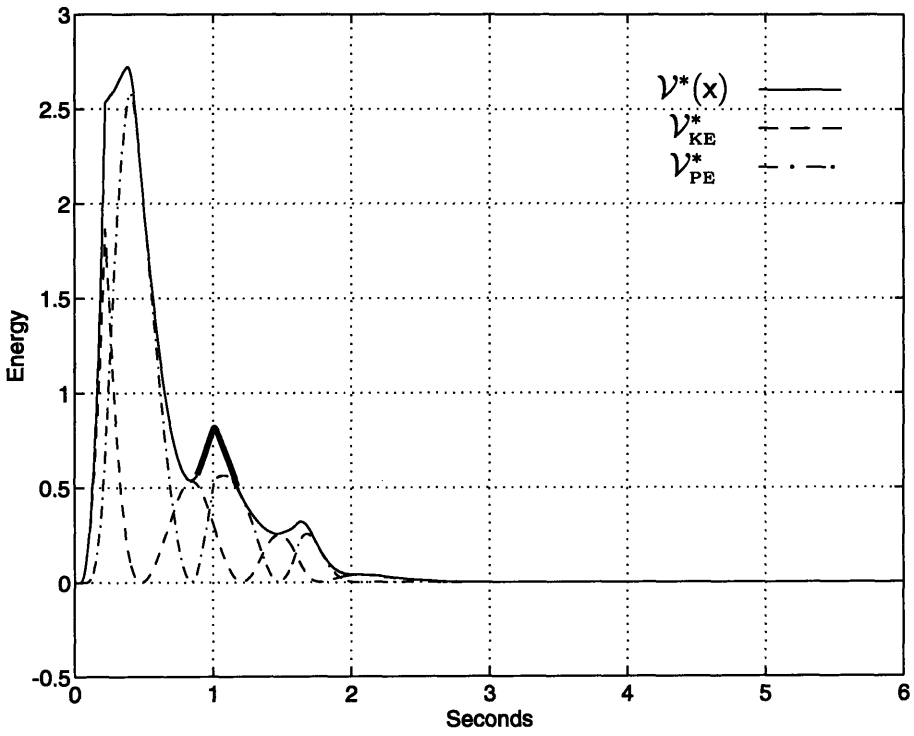

Figure 4.36: Transient, Kinetic and Potential Energy: Noninteracting Voltage Control.

simulations, a clearing time of $t_{cl} = 0.22$ sec. is used in the case 1 scenario. The gain k_v for the noninteracting control of (4.74) is 1. This gives good voltage control while minimizing the impact on the power/angle dynamics during control saturation. Poles on all machines are set at -3, -5 and -10, a somewhat arbitrary choice. The issue of pole placement for feedback linearizing excitation control is somewhat difficult to address. In previous work by this author [6, 8, 26], the three poles were set at -5, based on the heuristic guideline that the FBLC poles should be at least a decade less in magnitude than the lowest range of possible unmodeled dynamics in the system. The problem that is of most concern in designing excitation controls is that of generator shaft resonance, which tends to occur at frequencies above 62 radians/sec, hence the poles were set to be comfortably below this margin. In the present case the pole placement was determined experimentally to yield somewhat better performance. The information gained through the simulations in this and previous sections will lead to a somewhat more effective method of pole placement, however.

Figure 4.29 shows the rotor-angle response of the basic FBLC control. In this case,

the norm of $\boldsymbol{\lambda}_{\|}$ is minimized pointwise as the simulation proceeds (*i.e.* the pseudoinverse is used to yield the minimum-norm solution at each point of the simulation). Superimposed upon the plot (bold traces) is the response of a linear system whose poles match the design poles of the test system with FBLC. These plots start at the point at which all field voltages first come out of saturation. The small discrepancy that is seen is due to a short additional period of field-voltage saturation on Generator 3 that occurs roughly in the interval between 2.3 – 2.6 sec. The response does match exactly if the linear test model is initialized after this last period of saturation, however, the match is quite good over the longer period that is plotted here. It is telling to observe the state of the system at the point at which saturation becomes insignificant; in terms of the magnitude of the state deviations, this occurs very late in the course of the transient, which gives a graphic example of the severity of the field voltage saturation limits in the context of power/angle control.

Figures 4.30 and 4.31 compare the rotor-angle response with and without noninteracting voltage control. The responses are all but indistinguishable in Figure 4.30. The difference between the two simulations appears in Figure 4.31, showing that the maximum deviation is less than 2 degrees. As noted in the foregoing section, this difference results from the application of the voltage correction signal during the period when field voltage saturation is occurring. These plots make it clear that the voltage correction signal has minimal impact on the power/voltage dynamics. In this case at least, the effect of the noninteracting control is minimal even when one or more control inputs is in saturation.

The voltage correction signal is effective in bringing the voltages back to the desired levels, however, as Figures 4.32 and 4.33 demonstrate. The disparity in the responses is apparent. Note that the use of noninteracting voltage control does not eliminate the requirement that the postfault reference rotor angles $\boldsymbol{\delta}_o$ be chosen correctly, since the supplementary voltage correction signal cannot change the equilibrium rotor angle; it can only select the most favorable voltage profile that is consistent with the chosen equilibrium angle.

In previous work [6, 8], a variant of the Observation Decoupled State Space was

utilized as a means of calculating an appropriate postfault equilibrium angle, but it was noted that the voltage control achieved with this method was slow to correct errors in the voltage profile, even after the initial transient behavior had essentially disappeared. In this earlier work, a lossy system model was used, yielding a nonsingular $\mathbf{J}_{\|}^{p}$. It may be conjectured that the persistent terminal voltage offset occurred along directions for which the gain of $\mathbf{J}_{\|}^{p}$ was small, *i.e.* along singular vectors associated with small singular values. In this situation it may be possible to design a weakly-interacting voltage control signal to work in conjunction with the ODSS in order to improve the voltage response of the system.

An interesting phenomenon is evident in Figures 4.34 and 4.35. The second of these two plots depicts the response of the field voltage with the noninteracting voltage control signal, which also shows less field-voltage saturation than the pointwise minimum-norm method, which does not incorporate any supplementary control. Clearly, the pointwise minimization of the control signal does not reduce the amount of control saturation, as compared with the control that incorporates noninteracting voltage correction. The problem of devising a more meaningful minimization of the control energy in a large-signal context is a difficult matter, however, due both to the system nonlinearity and the strict limits on the control magnitude.

The final figure in this series (Figure 4.36) is a plot of the STEF for FBLC with noninteracting voltage control. Clearly, FBLC does not result in a monotonic decline of the STEF, but instead allows the total energy to rise at points where the KE is decreasing, *i.e.* when KE is being converted into PE. The control acts to increase the KE/PE gradient at these times, which increases the rate of the conversion at the expense of an overall gain in the value of the STEF. The bold overlay on the transient energy trace is a section for which there is no equilibrium: The stable equilibrium does not exist for the voltage magnitudes extant during that part of the simulation. In this portion of the simulation, the equilibrium is taken as the last converged load-flow solution along the system trajectory. The STEF is clearly not a valid measure of the system energy during this part of the simulation, at least in the characterization of the "potential" energy, but the incremental exchange of kinetic and potential energy

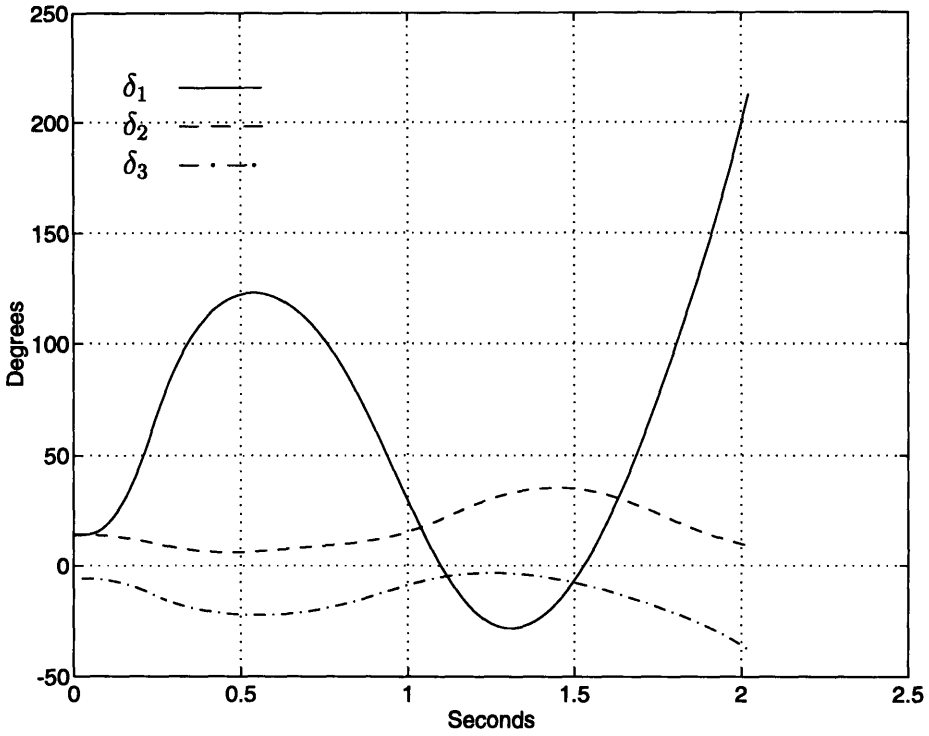

Figure 4.37: Rotor Angles, Second-Swing Unstable.

is preserved. What is lost is the effect of voltage variation on the potential energy term. The temporary loss of the stable equilibrium point does not result in loss of synchronism, since the equilibrium is recovered as the angle trajectory returns toward the prefault equilibrium. This is not always the case, however, as will presently be seen.

4.7.5 FBLC Pole Placement

In FBLC, the question of where to assign the design poles of the system may be difficult to address. Typical linear design strategies that seek to minimize some measure of the control response as an input to the design process are not directly applicable, since there is no methodical procedure for expressing the control effort required to cancel the system nonlinearity, and the control effort expressed as a linear combination of the transformed states must be mapped back through $\mathbf{J}_{\|}^{p}$ to arrive at the actual control magnitude. Since $\mathbf{J}_{\|}^{p}$ is nonlinearly state-dependent, it is difficult to penalize the control effort in an optimization routine, as is typically done in linear control design. Moreover, the severity of the control saturation limits is difficult to account for in any direct

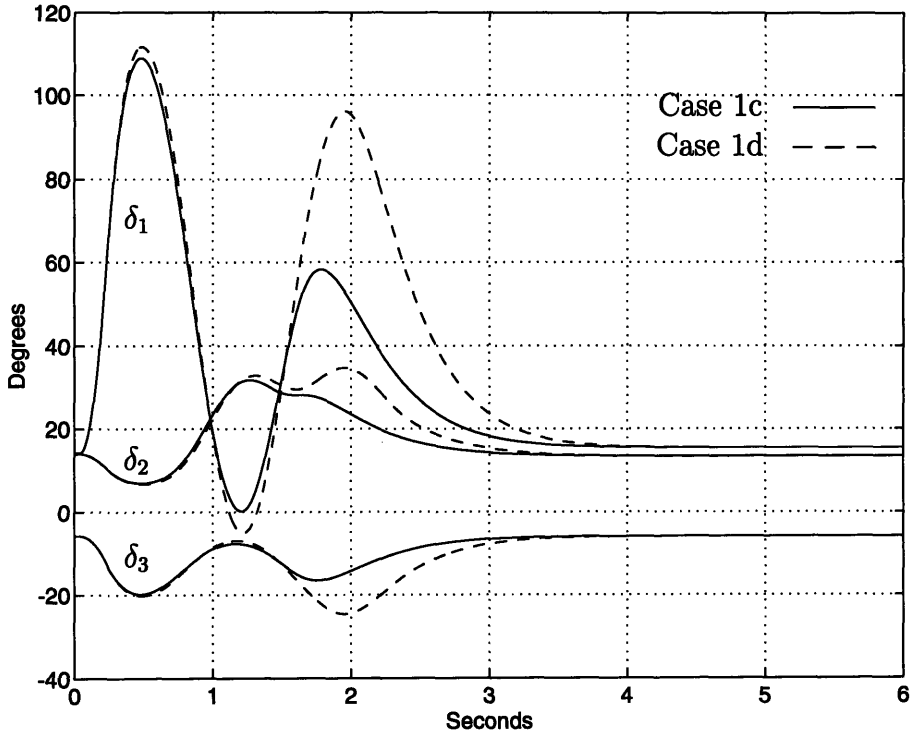

Figure 4.38: Rotor Angle Comparison, Case 1c & Case 1d.

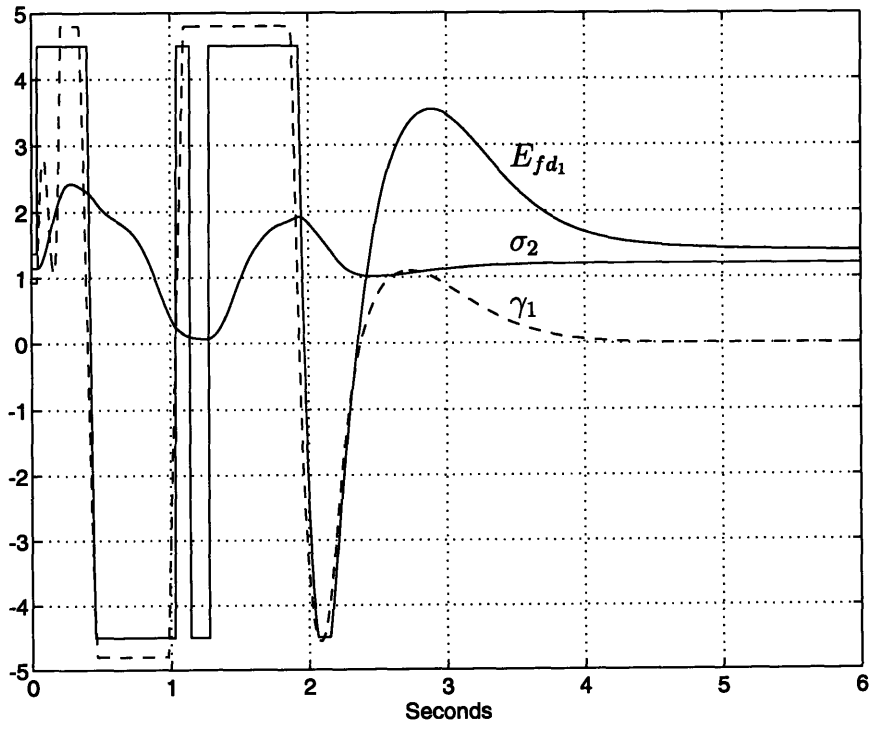

Figure 4.39: Minimum Nonzero Singular Value, Gen. 1 Field Voltage, Pre-input.

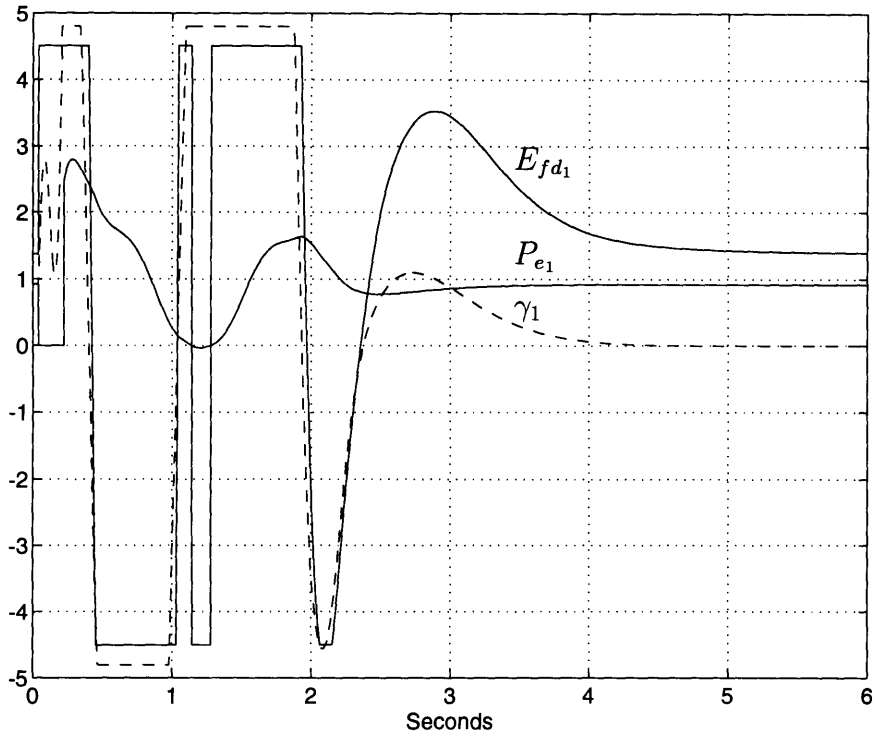

Figure 4.40: Gen. 1 Power, Gen. 1 Field Voltage, Pre-input.

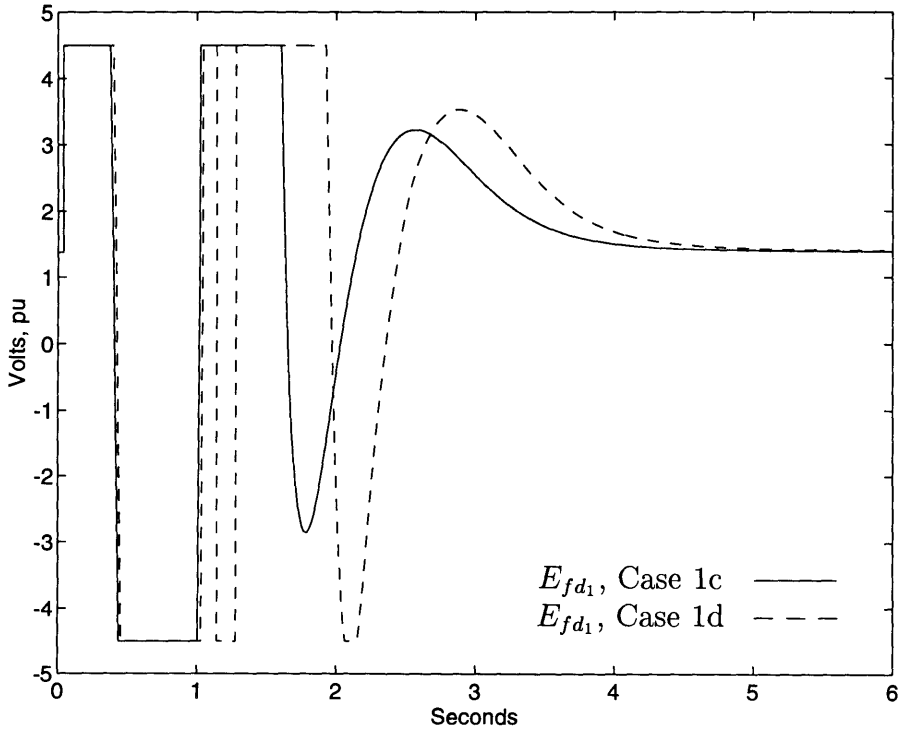

Figure 4.41: Field Voltage Comparison, Case 1c & Case 1d.

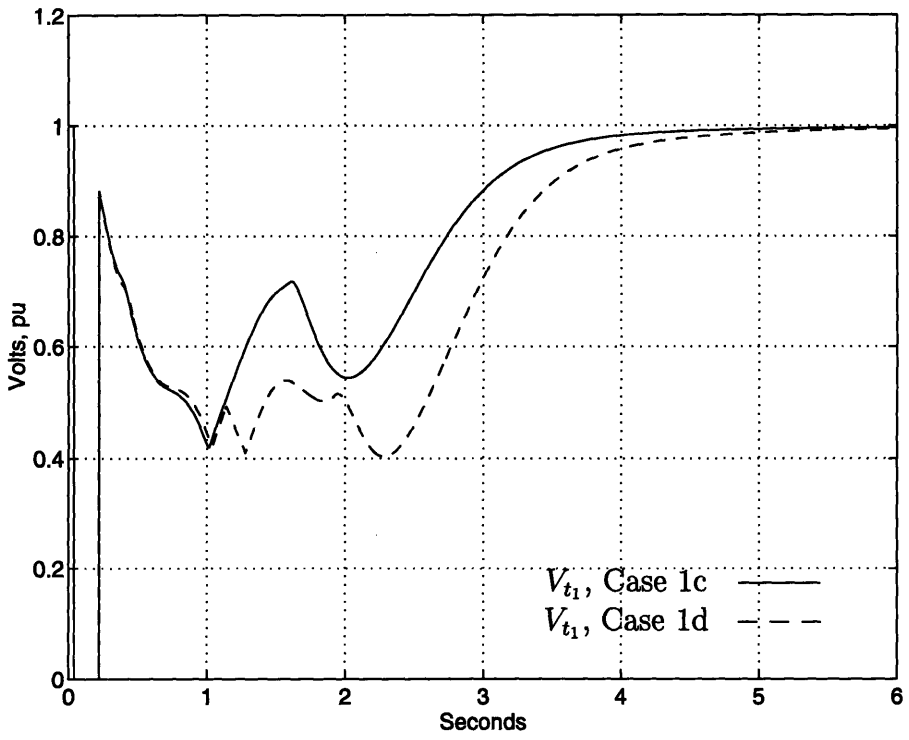

Figure 4.42: Terminal Voltage Comparison, Case 1c & Case 1d.

fashion.

In this section, the time-scale separation of control objectives and the state decomposition into variables associated with the fast objective and those associated with the slow objective will be used to guide the pole assignment process. Some comparative simulations will also be presented and analyzed, in which some of the difficulties related to ill-conditioning of the input matrix $\mathbf{J}_{\|}^{p}$ at certain points in the state space will become clear. These are of particular concern with FBLC, but also bear on the design of other types of excitation control. The characteristics of FBLC with respect to the PE gradient and the singularity of $\mathbf{J}_{\|}^{p}$ will be analyzed and their relationship to the control objectives will be identified.

Note that the pole placement in the foregoing FBLC simulations does not reflect any time-scale separation. In these simulations, the poles were placed based on previous experience with FBLC on other systems. Pole placement was a compromise between the desire for rapid damping of oscillations, avoidance of excessive input saturation, and the need to avoid exciting unmodeled higher-order dynamics. In any event, the performance

of the control (in terms of transient stability) appeared to be quite insensitive to the pole configuration on other system models . Such is not the case with the test system used here; it will be seen that the pole placement is crucial to the security of the system. A pole-placement scheme that reflects the time-scale separation of control objectives is seen to be considerably more effective in preventing loss of synchronism.

In the previous section, the fault clearing time used in all simulations was $t_{c\ell} = 0.22$. This is well within the limits of first-swing stability for this control. If the clearing time is increased to $t_{c\ell} = 0.23125$, an interesting phenomenon is observed. Although FBLC significantly increases the first-swing stability of the system, generator 1 loses stability on the second swing, as shown in Figure 4.37. A more informative comparison is shown in Figure 4.38. In this figure, the rotor angle plots of two simulations are superimposed. The first, plotted with solid lines, is the same case as was used in the previous section, with a clearing time $t_{c\ell} = .220$. This will be referred to as case 1c. The second, plotted with broken lines, has a clearing time $t_{c\ell} = 0.2225$ and will be referred to as case 1d. The response of the two simulations is quite similar over the first swing, as might be expected, given the small change in the clearing time. The second-swing response is dramatically different, however. The system is actually unstable on the second swing for clearing times much in excess of 0.2225. The change in behavior appears to be due to structural changes that occur in $\mathbf{J}_{\|}^{p}$ as the difference in rotor angles of generators 1 and 3 approaches zero.

An examination of several relevant quantities for $t_{c\ell} = 0.2225$ provides some insight into this problem. Figure 4.39 depicts the evolution of the smallest nonzero singular value of $\mathbf{J}_{\|}^{p}$, which is denoted σ_2. The second trace is the field voltage of generator 1, while the dashed trace shows the value of the first element of $\mathbf{J}_{\perp}^{p}\boldsymbol{\lambda}_{\perp} + \mathbf{M}\mathbf{A}_3\mathbf{z}$, that is, the first element of the feedback linearizing input prior to being multiplied by $(\mathbf{J}_{\|}^{p})^{-1}$. This quantity has been denoted γ_1 in the plot, and its value has been limited to $|\gamma_1| \leq 4.8$ for clarity in the comparison. Observe the close correlation between the signs of E_{fd_1} and γ_1, up until the first minimum of σ_2, at which point the two signals assume opposite signs. Shortly thereafter, the two signals again assume the same signs. These changes coincide with the point at which the power flow along the transmission line connecting

generators 1 and 2 is reversed, as shown in Figure 4.40. When this occurs, the increment in power associated with a voltage change at generator 1 is also reversed, which accounts for the reversal in E_{fd_1}. Up to the point at which the polarity reversal occurs, the field voltage response at generator 1 is almost identical in both cases, but the responses diverge after the change. As shown in Figure 4.42, the momentary reversal in the field voltage causes the terminal voltage to decline sharply, following which it never achieves the level seen in the the milder fault.

From the foregoing comparison, it seems clear that the polarity reversal observed in the field-voltage response of generator 1 is detrimental to the transient stability of the system. Two factors appear to contribute to the problem. The first is the small value of σ_2, which of course translates into a large gain in $(\mathbf{J}_{\|}^{p})^{-1}$ along the associated singular vector. Concurrently, the reversal of power flow at generator 1 causes a sign change in the singular vector associated with σ_2, which causes the observed sign change in the field voltage. This change first occurs at $t \approx 1.14003$ seconds, a point at which $\sigma_2 = 0.1084$. Evaluating $(\mathbf{J}_{\|}^{p})^{+}$ shortly before and after this time, we have

$$(\mathbf{J}_{\|}^{p})^{+}|_{(t=1.14001)} = \begin{bmatrix} 0.0019 & 0.0014 & -0.0033 \\ -5.3274 & 2.7615 & 2.5659 \\ 5.3273 & -2.5659 & -2.7614 \end{bmatrix}, \tag{4.75}$$

and

$$(\mathbf{J}_{\|}^{p})^{+}|_{(t=1.14005)} = \begin{bmatrix} -0.0019 & 0.0033 & -0.0015 \\ -5.3284 & 2.7619 & 2.5665 \\ 5.3284 & -2.5664 & -2.7620 \end{bmatrix} \tag{4.76}$$

for which the singular vector $\mathbf{v}_2$ associated with $1/\sigma_2$ is

$$\mathbf{v}_2(t = 1.14001) = \begin{bmatrix} 0.0003 \\ -0.7071 \\ 0.7071 \end{bmatrix}; \quad \mathbf{v}_2(t = 1.14005) = \begin{bmatrix} -0.0002 \\ -0.7071 \\ 0.7071 \end{bmatrix}. \tag{4.77}$$

σ_2 remains essentially constant over this interval. The small magnitude of σ_2, coupled

with the large deviation of δ_1, amplify the effect of the sign change in v_2. Note also that the interval between the two cases (4.75) and (4.76) is very short. Following this interval, the effect of the sign change on $(\mathbf{J}_{\|}^{p})^{+}$ first increases, then decreases and is finally reversed, causing E_{fd_1} to become positive again. This momentary inversion of the voltage/power characteristic of generator 1 does not represent any global change in the behavior of the potential energy surface, hence the sign change in E_{fd_1} is presumably counterproductive, in view of the fact that the Generator 1 power inversion is a transient effect. The comparative simulations support this conclusion.

In view of the foregoing information, some observations may be made regarding placement of the design poles in FBLC. To begin with, most severe faults on the power system tend to create a momentary distribution of load in which one generator or group of generators decelerates while another accelerates. This typically causes an overall increase in relative angles across the transmission lines that are involved in the fault. Because the reversal of the power/voltage characteristic associated with reversal of the power flow of a generator appears to result in undesirable transient control behavior, it is of interest to limit the magnitude not only of the initial swing of the generators, but of the backswing as well. Moreover, the magnitude of the singular values relates directly to the level of control effort necessary to affect the system behavior. Note that for a lossless single-machine infinite-bus system,

$$J_{\|}^{p} = \frac{E_{\infty}}{Ex_{eq}} sin(\delta), \tag{4.78}$$

which increases monotonically with δ, up to a maximum of $\frac{E_{\infty}}{Ex_{eq}}$. The singular values of $\mathbf{J}_{\|}^{p}$ are the multimachine equivalent of $|J_{\|}^{p}|$, and also tend to be larger when angle differences are large, as seen in our example. It is of interest therefore to choose poles that avoid trajectories along which the singular values become small. Because of control saturation, limitation of the backswing cannot always be achieved by designing the control with fast real poles. Clearly, in the foregoing example, the poles chosen should have prevented the large backswing that was observed, but control saturation prevented this from occurring.

The direction of acceleration of a particular generator is determined by the gradient of the PE surface with respect to $\boldsymbol{\delta}$, and this is beyond direct control of the field voltage, which only affects the *rate of change* of the gradient. Indeed, the only point at which the direction of acceleration of the system generators is fully under control is when the gradient $\nabla_{\delta}\mathcal{V}_{\text{KE}} = 0$, which is an equilibrium point of the system if the voltage magnitudes do not change. This is also the only condition under which the conversion of PE into KE is under full control of the field voltage control. It was seen that the steepest-descent methods attempted (unsuccessfully) to flatten $\nabla_{\delta}\mathcal{V}_{\text{KE}}$ — the virtual equilibrium point tended to follow the system trajectories. In the simulations presented in this section, the system regained a large amount of KE following the first swing, resulting in an unacceptably large swing magnitude on the backswing, with subsequent loss of synchronism for severe faults. We may conjecture that it would be most advantageous, if possible, to arrange for the flattest possible KE gradient at the turning point of the first swing, provided that it can be achieved without the loss of first-swing stability that was evident in the steepest-descent controls. Some reflection will reveal that this statement is equivalent to requiring (or desiring!) that the system be close to the objective manifold at the end of the first swing.

Since it is in some sense the kinetic energy gained during a disturbance that puts the system at risk, the immediate objective of the control is to convert kinetic energy to potential energy, and FBLC achieves this. Over a longer time scale (*i.e.* second swing), the goal is minimize risk by preventing the conversion of excess PE back into KE. This requires that the frequency deviations be corrected quickly, and that the PE gradient at the turning point be as flat as possible (in order to reduce the conversion of PE to KE without control saturation). This is just a restatement of the fast control objective. The reduction in KE says that we must have $\|\boldsymbol{\omega}\| \approx 0$ and the flat gradient condition is equivalent to $\|\boldsymbol{\alpha}\| \approx 0$, *i.e.*, the system should be as close as possible to $\mathcal{O}$ at the end of the first swing. Thus the geometric intuition provided through an understanding of the interactions between the control, the PE surface and the system KE is in precise alignment with the fast control objective as we have defined it.

Finally, with less urgency, we require that the angles be brought to the nominal

equilibrium value, which is the slow objective. This requirement is actually an indirect result of the need to restore desired voltage levels, but in the context of FBLC it is not possible to work directly with the voltages. It remains to develop a pole-placement strategy that reflects this time-scale decoupling.

Suppose that $\mathbf{A}_3$ is of the form of (4.63). Then the characteristic polynomial for each machine subsystem is

$$p(\mathbf{A}_i) = s^3 + a_2 s^2 + a_1 s + a_0. \tag{4.79}$$

If $a_0 = 0$, then the subsystem has a zero eigenvalue, associated with the eigenvector $v_0 = [1 \quad 0 \quad 0]^t$. If the remaining coefficients are selected to place the remaining eigenvalues on the real axis, well into the left half-plane, then the rotor angles do not participate in the associated eigenmodes. As an example, suppose that the coefficients are chosen as $a_0 = 0$, $a_1 = -110$, $a_2 = -21$. Then the eigenvalues are at 0, -10 and -11. The associated participation factors (see [40]), in columns associated with the eigenvalues 0, -10 and -11, from left to right, are

$$\begin{bmatrix} 1 & 0 & 0 \\ 0 & 11.0000 & -10.0000 \\ 0 & -10.0000 & 11.0000 \end{bmatrix} \tag{4.80}$$

If a_0 is made negative and its magnitude increased, the zero eigenvalue takes on increasingly negative values, but the above situation remains approximately true.

In order to avoid persistent depressions in the system voltages, the zero eigenvalue must be set at about -0.7, which, given the above values for a_1 and a_2, requires that $a_0 = -70$. For these values, the eigenvalues are -0.74, -7.4 and -12.9, but the approximate decoupling of the modes is still quite apparent in the participation factors:

$$\begin{bmatrix} 1.1781 & -0.2594 & 0.0813 \\ -0.1849 & 2.7488 & -1.5639 \\ 0.0067 & -1.4894 & 2.4827 \end{bmatrix} \tag{4.81}$$

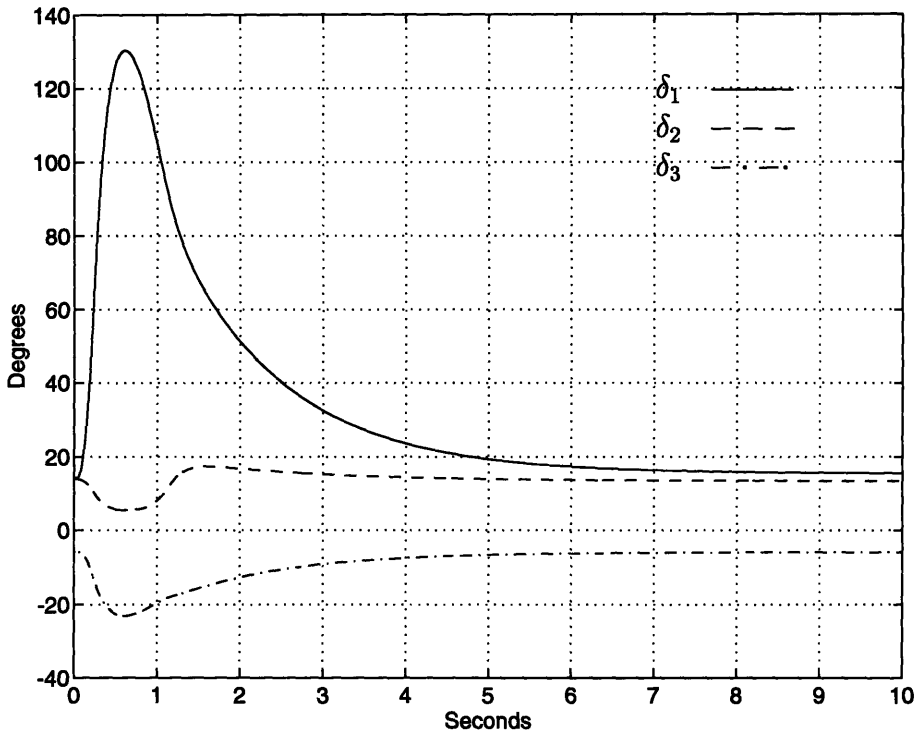

Figure 4.43: Rotor Angles, Decoupled Pole Placement.

The response of the system with these parameters is illustrated in Figures 4.43 – 4.48. The rotor angle plot (Figure 4.43) shows the slow return of the rotor angles to the equilibrium point following the first swing. In spite of control saturation in the early part of the disturbance, the response of the system is dominated by the slow eigenmode following the first swing, and the selection of FBLC poles has prevented the problem with the large backswing that was seen in the earlier simulations. Clearly, the time-scale separation of control objectives has been achieved, to the benefit of the control performance, at least from the perspective of security.

Figure 4.44 shows the slow recovery of the system voltages. Figure 4.45 shows that the attempt to avoid control saturation by ensuring that the KE gradient is as flat as possible at the end of the first swing is successful; the field voltages come out of saturation much earlier than in previous FBLC simulations, even though the fault is more severe. Sasaki's TEF for this case is plotted in Figure 4.46, with the points at which the load-flow solution vanishes depicted on the TEF plot as a bold line.

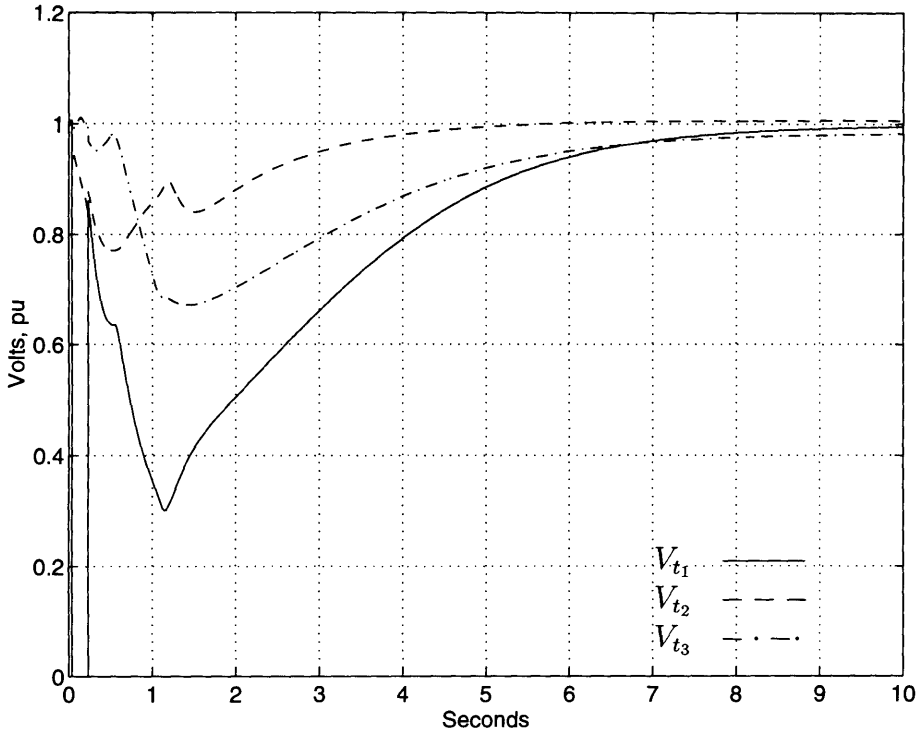

Figure 4.44: Terminal Voltage: Decoupled Pole Placement.

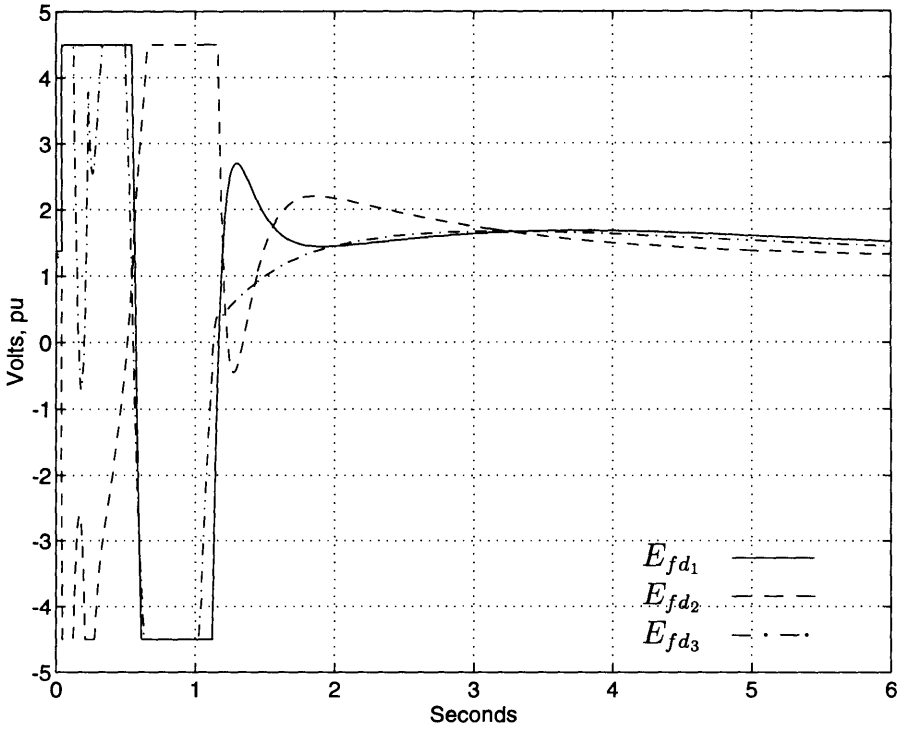

Figure 4.45: Field Voltage: Decoupled Pole Placement.

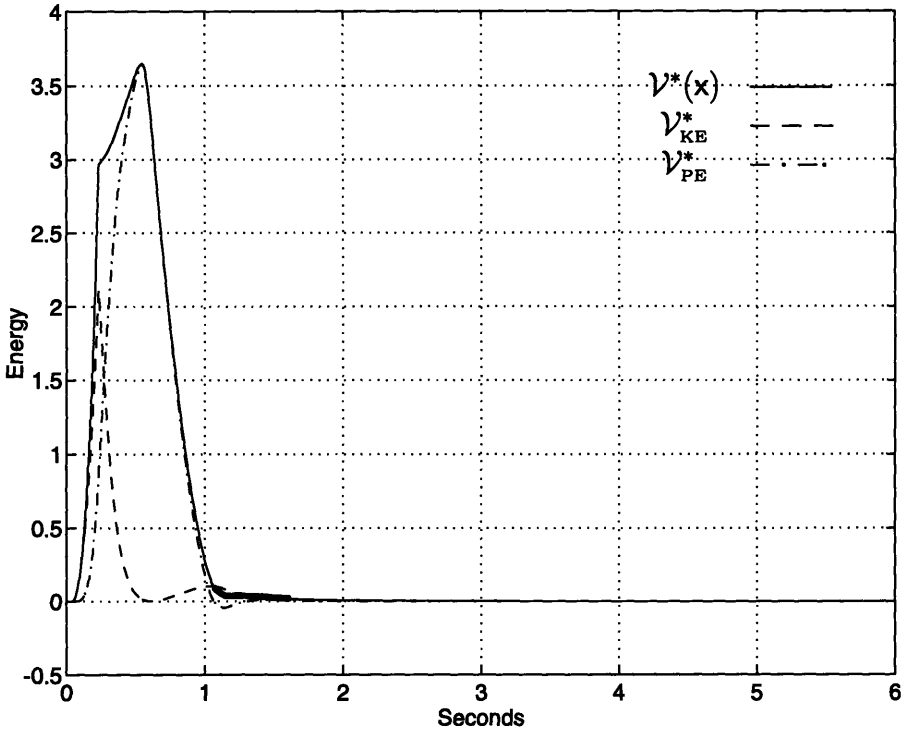

Figure 4.46: Transient, Kinetic, Potential Energy: Decoupled Pole Placement.

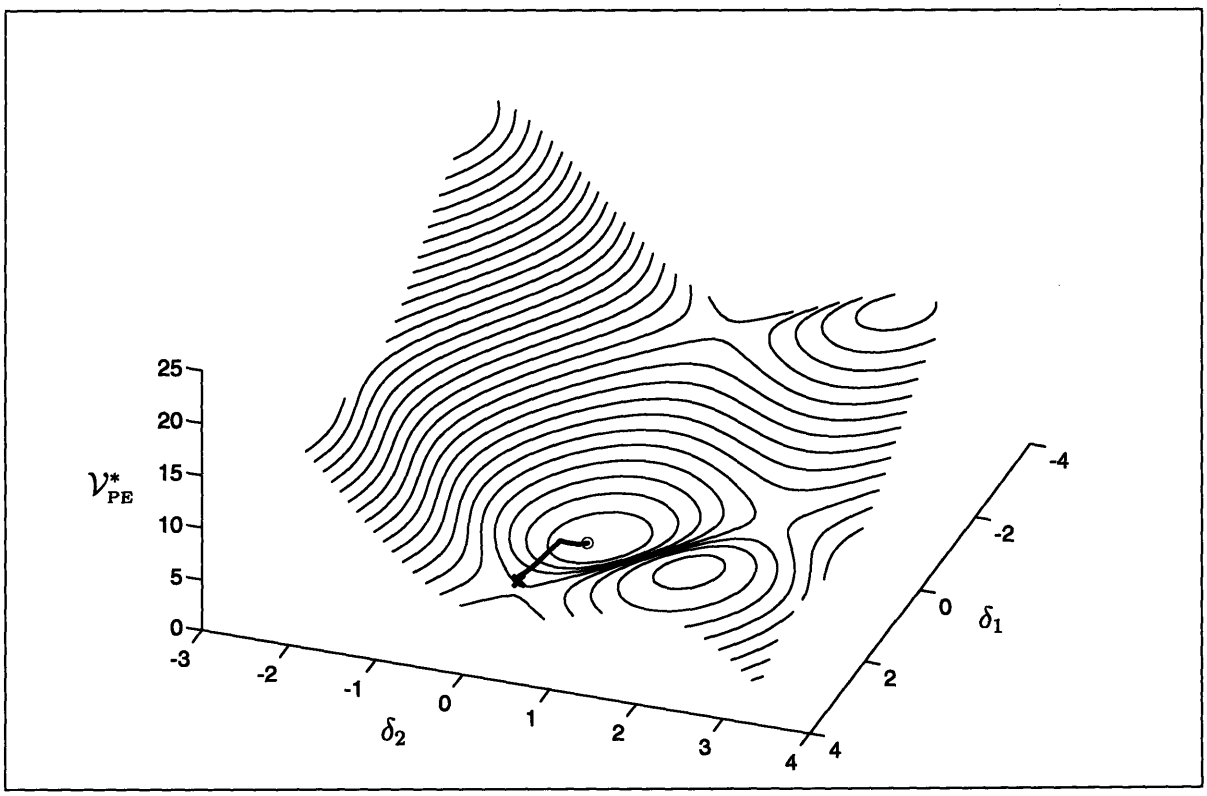

Figure 4.47: Potential Energy Surface: Decoupled Pole Placement.

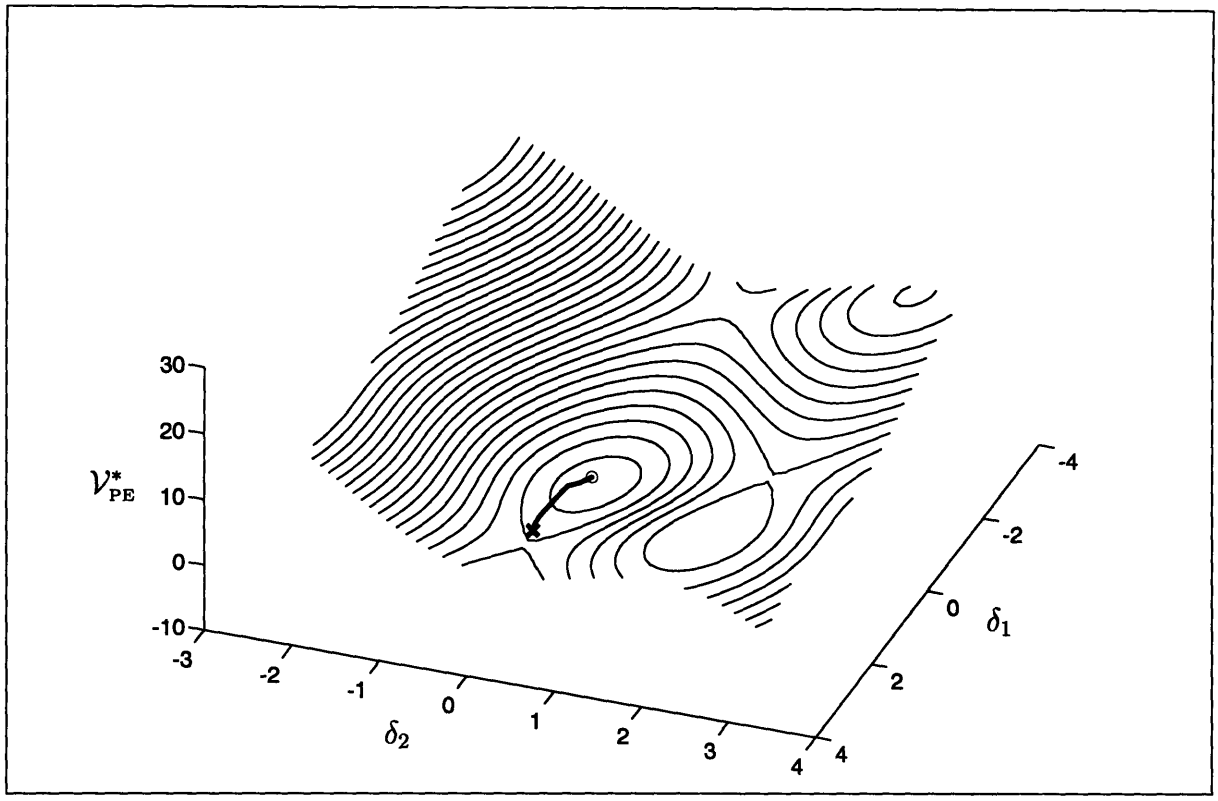

Figure 4.48: Potential Energy Surface, Milder Fault: Decoupled Pole Placement.

This plot very closely resembles the steepest-descent control, with the exception that the transient energy climbs sharply during the period between fault clearing and the turning point of the first swing. As we have seen, without this initial rise in transient energy, first-swing stability is seriously compromised. Hence, with this assignment of pole locations, FBLC appears to achieve much of what the steepest-descent control was intended to accomplish, without loss of first-swing stability margin. The rapid dissipation of transient energy minimizes the potential for loss of stability on the second and later swings by preventing the conversion of accumulated PE back into KE, while the initial rise in transient energy enhances the first-swing stability of the system by facilitating the most rapid conversion of KE to PE. Since the STEF is a measure of distance to $\mathcal{O}$, it is clear that this control achieves the fast objective in slightly over one second.

Figure 4.47 is a contour plot of the PE surface, taken at the top of the first swing of the generator 1 rotor angle. Note the proximity of the the unstable equilibrium

point to the trajectory at the turning point. At this point, the KE gradient is close to zero in all directions, hence it is a point at which the acceleration of the rotor angle is controllable within the field voltage saturation limits. It is also apparent that the difference in PE between the stable and unstable equilibria is larger than the prefault value; compare this figure to Figure 4.2. The proximity of the first turning point to the unstable equilibrium is a characteristic of this pole configuration, and not a consequence of the severity of the fault. Figure 4.48 is a contour plot of the PE surface for a milder fault, with clearing time $t_{c\ell} = 0.22$. Again, the gradient is small at the turning point of the first swing.

This section has outlined a pole-placement procedure that yields an improvement both in first-swing stability and in overall security over a longer time period. It appears to be capable of rapidly reducing the transient energy of the system (as expressed by the STEF) without sacrificing first-swing stability. Although the method is not rigorously rooted in any mathematical optimization procedure, it is meaningful in terms of its effects on the potential energy surface and in its ability to rapidly and effectively dissipate excess system energy. It also appears to be the first method proposed to date that has any meaningful connection with the nonlinear system dynamics. Moreover, to the extent that any given control design may be locally equivalent to an FBLC design, it should provide more general guidance in control design.

The fact that the system voltages are slow to return to desired values following a disturbance is of some concern, however. Moreover, the control does require an *a priori* knowledge of the postfault equilibrium rotor angle vector $\boldsymbol{\delta}_o$, and this is somewhat problematic, although this issue has been addressed to some extent by the modified observation decoupled state space method described in [8]. In the next section, a method is derived that incorporates the pole-placement approach described above, but achieves improved the voltage response and dispenses with the need to calculate a postfault angle equilibrium.

4.7.6 Toward Decentralized FBLC with Voltage Control

As noted in Section 4.7.5, if the coefficient a_o is set to 0 in the FBLC design, the system has a zero eigenvalue associated with the eigenvector $[1 \quad 0 \quad 0]^t$. Under these circumstances, the equilibrium angle to which the system settles following a disturbance is not well-defined, and will depend on the specifics of the disturbance. Alternatively, it might be said that the control so designed fails to distinguish between the various possible equilibria that make up the object manifold. Obviously, this does not lead to a viable control, and even in the presence of noninteracting voltage control, the system voltages will not return to any preset value, but it does effectively achieve the fast objective.

Suppose that the slow objective is to be achieved not by a slow pole in the FBLC configuration, but by the addition of a slow, conventional voltage feedback signal. Assuming that a sufficient time-scale separation is maintained between the two control objectives, it should be possible to bring the system voltages back to the desired level, returning the rotor angles to the point determined by the desired voltage profile, without seriously degrading the performance of the FBLC. This is particularly true if the performance of the FBLC is evaluated in terms of achieving the fast objective, rather than by the actual linearity of the system response. If the voltage profile is to be corrected in finite time, the decoupling will not be perfect and the two controls will obviously interact, but provided that a sufficient time-scale separation is provided, it may be possible to obtain an effective response.

The idea of adding a supplemental voltage control is not new, but in previous attempts it was found that a sufficiently fast voltage control loop led to an unacceptable degradation in the FBLC performance. In view of the input saturation problem, the ability to actually achieve a fast response with the two nonzero eigenvalues is enhanced by the decoupling, since driving the fast eigenvectors to zero is in some sense similar to stabilizing a second-order integrator, as opposed to a third-order integrator for non-decoupled eigenvectors. Any control that returns a third-order integrator to the origin certainly also returns the second-order subsystem to zero, but the converse does not

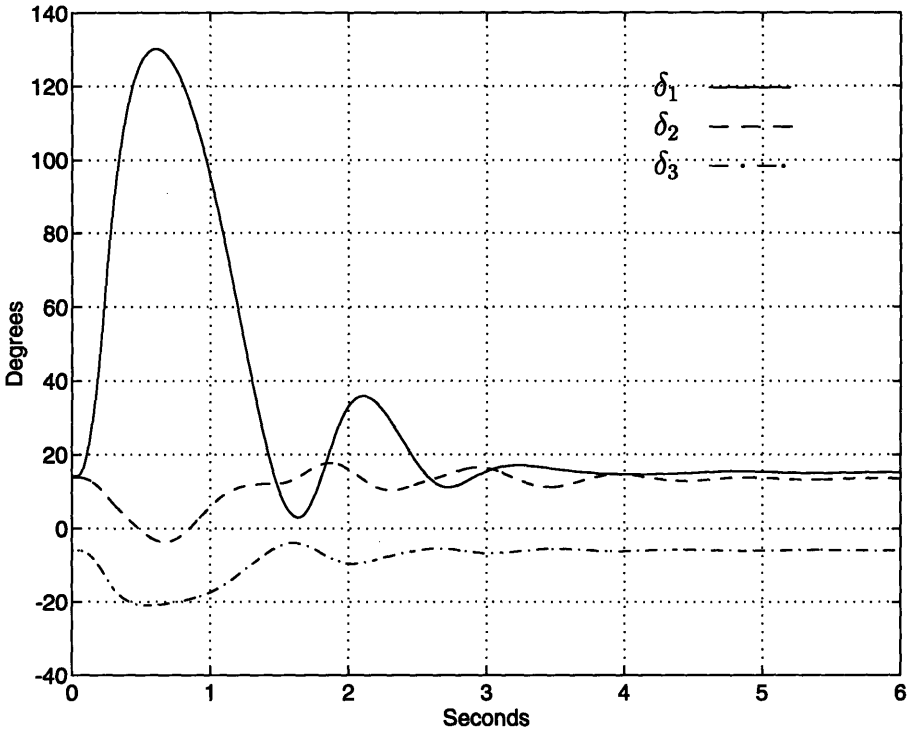

Figure 4.49: Rotor Angles: Direct Voltage Control.

hold. Therefore the use of a zero eigenvalue allow for greater time-scale separation by allowing for a faster FBLC response. In the present case we will attempt to utilize the time-scale separation to prevent significant interaction with the direct voltage error feedback.

In the following simulations, we define

$$\boldsymbol{\lambda}_{\|} = \boldsymbol{\lambda}_{\|}^{o} + k_{v2}(\mathsf{V} - \mathsf{V}_{ref}) \tag{4.82}$$

where $\boldsymbol{\lambda}_{\|}^{o}$ is the minimum-norm solution to the FBLC law, as defined in (4.63) and (4.64). Since $\boldsymbol{\lambda}_{\|}$ is related to the rate of change of the machine voltage magnitude, the added term implements a type of integral voltage control signal, whose speed of response is determined by the value of k_{v2}. In the following simulations, the value of k_{v2} is -15, while the FBLC coefficients are $a_o = 0$, $a_1 = -110$ and $a_2 = -21$, giving design pole locations at 0, -10 and -11. With these values in the case 1 simulation with $t_{cl} = 0.1925$, the voltage control causes some overshoot in the backswing of the

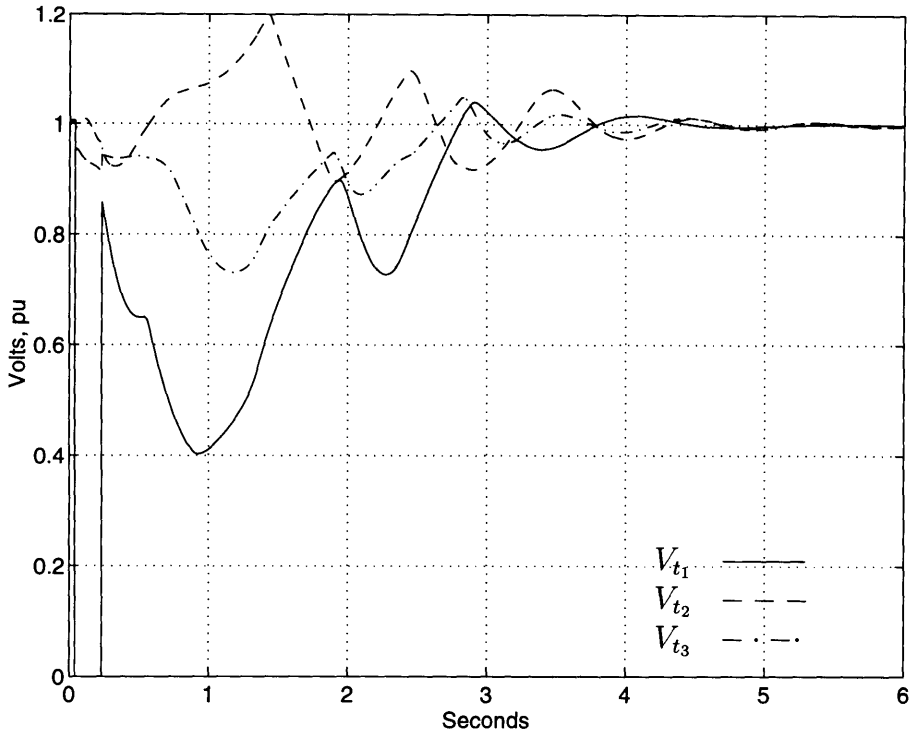

Figure 4.50: Terminal Voltage: Direct Voltage Control.

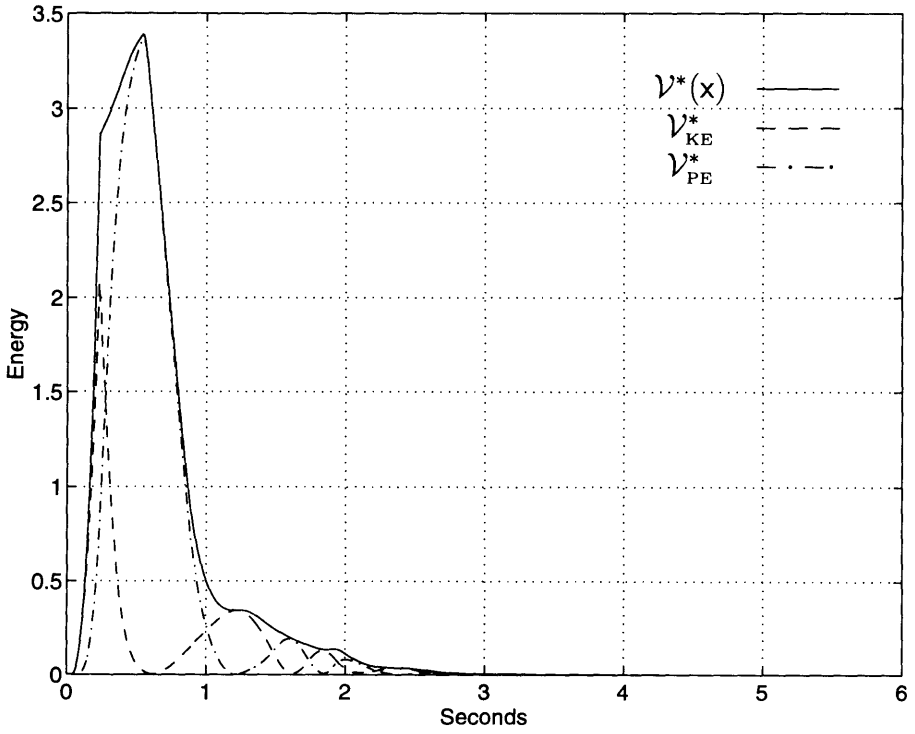

Figure 4.51: Transient, Kinetic, Potential Energy: Direct Voltage Control.

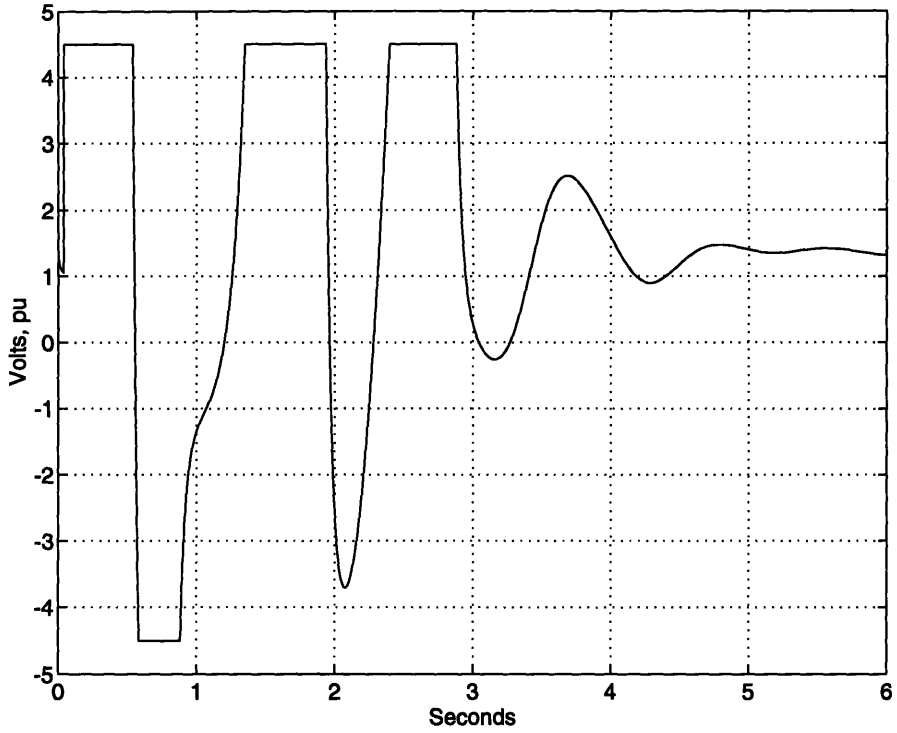

Figure 4.52: Generator 1 Field Voltage: Direct Voltage Control.

angle trajectories, but it is minimal considering the long fault clearing time (see Figure 4.49). On the other hand, as is evident in Figure 4.50, the terminal voltages recover much more rapidly than in the simulations of the previous section, and the system angles return quite smoothly to the desired equilibrium point. Moreover, the control is quite effective in arresting the first swing. The value of k_{v2} is quite large compared to the value of k_v that was used in the noninteracting voltage control. This appears to be caused by the interaction of FBLC with the voltage control. Since the rising system voltages tend to accelerate the machine rotors, the FBLC opposes this motion, hence the effect of the voltage control loop is canceled to some extent by the FBLC. This is not necessarily an adverse effect, though, since the FBLC also acts to minimize the overshoot on the backswing that is caused by the voltage control, and appears to be analogous to a rate feedback effect. The transient, kinetic and potential energy are plotted in Figure 4.51, and as is evident, the transient energy still declines quite steeply following the initial postfault rise that is necessary for limiting the first swing. Because of the fairly large voltage coefficient, there is some interaction between the

two control objectives. The more rapid return to the nominal equilibrium means that significant frequency deviations persist for longer than they would with a slower voltage control. This prevents the transient energy from returning to zero as rapidly as it would with a slower control. In this simulation, there is never a point at which the postfault equilibrium vanishes, as it did in previous FBLC simulations. The voltage control apparently supports the voltage to the extent that this never occurs. Finally, the generator 1 field voltage is shown in Figure 4.52. The field voltage remains in saturation for most of the initial 3 seconds, so that at least in the initial postfault period, this control appears to approximate a bang-bang type of control. One of the reasons for the sustained saturation is that the coefficient on the direct voltage control input was comparatively large; as mentioned earlier, there is actually significant interaction between the two control objectives.

Some very important simplifications are possible in the implementation of this control. To begin with, since $a_o = 0$, no measurement of the rotor angle is necessary, and no determination of the equilibrium value $\boldsymbol{\delta}^o$ is required. Additionally, this reduces the difficulty in obtaining measurements of the system variables in the COI frame of reference, since no measurement of $\boldsymbol{\delta}$ is required. Therefore, the control proposed in this section poses far fewer problems in terms of a decentralized implementation.

4.8 Applications to Linear Control

Although the subject has not been addressed in this chapter, many of the results presented here have application to linear control designs, particularly the concept of the objective manifold and the time-scale control decomposition that it motivates. In the field of power system stabilizer design, two commonly-used stabilizer inputs are the frequency and the so-called accelerating power, which is just $T_{m_i - P_{e_i}}$. It is not common to utilize any direct measurement of the rotor angle as an input to the stabilizer. The preceding development of a decoupled slow/fast FBLC design justifies this approach to some extent, although there are significant differences in the design of the controller that are not related to the linearity/nonlinearity of the control. We have allowed the

error measurement in the frequency and acceleration to directly affect the field voltage of the generator, whereas most PSSs add an offset signal to the voltage error measurement utilized by the automatic voltage regulator (AVR). Since the AVR is typically a fast control, there is no decoupling in this arrangement.

Because of the large state deviations inherent in disturbances that threaten transient stability, system nonlinearity may adversely affect linear control designs. This is in addition to variations in operating point that change the character of the system in which the control operates. Robust control techniques are only recently making an impact on control design for power systems. One issue in robust control design is the method used to characterize the uncertainty in the system. It is certainly within the realms of robust design to attempt to design controls that are insensitive in some sense to the system nonlinearity. In order to do this, it is necessary to characterize the effects of nonlinearity as some sort of bounded disturbance or perturbation to the nominal plant model. If a robust excitation control were to be designed using such an uncertainty model, it would yield a control with more predictable large-signal behavior.

The network-referenced system model allows for the construction of a bounded characterization of the system nonlinearity which is suitable for use in an $\mathcal{H}_\infty$ design framework. Since the design of such controls is somewhat peripheral to core material of this thesis, the development of this material has been placed in Appendix C.

4.9 Summary

It may be useful at this point to summarize the results of this chapter. The intent in this work was to attempt to identify some of the fundamental limitations inherent in the use of excitation control for the enhancement of system security in the sense of increasing transient stability margins, and to develop the concept of time-scale decoupling of the control response based on a time-scale separation of control objectives embodied in the concept of the objective manifold $\mathcal{O}$.

The STEF was selected as a tool for developing this topic because it is the simplest of the available Lyapunov-like functions that captures the essential aspects of the problem,

most notably the ability of the system to convert KE into PE and its close relationship to $\mathcal{O}$. The instantaneous rate of KE/PE conversion is captured as the dot product of the frequency vector $\boldsymbol{\omega}$ with the gradient of the PE surface $\nabla_\delta \mathcal{V}_{\mathrm{PE}}(\mathbf{x})$. Because the representation of KE is common to most if not all of the available TEFs, the PE surface as we have defined it controls the KE/PE energy interchange in many otherwise disparate energy functions. The various TEFs do differ in the rate of change of the "PE" terms, but the essential interchange between KE and PE is preserved, and is captured in the STEF, without cluttering the analysis with the dynamics of various added control devices such as voltage regulators. In order for these to be included in an energy function, an *a priori* assumption must be made as to their structure, which clouds the analysis.

The initial examples of the steepest-descent method are included for two reasons. First, they illustrate some of the difficulties in formulating the security problem, in particular that simple-minded schemes that seek only to reduce the overall transient energy fail to increase the system security, and second because they provide insight to the methods developed in ensuing parts of the chapter. In particular, they illustrate the close connection between the evolution of the PE surface and the power/angle dynamics of the multimachine system. The knowledge gained from these exercises bears directly on the design of more effective controls.

Several aspects of this problem make it difficult to solve in a general way. First, the ability of the system to successfully absorb the energy injected as a result of a disturbance depends directly on the topology of the PE surface, which in turn is a somewhat complex function of the machine voltages. Second, the strict control saturation limits pose a difficult analytical problem in the formulation of any optimization procedure. As noted earlier, the time-optimal control problem is conceptually attractive for such a strictly-limited control signal, but for excitation control at least is difficult to solve and appears to be impractical. Finally, the wide variation in the singular values of $\mathbf{J}_{\|}^{p}$ is difficult to account for, and creates a situation in which a control signal that is pointwise appropriate in the sense of creating the proper rate of change in the generator output power leads to control saturation and loss of stability in the ensuing parts of the system

response because of the ill-conditioning of $\mathbf{J}_{\|}^{p}$. Because of the difficulty of defining an appropriate control response in terms of the future value of $\mathbf{J}_{\|}^{p}$ when this is coupled with control saturation, the approach that was adopted was to avoid system responses that tend to lead to ill-conditioning of $\mathbf{J}_{\|}^{p}$. Clearly, this approach has not been derived rigorously in terms of an optimization of the control, but as noted previously, there do not appear to be any more systematic methods available that give consideration to the system nonlinearity. The sign change in the control signal that is illustrated in Figure 4.40 indicates that for the large disturbances considered here, a linearization of the model about the postfault equilibrium point will not capture the crucial variation in the character of $\mathbf{J}_{\|}^{p}$.

The three-machine lossless test model used in the simulations is a very severe test of the capabilities of any type of excitation control, since the absence of any voltage-dependent loads means that the total power consumed is always zero. Hence, it is the *distribution* of the total output power among the three generators that may be changed via the control. The transmitted power, summed over all generators, is always zero. This is not the case in a lossy system, since the presence of real, constant-impedance loads produces an overall voltage dependence in the total power dissipated. Moreover, although ignoring the real part of the reduced admittance matrix actually increases the critical clearing time for the classical model, it also reduces the ability of excitation control to dissipate energy, hence making it more difficult to realize any advantage in system security via excitation control. On the other hand, the lossless system brings several system characteristics into focus that are important in control design, but are only approximately true in a lossy system. In particular, the noninteracting voltage control depends on the generic singularity of $\mathbf{J}_{\|}^{p}$, which does not occur with a lossy grid. Nonetheless, even with a lossy grid, there exist directions for which the effect of $\boldsymbol{\lambda}_{\|}$ on $\dot{\mathsf{P}}_e$ remains small; these are directions in which voltage regulation may be implemented, in substantial independence of any power/angle control that may also be operative.

The decision to utilize the FBLC framework for developing excitation controls was based on the direct connection between $\frac{d}{dt}\nabla_{\delta}\mathcal{V}_{\mathrm{PE}}$ and the input signal v in (4.53). This allows the effect of the control to be directly related to the dynamics of the PE surface,

facilitating the incorporation of observations regarding the behavior of the PE surface into the control design process. In particular, it was noted that, given the limits on the magnitude of the control, the ability to exercise control over the conversion of accumulated PE back into KE after the first swing required that the gradient be small at the turning point of the first swing. This reinforced the idea that a composite two time-scale control would be most appropriate, and in turn led to the placement of the FBLC poles such that the rotor angle trajectory following the first swing was governed by a slow eigenvalue that was substantially decoupled from the dynamics of $\boldsymbol{\omega}$ and $\boldsymbol{\delta}$. This created a situation in which the fast control objective could be rapidly and effectively realized, leaving the system close to $\mathcal{O}$ as the trajectory approached the top of the first swing. Geometrically speaking, the PE gradient was small as the frequency deviations became small at the turning point of the first swing, thereby allowing the control to effectively limit the gain of KE on the second and later swings. This resulted in a control that improved the first-swing stability without creating stability problems on the second swing, as was observed in the original FBLC designs. The liability of this design was that it allowed a depression in the system voltages for an unacceptably long time. The final design presented in this chapter was motivated by the desire to limit the deviation in system voltages away from the desired values, and to exploit the small eigenvalue associated with the angle deviation to eliminate the need to measure $\boldsymbol{\delta}$, which may be problematic.

By allowing a zero eigenvalue in the FBLC and adding a voltage feedback signal, not only was improved voltage control realized, but the need to calculate an equilibrium value $\boldsymbol{\delta}^o$ (so that a meaningful measurement of the error in the rotor angle could be developed) was alleviated. This is a significant result, since the value of $\boldsymbol{\delta}^o$ is not easy to calculate in a decentralized control setting. The use of the modified observation decoupled state space concept that was proposed in [6] as a solution to this problem still requires a set of estimates or measurements of phasor quantities that may be difficult to obtain, and moreover was not as effective in regulating the system voltages as could be desired. The use of the supplementary voltage feedback with the zero eigenvalue eliminates this problem entirely, with one *caveat.* The use of the voltage feedback

signal will return the system to the reference values regardless of whether there exists a postfault equilibrium at that voltage level or not. If the system disturbance results in a significant loss of transmission capacity, there may be no stable equilibrium available if the prefault voltages are to be preserved. Therefore, while the FBLC will act to stabilize the first swing in a case such as this, the voltage control may subsequently drive the system into instability. A case of this nature was discussed in [26]. The modified ODSS, on the other hand, acts to control the voltage by changing the reference angle supplied to the FBLC. If no postfault equilibrium exists at prefault voltage levels, the ODSS will simply drive the system voltage to the lowest level for which a load-flow solution exists. Since FBLC is normally capable of maintaining stability at that point, the equilibrium is preserved, albeit in a very delicate state.

Chapter 5

Conclusions

In this chapter, the contributions of this thesis are summarized, their significance assessed, and candidate areas for further research are identified.

5.1 What's New

The bulk of Chapter 2 is drawn from established material, since it is primarily concerned with establishing the modeling framework that is used in following chapters. Well-known machine models that are commonly used in the dynamic analysis of power systems are presented, and some theoretical background material is included to facilitate understanding of the more advanced material that follows. The singular-perturbations-based derivation of the COI-referenced model appears to be new, however, as is the conversion of the models to the network frame of reference and the use of the block-form state ordering. The network-referenced model does lead to a simple norm-bounded characterization of the system nonlinearity, which was derived in Appendix C, but its main strength is that it simplifies many issues concerning the interaction of various dynamic subsystems in the interconnected network. The use of $\boldsymbol{\lambda}_{\|}$ and $\boldsymbol{\lambda}_{\perp}$ to resolve the rates of change of the machine voltages into a parallel and an orthogonal component also simplifies the equations a great deal and leads to a simpler characterization of some important properties of the load-flow Jacobians, such as the derivation of the left nullspace of $\mathbf{J}_{\|}^{p}$. The characterization of the system energy, the energy-related

interactions expressed in the STEF and the dynamics of the STEF itself are more cleanly expressed in the network frame of reference. These aspects of the network-referenced model significantly simplify the derivation of Claims 4.1, 4.2 and 4.3.

In Chapter 3 some introductory material is presented on Lyapunov-based nonlinear systems analysis, together with the transient stability framework that motivates much of the work in Chapter 4. This is for the most part standard material, but in Section 3.3.3, the derivation of the STEF dynamics in terms of the tracking voltages, culminating in Claim 3.1, is new. The use of the tracking voltages as a method for considering the STEF in a dynamic context is useful and clarifies much of the later work.

Chapter 4 formalizes the concept of a time-scale separation of control objectives by introducing the objective manifold $\mathcal{O}$. The objective manifold provides a framework for developing measures of control performance for operating security as measures of distance from the objective manifold. Reducing the distance to $\mathcal{O}$ is identified as the "fast" objective, in the sense that it takes precedence as long as there is risk of losing synchronism. Therefore in the immediate period following a disturbance, the primary concern is to achieve the fast objective, thereby reducing the risk of a system failure. The slow objective is defined as an adjustment of the operating point that takes precedence when the system is no longer considered to be at risk of failure, *i.e.*, when the fast objective is substantially complete. The objective manifold and the concept of a slow/fast decoupling of control objectives provides a framework for control evaluation that is new and useful. Much of Chapter 4 is concerned with developing links between the energy-based ideas inherent in transient stability work, the geometric interpretation of the conversion of KE to PE on the PE gradient surface, the impact of excitation control on the PE surface and its relationship with $\mathcal{O}$.

Except for the energy functions used in Section 4.5.2, in which a diagonally-loaded admittance matrix was used to cause a reactive-power minimum to appear at the desired equilibrium(s), all of the energy functions treated here are standard material. The use of the tracking voltages as a means of expressing the dynamic behavior of the various transient energy functions and in particular, the derivation of the STEF dynamics under excitation control (Claim 4.1) is new, as are the related expressions derived with respect

to the TEFs in Section 4.5.2. Although the steepest-descent controls derived from these expressions were unsuccessful, they were useful in the sense that they provided information about the interaction of field voltage control with the PE surface and its associated gradient, leading to more successful designs in ensuing sections of Chapter 4.

To begin with, the failure of the steepest-descent methods indicates that the most rapid dissipation of transient energy is not consistent with the maximization of the region of attraction, at least for the energy functions considered in this thesis. As was observed graphically in the contour plots of the PE surface, the pointwise minimization of the transient energy led to a flattening of the PE surface and consequent lowering of threshold values along the boundaries of the region of attraction. This caused a decrease in the system's ability to survive the first postfault swing. The transient energy plots show that in the immediate postfault period, the primary component of the TEF is kinetic energy, which must be converted to other forms of energy[1] in order for the first swing to be arrested. It was shown that the rate of conversion is directly related to the gradient of the PE surface, hence the brute-force minimization of transient energy actually reduces the capacity of the system to perform this function. In fact, this prevents the steepest-descent controls from fulfilling the fast objective of bringing the system onto the objective manifold $\mathcal{O}$, even when no supplemental slow-objective control exists.

It may certainly be conjectured that there exists a type of TEF for which the steepest-descent method (or some Lyapunov-based variant thereof), would yield a more effective control. The STEF simply constitutes a positive-definite function that captures the essential mechanism by which kinetic energy is transformed into other forms. The same might be said for other functions, and we have not provided a definitive answer to this question, although the approach was applied to other TEFs, most notably Kakimoto's [21], which were not included in the thesis. The simulations that are included here were chosen to provide the clearest possible picture of the issues that affect the system response to a particular control. Throughout Chapter 4, the transient,

[1]This is strictly true for the lossless system, and approximately true for the lossy system, since damping and other dissipative terms tend to be small.

kinetic and potential energy plots serve to relate the dynamic behavior of the system energy to the type of control that is implemented and the overall security of the system in terms of transient stability. This is also new work.

As noted by Petrov [43], the optimal control for system security is the time-optimal control. It was observed in Chapter 1 that this is the result of the fact that the time-optimal minimization problem is the only common method that explicitly includes control saturation as part of the minimization procedure, thereby limiting the set of control signals considered in the optimization to the set of achievable controls. The cost function associated with the time-optimal control is an energy function for which the steepest-descent control would also maximize security, but this problem has never been solved in the context of excitation control. Therefore, it is doubtful that any energy function can be rigorously justified as "best" in this sense, but the information gained by investigating the dynamic behavior of the STEF has at least provided some guidelines as to what constitutes an effective control for the enhancement of system security.

It was conjectured that an initial rise in the total transient energy might be justified, provided that the control is capable of limiting the amount of KE that can be regained on the backswing. Based on this, it seemed that the STEF, although it is a valid measure of distance to $\mathcal{O}$, was not the correct measure for defining the fast objective. This led to a refinement of the definition of $\mathcal{O}$, and a state transform in which new metrics based on the new definition could be applied. Since this transform from $(\mathsf{E}, \boldsymbol{\delta}, \boldsymbol{\omega})$ to $(\boldsymbol{\delta}, \boldsymbol{\omega}, \boldsymbol{\alpha})$ results in a system model that is feedback linearizable, FBLC control was investigated in the context of the slow/fast decoupled control.

Claim 4.2 provides motivation for the use of FBLC as a vehicle for refining the intuition gained in simulations of the steepest-descent controls. The direct connection between the time function v in the FBLC control law of (4.53) and the time rate of change of the KE gradient $\nabla_\delta \mathcal{V}_{\mathrm{PE}}$ appears to be hitherto unrecognized, and it provides a direct connection between the desired system behavior as expressed in v and the dynamics of the PE surface. Recall that the PE surface is plotted in a reduced-dimensional space that includes only the rotor angles. The gradient of this surface is important

since it is the negative of the KE gradient $\nabla_\delta \mathcal{V}_{\text{KE}}$.

Several nuts-and-bolts issues regarding the implementation of FBLC in a lossless system bear directly on the achievable dynamics of any set of excitation controls. The first fundamental limitation is expressed by the pole-matching requirement of Claim 4.3. Because *any* excitation control may be considered to act upon the power/angle dynamics of the system via the matrix $\mathbf{J}_{\|}^{p}$, the nullspace of this matrix constrains the type of behavior that is achievable through any type of excitation control. Moreover, this is not a local result, since it does not rely on a linearized system model for validity.

What the claim actually says for the lossless system is that a given multimachine control is achievable if it does not require an overall acceleration of the system, *i.e.*, if $\mathbf{1}^t\dot{\mathbf{P}}_e \equiv 0$. Since it is true that an overall acceleration of the system contributes nothing to the transient stability of the system, a pole configuration that requires this would be of questionable value, since the gain of $\mathbf{J}_{\|}^{p}$ is likely to be small in that direction, resulting in unnecessary control saturation. Therefore, even though a given multimachine control may be achievable in a lossy system and exhibit desirable small-signal behavior, it would be limited by saturation during large disturbances. Such a control would therefore compromise the short-term stability of the system. The adjustment of the overall system frequency that occurs when $\mathbf{1}^t\dot{\mathbf{P}}_e \neq 0$ is more properly the function of the governor control, via the governor droop characteristic and automatic generation control (AGC), over a somewhat longer time scale.

In Section 4.7.3, The singularity of $\mathbf{J}_{\|}^{p}$ was exploited in order to design a form of voltage control that does not interact with the power/angle control. Although this control only provides a single degree of freedom, it works well with FBLC to bring the generator terminal voltages back to a desired reference value. This method presupposes that the reference angle used by FBLC is known *a priori*, and serves to correct errors in the voltage profile that otherwise persist for an unacceptably long period of time. The fact that the correct reference angle vector $\boldsymbol{\delta}_o$ must be recalculated in order for the control to function properly when system loading and configuration change is a generic problem of feedback linearizing excitation control, particularly in the context of

decentralized control. Methods have been proposed for dealing with this problem[2], but the fact that $\mathbf{J}_{\|}^{p}$ is often ill-conditioned leads to fairly persistent offsets in the terminal voltage with respect to the reference values. Therefore, although this type of control is strictly noninteractive only in the lossless model, it is possible to define a weakly-interactive control that would correct precisely the problem encountered in the ODSS or any similar method.

Moreover, at least in the simulations performed on the test system, it was shown that noninteractive voltage control actually reduces the amount of control saturation encountered. This finding appears to be at odds with the observation that the most effective control strategy would be to place the design poles in accordance with Claim 4.3, but noninteracting voltage control differs from a pole configuration that demands an overall system acceleration in one important aspect. From (4.53) and (4.54), the portion of the FBLC control signal that controls the pole locations is defined by the term $(\mathbf{J}_{\|}^{p})^{-1}\mathbb{M}\mathbf{A}_{3}\mathbf{z}$. Because of the ill-conditioning of $\mathbf{J}_{\|}^{p}$ in the lossy case[3], there will tend to be a large gain associated with directions of $\mathbb{M}\mathbf{A}_{3}\mathbf{z}$ that correspond to an overall system acceleration, and this is likely to lead to control saturation. By contrast, the error signal for noninteracting voltage control is not multiplied by $(\mathbf{J}_{\|}^{p})^{-1}$, but instead is multiplied by a projection matrix whose maximum gain is always 1. The maximum gain of the voltage feedback loop is therefore entirely under the control of the designer, via the parameter k_v in (4.74), and a comparatively small gain is found to be effective in controlling the voltage.

The issue of effective pole placement was developed further in Section 4.7.5. Very little work appears to have been done previously in this area. The primary motivation for decoupled slow/fast pole placement is the decomposition of control objectives, but several factors specifically associated with FBLC also argue for the decoupled approach. First, if the magnitude of the first backswing is such that it causes a reversal of power transfer at a generator, associated with a small singular value of $\mathbf{J}_{\|}^{p}$, a reversal in the sign of the field voltage of the affected machine results. Consequently, the control exhibits

[2]Notably, the observation decoupled state space method, or ODSS [54, 8].

[3]as opposed to actual singularity in the lossless model

an extreme sensitivity to the severity of the fault. This is manifested as a severe increase in the magnitude of the second swing, leading to second-swing instability. Equation (4.78) leads to the conjecture that, in order to prevent the power reversal and maintain the magnitude of the nonzero singular values of $\mathbf{J}_{\|}^{p}$, the backswing should be limited to the greatest extent possible. In order to do this, the amount of KE regained on the backswing must be kept small.

The control saturation limits, together with the result of Claim 4.2, limit the ability of the control to affect the interchange of KE with PE when the gradient is large. This is a consequence of the fact that the control only affects the rate of change of the gradient, and the maximum rate of change is limited by control saturation. Although it is desirable for the gradient to be large in the direction of $\boldsymbol{\omega}$ in the immediate postfault period, a large gradient becomes a liability following the first swing, when the objective is to prevent the recovery of KE from PE. This presents a pair of conflicting objectives if defined solely in terms of the transient energy, such that the control should act to increase the KE gradient in the early postfault period, but only to the extent necessary to arrest the first swing. It must then act to reduce the gradient at the conclusion of the first swing, such that the system acceleration is under full control.

Therefore, as the system frequencies become small, the acceleration $\boldsymbol{\alpha}$ should also become small, and this is what is achieved by using the slow/fast decoupling of the FBLC eigenvectors. Since the fast eigenmodes that govern $\boldsymbol{\omega}$ and $\boldsymbol{\alpha}$ are substantially decoupled from the slower mode, the large deviations in $\boldsymbol{\delta}$ that exist as the frequencies approach zero at the conclusion of the first swing do not contribute to large values of $\boldsymbol{\alpha}$ at that point. The fact that real eigenvalues are selected for the fast modes means that as $\boldsymbol{\omega}$ approaches zero at the end of the first swing, $\boldsymbol{\alpha}$ also approaches zero, followed by a slow return of the rotor angles to the equilibrium values, governed by the slow eigenmode. This approach prevents the large backswing and attendant decrease in the singular values of $\mathbf{J}_{\|}^{p}$ that was seen in earlier simulations. This control was found to be much more effective in enhancing the overall system stability, but it led to a rather long period during which the system voltages were depressed.

The relative success of the decoupled pole-placement strategy, with its emphasis on

using the smallest value of a_o that yields an acceptably fast return to the equilibrium, suggests the method for implementing direct voltage control in conjunction with FBLC of Section 4.7.6. The idea of supplementing FBLC with a direct feedback loop is not new in itself, having been tested in [32], but previous approaches have typically resulted in unacceptable degradation of the FBLC performance. Several aspects of the decoupled pole placement strategy made it worthwhile to revisit this approach. In Figure 4.43, the portion of the response governed by the fast eigenmodes has essentially decayed to zero by the end of the first swing, at approximately 0.5 sec., after which the response of the system is almost exclusively that of the slow eigenmode associated with the rotor angle. The fast part of the response is confined to a short enough period as to make a reasonably fast voltage control possible, without materially degrading the fast part of the response. Within the limits of the control, it is impossible to get such a fast response with respect to the rotor angles, since the inertia of the generators slows the response. This was evident in the earlier simulations, where the the poles were placed at -3, -5 and -10. The response demanded by this pole configuration is not achievable within the limits of control saturation, as evidenced in Figure 4.35, where the field voltage saturation is more persistent than in Figure 4.45, in spite of the fact that the fault was not as severe as in the latter case.

When the coefficient a_o is set to 0, the fast part of the FBLC response is essentially the *only* response from that part of the control. Whatever value of $\boldsymbol{\delta}$ the system happens to take on as the fast eigenmodes approach zero becomes the new equilibrium value, at the expense of voltage control. A reasonably slow voltage feedback loop is added to this scenario, which returns the voltages to setpoint without significantly compromising the fast FBLC response, in the process returning the rotor angles to the appropriate equilibrium values. Once the voltages have returned to setpoint, both the voltage feedback loop and the FBLC are at equilibrium.

By adding a voltage error term to $\boldsymbol{\lambda}_{\|}$, a type of integral voltage control is achieved, since $\boldsymbol{\lambda}_{\|}$ is related to the rate of change of the magnitude of the generator voltage phasor. Given a small enough gain on this loop, the voltage control is slow enough to avoid deleterious interaction with the FBLC. In practice, it would be necessary

to limit the DC gain of the voltage feedback loop to allow for reactive power sharing between generators, but given the typically high gain of modern voltage regulators, the overall response of the control should be substantially the same. A major benefit of this method is that it makes the measurement of $\boldsymbol{\delta}$ and the calculation of the reference value $\boldsymbol{\delta}_o$ unnecessary. As the simulations show, this works rather well, and appears to be a significant advancement in feedback linearizing excitation control.

Finally, Appendix C utilizes the network-referenced model to characterize the nonlinearity as a bounded perturbation to the linearized system. The advantage of the network frame of reference over the machine frame of reference in this effort is that the nonlinearity appears in a form to which some standard results in robust control can be applied. This method can be used in the framework of $\mathcal{H}_\infty$ control design to develop controls with reduced sensitivity to system nonlinearity during large disturbances. This was not pursued in great depth, since our interest was primarily directed toward identifying fundamental structural limitations that apply to control design in a multimachine system. Thus the characterization of the system nonlinearity is the main result here, and was placed in an appendix.

5.2 Areas for Future Research

We introduce this section with the observation that the system model used and the control designs developed in this thesis were selected for the purpose of exposing the fundamental properties that impact the design of controls for system security. To some extent practicality was relegated to a secondary level in order to avoid clouding the analysis. Therefore there are several potential areas for further research related to practical implementation of the ideas that were uncovered in the course of the investigation.

The test model used in the simulations was a modified version of the one first presented in [4]. The original model utilized a lossy grid, constant-impedance loads and a classical (constant-voltage) machine model with uniform damping. This was converted to a lossless system with single-axis machine models. By comparison to the original model, the lossless system has somewhat stronger transmission links, which

translates into longer critical clearing times. Although the fault response of the lossless system is similar to that of the original system, it is a more difficult system to apply excitation control to, since there is no way to actually dissipate the energy gained as a result of a fault. Rather, the system must be stabilized by converting the excess energy into a constant offset in the system frequency, which vanishes in the COI frame of reference. This is reflected in the fact that any increase in generator output power at one machine must be balanced by a net decrease in the output power of the remaining machines, and this is what leads to the pole-matching requirement for FBLC.

It would be desirable to test some of the concepts developed in this document in a more realistic system model incorporating a lossy transmission grid. In particular, it would be of interest to test the pole-matching requirement and the noninteracting voltage control on a lossy system, to verify that the former leads to reduced control saturation, and to determine the extent to which the decoupling is preserved for the latter. Additionally, more complex machine models should be simulated. Much of the development in modeling, including the use of $\boldsymbol{\lambda}_{\|}$ and $\boldsymbol{\lambda}_{\perp}$, are applicable to the two-axis model, and it would be beneficial to generalize some of the energy-related results to the two-axis model. This would probably require refinements to the type of TEF that is used.

A second area of research would be an effort to develop decentralized implementations of concepts like noninteracting voltage control, and to characterize its utility in the context of currently-used controls such as PSS. Stated more plainly, one would ask whether the concept of noninteracting voltage control could be applied toward more effective utilization of existing PSS and voltage regulation controls. Another possibility would be to generalize the FBLC pole-matching requirement for use in analyzing existing PSS designs on multimachine systems. Certainly, a situation could exist in which the PSS designs at various locations interact to produce a control effort directed at an overall acceleration of the system. This would almost certainly be an undesirable effect.

Because of the growing influence of FACTS devices such as phase-shifting transformers, thyristor-controlled series capacitors and the like, it would be desirable to generalize some of the concepts developed here to include these devices. The network-referenced

model should provide a framework in which these interactions are more clearly defined, and the results regarding the interaction of excitation controls in the interconnected system would provide a starting point for this research.

It was observed in Section 4.7.6 that the use of decoupled pole placement in conjunction with a voltage feedback loop is attractive in the sense that it facilitates a decentralized implementation of the control. On the other hand, it was observed that in cases where no postfault equilibrium exists at the prefault terminal voltage setpoints this control may not be as effective as an FBLC design in which the postfault reference vector $\boldsymbol{\delta}_o$ is calculated via the modified ODSS of [8]. It would be valuable to revisit some of the cases used in previous research to demonstrate the capabilities of the FBLC/ODSS method in order to determine the relative value of the two methods.

In earlier work, comparisons were made between FBLC/ODSS and more conventional PSS designs. Similar comparisons should be made with the newer designs, and in particular, the dynamics of the system energy should be investigated with respect to more established control methodologies. The decentralized, voltage-controlled implementation of feedback linearizing control should also be tested to determine the potential for interaction with higher-order system dynamics such as shaft resonance modes. Some work in this area has already appeared with respect to earlier FBLC designs [1, 2].

The slow control objective has been expressed as a movement along $\mathcal{O}$, from the initial contact point following a disturbance to the nominal equilibrium. In reality, this movement cannot occur exactly on $\mathcal{O}$ if it is to be completed in finite time, but most occur in a region "close" to $\mathcal{O}$ in some sense. $\mathcal{O}$ is a rather complex surface, and it is not clear that the transition to the nominal equilibrium can be made on the manifold without encountering singularities. Therefore a more thorough study of the slow trajectory with respect to the object manifold would enhance understanding of how singularities in $\mathcal{O}$ might affect the control, both practically and in the limiting case where the slow objective is exactly confined to $\mathcal{O}$

With respect to Appendix C, one area for further research would be in the design and testing of $\mathcal{H}_\infty$-suboptimal excitation controllers analogous to a robust PSS. Some

work has already been done in this area, so the results would have to be compared to existing work in order to identify the strengths and weaknesses of the method. Although it has not been included in this thesis, it was observed in preliminary work that standard $\mathcal{H}_\infty$ design tools yield reasonable controls in some circumstances, but that when frequency feedback is utilized, the control gain is unreasonably high, even with heavy weighting on the input. Since the only requirement on the uncertain matrix is that it be norm-bounded and its elements be Lebesgue-measurable functions of time, there is no frequency information implicit in the formulation of Appendix C. It appears, based on initial work, that appropriate weighting functions will be required in order to limit the frequency content of the uncertainty to an appropriate range, in addition to any weights that would be required to express the desired performance of the controller. In spite of the fact that the practical aspects of the method were not developed in detail, the method may be of practical value in both design and analysis of excitation and other types of control.

5.3 Conclusions

This thesis attempts to link two fields of study that have been somewhat disparate to this point, *i.e.* control design and transient stability. In the field of power systems, both fields present significant technical challenges, and on the face of it, the breadth of the two subjects makes the task of providing a comprehensive unifying theory in an effort such as this impossibly broad in scope. At best, this work provides a beginning, by identifying some of the mechanisms by which excitation control interacts with commonly-understood notions of system energy and its component quantities of kinetic and potential energy. Some time-scale separations have been proposed which divide the objectives of controls acting on the transient time scale into distinct components, *i.e.* the immediate postfault period during which the primary objective is to effectively convert kinetic energy into potential energy and the period following the first swing, during which the concern is to prevent the conversion of PE to KE and restore the nominal equilibrium in a secure fashion.

In the course of this effort, control designs have been proposed that have some potential for improving system security with respect to disturbances that push the stability of the system to the limit, and metrics have been proposed to quantify security-related control performance and provide design objectives. The insights developed through this process may be of value, both in deriving practical control designs from the academic examples presented in these pages, and in forging a rigorous mathematical framework for the phenomena observed here. In addition, the results derived in this thesis may provide analytical tools for identifying unwanted control interactions. These may be of some value, since the widespread use of highly simplified models for control design and the overall decentralization of power system controls tend to mask these effects.

Many challenges remain, in identifying the most appropriate functions for expressing the system energy, in generalizing the method to include a wider range of control devices and in providing some framework for deriving a more meaningful optimization of control designs, but the findings presented here are based on fundamental characteristics of the interconnected power system, and as such are substantially independent of any particular control structure. Hence it is to be hoped that they will prove useful in guiding future work.

Appendix A

Dynamics of the Tracking Voltages

A.1 Introduction

It was mentioned in Chapter 3 that the tracking variables are actually related algebraically to the state variables of the system model. Given a "snapshot" of the system variables at a given time t, it is possible to calculate the value of the tracking variables at that point via a load flow computation. Unfortunately, since no closed-form solution exists for the load flow problem, it is not possible to substitute algebraically for the tracking variables in an expression like the STEF. In order to calculate the dynamic behavior of the STEF, and to calculate the control suggested by Claim 3.1 and (4.6), we may define a tracking system via a set of dynamic equations such that, if once initialized at an equilibrium point, the states of the tracking system become the tracking variables. It is also possible to define correction terms such that small errors vanish asymptotically from the solution. It is then possible to substitute dynamics of the tracking system into the STEF, for example, to derive its time-domain behavior without having to deal explicitly with the load-flow equations.

The tracking system is driven exclusively by the rate of change of the machine voltage magnitudes, and it is most convenient to express this in terms of the variable $\boldsymbol{\lambda}_{\|}$, which was briefly introduced in Chapter 3 and will be dealt with in more detail in this appendix. In the case of the tracking system, it is particularly convenient to utilize $\boldsymbol{\lambda}_{\|}$ as an input to the tracking system, since it is independent of the underlying machine

model, *i.e.*, the tracking equations are identical for the single-axis or two-axis model.

A final issue that is addressed here is the singularity of the load-flow Jacobian (which appears in the tracking system equations) when taken with respect to the phase angles of the machine voltages. A method is presented for avoiding the problem of the slack bus by causing any error in the solution to be projected as a uniform accelerating power, which vanishes in the COI model. This is shown to result in a unique trajectory, at least in some neighborhood of the nominal stable equilibrium. It is always possible for all solutions to vanish for some voltage levels, so local results are the best that can be expected.

A.2 Defining the Tracking System

The D and Q components of the "tracking" voltages are defined as

$$\begin{bmatrix} \mathsf{E}_{\mathrm{D}}^{*} \\ \mathsf{E}_{\mathrm{Q}}^{*} \end{bmatrix} = \begin{bmatrix} \mathbb{C}(\boldsymbol{\delta}^{*}) & \mathbb{S}(\boldsymbol{\delta}^{*}) \\ \mathbb{S}(\boldsymbol{\delta}^{*}) & \mathbb{C}(\boldsymbol{\delta}^{*}) \end{bmatrix} \begin{bmatrix} \mathsf{E}_{d}' \\ \mathsf{E}_{q}' \end{bmatrix}, \tag{A.1}$$

which for the single-axis model can be simplified to

$$\begin{bmatrix} \mathsf{E}_{\mathrm{D}}^{*} \\ \mathsf{E}_{\mathrm{Q}}^{*} \end{bmatrix} = \begin{bmatrix} \mathbb{C}(\boldsymbol{\delta}^{*}) \\ \mathbb{S}(\boldsymbol{\delta}^{*}) \end{bmatrix} \mathsf{E}. \tag{A.2}$$

In order for the tracking variables to follow the virtual equilibrium, two conditions must be satisfied:

$$|E_{\mathrm{D}_i} + jE_{\mathrm{Q}_i}| = |E_{\mathrm{D}_i}^{*} + jE_{\mathrm{Q}_i}^{*}| \tag{A.3}$$

and

$$\mathsf{P}^{*} = \mathsf{T}_m = \left[\mathbb{E}_{\mathrm{D}}^{*} \,\middle|\, \mathbb{E}_{\mathrm{Q}}^{*} \right] \mathbf{Y}_r \begin{bmatrix} \mathsf{E}_{\mathrm{D}}^{*} \\ \mathsf{E}_{\mathrm{Q}}^{*} \end{bmatrix}. \tag{A.4}$$

This latter is somewhat problematic, since it represents a load-flow solution that must be satisfied at each bus, and is therefore overdetermined. However, as will be seen, it is possible to project the error in such a way that it appears as a uniform accelerating

power at each machine. In the COI model, such an error is canceled by the term P_{COI} in the system dynamic equations (see (2.125)) and therefore does not conflict with the equilibrium point. Now, setting

$$\begin{bmatrix} \mathsf{i}_{\mathrm{D}}^* \\ \mathsf{i}_{\mathrm{Q}}^* \end{bmatrix} = \mathbf{Y}_r \begin{bmatrix} \mathsf{E}_{\mathrm{D}}^* \\ \mathsf{E}_{\mathrm{Q}}^* \end{bmatrix} \tag{A.5}$$

and observing that T_m is constant, we must have that

$$\dot{\mathsf{P}}^* = \left(\left[\mathbb{E}_{\mathrm{D}}^* \,\middle|\, \mathbb{E}_{\mathrm{Q}}^* \right] \mathbf{Y}_r + \begin{bmatrix} \mathbb{I}_{\mathrm{D}}^* & \mathbb{I}_{\mathrm{Q}}^* \end{bmatrix} \right) \begin{bmatrix} \dot{\mathsf{E}}_{\mathrm{D}}^* \\ \dot{\mathsf{E}}_{\mathrm{Q}}^* \end{bmatrix} = 0. \tag{A.6}$$

Proceeding from these conditions, it is possible to derive the required dynamics such that the tracking variables will follow the virtual equilibrium. Let $|\mathsf{E}^*|$ denote the vector of magnitudes of the tracking voltages. Similarly, $|\mathbb{E}^*|$ will represent the diagonal matrix of magnitudes. For a single phasor expressed in rectangular form, the time derivative of the magnitude is

$$\frac{1}{|E|}(E_{\mathrm{D}}\dot{E}_{\mathrm{D}} + E_{\mathrm{Q}}\dot{E}_{\mathrm{Q}}). \tag{A.7}$$

From this it is straightforward to show that

$$\frac{d}{dt}|\mathsf{E}^*| = |\mathbb{E}^*|^{-1} \left[\mathbb{E}_{\mathrm{D}}^* \,\middle|\, \mathbb{E}_{\mathrm{Q}}^* \right] \begin{bmatrix} \dot{\mathsf{E}}_{\mathrm{D}}^* \\ \dot{\mathsf{E}}_{\mathrm{Q}}^* \end{bmatrix}. \tag{A.8}$$

The time derivative of the tracking components is decomposed into "parallel" and "perp" components as follows:

$$\frac{d}{dt} \begin{bmatrix} \mathsf{E}_{\mathrm{D}}^* \\ \mathsf{E}_{\mathrm{Q}}^* \end{bmatrix} = \begin{bmatrix} \mathbb{E}_{\mathrm{D}}^* \\ \mathbb{E}_{\mathrm{Q}}^* \end{bmatrix} \boldsymbol{\lambda}_{\parallel}^* + \begin{bmatrix} -\mathbb{E}_{\mathrm{Q}}^* \\ \mathbb{E}_{\mathrm{D}}^* \end{bmatrix} \boldsymbol{\lambda}_{\perp}^* \tag{A.9}$$

This may always be done provided the magnitude of each machine voltage is nonzero, since in that case the matrix

$$\begin{bmatrix} \mathbb{E}_{\mathrm{D}}^* & -\mathbb{E}_{\mathrm{Q}}^* \\ \mathbb{E}_{\mathrm{Q}}^* & \mathbb{E}_{\mathrm{D}}^* \end{bmatrix}$$

is always nonsingular. Thus we may write

$$\begin{bmatrix} \boldsymbol{\lambda}_{\|}^* \\ \boldsymbol{\lambda}_{\perp}^* \end{bmatrix} = \begin{bmatrix} \mathbb{E}_{\mathrm{D}}^* & -\mathbb{E}_{\mathrm{Q}}^* \\ \mathbb{E}_{\mathrm{Q}}^* & \mathbb{E}_{\mathrm{D}}^* \end{bmatrix}^{-1} \begin{bmatrix} \dot{\mathsf{E}}_{\mathrm{D}}^* \\ \dot{\mathsf{E}}_{\mathrm{Q}}^* \end{bmatrix} = |\mathbb{E}^*|^{-2} \begin{bmatrix} \mathbb{E}_{\mathrm{D}}^* & \mathbb{E}_{\mathrm{Q}}^* \\ -\mathbb{E}_{\mathrm{Q}}^* & \mathbb{E}_{\mathrm{D}}^* \end{bmatrix} \begin{bmatrix} \dot{\mathsf{E}}_{\mathrm{D}}^* \\ \dot{\mathsf{E}}_{\mathrm{Q}}^* \end{bmatrix} \tag{A.10}$$

where $|\mathbb{E}^*| = \mathrm{diag}(|E_{\mathrm{D}_1}^* + jE_{\mathrm{Q}_1}^*|, \ \ldots, \ |E_{\mathrm{D}_p}^* + jE_{\mathrm{Q}_p}^*|)$. Substituting (A.9) into (A.8) annihilates the perp component and leaves

$$\begin{aligned} \frac{d}{dt}|\mathsf{E}^*| &= |\mathbb{E}^{*-1}| \begin{bmatrix} \mathbb{E}_{\mathrm{D}}^* \,\middle|\, \mathbb{E}_{\mathrm{Q}}^* \end{bmatrix} \begin{bmatrix} \mathsf{E}_{\mathrm{D}}^* \\ \mathsf{E}_{\mathrm{Q}}^* \end{bmatrix} \boldsymbol{\lambda}_{\|}^* \\ &= |\mathsf{E}^*| \boldsymbol{\lambda}_{\|}^*. \end{aligned} \tag{A.11}$$

This is actually just a collection of p independent equations (since the constituent matrices are diagonal), and we may derive another characterization for $\boldsymbol{\lambda}_{\|}^*$ as

$$\boldsymbol{\lambda}_{\|}^* = |\mathbb{E}^*|^{-1} \frac{d}{dt}|\mathsf{E}^*| = \frac{d}{dt}\ln|\mathsf{E}^*|. \tag{A.12}$$

If we let θ_i^* represent the phase angle of $E_{\mathrm{D}_i}^* + j\,E_{\mathrm{Q}_i}^*$ (of course, if the underlying generator model is single-axis, then $\theta^* = \delta^*$), then we may derive a similar relationship for $\boldsymbol{\lambda}_{\perp}^*$ as the rate of change of $\boldsymbol{\theta}^*$. This is clear from the scalar equation

$$\dot{\theta}_i^* = \frac{d}{dt}\tan^{-1}\left(\frac{E_{\mathrm{Q}_i}^*}{E_{\mathrm{D}_i}^*}\right) = |E_i^*|^{-2} \begin{bmatrix} -E_{\mathrm{Q}_i} & E_{\mathrm{D}_i} \end{bmatrix} \begin{bmatrix} \dot{E}_{\mathrm{D}_i}^* \\ E_{\mathrm{Q}_i}^* \end{bmatrix} = \lambda_{\perp_i}. \tag{A.13}$$

Note that the parallel and perp components of the actual machine voltages can be extracted in the same way, so we may express the change in magnitude of the machine voltages as

$$\frac{d}{dt}|\mathbb{E}| = |\mathbb{E}|\boldsymbol{\lambda}_{\|}. \tag{A.14}$$

Since we require that

$$\frac{d}{dt}|\mathbb{E}^*| = \frac{d}{dt}|\mathbb{E}|, \tag{A.15}$$

we have

$$\boldsymbol{\lambda}_{\|}^{*} = |\mathbb{E}^{*}|^{-1}|\mathbb{E}|\boldsymbol{\lambda}_{\|}. \tag{A.16}$$

When $|\mathbb{E}^{*}| = |\mathbb{E}|$, this reduces to

$$\boldsymbol{\lambda}_{\|}^{*} = \boldsymbol{\lambda}_{\|}, \tag{A.17}$$

i.e.,

$$\boldsymbol{\lambda}_{\|}^{*} = |\mathbb{E}|^{-2} \left[\begin{array}{c|c} \mathbb{E}_{\mathrm{D}} & \mathbb{E}_{\mathrm{Q}} \end{array} \right] \left[\begin{array}{c} \dot{\mathrm{E}}_{\mathrm{D}} \\ \dot{\mathrm{E}}_{\mathrm{Q}} \end{array} \right]. \tag{A.18}$$

In the sequel, it will generally be assumed that $|\mathbb{E}^{*}| = |\mathbb{E}|$, which is a requirement if the virtual equilibrium is to be correctly represented by the tracking voltages. It remains to solve for $\boldsymbol{\lambda}_{\perp}^{*}$. The defining relationship that allows us to do this follows from the fact that the tracking voltages must follow the virtual equilibrium, so we must satisfy $\mathsf{P}^{*} \equiv \mathsf{T}_{m}$, where P_{e}^{*} is a virtual system power. With respect to the tracking voltage magnitude and phase, the required relationship is written symbolically as

$$0 = \frac{d}{dt}\mathsf{P}^{*} = \mathbf{J}_{\|}^{*}\boldsymbol{\lambda}_{\|}^{*} + \mathbf{J}_{\perp}^{*}\boldsymbol{\lambda}_{\perp}^{*}, \tag{A.19}$$

where $\mathbf{J}_{\|}^{*}$ and $\mathbf{J}_{\perp}^{*}$ are the load flow Jacobians with respect to the log magnitude and phase, respectively, of the tracking voltages. If it were not for the fact that $\mathbf{J}_{\perp}^{*}$ is singular, the solution would be

$$\boldsymbol{\lambda}_{\perp}^{*} = -(\mathbf{J}_{\perp}^{*})^{-1}\mathbf{J}_{\|}^{*}\boldsymbol{\lambda}_{\|}^{*}. \tag{A.20}$$

For the present, it will be assumed that this is true, and treatment of the singularity problem will be briefly deferred. In the rectangular coordinates, (A.19) can be expanded by differentiating (A.4) using the chain rule:

$$\frac{d}{dt}\mathsf{P}^{*} = \left\{ \left[\begin{array}{cc} \mathbb{E}_{\mathrm{D}}^{*} & \mathbb{E}_{\mathrm{Q}}^{*} \end{array} \right] \mathbf{Y}_{r} + \left[\begin{array}{cc} \mathbb{I}_{\mathrm{D}} & \mathbb{I}_{\mathrm{Q}} \end{array} \right] \right\} \left\{ \left[\begin{array}{c} \mathbb{E}_{\mathrm{D}}^{*} \\ \mathbb{E}_{\mathrm{Q}}^{*} \end{array} \right] \boldsymbol{\lambda}_{\|}^{*} + \left[\begin{array}{c} -\mathbb{E}_{\mathrm{Q}}^{*} \\ \mathbb{E}_{\mathrm{D}}^{*} \end{array} \right] \boldsymbol{\lambda}_{\perp}^{*} \right\} \tag{A.21}$$

(note that $\mathbb{I}_D = \mathrm{diag}(\mathsf{i}_D)$). From (A.21) the elements of the Jacobian can be identified:

$$\mathbf{J}_{\parallel}^{*} = \begin{bmatrix} \mathbb{E}_D^* & \mathbb{E}_Q^* \end{bmatrix} \mathbf{Y}_r \begin{bmatrix} \mathbb{E}_D^* \\ \mathbb{E}_Q^* \end{bmatrix} + \mathrm{diag}(\mathsf{P}^*) \tag{A.22}$$

$$\mathbf{J}_{\perp}^{*} = \begin{bmatrix} \mathbb{E}_D^* & \mathbb{E}_Q^* \end{bmatrix} \mathbf{Y}_r \begin{bmatrix} -\mathbb{E}_Q^* \\ \mathbb{E}_D^* \end{bmatrix} - \mathrm{diag}(\mathsf{Q}^*) \tag{A.23}$$

It is well-known that the load-flow Jacobian, taken with respect to $\boldsymbol{\delta}$, is singular, since the load-flow equations only depend on the *relative* machine angles. Any uniform increment, when added to each angle, leaves the flow unchanged. A similar situation holds for $\mathbf{J}_{\perp}^{*}$. In load-flow calculations, this difficulty is typically avoided by deleting the row and column of the Jacobian corresponding to an arbitrarily-selected slack bus, proceeding thence with the reduced-dimension, nonsingular matrix. This creates a problem, however, in that the power at the slack bus is undetermined *a priori* and becomes a by-product of the solution for the $p-1$ remaining busses.

In the present case this is unacceptable, since we require that $P_i^* = T_{mi}$ at each bus, hence the problem is overspecified. If a slack bus is assigned, the entire error occurs at that bus, which would hardly reflect an equilibrium point. If the error appears as a uniform acceleration of the entire system, however, then at least in the case of uniform damping, the COI equilibrium is preserved (Recall that a uniform error in the frequency at all machines is annihilated by the COI transform). In order to achieve this, the following approach is taken: the angle of an arbitrary generator is declared as a reference angle, so that for that bus, $\lambda_{\perp} = 0$. We may then delete the corresponding column of $\mathbf{J}_{\perp}^{*}$ and solve the following problem:

$$d\mathsf{P} = \begin{bmatrix} | & & | \\ \mathsf{j}_1 & \cdots & \mathsf{j}_{p-1} \\ | & & | \end{bmatrix} \begin{bmatrix} d\lambda_{\perp_1} \\ \vdots \\ d\lambda_{\perp_{p-1}} \end{bmatrix} + \frac{1}{m_T} \begin{bmatrix} m_1 \\ \vdots \\ m_p \end{bmatrix} d\lambda_e \tag{A.24}$$

$$= \underbrace{\begin{bmatrix} | & & | & \frac{m_1}{m_T} \\ \mathrm{j}_1 & \cdots & \mathrm{j}_{p-1} & \vdots \\ | & & | & \frac{m_p}{m_T} \end{bmatrix}}_{\mathbf{J}_\perp^a} \begin{bmatrix} d\lambda_{\perp_1} \\ \vdots \\ d\lambda_{\perp_{p-1}} \\ d\lambda_e \end{bmatrix} \tag{A.25}$$

This is straightforward to solve, as long as $\mathbf{J}_\perp^a$ (identified by the underbrace above) is nonsingular. This appears to hold in the great majority of cases. This forces any error in the solution to appear as a uniform system accelerating power. Moreover, the solution is unique, *i.e.* there is no better solution that satisfies the conditions for the virtual equilibrium.

A.3 Correcting Numerical Errors

In order to simulate controls such as the steepest-descent control based on the STEF, it is necessary to create a computer implementation of the tracking voltage dynamics. The problem that remains is that the tracking system equations provide no means of correcting for errors in numerical integration. In particular, any error in the tracking voltage magnitude is preserved; nothing in the equations derived to this point acts to reduce it. It is now necessary to derive an error feedback such that the tracking variables will approach the correct values in the presence of errors in the initial conditions. Since the tracking variables are not physical states of the system, the function of the error feedback terms is to assure that any discrepancies resulting from the numerical integration of the tracking equations remain small. This is a fairly simple matter, and will therefore not be dwelt upon. Let $\mathbf{J}_\perp^a$ be the perp Jacobian, with the last column replaced by the vector of scaled inertias, as suggested by (A.25). Then (A.20) becomes

$$\boldsymbol{\lambda}_\perp^* = -(\mathbf{J}_\perp^a)^{-1}\mathbf{J}_\parallel^*\boldsymbol{\lambda}_\parallel^*. \tag{A.26}$$

and the dynamic equations which cause the tracking system to follow the virtual equilibrium are then

$$\frac{d}{dt}\begin{bmatrix} \mathsf{E}_{\mathrm{D}}^{*} \\ \mathsf{E}_{\mathrm{Q}}^{*} \end{bmatrix} = \begin{bmatrix} \mathbb{E}_{\mathrm{D}}^{*} \\ \mathbb{E}_{\mathrm{Q}}^{*} \end{bmatrix} \left(\boldsymbol{\lambda}_{\|}^{*} + k_{\|}(|\mathsf{E}| - |\mathsf{E}^{*}|) \right) + \begin{bmatrix} -\mathbb{E}_{\mathrm{Q}}^{*} \\ \mathbb{E}_{\mathrm{D}}^{*} \end{bmatrix} \mathbf{J}_{\|}^{*}(\mathbf{J}_{\perp}^{a})^{-1}\boldsymbol{\lambda}_{\|}^{*} + k_{\perp}\mathbf{J}_{\perp}^{*}(\mathsf{T}_{m} - \mathsf{P}^{*}). \tag{A.27}$$

where $k_{\|}$ and $k_{\perp}$ are scalar feedback gains. Note that, absent errors in initial conditions, the dynamics of this subsystem are entirely dependent on the change in magnitude of the machine voltages.

This is the tracking system that was used to simulate the steepest-descent controls using the STEF and related functions in Chapter 4. Of course, in deriving the dynamic behavior of the STEF and in other similar applications, one may assume that the system tracks perfectly, and dispense with the correction terms.

Appendix B

A Single-Machine FBLC Example

The state transformation into Brunovsky canonical form is repeated here for convenience, and we do not assume that modeling is in the COI frame of reference, hence the equilibrium value of $\boldsymbol{\omega}$ is $\omega_o 1$:

$$\mathsf{z} = \begin{bmatrix} (\boldsymbol{\delta} - \boldsymbol{\delta}_o) \\ (\boldsymbol{\omega} - \omega_o) \\ \boldsymbol{\alpha} \end{bmatrix} = \mathsf{T}(\mathsf{E}'_q, \boldsymbol{\delta}, \boldsymbol{\omega}), \tag{B.1}$$

where $\boldsymbol{\alpha}$ is the angular acceleration of the rotor, $\boldsymbol{\alpha} = \dot{\boldsymbol{\omega}}$. This transform is locally C^1 for most operating points, as was shown in [6]. For the single-axis model, the system dynamics in the new coordinates are expressed as

$$\dot{\boldsymbol{\delta}} = \boldsymbol{\omega} - \omega_o \tag{B.2}$$

$$\dot{\boldsymbol{\omega}} = \boldsymbol{\alpha} \tag{B.3}$$

$$\dot{\boldsymbol{\alpha}} = -\mathbb{M}^{-1}(\mathbf{J}_e^p \dot{\mathsf{E}}'_q + \mathbf{J}_\delta^p(\boldsymbol{\omega} - \omega_o)), \tag{B.4}$$

where J_e^p is the derivative of the power vector P_e, taken with respect to E'_q, and J_δ^p is the derivative with respect to $\boldsymbol{\delta}$. For convenience, it will be assumed in this section that the damping constants vanish, *i.e.* $\mathbb{D} = 0$. It is straightforward to include damping, but for the purposes of this section, consideration of damping adds nothing to the discussion.

For the single-machine case we may substitute (2.9) into (B.4) as follows:

$$\dot{\alpha} = \frac{1}{m}\left(\frac{\partial P_e}{\partial E'_q}\frac{1}{T'_{do}}(E'_q + (x_q - x'_q)i_q) - \frac{\partial P_e}{\partial \delta}(\omega - \omega_o)\right) - \frac{\partial P_e}{\partial E'_q}\frac{1}{mT'_{do}}E_{fd} \tag{B.5}$$

which is affine in the control, so that (B.2), (B.3) and (B.5) express the system dynamics in the Brunovsky form. Now, provided there is a neighborhood of the equilibrium point on which $\frac{\partial P_e}{\partial E'_q}$ is nonzero, we may define the feedback-linearizing control signal as

$$\begin{aligned} u = E_{fd} &= -mT'_{do}\left(\tfrac{\partial P_e}{\partial E'_q}\right)^{-1}\frac{1}{m}\left(-\tfrac{\partial P_e}{\partial \delta}(\omega - \omega_o) + \tfrac{\partial P_e}{\partial E'_q}\tfrac{1}{T'_{do}}(E'_q + (x_q - x'_q)i_q)\right) \\ &+ mT'_{do}\left(\tfrac{\partial P_e}{\partial E'_q}\right)^{-1}(a_0(\delta - \delta_o) + a_1(\omega - \omega_o) + a_2\alpha) \end{aligned} \tag{B.6}$$

or

$$u = -T'_{do}(\tfrac{\partial P}{\partial E'_q})^{-1}\tfrac{\partial P}{\partial \delta} + E'_q + (x_q - x'_q)i_q - mT'_{do}\left(\tfrac{\partial P_e}{\partial E'_q}\right)^{-1}(a_0(\delta - \delta_o) + a_1(\omega - \omega_o) + a_2\alpha) \tag{B.7}$$

The feedback signal defined in (B.7), forces the closed-loop dynamics to take the form of (4.52), where the specific behavior of the feedback-linearized system is determined by selection of the parameters a_0, a_1 and a_2. This form is only valid for the single machine infinite bus case, since if other field voltage inputs are active they affect the control at the local machine. This creates difficulties for the implementation of a decentralized control, an issue that is addressed in [6], but is bypassed here, since this example is presented primarily to motivate the multimachine case in the main text of this thesis, which is of more direct interest when the impact of the control on the STEF is investigated.

Appendix C

Characterizing System Nonlinearity as a Norm-Bounded Perturbation

C.1 Introduction

As mentioned in Chapter 1, the problem of designing viable controls for power system is complicated by both the system nonlinearity and the fact that the operating point varies widely in day-to-day operation. The variation in the operating point is driven primarily by variation in the load that tits to be served, but may also be responsive to economic pressures and operating concerns such as scheduled maintenance of transmission and generation facilities. It is generally the case that the operating point changes slowly, particularly relative to the time scale over which the controls considered in this document operate, *i.e.* over a range of up to thirty seconds. It is true that equipment failures and transmission outages may create shifts in the operating point that are essentially instantaneous, however. In addition, large disturbances are typically accompanied by large swings in the state variables away from the equilibrium, so that any control that is placed into operation is faced with uncertainty in the system parameters as well as excursions in the state variables that challenge the small-signal assumptions

upon which linear control design is based. This quite clearly calls for consideration of control robustness in both design and analysis. Obviously, the tendency towards conservativeness in the design of power system controls has been well-founded in terms of practical system operation, but the changing environment of the power industry is placing increasing pressure on designers to extract a higher level of performance from both new and existing equipment.

In many cases, the ability of a utility to operate most efficiently, *e.g.* by maximizing the utilization of more-efficient generating plants or by contracting for imported power, is limited by security concerns, since the dynamic coupling between generators that is provided by the transmission grid is progressively weakened as the transmission lines become more heavily-loaded. This leads to a situation in which a disturbance that would be survivable under light loads becomes catastrophic. Because of the weakened coupling, generators are more prone to losing synchronism with the system frequency, causing the protective relaying to remove them from service. This creates a further disturbance, which can in turn lead to cascading failures and the complete shutdown of large sections of the system. An example of this was the blackout that occurred in the northeastern United States in 1972.

The field of robust linear control has seen great advances in recent years, and has been applied in several cases to power system controls. One area that has not been specifically addressed, however, is robustness of controls with respect to variations in the system behavior due to the system nonlinearity when large state deviations occur. Since the security of the system depends on its ability to survive such events, it is of interest to investigate this area.

The first task in approaching a robust control problem is to characterize the system uncertainty in the form of a disturbance signal that is bounded in some sense; several standard methods exist for including uncertainties in the system model as fictitious disturbances, which take the form of exogenous inputs whose magnitudes are subject to some type of norm bound, filtered by fictitious systems whose gain and frequency-domain characteristics reflect the level of uncertainty as well as any knowledge of the frequency at which the uncertainty occurs. As an example, $\mathcal{H}_\infty$ methods [15] seek to

minimize the gain of the system, taken from the disturbance input to the controlled output, in the sense of the $\mathcal{L}_2$ norm, such that for a vector disturbance input $\mathbf{w}(t)$ and a controlled output $\mathbf{z}(t)$, the $\mathcal{L}_2$-gain of the system (including the fictitious blocks) is given by

$$\|\mathbf{z}(t)\|_{\mathcal{L}_2} \leq \gamma_{min}, \ \forall \mathbf{w}(t) \in \mathcal{W}, \tag{C.1}$$

where $\mathcal{W} = \{\mathbf{w}(t) \mid \|\mathbf{w}(t)\|_{\mathcal{L}_2} \leq 1\}$ and the $\mathcal{L}_2$ norm of a right-sided signal is given by

$$\|\mathbf{x}(t)\|_{\mathcal{L}_2}^2 = \int_0^\infty \langle \mathbf{x}, \mathbf{x} \rangle(t)\, dt. \tag{C.2}$$

The notation $\langle \cdot, \cdot \rangle$ is the standard vector inner product. Provided one can concoct an appropriate representation of the uncertainty in the form discussed above, the solution of the control problem is standard material, and may be solved using a state-space representation, as shown in [15].

Another approach to the robust stabilization problem involves *quadratic stabilizability*, first developed in [42, 41]. This approach is formulated as a "robust linear-quadratic" problem, and has attracted the attention of other researchers [14]. Khargonekar *et. al.* later showed that this approach is equivalent to an $\mathcal{H}_\infty$ problem, and this work was extended in [53]. It happens that the nonlinearity of the network-referenced power system model may be characterized in the form required by this method and thereby reduced to the so-called *robust performance* problem, which may then be solved in state-space form, following [15]. In this manner, the effect of the system nonlinearity during large disturbances may be accounted for in the design process, while maintaining the freedom to simultaneously consider performance criteria as well. Before developing this approach, however, some introductory material must be presented.

C.2 Preliminary Definitions

The various types of stability that must be considered when dealing with nonlinear systems, including the notion of asymptotic stability, were defined in Chapter 3. An analytically tractable definition of stability that is somewhat stricter than asymptotic

stability is quadratic stability. As noted in the introduction to this chapter, quadratic stability forms the basis for a robust control method that may be applied to the network-referenced model. Several theorems exist which allow the stability of uncertain systems with a particular type of norm-bounded uncertainty to be characterized in terms of quadratic stability and quadratic stabilizability. The aspects of this theory that will be useful in the sequel will now be outlined, beginning with a definition of quadratic stability itself.

Adopting the notational convention that $\mathbf{P} > \mathbf{0}$, $(\geq \mathbf{0})$ means that $\mathbf{P}$ is positive (semi)definite, the following definition is applied:

Definition C.1 *The system (1.3) is said to be* quadratically stable *if there exist a constant $k > 0$ and a symmetric matrix $\mathbf{P} > \mathbf{0}$ such that $\frac{d}{dt}(\mathsf{x}^t\mathbf{P}\mathsf{x}) \leq -k\|\mathsf{x}\|^2$.*

In order to utilize the results that have been developed with respect to the quadratic stability of uncertain linear systems, it will be necessary to define the form of the system and the uncertainty to which these results are applied. This introduction closely follows the treatment in [53]. We consider a system with a norm-bounded, time-varying real parameter uncertainty of the form:

$$\begin{aligned} \dot{\mathsf{x}}(t) &= \left[\mathbf{A}_s + \Delta\mathbf{A}(t)\right]\mathsf{x}(t) + \mathbf{B}_1\,\mathsf{w}(t) + \left[\mathbf{B}_2 + \Delta\mathbf{B}(t)\right]\mathsf{u}(t) \\ \mathsf{z}(t) &= \mathbf{C}_1\,\mathsf{x}(t) + \mathbf{D}_{12}\,\mathsf{u}(t) \\ \mathsf{y}(t) &= \left[\mathbf{C}_2 + \Delta\mathbf{C}(t)\right]\mathsf{x}(t) + \mathbf{D}_{21}\,\mathsf{w}(t) + \left[\mathbf{D}_{22} + \Delta\mathbf{D}(t)\right]\mathsf{u}(t), \end{aligned} \tag{C.3}$$

Here, following notation that is quite widespread, the control input is u, the exogenous input is w, the measured output is y, the controlled output is z, and the uncertainty must be expressible in the form

$$\begin{bmatrix} \Delta\mathbf{A}(\cdot) & \Delta\mathbf{B}(\cdot) \\ \Delta\mathbf{C}(\cdot) & \Delta\mathbf{D}(\cdot) \end{bmatrix} = \begin{bmatrix} \mathbf{G}_1 \\ \mathbf{G}_2 \end{bmatrix} \mathbf{F}(\cdot) \begin{bmatrix} \mathbf{H}_1 & \mathbf{H}_2 \end{bmatrix} \tag{C.4}$$

and $\mathbf{F}(\cdot)$ is a time-varying matrix whose entries are Lebesgue-measurable and for which

$$\|\mathbf{F}(\cdot)\|_2 \leq \rho. \tag{C.5}$$

Note that Definition C.1 is equivalent to the following:

Definition C.2 *The system of (C.3) is quadratically stable if there exists a constant, matrix* $\mathbf{P} > \mathbf{0}$ *such that*

$$\left[\mathbf{A} + \Delta\mathbf{A}(t)\right]^t \mathbf{P} + \mathbf{P}\left[\mathbf{A} + \Delta\mathbf{A}(t)\right] < 0, \ \forall t > t_o \tag{C.6}$$

Now, consider the class $\mathcal{K}$ of strictly-proper output-feedback controllers $\mathbf{K}(s)$ characterized by:

$$\begin{aligned} \dot{\boldsymbol{\xi}} &= \mathbf{A}_c\boldsymbol{\xi} + \mathbf{B}_c\mathsf{y} \\ \mathsf{u} &= \mathbf{C}_c\boldsymbol{\xi}. \end{aligned} \tag{C.7}$$

Then we have the following:

Definition C.3 *The system (C.3) is said to be* quadratically stabilizable *via output feedback if there exists a controller* $\mathbf{K}(s) \in \mathcal{K}$ *such that the closed-loop system is quadratically stable.*

The quadratic stabilizability problem was initially developed in several papers by Peterson and Hollot in terms of a Ricatti equation condition utilizing full state feedback [42, 41]. Khargonekar *et al.* later showed that the quadratic stabilizability of (C.3) via output feedback is equivalent to the existence of a linear dynamic controller $\mathbf{K}(s)$ such that the gain of the closed-loop transfer function

$$\mathbf{H}_o(s) = (\mathbf{H}_1 - \mathbf{H}_2\mathbf{K}(s)\mathbf{C}_2)(s\mathbf{I} - \mathbf{A}_s + \mathbf{B}\mathbf{K}(s)\mathbf{C}_2)^{-1}\mathbf{D}, \tag{C.8}$$

is bounded as follows:

$$\|\mathbf{H}_o(s)\|_\infty < \rho^{-1}. \tag{C.9}$$

In other words, the stabilizability question may be reduced to an $\mathcal{H}_\infty$ optimization over the set of stabilizing controllers for the nominal system[25]. Xie *et. al.* [53] generalized the results of [25] further to include performance constraints, as follows:

Consider the following system model:

$$\begin{aligned} \dot{\mathsf{x}} &= \mathbf{A}\mathsf{x} + \begin{bmatrix} \sqrt{\epsilon}\,\rho\,\mathbf{G}_1 & \gamma^{-1}\mathbf{B}_1 \end{bmatrix} \mathsf{w} + \mathbf{B}_2\,\mathsf{u} \\ \hat{\mathsf{z}} &= \begin{bmatrix} \epsilon^{-1/2}\mathbf{H}_1 \\ \mathbf{C}_1 \end{bmatrix} \mathsf{x} + \begin{bmatrix} \epsilon^{-1/2}\mathbf{H}_2 \\ \mathbf{D}_{12} \end{bmatrix} \mathsf{u} \\ \mathsf{y} &= \mathbf{C}_2\,\mathsf{x} + \begin{bmatrix} \sqrt{\epsilon}\,\rho\,\mathbf{G}_2 & \gamma^{-1}\mathbf{D}_{21} \end{bmatrix} \mathsf{u}. \end{aligned} \tag{C.10}$$

With regard to (C.3, we may define a transfer function from the disturbance w to the output z, which we will call $\mathbf{H}_{zw}(s)$. The disturbance attenuation of the system is then defined as $\|\mathbf{H}_{zw}(s)\|_\infty$. The following theorem concerns robust stability with a guaranteed level of disturbance rejection for the system of (C.3):

Theorem C.1 *Let γ represent a given level of disturbance attenuation and $\mathbf{K}(s)$ denote a given linear dynamic controller. Then the system of (C.3) is quadratically stable with disturbance attenuation γ if and only if there exists an ϵ such that the system of (C.10) with feedback controller $\mathbf{K}(s)$ is stable with unitary disturbance rejection.*

Referring to [15], it is clear that the model defined by (C.10) has the necessary form for the synthesis of controls, provided the following definitions are made:

$$\begin{aligned} \mathbf{B}_1' &= \begin{bmatrix} \sqrt{\epsilon}\,\rho\,\mathbf{G}_1 & \gamma^{-1}\mathbf{B}_1 \end{bmatrix}, \\ \mathbf{B}_2' &= \mathbf{B}_2, \\ \mathbf{C}_1' &= \begin{bmatrix} \epsilon^{-1/2}\mathbf{H}_1 \\ \mathbf{C}_1 \end{bmatrix}, \\ \mathbf{C}_2' &= \mathbf{C}_2, \\ \mathbf{D}_{12}' &= \begin{bmatrix} \epsilon^{-1/2}\mathbf{H}_2 \\ \mathbf{D}_{12} \end{bmatrix}, \end{aligned}$$

$$\mathbf{D}'_{21} = \left[\sqrt{\epsilon}\,\rho\,\mathbf{G}_2 \quad \gamma^{-1}\mathbf{D}_{21} \right].$$

It is somewhat unfortunate that the standard notation for the input matrix is the same as the standard notation for a susceptance matrix *i.e.* $\mathbf{B}$. However, in this chapter, the susceptance matrix will always carry the subscript r, as in $\mathbf{B}_r$. Moreover, the distinction will be obvious from the context, so we will adhere to the notational standard in both cases.

Theorem C.1 will be used to develop controls that are insensitive to variations in the linearized model due to the system nonlinearity. In the process we will develop a model of the form of (C.3) in which straightforward bounds on $\|\mathbf{F}(\cdot)\|$ may be calculated and which is an exact expression of the nonlinear state equations. This formulation allows controls to be designed for the linearized system which are guaranteed to be stable for a given magnitude of state perturbations about the origin, with consideration of performance objectives. It is conservative to the extent that the matrix $\mathbf{F}(\cdot)$ as it is defined with reference to the power system model has a structure that is not fully characterized by the norm condition, thus the worst-case perturbation is likely to lie outside the set of achievable perturbations. However, in the process of defining the uncertain linear power system model, several parameters are available that allow the relative magnitudes of various perturbations to be scaled to suit the problem, and therefore provide some insight into the various trade-offs that restrict performance versus robustness to model variation due to nonlinearity when state deviations are large.

C.3 Characterization of the Nonlinearity

One attribute of the network-referenced system model is that it allows for a fairly straightforward characterization of the system nonlinearity as a linear system plus a norm-bounded uncertainty. For convenience, we repeat equations (2.90) here:

$$\dot{\mathsf{E}}_{\mathrm{DQ}} = \left\{ \mathbf{A}_1 + \mathbf{R}_{\mathrm{N}}(2\boldsymbol{\delta})\,\mathbf{A}_2 + \mathbf{W}(\boldsymbol{\omega}) \right\} \mathsf{E}_{\mathrm{DQ}} + \mathbf{U}(\boldsymbol{\delta})\mathsf{E}_{fd}, \tag{C.11}$$

$$\dot{\delta} = \omega - \omega_o \tag{C.12}$$

$$\dot{\omega} = \mathbb{M}^{-1}\left\{\mathsf{T}_m - \begin{bmatrix} \mathbb{E}_D & \mathbb{E}_Q \end{bmatrix} \mathbf{Y}_r \begin{bmatrix} \mathsf{E}_D \\ \mathsf{E}_Q \end{bmatrix} - \mathbb{D}\frac{(\omega - \omega_o)}{\omega_o}\right\} \tag{C.13}$$

In this case we utilize an absolute frame of reference, so that both δ and ω will be measured against a fixed reference. This means that the system has an uncontrollable zero eigenvalue, but it simplifies the derivation of the bounded-norm characterization of the uncertainty. Following this derivation, the conversion will be made to the relative-angle model, which is most suitable for linear design techniques. In order to utilize Theorem C.1, the system (C.11)–(C.13) must be written in the form of (C.3), and the bounds of the uncertainty must be established. For the network-referenced model, this may be done exactly. First, however, the issue of the system equilibrium must be addressed. In general, if linear design techniques are to be applied to a nonlinear system, the system is first linearized about the operating point x_o, as in (1.5). A new state vector, $\tilde{\mathsf{x}} = \mathsf{x} - \mathsf{x}_o$, is defined that expresses the deviation of the state from the nominal equilibrium, with the result that the equilibrium is translated to 0.

In the following paragraphs, the linearized model will be derived, but we will not proceed immediately by differentiation. Rather, we will first perform the translation of the state to the zero equilibrium point by explicitly expressing the state variables in terms of the equilibrium value plus a perturbation, then performing the translation algebraically. This method yields a model in which the equilibrium point may be taken as 0, but it is exact. The linearized model of (1.5) will then be derived, but the higher-order terms will be preserved and placed in the form of (C.4). The linearized system matrix $\mathbf{A}_s$ will be of the form:

$$\mathbf{A}_s = \begin{bmatrix} \mathbf{A}_{ee} & \mathbf{A}_{e\delta} & \mathbf{A}_{e\omega} \\ \mathbf{0} & \mathbf{0} & \mathbf{A}_{\delta\omega} \\ \mathbf{A}_{\omega e} & \mathbf{0} & \mathbf{A}_{\omega\omega} \end{bmatrix}. \tag{C.14}$$

and the component blocks will be identified as we proceed with the linearization.

In order to perform the translation for the voltage vector E_{DQ}, we first address the

state-dependent matrix $\mathbf{R}_{\text{N}}(2\boldsymbol{\delta})$ which, like $\mathbf{R}(\boldsymbol{\delta})$ in (2.34), is a pairwise coordinate rotation with a sign change. For a general rotation matrix it is true that $\mathbf{R}(\phi+\theta) = \mathbf{R}(\phi)\mathbf{R}(\theta)$, which allows $\mathbf{R}_{\text{N}}(2\boldsymbol{\delta})$ to be factored into a constant matrix plus a matrix that depends only on the change in $\boldsymbol{\delta}$:

$$\mathbf{R}_{\text{N}}(2\boldsymbol{\delta}) = \begin{bmatrix} \mathbf{I} & \mathbf{0} \\ \mathbf{0} & -\mathbf{I} \end{bmatrix} \begin{bmatrix} \mathbb{C}(2\tilde{\boldsymbol{\delta}}) & \mathbb{S}(2\tilde{\boldsymbol{\delta}}) \\ -\mathbb{S}(2\tilde{\boldsymbol{\delta}}) & \mathbb{C}(2\tilde{\boldsymbol{\delta}}) \end{bmatrix} \begin{bmatrix} \mathbb{C}(2\boldsymbol{\delta}_o) & \mathbb{S}(2\boldsymbol{\delta}_o) \\ -\mathbb{S}(2\boldsymbol{\delta}_o) & \mathbb{C}(2\boldsymbol{\delta}_o) \end{bmatrix} \tag{C.15}$$

Some shuffling of signs yields

$$\begin{aligned} \mathbf{R}_{\text{N}}(2\boldsymbol{\delta}) &= \begin{bmatrix} \mathbb{C}(2\tilde{\boldsymbol{\delta}}) & -\mathbb{S}(2\tilde{\boldsymbol{\delta}}) \\ \mathbb{S}(2\tilde{\boldsymbol{\delta}}) & \mathbb{C}(2\tilde{\boldsymbol{\delta}}) \end{bmatrix} \begin{bmatrix} \mathbb{C}(2\boldsymbol{\delta}_o) & \mathbb{S}(2\boldsymbol{\delta}_o) \\ \mathbb{S}(2\boldsymbol{\delta}_o) & -\mathbb{C}(2\boldsymbol{\delta}_o) \end{bmatrix} \\ &= \left\{ \mathbf{I} + \begin{bmatrix} \mathbb{C}(2\tilde{\boldsymbol{\delta}}) - \mathbf{I} & -\mathbb{S}(2\tilde{\boldsymbol{\delta}}) \\ \mathbb{S}(2\tilde{\boldsymbol{\delta}}) & \mathbb{C}(2\tilde{\boldsymbol{\delta}}) - \mathbf{I} \end{bmatrix} \right\} \mathbf{R}_{\text{N}}(2\boldsymbol{\delta}_o) \\ \mathbf{R}_{\text{N}}(2\boldsymbol{\delta}) &= \mathbf{R}^o_{\text{N}} + \tilde{\mathbf{R}}_{\text{N}}(2\tilde{\boldsymbol{\delta}})\mathbf{R}^o_{\text{N}} \end{aligned} \tag{C.16}$$

Note that the second term in (C.16) depends only on $\tilde{\boldsymbol{\delta}}$ and is zero when $\tilde{\boldsymbol{\delta}} = 0$. By a similar procedure, the input matrix $\mathbf{U}(\boldsymbol{\delta})$ may be resolved into a constant matrix plus a matrix that depends only on the increment in $\boldsymbol{\delta}$:

$$\begin{aligned} \mathbf{U}(\boldsymbol{\delta}) &= \left\{ \begin{bmatrix} \mathbb{C}(\boldsymbol{\delta}_o) \\ \mathbb{S}(\boldsymbol{\delta}_o) \end{bmatrix} + \begin{bmatrix} \mathbb{C}(\boldsymbol{\delta}_o) & -\mathbb{S}(\boldsymbol{\delta}_o) \\ \mathbb{S}(\boldsymbol{\delta}_o) & \mathbb{C}(\boldsymbol{\delta}_o) \end{bmatrix} \begin{bmatrix} \mathbb{C}(\tilde{\boldsymbol{\delta}}) - \mathbf{I} \\ \mathbb{S}(\tilde{\boldsymbol{\delta}}) \end{bmatrix} \right\} \mathbb{T}_{do}^{-1} \\ &= \mathbf{U}(\boldsymbol{\delta}_o) + \tilde{\mathbf{U}}(\tilde{\boldsymbol{\delta}}) \end{aligned} \tag{C.17}$$

These expressions are substituted into (C.11) and the constant terms dropped, giving a model with a zero equilibrium:

$$\begin{aligned} \dot{\tilde{\mathsf{E}}}_{\text{DQ}} &= \left\{ \mathbf{A}_1 + \mathbf{R}^o_{\text{N}}\mathbf{A}_2 \right\} \tilde{\mathsf{E}}_{\text{DQ}} + \tilde{\mathbf{R}}_{\text{N}}(2\tilde{\boldsymbol{\delta}})\mathbf{R}^o_{\text{N}}\mathbf{A}_2\, \mathsf{E}^o_{\text{DQ}} + \mathbf{W}(\tilde{\boldsymbol{\omega}})\, \mathsf{E}^o_{\text{DQ}} \\ &+ \tilde{\mathbf{R}}_{\text{N}}(2\tilde{\boldsymbol{\delta}})\mathbf{R}^o_{\text{N}}\mathbf{A}_2\, \tilde{\mathsf{E}}_{\text{DQ}} + \mathbf{W}(\tilde{\boldsymbol{\omega}})\tilde{\mathsf{E}}_{\text{DQ}} + \mathbf{U}(\boldsymbol{\delta}_o)\, \tilde{\mathsf{E}}_{fd} + \tilde{\mathbf{U}}(\tilde{\boldsymbol{\delta}})(\mathsf{E}^o_{fd} + \tilde{\mathsf{E}}_{fd}). \end{aligned} \tag{C.18}$$

From this equation, $\mathbf{A}_{ee}$ may be identified:

$$\mathbf{A}_{ee} = \mathbf{A}_1 + \mathbf{R}_{\mathrm{N}}^o \mathbf{A}_2, \tag{C.19}$$

where $\mathbf{A}_1$ and $\mathbf{A}_2$ are defined in (2.85) and (2.86), respectively. Now, expanding the term $\mathbf{W}(\tilde{\boldsymbol{\omega}})\,\mathsf{E}_{\mathrm{DQ}}^o$, we have

$$\mathbf{W}(\tilde{\boldsymbol{\omega}})\,\mathsf{E}_{\mathrm{DQ}}^o = \begin{bmatrix} \mathbf{0} & -\mathbb{W} \\ \mathbb{W} & \mathbf{0} \end{bmatrix} \begin{bmatrix} \mathsf{E}_{\mathrm{D}}^o \\ \mathsf{E}_{\mathrm{Q}}^o \end{bmatrix} = \begin{bmatrix} -\mathbb{E}_{\mathrm{Q}}^o \\ \mathbb{E}_{\mathrm{D}}^o \end{bmatrix} \boldsymbol{\omega}. \tag{C.20}$$

Hence,

$$\mathbf{A}_{e\omega} = \begin{bmatrix} -\mathbb{E}_{\mathrm{Q}}^o \\ \mathbb{E}_{\mathrm{D}}^o \end{bmatrix}. \tag{C.21}$$

We resort to differentiation of the terms $\tilde{\mathbf{R}}_{\mathrm{N}}(2\tilde{\boldsymbol{\delta}})\mathbf{R}_{\mathrm{N}}^o\mathbf{A}_2\,\mathsf{E}_{\mathrm{DQ}}^o$ and $\tilde{\mathbf{U}}(\tilde{\boldsymbol{\delta}})\mathsf{E}_{fd}^o$ in order to extract $\mathbf{A}_{e\delta}$ plus a higher-order residual. Defining $\tilde{\Delta}$ as $\mathrm{diag}(\tilde{\boldsymbol{\delta}})$ and referring to (C.16), (C.17) we differentiate $\tilde{\mathbf{R}}_{\mathrm{N}}(2\tilde{\boldsymbol{\delta}})\mathbf{R}_{\mathrm{N}}^o$ and $\tilde{\mathbf{U}}(\tilde{\boldsymbol{\delta}})$, which yields

$$\begin{aligned} &\tilde{\mathbf{R}}_{\mathrm{N}}(2\tilde{\boldsymbol{\delta}})\mathbf{R}_{\mathrm{N}}^o\,\mathsf{E}_{\mathrm{DQ}}^o + \tilde{\mathbf{U}}(\tilde{\boldsymbol{\delta}})\,\mathsf{E}_{fd}^o \;= \\ &\begin{bmatrix} 2\tilde{\Delta} & \mathbf{0} \\ \mathbf{0} & 2\tilde{\Delta} \end{bmatrix} \underbrace{\begin{bmatrix} \mathbf{0} & -\mathbf{I} \\ \mathbf{I} & \mathbf{0} \end{bmatrix} \mathbf{R}_{\mathrm{N}}^o\,\mathbf{A}_2\,\mathsf{E}_{\mathrm{DQ}}^o}_{\mathsf{A}_d} + \begin{bmatrix} -\mathbb{S}(\boldsymbol{\delta}_o) \\ \mathbb{C}(\boldsymbol{\delta}_o) \end{bmatrix} \mathbb{T}_{do}^{-1}\,\mathbb{E}_{fd}^o\tilde{\boldsymbol{\delta}} \\ &+ \begin{bmatrix} \mathbb{C}(2\tilde{\boldsymbol{\delta}}) - \mathbf{I} & 2\boldsymbol{\delta} - \mathbb{S}(2\tilde{\boldsymbol{\delta}}) \\ \mathbb{S}(2\tilde{\boldsymbol{\delta}}) - 2\tilde{\boldsymbol{\delta}} & \mathbb{C}(2\tilde{\boldsymbol{\delta}}) - \mathbf{I} \end{bmatrix} \mathbf{A}_2\,\mathsf{E}_{\mathrm{DQ}}^o + \begin{bmatrix} \mathbb{C}(\boldsymbol{\delta}_o) & -\mathbb{S}(\boldsymbol{\delta}_o) \\ \mathbb{S}(\boldsymbol{\delta}_o) & \mathbb{C}(\boldsymbol{\delta}_o) \end{bmatrix} \begin{bmatrix} \mathbb{C}(\tilde{\boldsymbol{\delta}}) - \mathbf{I} \\ \mathbb{S}(\tilde{\boldsymbol{\delta}}) - \tilde{\boldsymbol{\delta}} \end{bmatrix} \mathbb{T}_{do}^{-1}\mathsf{E}_{fd}^o, \end{aligned} \tag{C.22}$$

Utilizing the constant vector $\mathsf{A}_d = [\ \mathsf{A}_{d1}^t \quad \mathsf{A}_{d2}^t\ ]^t$ as defined by the underbrace in the equation above, $\mathbf{A}_{e\delta}$ may be defined:

$$\mathbf{A}_{e\delta} = \begin{bmatrix} 2\mathbf{A}_{d1} - \mathbb{S}(\boldsymbol{\delta}_o)\mathbb{T}_{do}^{-1}\mathbb{E}_{fd}^o \\ 2\mathbf{A}_{d2} + \mathbb{C}(\boldsymbol{\delta}_o)\mathbb{T}_{do}^{-1}\mathbb{E}_{fd}^o \end{bmatrix}. \tag{C.23}$$

Examination of (C.12) reveals that the equation for the $\tilde{\boldsymbol{\delta}}$ dynamics is linear and

expressed in terms of the incremental variables, so no linearization of (C.12) is needed, and the translation to the zero equilibrium is trivial. Turning to (C.13), we may expand the equation by writing the power equation as:

$$\mathsf{P}_e = \left[\begin{array}{cc} (\mathbb{E}_{\mathrm{D}}^o + \tilde{\mathbb{E}}_{\mathrm{D}}) & (\mathbb{E}_{\mathrm{Q}}^o + \tilde{\mathbb{E}}_{\mathrm{Q}}) \end{array} \right] \mathbf{Y}_r \left[\begin{array}{c} (\mathsf{E}_{\mathrm{D}}^o + \tilde{\mathsf{E}}_{\mathrm{D}}) \\ (\mathsf{E}_{\mathrm{Q}}^o + \tilde{\mathsf{E}}_{\mathrm{Q}}) \end{array} \right]. \tag{C.24}$$

Performing the multiplication and again dropping constant terms, we have (*cf* (C.13)):

$$\begin{aligned} \dot{\tilde{\omega}} \;=\; \mathbb{M}^{-1} \Bigg\{ & \left[\begin{array}{cc} \mathbb{E}_{\mathrm{D}}^o & \mathbb{E}_{\mathrm{Q}}^o \end{array} \right] \mathbf{Y}_r \left[\begin{array}{c} \tilde{\mathsf{E}}_{\mathrm{D}} \\ \tilde{\mathsf{E}}_{\mathrm{Q}} \end{array} \right] + \left[\begin{array}{cc} \tilde{\mathbb{E}}_{\mathrm{D}} & \tilde{\mathbb{E}}_{\mathrm{Q}} \end{array} \right] \mathbf{Y}_r \left[\begin{array}{c} \mathsf{E}_{\mathrm{D}}^o \\ \mathsf{E}_{\mathrm{Q}}^o \end{array} \right] \\ & + \left[\begin{array}{cc} \tilde{\mathbb{E}}_{\mathrm{D}} & \tilde{\mathbb{E}}_{\mathrm{Q}} \end{array} \right] \mathbf{Y} \left[\begin{array}{c} \tilde{\mathsf{E}}_{\mathrm{D}} \\ \tilde{\mathsf{E}}_{\mathrm{Q}} \end{array} \right] - \mathbb{D} \frac{\tilde{\omega}}{\omega_o} \Bigg\}. \end{aligned} \tag{C.25}$$

The first two terms are linear with respect to $\tilde{\mathsf{E}}_{\mathrm{DQ}}$, but the second term needs some manipulation. Observe:

$$\begin{aligned} \left[\begin{array}{cc} \tilde{\mathbb{E}}_{\mathrm{D}} & \tilde{\mathbb{E}}_{\mathrm{Q}} \end{array} \right] \mathbf{Y}_r \left[\begin{array}{c} \mathsf{E}_{\mathrm{D}}^o \\ \mathsf{E}_{\mathrm{Q}}^o \end{array} \right] &= \left[\begin{array}{cc} \tilde{\mathbb{E}}_{\mathrm{D}} & \tilde{\mathbb{E}}_{\mathrm{Q}} \end{array} \right] \left[\begin{array}{c} \mathsf{i}_{\mathrm{D}}^o \\ \mathsf{i}_{\mathrm{Q}}^o \end{array} \right] \\ &= \left[\begin{array}{cc} \mathbb{I}_{\mathrm{D}}^o & \mathbb{I}_{\mathrm{Q}}^o \end{array} \right] \left[\begin{array}{c} \tilde{\mathsf{E}}_{\mathrm{D}} \\ \tilde{\mathsf{E}}_{\mathrm{Q}} \end{array} \right], \end{aligned} \tag{C.26}$$

which allows $\mathbf{A}_{\omega e}$ to be identified as:

$$\mathbf{A}_{\omega e} = -\mathbb{M}^{-1} \left\{ \left[\begin{array}{cc} \tilde{\mathbb{E}}_{\mathrm{D}} & \tilde{\mathbb{E}}_{\mathrm{Q}} \end{array} \right] \mathbf{Y}_r + \left[\begin{array}{cc} \mathbb{I}_{\mathrm{D}}^o & \mathbb{I}_{\mathrm{Q}}^o \end{array} \right] \right\}. \tag{C.27}$$

Finally, $\mathbf{A}_{\omega\omega}$ is identified by inspection of (C.25) as

$$A_{\omega\omega} = -\frac{1}{\omega_o} \mathbb{M}^{-1} \mathbb{D}. \tag{C.28}$$

The linearized system matrix $\mathbf{A}_s$ is now completely characterized in terms of its com-

ponent blocks, whose definitions will be summarized here:

$$\mathbf{A}_{ee} = \mathbf{A}_1 + \mathbf{R}_{\mathrm{N}}^o \mathbf{A}_2 \tag{C.29}$$

$$\mathbf{A}_{e\delta} = \begin{bmatrix} 2\mathbf{A}_{d1} - \mathbb{S}(\boldsymbol{\delta}_o)\mathbb{T}_{do}^{-1}\mathbb{E}_{fd}^o \\ 2\mathbf{A}_{d2} + \mathbb{C}(\boldsymbol{\delta}_o)\mathbb{T}_{do}^{-1}\mathbb{E}_{fd}^o \end{bmatrix} \tag{C.30}$$

$$\left(\begin{bmatrix} \mathsf{A}_{d1} \\ \mathsf{A}_{d2} \end{bmatrix} = \begin{bmatrix} \mathbf{0} & -\mathbf{I} \\ \mathbf{I} & \mathbf{0} \end{bmatrix} \mathbf{R}_{\mathrm{N}}^o \, \mathbf{A}_2 \, \mathsf{E}_{\mathrm{DQ}}^o \right) \tag{C.31}$$

$$\mathbf{A}_{e\omega} = \begin{bmatrix} -\mathbb{E}_{\mathrm{Q}}^o \\ \mathbb{E}_{\mathrm{D}}^o \end{bmatrix} \tag{C.32}$$

$$\mathbf{A}_{\delta\omega} = \mathbf{I} \tag{C.33}$$

$$\mathbf{A}_{\omega e} = -\mathbb{M}^{-1} \left\{ \begin{bmatrix} \tilde{\mathbb{E}}_{\mathrm{D}} & \tilde{\mathbb{E}}_{\mathrm{Q}} \end{bmatrix} \mathbf{Y}_r + \begin{bmatrix} \mathbb{I}_{\mathrm{D}}^o & \mathbb{I}_{\mathrm{Q}}^o \end{bmatrix} \right\} \tag{C.34}$$

$$A_{\omega\omega} = -\frac{1}{\omega_o} \mathbb{M}^{-1} \mathbb{D}. \tag{C.35}$$

The task that remains is to characterize the higher-order terms in the form of (C.4). The uncertain matrix $\mathbf{F}(\cdot)$ will have a block-diagonal form, so that each nonlinear residual term will be cast into the form $\Delta\mathbf{A}_{\mathsf{x}_i\mathsf{x}_j}^k(\cdot) = \mathbf{G}_{\mathsf{x}_i,k}\mathbf{F}_{k,k}(\cdot)\mathbf{H}_{k,\mathsf{x}_j}$. Each term $\Delta\mathbf{A}_{\mathsf{x}_i,\mathsf{x}_j}^k$ appears in the dynamic equation for the state variables x_i, and multiplies the state variables x_j. The k superscript locates the block $\mathbf{F}_{kk}(\cdot)$ in the block-diagonal matrix $\mathbf{F}(\cdot)$. Assuming an ordering $k \in \{1, \cdots, k_{ee}, k_{ee}+1, \cdots, k_{e\delta}, \cdots\}$, the system equations may be written in a certain general form, illustrated here with the machine voltage equations:

$$\dot{\tilde{\mathsf{E}}}_{\mathrm{DQ}} = \begin{bmatrix} \mathbf{A}_{ee} & \mathbf{A}_{e\delta} & \mathbf{A}_{e\omega} \end{bmatrix} \tilde{\mathsf{x}} + \sum_{i=1}^{k_e} \Delta\mathbf{A}_{ee}(\cdot)\tilde{\mathsf{E}} + \sum_{i=k_e+1}^{k_\delta} \Delta\mathbf{A}_{e\delta}(\cdot)\tilde{\boldsymbol{\delta}} + \sum_{i=k_\delta+1}^{k_\omega} \Delta\mathbf{A}_{e\omega}(\cdot)\tilde{\boldsymbol{\omega}}. \tag{C.36}$$

We may now collect the linear and residual terms in the voltage equation as follows, where each nonlinear term is identified by the underbraces.

$$\dot{\tilde{\mathsf{E}}}_{\mathrm{DQ}} = \mathbf{A}_{se}\tilde{\mathsf{x}} + \underbrace{\tilde{\mathbf{R}}_{\mathrm{N}}(2\tilde{\boldsymbol{\delta}})\mathbf{R}_{\mathrm{N}}^o\mathbf{A}_2\,\tilde{\mathsf{E}}_{\mathrm{DQ}}}_{\Delta\mathbf{A}_{ee}^1} + \underbrace{\begin{bmatrix} \mathbb{C}(2\tilde{\boldsymbol{\delta}}) - \mathbf{I} & 2\boldsymbol{\delta} - \mathbb{S}(2\tilde{\boldsymbol{\delta}}) \\ \mathbb{S}(2\tilde{\boldsymbol{\delta}}) - 2\tilde{\boldsymbol{\delta}} & \mathbb{C}(2\tilde{\boldsymbol{\delta}}) - \mathbf{I} \end{bmatrix} \mathbf{A}_2\,\mathsf{E}_{\mathrm{DQ}}^o}_{\Delta\mathbf{A}_{e\delta}^2}$$

$$+ \underbrace{\begin{bmatrix} \mathbb{C}(\delta_o) & -\mathbb{S}(\delta_o) \\ \mathbb{S}(\delta_o) & \mathbb{C}(\delta_o) \end{bmatrix} \begin{bmatrix} \mathbb{C}(\tilde{\delta}) - \mathbf{I} \\ \mathbb{S}(\tilde{\delta}) - \tilde{\delta} \end{bmatrix} \mathbb{T}_{do}^{-1} \mathsf{E}_{fd}^{o}}_{\Delta \mathbf{A}_{e\delta}^{3}} + \underbrace{\mathbf{W}(\tilde{\omega}) \tilde{\mathsf{E}}_{\mathrm{DQ}}}_{\Delta \mathbf{A}_{e\omega}^{4}} + \underbrace{\tilde{\mathbf{U}}(\tilde{\delta}) \tilde{\mathsf{E}}_{fd}}_{\Delta \mathbf{B}_{eu}^{5}}$$

$$+ \underbrace{\mathbf{U}(\delta^o)}_{\mathbf{B}_e} \tilde{\mathsf{E}}_{fd}. \tag{C.37}$$

$$\dot{\tilde{\omega}} = \mathbf{A}_{\omega e} \tilde{\mathsf{E}}_{\mathrm{DQ}} + \mathbf{A}_{\omega\omega} \tilde{\omega} - \mathbb{M}^{-1} \begin{bmatrix} \tilde{\mathbb{E}}_{\mathrm{D}} & \tilde{\mathbb{E}}_{\mathrm{Q}} \end{bmatrix} \mathbf{Y}_r \tilde{\mathsf{E}}_{\mathrm{DQ}} \tag{C.38}$$

The nonlinear terms must now be manipulated into the proper form. Note that (C.4) requires that the bounded uncertainty matrix must multiply the state. In general, the fact that the residual terms approach zero as $\tilde{\mathbf{x}} \to 0$ will allow flexibility in defining scaling factors to be defined that characterize the magnitude of allowable state deviation that is to be considered in a given design. As mentioned earlier, the matrix $\mathbf{F}(\cdot)$ is of a block-diagonal form, whereas the design of the controller proceeds solely upon the assumption that $\|\mathbf{F}(\cdot)\|_2 \leq 1$, without constraining the form of the matrix in any way. Since it is unlikely that the worst-case perturbation of the matrix is within the set of achievable perturbations, the method will be conservative. However, at worst, the uncertain matrix may be scaled by a small factor, in which case the model approaches the nominal plant. Other types of structured or unstructured uncertainty may also be included to reflect other types of plant perturbations or disturbances.

Referring to (C.38), it is evident that the term $\Delta \mathbf{A}_{ee}^{1}$, is already in the required form, *i.e.* $\Delta \mathbf{A}_{ee}^{1} = \mathbf{G}_{e1} \mathbf{F}_{11}(\tilde{\delta}) \mathbf{H}_{1e}$, where

$$\mathbf{G}_{e1} = \mathbf{I}; \qquad \mathbf{F}_{11}(\tilde{\delta}) = \tilde{\mathbf{R}}_{\mathrm{N}}(2\tilde{\delta}); \qquad \mathbf{H}_{1e} = \mathbf{R}_{\mathrm{N}}^{o} \mathbf{A}_2 \tag{C.39}$$

In order to quantify the norm of $\mathbf{F}_{11}(\tilde{\delta})$, we define

$$\bar{\delta} = \|\tilde{\delta}\|_{\infty}. \tag{C.40}$$

Since the blocks of $\mathbf{F}_{11}(\tilde{\delta})$ are diagonal, this is completely analogous to a calculation

performed on a 2×2 matrix, and

$$\|\mathbf{F}_{11}(\tilde{\boldsymbol{\delta}})\|_2^2 = 2(1 - \cos\bar{\delta}). \tag{C.41}$$

Turning now to $\Delta\mathbf{A}^2_{e\delta}$, it is clear that some manipulation will be required, since there is no affine multiplication of the state. We have:

$$\Delta\mathbf{A}^2_{e\delta} = \underbrace{\begin{bmatrix} \mathbb{C}(2\tilde{\boldsymbol{\delta}}) - \mathbf{I} & -(\mathbb{S}(2\tilde{\boldsymbol{\delta}}) - 2\boldsymbol{\delta}) \\ \mathbb{S}(2\tilde{\boldsymbol{\delta}}) - 2\tilde{\boldsymbol{\delta}} & \mathbb{C}(2\tilde{\boldsymbol{\delta}}) - \mathbf{I} \end{bmatrix} \mathbf{A}_2 \mathsf{E}^o_{\mathsf{DQ}}}_{\mathsf{Z}_d}. \tag{C.42}$$

Taking $\mathsf{Z}_d = \begin{bmatrix} \mathsf{Z}^t_{d1} & \mathsf{Z}^t_{d2} \end{bmatrix}^t$ and defining the diagonal matrices $\mathbb{Z}_{dq}$ and $\mathbb{Z}_{d1}$ in the obvious way, we have

$$\Delta\mathbf{A}^2_{e\delta} = \begin{bmatrix} \mathbb{C}(2\tilde{\boldsymbol{\delta}}) - \mathbf{I} & -(\mathbb{S}(2\tilde{\boldsymbol{\delta}}) - 2\boldsymbol{\delta}) \\ \mathbb{S}(2\tilde{\boldsymbol{\delta}}) - 2\tilde{\boldsymbol{\delta}} & (\mathbb{C}(2\tilde{\boldsymbol{\delta}}) - \mathbf{I}) \end{bmatrix} \begin{bmatrix} \mathbb{Z}_{d1} \\ \mathbb{Z}_{d2} \end{bmatrix} \tag{C.43}$$

Now, because the system has been linearized, all nonlinear terms are at least quadratic, hence terms of the form $f(\tilde{x})/\tilde{x} \to 0$ as $\tilde{x} \to 0$, so after a certain amount of algebraic manipulation, we may cast the expression in the form

$$\Delta\mathbf{A}^2_{e\delta} = \underbrace{\begin{bmatrix} \mathbb{Z}_{d1} & -\mathbb{Z}_{d2} \\ \mathbb{Z}_{d2} & \mathbb{Z}_{d1} \end{bmatrix}}_{\mathbf{G}_{e2}} \underbrace{\begin{bmatrix} \mathbb{C}(2\tilde{\boldsymbol{\delta}}) - \mathbf{I} \\ \mathbb{S}(2\tilde{\boldsymbol{\delta}}) - 2\tilde{\boldsymbol{\delta}} \end{bmatrix} \tilde{\Delta}^{-1} \quad \mathbf{I}}_{\mathbf{F}_{22}} \underbrace{\quad}_{\mathbf{H}_{2\delta}} \tilde{\boldsymbol{\delta}}. \tag{C.44}$$

Once again, the problem of finding the norm of $\mathbf{F}_{22}$ reduces to a 2×2 case, whence we have

$$\|\mathbf{F}_{22}\|_2^2 = \frac{1}{\bar{\delta}^2}\left[2 - 2\cos(2\bar{\delta}) - 4\bar{\delta}\sin(2\bar{\delta}) + 4\bar{\delta}^2\right] \tag{C.45}$$

Now, by a procedure similar to that applied to $\Delta\mathbf{A}^2_{e\delta}$, $\Delta\mathbf{A}^3_{e\delta}$ may be decomposed as:

$$\Delta\mathbf{A}^3_{e\delta} = \underbrace{\begin{bmatrix} \mathbb{C}(\boldsymbol{\delta}^o) & -\mathbb{S}(\boldsymbol{\delta}^o) \\ \mathbb{S}(\boldsymbol{\delta}^o) & \mathbb{C}(\boldsymbol{\delta}^o) \end{bmatrix}}_{\mathbf{G}_{e3}} \underbrace{\begin{bmatrix} \mathbb{C}(\tilde{\boldsymbol{\delta}}) - \mathbf{I} \\ \mathbb{S}(\tilde{\boldsymbol{\delta}}) - \tilde{\boldsymbol{\delta}} \end{bmatrix}}_{\mathbf{F}_{33}} \underbrace{\mathbb{T}^{-1}_{do}\mathbb{E}^o_{fd}}_{\mathbf{H}_{3\delta}} \tilde{\boldsymbol{\delta}}. \tag{C.46}$$

$\Delta\mathbf{A}^4_{e\omega}$ can be rewritten as

$$\Delta\mathbf{A}^4_{e\omega} = \begin{bmatrix} \tilde{\mathbb{E}}_{\mathrm{Q}} \\ -\tilde{\mathbb{E}}_{\mathrm{D}} \end{bmatrix} \tilde{\boldsymbol{\omega}}, \tag{C.47}$$

so we may choose

$$\mathbf{G}_{e4} = \mathbf{I}, \;\; \mathbf{F}_{44} = \begin{bmatrix} \tilde{\mathbb{E}}_{\mathrm{Q}} \\ -\tilde{\mathbb{E}}_{\mathrm{D}} \end{bmatrix}, \;\; \mathbf{H}_{4\omega} = \mathbf{I}. \tag{C.48}$$

In this case, it would have been possible to choose $\mathbf{F}_{44} = \mathbb{W}(\tilde{\boldsymbol{\omega}})$, but this increases the dimension of $\mathbf{F}(\cdot)$. The norm of $\mathbf{F}_{44}$ is just the maximum magnitude of the change in the machine voltage phasors, which is given by the law of cosines:

$$\|\mathbf{F}_{44}\|_2^2 = \max_{1\le i\le p} \left\{ |E_i^o|^2 + |E_i|^2 - 2|E_i^o|\,|E_i|\,\cos\phi_i \right\}, \tag{C.49}$$

where ϕ is the change in phase angle. This has a natural bound, since the cosine is bounded and the change in magnitude is bounded above by magnetic saturation of the generator and below by 0.

The uncertainty in the input matrix may be expressed as

$$\Delta\mathbf{B}_{11} = \underbrace{\begin{bmatrix} \mathbb{C}(\boldsymbol{\delta}^o) & -\mathbb{S}(\boldsymbol{\delta}^o) \\ \mathbb{S}(\boldsymbol{\delta}^o) & \mathbb{C}(\boldsymbol{\delta}^o) \end{bmatrix}}_{\mathbf{G}_{15}} \underbrace{\begin{bmatrix} \mathbb{C}(\tilde{\boldsymbol{\delta}}) - \mathbf{I} \\ \mathbb{S}(\tilde{\boldsymbol{\delta}}) \end{bmatrix}}_{\mathbf{F}_{55}} \underbrace{\mathbb{T}_{do}^{-1}\,\tilde{\mathbb{E}}_{fd}}_{\mathbf{H}_{54}} \tag{C.50}$$

Moving to Equation (C.38), the last term on the right-hand side may be taken as-is:

$$\Delta\mathbf{A}_{\omega 1} = \underbrace{\mathbb{M}^{-1}}_{\mathbf{G}_{\omega 6}} \underbrace{\begin{bmatrix} \tilde{\mathbb{E}}_{\mathrm{D}} & \tilde{\mathbb{E}}_{\mathrm{Q}} \end{bmatrix}}_{\mathbf{F}_{66}} \underbrace{\mathbf{Y}_r\,\tilde{\mathbb{E}}_{\mathrm{DQ}}}_{\mathbf{H}_{6e}} \tag{C.51}$$

A final uncertainty that must be addressed is the "measurement" uncertainty inherent in a voltage magnitude measurement. The problem is that the voltage magnitude is a nonlinear function of the state, so that, again, the nonlinearity may be accounted for as a bounded perturbation of the $\mathbf{C}_2$ matrix. We begin by recalling equation (2.40). In

the network frame of reference when saliency is ignored, this is just

$$\begin{bmatrix} \mathsf{V}_D \\ \mathsf{V}_Q \end{bmatrix} = \{\mathbf{I} + \mathbf{Z}\mathbf{Y}_r\} \begin{bmatrix} \mathsf{E}_{\mathrm{D}} \\ \mathsf{E}_{\mathrm{Q}} \end{bmatrix} \tag{C.52}$$

$$= \mathbf{K}_v \mathsf{E}_{\mathrm{DQ}} \tag{C.53}$$

Letting $|V_i|^2 = V_{\mathrm{D}_i}^2 + V_{\mathrm{Q}_i}^2 = |V_{\mathrm{D}_i} + jV_{\mathrm{Q}_i}|^2$,

$$\begin{bmatrix} |V_1|^2 \\ \vdots \\ |V_p|^2 \end{bmatrix} = \begin{bmatrix} \mathbb{E}_{\mathrm{D}} & \mathbb{E}_{\mathrm{Q}} \end{bmatrix} \mathbf{K}_v^t \mathbf{K}_v \begin{bmatrix} \mathsf{E}_{\mathrm{D}} \\ \mathsf{E}_{\mathrm{Q}} \end{bmatrix}, \tag{C.54}$$

Note that this form is exactly like the power equation (2.28), and we may treat it in the same way in order to define the incremental change in $|V_i|^2$. We now define the vector

$$\mathsf{k}_v = \begin{bmatrix} \mathsf{k}_{v1} \\ \mathsf{k}_{v2} \end{bmatrix} = \mathbf{K}_v^t \mathbf{K}_v \begin{bmatrix} \mathsf{E}_{\mathrm{D}} \\ \mathsf{E}_{\mathrm{Q}} \end{bmatrix}, \tag{C.55}$$

so that

$$\begin{bmatrix} |V_1|^2 - |V_1^o|^2 \\ \vdots \\ |V_p|^2 - |V_p^o|^2 \end{bmatrix} = \underbrace{\left\{ \begin{bmatrix} \mathbb{E}_{\mathrm{D}}^o & \mathbb{E}_{\mathrm{Q}}^o \end{bmatrix} \mathbf{K}_v^t \mathbf{K}_v + \begin{bmatrix} \mathbb{K}_{v1} & \mathbb{K}_{v2} \end{bmatrix} \right\}}_{C_2} \tilde{\mathsf{E}}_{\mathrm{DQ}} + \underbrace{\mathbf{I}}_{\mathbf{G}_{47}} \underbrace{\begin{bmatrix} \tilde{\mathbb{E}}_{\mathrm{D}} & \tilde{\mathbb{E}}_{\mathrm{Q}} \end{bmatrix}}_{F_{77}} \underbrace{\mathbf{K}_v^t \mathbf{K}_v}_{H_{71}} \tilde{\mathsf{E}}_{\mathrm{DQ}}. \tag{C.56}$$

Collecting all the terms defined up to this point, we have:

$$\mathbf{G} = \left[\begin{array}{c|cc|cc|c|c} -\mathbf{I}_{2p\times 2p} & \begin{matrix}\mathbb{Z}_1 & -\mathbb{Z} \\ \mathbb{Z}_2 & \mathbb{Z}_1\end{matrix} & \begin{matrix}\mathbb{C}(\boldsymbol{\delta}_o) & -\mathbb{S}(\boldsymbol{\delta}_o) \\ \mathbb{S}(\boldsymbol{\delta}_o) & \mathbb{C}(\boldsymbol{\delta}_o)\end{matrix} & \mathbf{I}_{2p\times 2p} & \begin{matrix}\mathbb{C}(\boldsymbol{\delta}_o) & -\mathbb{S}(\boldsymbol{\delta}_o) \\ \mathbb{S}(\boldsymbol{\delta}_o) & \mathbb{C}(\boldsymbol{\delta}_o)\end{matrix} & \mathbf{0}_{2p\times p} & \mathbf{0} \\ \hline \mathbf{0}_{p\times 2p} & \mathbf{0} & \mathbf{0} & \mathbf{0} & \mathbf{0} & \mathbf{0}_{p\times p} & \mathbf{0} \\ \mathbf{0}_{p\times 2p} & \mathbf{0} & \mathbf{0} & \mathbf{0} & \mathbf{0} & \mathbb{M}^{-1} & \mathbf{0} \\ \hline \mathbf{0} & \mathbf{0} & \mathbf{0} & \mathbf{0} & \mathbf{0} & \mathbf{0} & \mathbf{I} \end{array}\right], \tag{C.57}$$

$$F(\underline{x}) = \begin{bmatrix} \begin{bmatrix} \mathbb{C}(2\tilde{\boldsymbol{\delta}}) - \mathbf{I} & -\mathbb{S}(2\tilde{\boldsymbol{\delta}}) \\ \mathbb{S}(2\tilde{\boldsymbol{\delta}}) & \mathbb{C}(2\tilde{\boldsymbol{\delta}}) - \mathbf{I} \end{bmatrix} & \mathbf{0} & \mathbf{0} & \mathbf{0} & \mathbf{0} & \mathbf{0} & \mathbf{0} \\ \mathbf{0} & \begin{bmatrix} \mathbb{C}(2\tilde{\boldsymbol{\delta}}) - \mathbf{I} \\ \mathbb{S}(2\tilde{\boldsymbol{\delta}}) - 2\tilde{\boldsymbol{\delta}} \end{bmatrix} \tilde{\Delta}^{-1} & \mathbf{0} & \mathbf{0} & \mathbf{0} & \mathbf{0} & \mathbf{0} \\ \mathbf{0} & \mathbf{0} & \begin{bmatrix} \mathbb{C}(\tilde{\boldsymbol{\delta}}) - \mathbf{I} \\ \mathbb{S}(\tilde{\boldsymbol{\delta}}) - \tilde{\boldsymbol{\delta}} \end{bmatrix} \tilde{\Delta}^{-1} & \mathbf{0} & \mathbf{0} & \mathbf{0} & \mathbf{0} \\ \mathbf{0} & \mathbf{0} & \mathbf{0} & \begin{bmatrix} \tilde{\mathbb{E}}_{\mathrm{Q}} \\ -\tilde{\mathbb{E}}_{\mathrm{D}} \end{bmatrix} & \mathbf{0} & \mathbf{0} & \mathbf{0} \\ \mathbf{0} & \mathbf{0} & \mathbf{0} & \mathbf{0} & \begin{bmatrix} \mathbb{C}(\tilde{\boldsymbol{\delta}}) - \mathbf{I} \\ \mathbb{S}(\tilde{\boldsymbol{\delta}}) \end{bmatrix} & \mathbf{0} & \mathbf{0} \\ \mathbf{0} & \mathbf{0} & \mathbf{0} & \mathbf{0} & \mathbf{0} & \begin{bmatrix} \tilde{\mathbb{E}}_{\mathrm{D}} & \tilde{\mathbb{E}}_{\mathrm{Q}} \end{bmatrix} & \mathbf{0} \\ \mathbf{0} & \mathbf{0} & \mathbf{0} & \mathbf{0} & \mathbf{0} & \mathbf{0} & \begin{bmatrix} \tilde{\mathbb{E}}_{\mathrm{D}} & \tilde{\mathbb{E}}_{\mathrm{Q}} \end{bmatrix} \end{bmatrix} \tag{C.58}$$

and

$$\mathbf{H} = \left[\begin{array}{c|c|c|c} \mathbf{R}_{\mathrm{N}}^{o}\mathbf{A}_2 & \mathbf{0}_{2p\times p} & \mathbf{0}_{2p\times p} & \mathbf{0}_{2p\times p} \\ \hline \mathbf{0}_{p\times 2p} & \mathbf{I}_{p\times p} & \mathbf{0}_{p\times p} & \mathbf{0}_{p\times p} \\ \hline \mathbf{0}_{p\times 2p} & \mathbb{T}_{do}^{-1}\mathbb{E}_{fdo} & \mathbf{0}_{p\times p} & \mathbf{0}_{p\times p} \\ \hline \mathbf{0}_{2p\times p} & \mathbf{0}_{p\times p} & \mathbf{I}_{p\times p} & \mathbf{0}_{2p\times p} \\ \hline \mathbf{0}_{p\times 2p} & \mathbf{0}_{p\times p} & \mathbf{0}_{p\times p} & \mathbb{T}_{do}^{-1} \\ \hline \mathbf{Y}_r & \mathbf{0}_{2p\times p} & \mathbf{0}_{2p\times p} & \mathbf{0}_{2p\times p} \\ \hline\hline \mathbf{K}_v^t\mathbf{K}_v & \mathbf{0} & \mathbf{0} & \mathbf{0} \end{array}\right] \tag{C.59}$$

We have now defined all the matrices and associated submatrices necessary to begin the design of a suboptimal $\mathcal{H}_\infty$ control, using the methods outlined in [15]. One issue remains to be dealt with, however, and that is the problem of the zero eigenvalue, which has been postponed in the interest of simplicity.

The dynamic equations derived in the earlier parts of this chapter must now be modified to reflect the relative angle reference. Observe that, in addition to the fact that two states vanish from the relative-angle model, the "uncertainty" in the angle δ_p and the corresponding frequency ω_p also vanishes. Therefore, given the block-diagonal structure of both $\mathbf{F}(\tilde{\mathrm{x}})$ and its component submatrices, it is easily seen that the rows and columns corresponding to the variation in the reference variables must be eliminated. Moreover, since the $\mathbf{H}$ matrix multiplies the incremental state vector $\tilde{\mathrm{x}}$, the columns of $\mathbf{H}$ corresponding to the reference variables are also eliminated. As noted in Section 2.8, if the voltage dynamics of the reference machine are to be preserved, then the modifications suggested in (2.112) and (2.113) are incorporated into the voltage equations, but this is just a matter of expressing the equilibrium in the relative-angle coordinates. Moreover, the fact that the uncertainty vanishes from the nonlinear terms associated with the reference machine is already accounted for by the elimination of the rows and columns of G, $F(\mathrm{x})$ and H associated with the reference variables. Hence, passing from the full-order model derived above to the relative-angle model is trivial.

Bibliography

[1] E. A. Allen, J. W. Chapman, and M. D. Ilić. Effects of torsional dynamics on nonlinear generator control: Part I. In *Proceedings,* 34^{th} *IEEE Conference on Decision and Control*, pages 3887–3894, New Orleans, LA, December 1995.

[2] E. A. Allen, J. W. Chapman, and M. D. Ilić. Effects of torsional dynamics on nonlinear generator control: Part II. In *Proceedings,* 34^{th} *IEEE Conference on Decision and Control*, pages 3479–3485, New Orleans, LA, December 1995.

[3] P. M. Anderson and A. A. Fouad. *Power System Control and Stability.* Iowa State University Press, 1977.

[4] T. Athay, R. Podmore, and S. Virmani. A practical method for the direct analysis of transient stability. *IEEE Transactions on Power Apparatus and Systems*, PAS-98(2):573–584, March 1979.

[5] Yijin Cao, Jiang Lin, et al. A nnonlinear variable structure stabilizer for power system stability. In *Proceedings, IEEE Power Engineering Society Winter Meeting*, 1994. Paper #94 WM 126-3 EC.

[6] J. W. Chapman. Feedback linearizing generator excitation control for enhanced power system stability. Master's thesis, Massachusetts Institute of Technology, 1992.

[7] J. W. Chapman and M. D. Ilic. Some robustness results for feedback linearizing control of generator excitation. In *Proceedings,* 31^{st} *IEEE Conference on Decision and Control*, pages 1123–28, Tucson, AZ, December 1992.

[8] J. W. Chapman, M. D. Ilic, C. A. King, et al. Stabilizing a multimachine power system via decentralized feedback linearizing excitation control. *IEEE Transactions on Power Systems*, PWRS-8:830–839, August 1993.

[9] H. D. Chiang. Analytical results on direct methods for power system transient stability analysis. In *Control and Dynamic Systems*, volume 43. Academic Press, 1991.

[10] H. D. Chiang, F. F. Wu, and P. P. Varaiya. Foundations of direct methods for power system transient stability analysis. *IEEE Transactions on Circuits and Systems*, CAS-34:160–172, February 1987.

[11] H. D. Chiang, F. F. Wu, and P. P. Varaiya. Foundations of the potential energy boundary surface method for power system transient stability analysis. *IEEE Transactions on Circuits and Systems*, CAS-35(6):712–728, June 1988.

[12] H. D. Chiang, F. F. Wu, and P. P. Varaiya. A BCU method for direct analysis of power system stability. *IEEE Transactions on Power Systems*, PWRS-9(3):1194–1208, August 1994.

[13] I. Dobson and L. Lu. Immediate change in stability and voltage collapse when generator reactive power limits are encountered. In *Proceedings, Symposium on Bulk Power System Voltage Phenomena II*, pages 65–73, August 1991.

[14] J. Douglas and M. Athans. Robust linear quadratic designs with real parameter uncertainty. *IEEE Transactions on Automatic Control*, 39(1):107–111, January 1994.

[15] J. C. Doyle, K. Glover, P. P. Khargonekar, and B. A. Francis. State space solutions to standard $\mathcal{H}_2$ and $\mathcal{H}_\infty$ control problems. *IEEE Transactions on Automatic Control*, 34(8):831–847, 1989.

[16] J. F. Gronquist, W. A. Sethares, F. L. Alvarado, and R. H. Lasseter. Power oscillation damping control strategies for facts devices using locally measurable

quantities. In *IEEE Power Engineering Society Winter Meeting*, New York, NY, January 1995. Paper #95 WM 185-9 PWRS.

[17] J. F. Hauer. Robust damping controls for large power systems. *IEEE Control Systems Magazine*, pages 12–18, January 1989.

[18] T. Hiyama, M. Kugimiya, and S. Hironori. Advanced PID type fuzzy logic power system stabilizer. In *IEEE Power Engineering Society 1994 Winter Meeting*, February 1994. Paper # 94 WM 127-1 PWRS.

[19] M. D. Ilić. Fundamental engineering porblems and opportunities in operating power transmission grids of the future. *To Appear: International Journal of Electrical Power & Energy Systems, Special Issue on FACTS*, February 1995.

[20] Alberto Isidori. *Nonlinear Control Systems.* Springer-Verlag, 1989.

[21] N. Kakimoto, Y. Ohnogi, H. Matsuda, and H. Shibuya. Transient stability analysis of large-scale power system by lyapunov's direct method. *IEEE Transactions on Power Apparatus and Systems*, PAS-103(1), January 1984.

[22] N. Kakimoto, Y. Ohsawa, and M. Hayashi. Transient stability analysis of multimachine power systems with field flux decays via lyapunov's ditect method. *IEEE Transactions on Power Apparatus and Systems*, PAS-99(5), September 1980.

[23] Hassan K. Khalil. *Nonlinear Systems.* MacMillan, 1992.

[24] M. H. Khammash, V. Vittal, and C. D. Pawloski. Analysis of control performance for stability robustness of power systems. In *Proceedings, IEEE Power Engineering Society Winter Meeting*, 1994. Paper #94 WM 171-9 PWRS.

[25] P. P. Khargonekar, I. R. Peterson, and K. Zhou. Robust stabilization of uncertain linear systems: Quadratic stabilizability and $\mathcal{H}_\infty$ control theory. *IEEE Transactions on Automatic Control*, 35(3):356 – 361, March 1990.

[26] Charles A. King, J. W Chapman, and M. D. Ilić. Feedback linearizing excitation control on a full-scale power system model. *IEEE Transactions of Power Systems*, 9(2):1102–1109, May 1994.

[27] M. Klein, G. J. Rogers, and P. Kundur. A fundamental study of inter-area oscillations in power systems. *IEEE Transactions on Power Systems*, 6(3):914–921, August 1991.

[28] P. V. Kokotovic, H. K. Khalil, and J. O'Reilly. *Singular Perturbations Methods in Control: Analysis and Design.* Academic Press, 1986.

[29] D. N. Kosterev and J. K. Wojtek. Bang-bang series capacitor transient stability control. *IEEE Transactions on Power Systems*, PWRS-10(2):915–924, May 1995.

[30] Paul C. Krause. *Analysis of Electric Machinery.* McGraw-Hill, 1986.

[31] A Llamas, J. De La Ree Lopez, et al. Clarifications of the BCU method for transient stability analysis. In *IEEE Power Engineering Society 1994 Winter Meeting*, January 1994. Paper # 94 WM 179-2 PWRS.

[32] F. K. Mak. *Analysis and Control of Voltage Dynamics in Electric Power Systems.* PhD thesis, University of Illinois at Urbana-Champaign, 1990.

[33] R. Marino. An example of a nonlinear regulator. *IEEE Transactions on Automatic Control*, AC-29(3), March 1989.

[34] W. Mielczarski and A. M. Zajaczkowski. Nonlinear stabilization of synchronous generator. In *Proceedings, IFAC Nonlinear Control Symposium*, Capri, Italy, June 1989.

[35] Y. Morioka, H. Tanaka, et al. Application of multivariable optimal controller to real power systems. In *IEEE Power Engineering Society 1994 Winter Meeting*, February 1994. Paper # 94 WM 158-8 PWRS.

[36] H. A. Othman, J. H. Chow, and G. N. Taranto. Modeling of impedance uncertainty in power system networks. In *Proceedings, 31st IEEE Conference on Decision and Control*, pages 591–592, December 1992.

[37] K. R. Padiyar and K. K. Ghosh. Dynamic security assessment of power systems using structure-preserving energy functions. *Electrical Power & Energy Systems*, 11(1):39–46, January 1989.

[38] M. A. Pai. *Power System Stability: Analysis by the Direct Method of Lyapunov.* North-Holland systems and control series; v.3, 1981.

[39] M. A. Pai. *Energy Function Analysis for Power System Stability.* Kluwer, 1989.

[40] I. J. Pérez, G. C. Verghese, F. L. Pagola, et al. Developments in selective modal analysis of small-signal stability in electric power systems. *Automatica*, 26(2):215–231, 1990.

[41] I. R. Peterson and C. V. Hollot. A Riccati equation approach to the stabilization of uncertain linear systems. *Automatica*, 22(4):397–411, 1986.

[42] Ian R. Peterson. A stabilization algorithm for a class of uncertain linear systems. *Systems and Control Letters*, 8:351–357, 1987.

[43] IUrii P. Petrov. *Variational Methods in Optimum Control Theory.* Academic Press, 1968.

[44] A. H. M. A. Rahim and A. I. J. Al-Sammak. Optiomal switching of dynamic braking resistor, reactor or capacitor for transient stability of power systems. *IEE Proceedings-C*, 138(1):89–93, January 1991.

[45] M. Ribbens-Pavella and F. J. Evans. Direct methods for studying dynamics of large-scale electric power systems – a survey. *Automatica*, 21(1):1–21, 1985.

[46] H. Sasaki. An approximate incorporation of field flux decay into transient stability abalyses of multimachine power systems by the second method of lyapunov. *IEEE Transactions on Power Apparatus and Systems*, PAS-98(2):473–483, March 1979.

[47] P. W. Sauer and M. A. Pai. Modeling and simulation of dynamic systems. In *Advances in Control and Dynamic Systems*, volume 43. Academic Press, 1991.

[48] J-J. E. Slotine and Weiping Li. *Applied Nonlinear Control.* Prentice Hall, 1991.

[49] J. R. Smith, D. A. Pierre, D. A. Rudberg, I. Sadighi, A. P. Johnson, and J. F. Hauer. An enhanced LQ adaptive VAR unit controller for power system damping. *IEEE Transactions on Power Systems*, 4(2):443–451, May 1989.

[50] M. Vidyasagar. *Nonlinear Systems Analysis.* Prentice-Hall, 1993.

[51] V. Vittal, N. Bhatia, and A. A. Fouad. Analysis of the inter-area mode phenomenon in power systems following large disturbances. *IEEE Transactions on Power Systems*, 6(4):1515–1521, November 1989.

[52] Y. Wang, W. A. Mittlestadt, and D.J. Maratukulam. Variable-structure braking resistor control in a multimachine power system. In *IEEE Power Engineering Society 1993 Summer Meeting*, July 1993. Paper # 93 SM 480-4 PWRS.

[53] L Xie, M. Fu, and C. E. de Souza. $\mathcal{H}_\infty$ control and quadratic stabilization of systems with parameter uncertainty via output feedback. *IEEE Transactions on Automatic Control*, 37(8):1253 – 1256, August 1992.

[54] J. Zaborszky, K. V. Prasad, and K. W. Whang. Stabilizing control in emergencies, part 2. *IEEE Transactions on Power Apparatus and Systems*, PAS-100(5):2381–2389, 1981.

[55] J. Zaborszky and K. W. Whang. Local feedback stabilization of large interconnected power systems in emergencies. *Automatica*, 17(5):673–686, 1981.